

INFORMATION TO USERS

This manuscript has been reproduced from the microfilm master. UMI films the text directly from the original or copy submitted. Thus, some thesis and dissertation copies are in typewriter face, while others may be from any type of computer printer.

The quality of this reproduction is dependent upon the quality of the copy submitted. Broken or indistinct print, colored or poor quality illustrations and photographs, print bleedthrough, substandard margins, and improper alignment can adversely affect reproduction.

In the unlikely event that the author did not send UMI a complete manuscript and there are missing pages, these will be noted. Also, if unauthorized copyright material had to be removed, a note will indicate the deletion.

Oversize materials (e.g., maps, drawings, charts) are reproduced by sectioning the original, beginning at the upper left-hand corner and continuing from left to right in equal sections with small overlaps.

ProQuest Information and Learning
300 North Zeeb Road, Ann Arbor, MI 48106-1346 USA
800-521-0600

UMI[®]

THE UNIVERSITY OF OKLAHOMA

GRADUATE COLLEGE

**IN-SITU ANALYSIS OF VOLATILES OBTAINED BY CATALYTIC CRACKING OF
POLYETHYLENE WITH HZSM-5, HY, AND HMCM-41**

A DISSERTATION

SUBMITTED TO THE GRADUATE FACULTY

In partial fulfillment of the requirements for the

degree of

DOCTOR OF PHILOSOPHY

By

NATHAN D. HESSE

Norman, Oklahoma

2002

UMI Number: 3063954

UMI[®]

UMI Microform 3063954

**Copyright 2002 by ProQuest Information and Learning Company.
All rights reserved. This microform edition is protected against
unauthorized copying under Title 17, United States Code.**

**ProQuest Information and Learning Company
300 North Zeeb Road
P.O. Box 1346
Ann Arbor, MI 48106-1346**

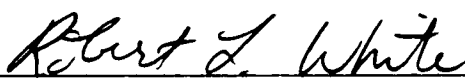
©Copyright by NATHAN D. HESSE 2002

All Rights Reserved.

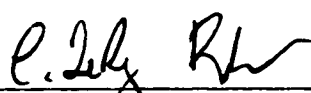
IN-SITU ANALYSIS OF VOLATILES OBTAINED BY CATALYTIC CRACKING OF
POLYETHYLENE WITH HZSM-5, HY, AND HMCM-41

A DISSERTATION APPROVED FOR THE
DEPARTMENT OF CHEMISTRY AND BIOCHEMISTRY

BY



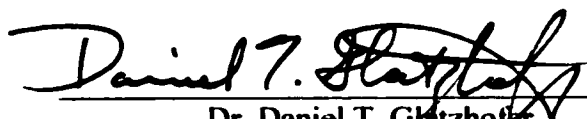
Dr. Robert L. White



Dr. C. LeRoy Blank



Dr. Richard W. Taylor



Dr. Daniel T. Glatzhofer



Dr. Lance L. Lobban

ACKNOWLEDGEMENTS

The completion of this dissertation is the final requirement to obtain my doctoral degree. This has been my greatest accomplishment to date and I could not have done it without the help and support of a many people.

I would first like to sincerely thank Dr. Robert L. White, my mentor, for his dedication and thoughtful guidance and advice throughout my entire graduate career at the University of Oklahoma. I really appreciated the scientific discussions that we have had over the years, but most importantly I will value our personal kinship. My appreciation goes to the other members of my graduate committee: Dr. C. Leroy Blank, Dr. Richard W. Taylor, Dr. Daniel T. Glatzhofer, and Dr. Lance L. Lobban for their interest in my research and motivation to help me succeed.

I must express my gratitude to the past and present members of Dr. White's research group for their comradery. I would especially like to thank Dr. Edouard Bonnet, Mr. Darrel Negelein, Dr. Rong Lin, Dr. Emmanuel Sikabwe, Mr. Jesse Cooper III, Ms. Lihong Du, and future Dr. Ling Huang for their supportive discussions.

Finally, I wish to express my infinite admiration to all of my family. None of this would have been possible without their love and encouraging support.

TABLE OF CONTENTS

	Page
LIST OF TABLES	ix
LIST OF FIGURES	x
ABSTRACT	xvi
CHAPTER 1 - INTRODUCTION	
1.1 Background	1
1.2 Catalytic Cracking and Hydrocracking of Polyethylene	5
1.3 Acid Catalyzed Chain Reaction Cracking Mechanisms	12
1.3.1 Bifunctional Catalyst Cracking Mechanisms	14
1.4 Project Description	17
1.5 References	19
CHAPTER 2 - EXPERIMENTAL	
2.1 Introduction	26
2.2 Materials	26
2.3 Sample Preparation	30
2.4 Thermogravimetric Analysis (TGA)	30
2.5 Thermal Analysis Coupled with Mass Spectrometry (TA-MS)	36
2.5.1 Thermal Analysis Coupled with Gas Chromatography/Mass Spectrometry (TA-GC/MS)	42
2.6 Ammonia Temperature Programmed Desorption (NH ₃ -TPD)	55
2.7 References	63

CHAPTER 3 - ISOCONVERSION EFFECTIVE ACTIVATION ENERGY

3.1	Introduction	69
3.2	Theory/Background	70
3.3	Experimental	74
3.4	References	88

CHAPTER 4 - RESULTS OF LPE CRACKING AND ISOCONVERSION E_a EXPERIMENTS

4.1	Introduction	93
4.2	Experimental Results	93
4.2.1	LPE/HZSM-5 (He)	
4.2.1a	TA-GC/MS Results	94
4.2.1b	TA-MS Results	99
4.2.2	LPE/HZSM-5 (H ₂)	
4.2.2a	TA-GC/MS Results	103
4.2.2b	TA-MS Results	109
4.2.3	LPE/PtHZSM-5 (He)	
4.2.3a	TA-GC/MS Results	113
4.2.3b	TA-MS Results	116
4.2.4	LPE/PtHZSM-5 (H ₂)	
4.2.4a	TA-GC/MS Results	122
4.2.4b	TA-MS Results	126
4.2.5	LPE/HY (He)	
4.2.5a	TA-GC/MS Results	128
4.2.5b	TA-MS Results	133
4.2.6	LPE/HY (H ₂)	
4.2.6a	TA-GC/MS Results	133
4.2.6b	TA-MS Results	139
4.2.7	LPE/PtHY (He)	
4.2.7a	TA-GC/MS Results	139
4.2.7b	TA-MS Results	145

4.2.8	LPE/PtHY (H ₂)	
4.2.8a	TA-GC/MS Results	147
4.2.8b	TA-MS Results	151
4.2.9	LPE/HMCM-41 (He)	
4.2.9a	TA-GC/MS Results	151
4.2.9b	TA-MS Results	157
4.2.10	LPE/HMCM-41 (H ₂)	
4.2.10a	TA-GC/MS Results	157
4.2.10b	TA-MS Results	160
4.2.11	LPE/PtHMCM-41 (He)	
4.2.11a	TA-GC/MS Results	164
4.2.11b	TA-MS Results	168
4.2.12	LPE/PtHMCM-41 (H ₂)	
4.2.12a	TA-GC/MS Results	168
4.2.12b	TA-MS Results	174

CHAPTER 5 - DISCUSSION OF EXPERIMENTAL RESULTS

5.1	Introduction	176
5.2	Temperature Changes During LPE Cracking	176
5.2.1	LPE/catalyst in Helium	177
5.2.2	LPE/catalyst in Hydrogen	179
5.2.3	LPE/Ptcatalyst in Helium	180
5.2.4	LPE/Ptcatalyst in Hydrogen	182
5.3	Volatile Product Slate Comparisons	184
5.3.1a	LPE/HZSM-5 (He) vs. LPE/HZSM-5 (H ₂)	184
5.3.1b	LPE/HZSM-5 (He) vs. LPE/PtHZSM-5 (He)	191
5.3.1c	LPE/PtHZSM-5 (He) vs. LPE/PtHZSM-5 (H ₂)	193
5.3.2a	LPE/HY (He) vs. LPE/HY (H ₂)	195
5.3.2b	LPE/HY (He) vs. LPE/PtHY (He)	198

5.3.2c	LPE/PtHY (He) vs. LPE/PtHY (H ₂)	200
5.3.3a	LPE/HMCM-41 (He) vs. LPE/HMCM-41 (H ₂)	201
5.3.3b	LPE/HMCM-41 (He) vs. LPE/PtHMCM-41 (He)	204
5.3.3c	LPE/HMCM-41 (He) vs. LPE/HMCM-41 (H ₂)	205
5.4	Isoconversion E _a of LPE Cracking	205
5.4.1	LPE/HZSM-5 Paraffin Formation E _a	206
5.4.2	LPE/HZSM-5 Olefin Formation E _a	214
5.4.3	LPE/HZSM-5 and LPE/PtHZSM-5 Alkyl Aromatic Formation E _a	218
5.4.4	LPE/HY Paraffin Formation E _a	218
5.4.5	LPE/HY Olefin Formation E _a	223
5.4.6	LPE/HY Alkyl Aromatics Formation E _a	223
5.4.7	LPE/HMCM-41 Paraffin Formation E _a	225
5.4.8	LPE/HMCM-41 Olefin Formation E _a	225
5.4.9	LPE/HMCM-41 Alkyl Aromatics Formation E _a	229
5.5	Conclusions	229
5.6	References	234

LIST OF TABLES

TABLE	Page
CHAPTER 1 - INTRODUCTION	
No Tables	
CHAPTER 2 - EXPERIMENTAL	
No Tables	
CHAPTER 3 - ISOCONVERSION EFFECTIVE ACTIVATION ENERGY	
3-1	Identities of the numbered peaks from Figures 3-4 to 3-6 85
CHAPTER 4 - RESULTS OF LPE CRACKING AND ISOCONVERSION E_a EXPERIMENTS	
No Tables	
CHAPTER 5 - DISCUSSION OF EXPERIMENTAL RESULTS	
5-1	Volatile product evolution Temperatures for LPE/Catalysts 178
5-2	Percentage yields for LPE/HMCM-41 samples 185
5-3	Percentage yields for LPE/HMCM-41 samples 196
5-4	Percentage yields for LPE/HMCM-41 samples 202

LIST OF FIGURES

FIGURE	Page
CHAPTER 1 - INTRODUCTION	
1-1 Percent Composition of Plastics in MSW	6
CHAPTER 2 - EXPERIMENTAL	
2-1 Acid catalyst framework structure	28
2-2 Thermogravimetric balance	31
2-3 TGA of neat LPE	33
2-4 TGA and CBO of LPE/PtHY (He)	35
2-5 TA-GC/MS system	37
2-6 TA-GC/MS flow diagram	38
2-7 Tube furnace sample location	40
2-8 Sample position versus furnace temperature	41
2-9 Eight-port injection valve positions	45
2-10 Six-port injection valve positions	46
2-11 Repetitive injection chromatograms for LPE/PtHZSM-5 (He)	49
2-12 Sample injection at 150 °C for LPE/PtHZSM-5 (He)	50
2-13 Sample injection at 240 °C for LPE/PtHZSM-5 (He)	51
2-14 Sample injection at 300 °C for LPE/PtHZSM-5 (He)	52
2-15 NH ₃ -TPD correction for water	57
2-16 Normalized NH ₃ -TPD curves a) HZSM-5 b) PtHZSM-5	58
2-17 Normalized NH ₃ -TPD curves a) HY b) PtHY	59

2-18	Normalized NH ₃ -TPD curves a) HMCM-41 b) PtHMCM-41	60
2-19	Corrected NH ₃ -TPD curves for the metal-free catalysts	62

CHAPTER 3 - ISOCONVERSION EFFECTIVE ACTIVATION ENERGY

3-1	Normalized integrated ion signal versus temperature	77
3-2	ln(H) versus 1/T plots for LPE/HY	78
3-3	Paraffin E _a plots for LPE/HY	79
3-4	Selectivity of m/z 55 for olefins at 150 °C for LPE/HZSM-5	81
3-5	Selectivity of m/z 55 for olefins at 230 °C for LPE/HZSM-5	82
3-6	Selectivity of m/z 55 for olefins at 290 °C for LPE/HZSM-5	83
3-7	Volatile evolution profile comparison	87

CHAPTER 4 - RESULTS OF LPE CRACKING AND ISOCONVERSION E_a EXPERIMENTS

4-1	Repetitive injection chromatogram and negative derivative TGA for LPE/HZSM-5 (He)	95
4-2	Sample injections at a) 150, b) 240, and c) 300 °C for LPE/HZSM-5 (He)	96
4-3	Volatile product evolution profiles for LPE/HZSM-5 (He)	98
4-4	Paraffin E _a plots for LPE/HZSM-5 (He)	100
4-5	Olefin E _a plots for LPE/HZSM-5 (He)	102
4-6	Alkyl aromatics E _a plots for LPE/HZSM-5 (He)	104
4-7	Repetitive injection chromatogram and negative derivative TGA for LPE/HZSM-5 (H ₂)	105
4-8	Sample injections at a) 150, b) 240, and c) 300 °C for LPE/HZSM-5 (H ₂)	107

4-9	Volatile product evolution profiles for LPE/HZSM-5 (H ₂)	108
4-10	Olefin E _a plots for LPE/HZSM-5 (H ₂)	110
4-11	Paraffin E _a plots for LPE/HZSM-5 (H ₂)	112
4-12	Repetitive injection chromatogram and negative derivative TGA for LPE/PtHZSM-5 (He)	114
4-13	Sample injections at a) 150, b) 240, and c) 300 °C for LPE/PtHZSM-5 (He)	115
4-14	Volatile product evolution profiles for LPE/PtHZSM-5 (He)	117
4-15	Paraffin and Olefin E _a plots for LPE/PtHZSM-5 (He)	118
4-16	Alkyl aromatics E _a plots for LPE/HZSM-5 (He)	121
4-17	Repetitive injection chromatogram and negative derivative TGA for LPE/PtHZSM-5 (H ₂)	123
4-18	Sample injections at a) 150, b) 240, and c) 300 °C for LPE/PtHZSM-5 (H ₂)	124
4-19	Volatile product evolution profiles for LPE/PtHZSM-5 (H ₂)	125
4-20	Paraffin E _a plots for LPE/PtHZSM-5 (H ₂)	127
4-21	Repetitive injection chromatogram and negative derivative TGA for LPE/HY (He)	129
4-22	Sample injections at a) 170, b) 210, and c) 260 °C for LPE/HY (He)	131
4-23	Volatile product evolution profiles for LPE/HY (He)	132
4-24	Paraffin E _a plots for LPE/HY (He)	134
4-25	Repetitive injection chromatogram and negative derivative TGA for LPE/HY (H ₂)	135
4-26	Sample injections at a) 170, b) 210, and c) 260 °C for LPE/HY (H ₂)	137
4-27	Volatile product evolution profiles for LPE/HY (H ₂)	138

4-28	Paraffin E_a plots for LPE/HY (H_2)	140
4-29	Repetitive injection chromatogram and negative derivative TGA for LPE/PtHY (He)	141
4-30	Sample injections at a) 170, b) 210, and c) 260 °C for LPE/PtHY (He)	143
4-31	Volatile product evolution profiles for LPE/PtHY (He)	144
4-32	Paraffin and alkyl aromatics E_a plots for LPE/PtHY (He)	146
4-33	Repetitive injection chromatogram and negative derivative TGA for LPE/PtHY (H_2)	148
4-34	Sample injections at a) 220, b) 260, and c) 300 °C for LPE/PtHY (H_2)	149
4-35	Volatile product evolution profiles for LPE/PtHY (H_2)	150
4-36	Paraffin E_a plots for LPE/PtHY (H_2)	152
4-37	Repetitive injection chromatogram and negative derivative TGA for LPE/HMCM-41 (He)	153
4-38	Sample injections at a) 250, b) 270, and c) 290 °C for LPE/HMCM-41 (He)	155
4-39	Volatile product evolution profiles for LPE/HMCM-41 (He)	156
4-40	Olefin E_a plots for LPE/HMCM-41 (He)	158
4-41	Repetitive injection chromatogram and negative derivative TGA for LPE/HMCM-41 (H_2)	159
4-42	Sample injections at a) 250, b) 270, and c) 290 °C for LPE/HMCM-41 (H_2)	161
4-43	Volatile product evolution profiles for LPE/HMCM-41 (H_2)	162
4-44	Olefin E_a plots for LPE/HMCM-41 (H_2)	163
4-45	Repetitive injection chromatogram and negative derivative TGA for LPE/PtHMCM-41 (He)	165

4-46	Sample injections at a) 200, b) 250, and c) 290 °C for LPE/PtHMCM-41 (He)	166
4-47	Volatile product evolution profiles for LPE/PtHMCM-41 (He)	167
4-48	Olefin E_a plots for LPE/PtHMCM-41 (He)	169
4-49	Repetitive injection chromatogram and negative derivative TGA for LPE/PtHMCM-41 (H ₂)	170
4-50	Sample injections at a) 250, b) 270, and c) 280 °C for LPE/PtHMCM-41 (H ₂)	172
4-51	Volatile product evolution profiles for LPE/PtHMCM-41 (H ₂)	173
4-52	Paraffin E_a plots for LPE/PtHMCM-41 (H ₂)	175

CHAPTER 5 - DISCUSSION OF EXPERIMENTAL RESULTS

5-1	Normalized volatile paraffin profiles for a) LPE/HZSM-5 (He) b) LPE/HZSM-5 (H ₂)	189
5-2	P/O ratio vs. temperature plots for LPE/HZSM-5 (He) and (H ₂)	190
5-3	Normalized volatile paraffin and alkyl aromatics profiles for a) LPE/HY (He) b) LPE/PtHY (He)	199
5-4	Paraffin selectivity vs. temperature plot for LPE/HZSM-5 (He)	207
5-5	Paraffin E_a vs. temperature plots for a) LPE/HZSM-5 (He) and (H ₂) b) LPE/PtHZSM-5 (He)	209
5-6	Paraffin E_a vs. temperature plot for LPE/PtHZSM-5 (H ₂)	212
5-7	Olefin selectivity vs. temperature plot for LPE/HZSM-5 (He)	215
5-8	Paraffin E_a vs. temperature plots for LPE/HZSM-5 (He), LPE/HZSM-5 (H ₂), and LPE/PtHZSM-5 (He)	216
5-9	Alkyl aromatics E_a vs. temperature plots for LPE/HZSM-5 (He) and LPE/PtHZSM-5 (He)	219
5-10	Paraffin E_a vs. temperature plots for LPE/HY (He) and LPE/HY (H ₂)	220

5-11	Paraffin E_a vs. temperature plots for LPE/PtHY (He) and LPE/PtHY (H_2)	222
5-12	Alkyl aromatics E_a vs. temperature plots for LPE/PtHY (He)	224
5-13	Paraffin E_a vs. temperature plots for LPE/PtHMCM-41 (H_2)	226
5-14	Paraffin E_a vs. temperature plots for a) LPE/HMCM-41 (He) and (H_2) b) LPE/PtHMCM-41 (He)	227

IN-SITU ANALYSIS OF VOLATILES OBTAINED BY CATALYTIC CRACKING OF POLYETHYLENE WITH HZSM-5, HY, AND HMCM-41

Nathan D. Hesse

ABSTRACT

A variety of plastic waste recycling methods have been established and new recycling approaches are being developed to avoid placing polymers into landfills. One approach to waste plastic recycling, known as tertiary recycling, consists of decomposing plastics into useful chemicals or fuels. Repetitive injection thermal analysis gas chromatography mass spectrometry and thermal analysis mass spectrometry allow us to identify and quantify volatile products evolved from complex temperature-dependent systems. Volatile products from cracking/hydrocracking of low molecular weight polyethylene (LPE) were analyzed and activation energies of formation were determined when HZSM-5, HY, HMCM-41, and their platinum loaded analogs were employed as cracking catalysts.

When LPE is heated in helium with HZSM-5, paraffins are detected initially and olefins are produced at somewhat higher temperatures. Volatile paraffin formation by disproportionation reactions catalyzed by external HZSM-5 acid sites is favored due to the low activation energy values for this pathway at low temperatures. Small olefins (C_3 - C_5) are the most abundant products when HZSM-5 and HMCM-41 catalysts are employed for cracking LPE. In contrast, cracking with HY produces primarily paraffin

volatile products (C₄-C₈). HY pores are large enough and acid sites are strong enough to promote disproportionation reactions, which lead to formation of volatile paraffins.

When polymer/catalyst samples are heated in hydrogen, the extent of hydrogenation is reflected by reduced residue content and variations in E_a versus temperature curves. The addition of platinum increases volatile aromatic and olefin yields and/or residue content when polymer/catalyst samples are heated in helium. Bifunctional hydrogenation reactions dominate volatile product forming reactions, resulting in mainly paraffin products and small amounts of residue. Activation energy value differences between polymer/Ptcatalyst samples heated in hydrogen and the same samples heated in helium may be responsible for observed temperature shifts. The magnitudes of hydrogenation and/or platinum catalyzed effects appear to be related to catalyst pore size and acidity.

Volatile product slates derived from LPE cracking/hydrocracking differ significantly with temperature, reaction atmosphere, and catalyst physical characteristics (i.e. pore size, acidity, metal loading). When thermal analysis-gas chromatography mass spectrometry and thermal analysis-mass spectrometry results are considered, volatile product variations can be rationalized by effects of catalyst acidity and/or pore size on mono- and bifunctional cracking mechanisms.

CHAPTER 1 - INTRODUCTION

1.1 Background

The disposal of municipal solid waste (MSW) is recognized to be a major environmental problem. The amount of MSW generated annually in the United States has risen steadily from 88.1 million tons in 1960 to 231.9 million tons in 2000.¹ Currently, 30% of all MSW is recycled, leaving 162.0 million tons to be disposed. The most common method of MSW disposal is landfilling. However, landfills are becoming much more expensive to operate and new landfill sites are often vigorously opposed. An alternative to landfilling is desperately needed because the space available for waste disposal is shrinking. Between the years of 1988 and 2000, the number of landfills in operation in the United States decreased from 7924 to 1967.¹ Federal legislation and public distaste for landfills make it difficult to establish new landfill sites. Clearly, new waste treatment processes that reduce the volume of landfilled MSW are urgently needed.

The United States government has recognized this problem and has shown interest in recycling as a means for waste reduction. WasteWise is a free, voluntary, United States Environmental Protection Agency (U.S. EPA) program implemented in 1994 through which organizations are shown how to eliminate costly MSW, simultaneously benefiting their bottom line and the environment.² As of July 2001, over 1100 companies, state/local governments, and colleges were registered with the WasteWise program including: Eastman Kodak, GM, Anheuser-Busch, and Sandia National Laboratories.

In November 2001, a proclamation by the President of the United States was given commemorating November 15 as "America Recycles Day." George W. Bush stated:

"Our nation is making great progress by recycling, but we can and must do better. America Recycles Day 2001 represents a partnership among government, industry, and environmental organizations to promote recycling and to encourage the participation of all our citizens."

In September 2002, the U.S. EPA initiated another recycling program to urge all North Americans to take renewed responsibility for their individual impact on the environment.³ The "Resource Conservation Challenge" is a campaign challenging North Americans to meet or beat two goals by 2005: boosting the national recycling rate from 30 percent to at least 35 percent and limiting the generation of 30 harmful chemicals by 50 percent. To help meet the goals of the challenge, EPA has also announced 12 new innovative projects that will test creative approaches for waste minimization, energy recovery, recycling, and land revitalization. The goal of the resource conservation challenge and the innovative projects will be less waste, more economic growth, and greater energy savings and recovery.

MSW plastics constituted 10.7% of the total weight and about 20% of the total volume of MSW generated in the United States in 2000.¹ Increased plastic waste recycling is one response to the Resource Conservation Challenge. There are a variety of plastic waste recycling methods and the American Society for Testing Materials (ASTM) has categorized them into four different types. Primary recycling can be applied to waste that consist of polymers that are free from impurities. They can be used like virgin

plastic material during processing. Secondary recycling can be employed to convert plastic waste to new plastic materials that require less demanding performance characteristics than the original products. In tertiary recycling, waste plastics are degraded to produce chemicals or fuels. Plastic waste possesses high-energy content. Quaternary recycling, more commonly known as incineration, is used to convert plastic waste into thermal energy.

One advantage of tertiary and quaternary recycling is that commingled or contaminated waste, which makes up a majority of plastic MSW, can be recycled. However, quaternary recycling suffers from limited acceptability because of toxic emissions released by incineration and many volatile emission regulations restrict the use of this method. The U.S. is heavily dependent on liquid fuels, such as gasoline, diesel, and jet fuel. The present demands for these fuels far exceed domestic petroleum production capacity, and over one-half of these fuels are imported.⁴ Converting waste plastic into liquid fuels would not only supplement U.S. energy supplies, but could also help to mitigate environmental disposal problems.⁵ Therefore, one focus of current research is to convert plastic waste to useful fuels by tertiary recycling.

There are five different categories of tertiary recycling (otherwise known as feedstock or chemical recycling): chemical depolymerization, gasification, catalytic cracking and reforming, and hydrogenation.⁴ Chemical depolymerization involves chemical reaction with specific agents to recover monomers. Gasification with oxygen and/or steam is used to produce synthesis gas (CO and H₂). Catalytic cracking and reforming processes break down polymer chains to form smaller hydrocarbon products. In hydrogenation, the polymer is degraded by the combined actions of heat, hydrogen,

and in many cases, catalysts. Many different useful products may be formed through catalytic cracking, reforming, or hydrogenation reactions. Products depend on operating conditions and the type of catalyst employed.

Three main factors determine the profitability of tertiary recycling: the degree of separation required for the raw wastes, the value of the products obtained, and the capital investment in processing. In most tertiary recycling methods, some pretreatment and separation must be carried out on plastic waste prior to recycling, which results in increased recycling costs. According to the degree of separation required, feedstock recycling methods can be ordered as follows: gasification < thermal treatments, hydrogenation < catalytic cracking < chemical depolymerization.⁴ Many previous waste plastic recycling methods have failed because of the relatively low value of recycled products. However, as MSW amounts increase, landfill space decreases and the cost of landfilling increases. Eventually, government policies and legislation will demand recycling solutions that will make tertiary recycling methods viable.

A variety of plastic waste recycling methods have been established and new recycling approaches are being developed. Current large-scale recycling schemes do not incorporate catalytic cracking. However, the American Plastics Council (APC) and many other groups have sponsored extensive research in the area of feedstock recycling of plastics.⁶⁻⁷ During the period between 1990 and 1998, the plastics industry invested more than \$1 billion to support increased recycling within the United States.⁶⁻⁷ APC worked with Conrad Industries (Chehalis, Washington) to develop pyrolysis methods for converting plastic waste into petrochemical feedstocks. The plastic most studied has been a mixture of 60% high-density polyethylene, 20% polypropylene, and 20% polystyrene.

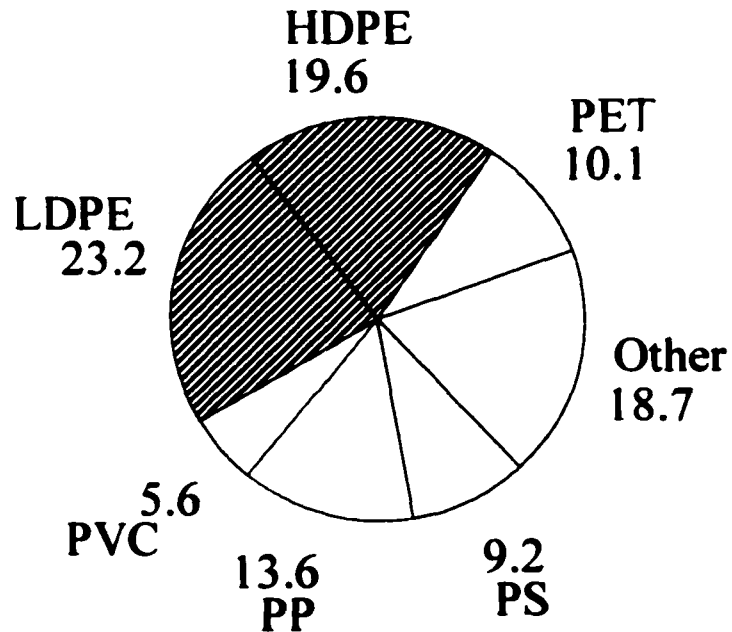
The U.S. Department of Energy has extensively investigated both the co-liquefaction and co-gasification of plastic waste with coal to produce petrochemical feedstocks and transportation fuels. Texaco and others have investigated the gasification of post-use plastic waste and other hydrocarbon feedstocks to produce synthesis gas (H_2 and CO). In Europe, BP Amoco continues to explore fluidized bed conversion of polyolefins to produce petrochemical feedstocks. Consequently, there is an ongoing need for research in the field of plastic waste tertiary recycling.

1.2 Catalytic Cracking and Hydrocracking of Polyethylene

Many polymer cracking studies have focused on polyethylene (PE) because it is the most abundant polymer in MSW plastics. Low density polyethylene (LDPE) and high density polyethylene (HDPE) constitute 42.8% of all MSW plastics (Figure 1-1).¹ During the late 1970s and 1980s, Uemichi and coworkers investigated the use of silica-alumina, activated carbon, Pt/silica-alumina, and Pt/alumina catalysts for PE cracking.⁸⁻¹¹ With the exception of the Pt/Alumina catalyst, most of the collected cracking products were hydrocarbons smaller than C_{12} . When the Pt/alumina catalyst was employed, a significant fraction (28%) of high boiling point products ($>C_{22}$) were detected. Whereas most of the volatile products obtained by using the silica alumina catalysts were C_3 - C_5 isoalkanes, activated carbon yielded small n-alkanes (C_1 - C_5) and aromatics (C_6 - C_8) as primary products.

In 1987, Takesue and coworkers reported that PE cracking under mild conditions with a silica-alumina catalyst could be used to shorten polymer chains and increase chain branching.¹² In their studies, catalytic reactions were conducted within glass reaction tubes heated to moderate temperatures (160-320 °C).

% Composition of Plastics in MSW



Total Plastic in MSW = 24.7 million tons

"Municipal Solid Waste in the U.S.: Facts and Figures", EPA 530-R-02-001 (2002)

HDPE = High density polyethylene
LDPE = Low density polyethylene
PVC = Poly(vinyl chloride)

PP = Polypropylene
PS = Polystyrene
PET = Poly(ethylene terephthalate)
Other = ?

Figure 1-1: Composition of plastics in municipal solid waste (MSW) in the United States for the year 2000¹

They employed polymer-to-catalyst ratios of unity for their experiments. Based on analysis of products isolated at different reaction temperatures, Takesue and coworkers determined that volatiles were not formed by chain end scissions, but were instead produced as a consequence of molecular weight decrease¹²⁻¹⁷, which was accompanied by skeletal rearrangements that enhanced branching in the degraded polymer. In a later report, Takesue and coworkers compared the cracking products obtained from their batch reactor with those obtained from a fixed bed flow reactor. As expected, the much longer residence times afforded by the batch reactor led to the formation of smaller hydrocarbon products than those generated by the fixed bed flow reactor at the same temperature. When NaY zeolite was employed to crack PE in a batch reactor at temperatures between 180 and 300 °C, volatile products were primarily isobutene and isopentane (75-93%), which were formed in nearly equal amounts. A “back biting” reaction scheme in which a C_9^+ intermediate was formed was proposed as the predominant low temperature reaction mechanism.

In 1989, Beltrame and Carntiti reported results from PE catalytic cracking in a batch reactor at reduced pressure (0.1-0.2 Torr).¹⁸ The activities of alumina, silica, HY, rare earth Y (REY), and silica-alumina catalysts were compared. Silica and alumina had little effect on polyethylene decomposition processes. Overall activation energies derived by applying the Freeman-Carrol method to thermogravimetric (TG) results confirmed that the zeolite catalysts (HY and REY) were more effective for cracking PE than silica-alumina.¹⁸

Ivanova et al. described the effects of Lewis acid catalysts on PE cracking in 1991.¹⁹ They reported that changing the composition of the Lewis acid catalyst could

alter volatile product slates. Product selectivity was found to increase as the catalyst acidity was reduced. For example, when PE was cracked by using AlCl_3 , 41% of the volatile products were C_4 hydrocarbons and 53% were hydrocarbons with five or more carbons. In contrast, when $\text{MgCl}_2 \cdot \text{AlCl}_3$ was employed as the cracking catalyst, the C_4 hydrocarbon yield rose to 85% and the abundance of hydrocarbons with more than five carbons was negligible.

During the early 1990s, several groups became interested in using catalysts to reform thermal decomposition products. Haskhimoto and coworkers evaluated the use of a variety of zeolite acid catalysts for reforming PE products generated by thermal decomposition.²⁰ REY was found to yield reformed products with the highest research octane number (RON = 67). Ng et al. produced gasoline fractions with RON values ranging from 70 to 85 by using HY to reform waxes derived from thermal decomposition of LDPE and HDPE.²¹ Using a similar approach, Ohkita et al. compared the reforming capabilities of HZSM-5 and silica-alumina catalysts.²² They found that the relative yield of gases (C_1 - C_4) increased with increasing acidity of the cracking catalyst.

Attempts have been made to blend polymers with other feedstocks prior to catalytic cracking. Ng demonstrated that a blend of PE with vacuum gas oil (VGO) could be cracked to yield fuels.²³ Unfortunately, the limited solubility of PE in VGO restricted blends to a maximum of 10% polymer by weight. Liu and Meuzelaar studied catalytic cracking of PE mixed with coal.²⁴ They found that HZSM-5 accelerated the rate of decomposition of coal commingled with plastic by a factor of 10 at 420 °C. Ding et al. reported that metal-loaded (Pt, Pd, Fe, and Ni) silica-alumina increased the catalytic activities of oil conversion for co-liquefaction of HDPE and coal mixtures at 430 °C

under 2000 psig hydrogen.²⁵ In a similar study, Joo et al. found that NiMo/HZSM-5 was more effective in forming liquid products than HZSM-5 for the co-liquefaction of LDPE and coal.²⁶

The number of published reports pertaining to PE cracking has increased substantially in the past few years. Ochoa and coworkers employed a series of silica-alumina catalysts with varying Brönsted/Lewis acid site ratios and determined that the oil yield from medium density polyethylene (MDPE) was determined by the Brönsted acidity.²⁷ Aguado et al. compared the activities and product selectivities of LDPE and HDPE cracking by using HZSM-5 and MCM-41 catalysts.²⁸⁻²⁹ They found that HZSM-5 was more active for PE cracking due to increased acid strength, but the selectivity toward the formation of gasoline and middle distillates (C₅-C₁₂) was clearly higher for MCM-41. Sakata and coworkers produced fuel oil from PE by using silica-alumina, ZSM-5, and non-acidic mesoporous silica.³⁰⁻³¹ Interestingly, mesoporous silica exhibited a catalytic effect that was similar to one of the silica-alumina catalysts. Sharratt and coworkers used a fluidized-bed reactor and HZSM-5 catalyst to crack HDPE with 90 wt. % yield at 360 °C³² and then extended the study to include silica-alumina, mordenite, and HY catalysts.³³ The same group characterized the deactivation of USY zeolite by monitoring changes in the TG properties of polymer/catalyst mixtures.³⁴

Garforth et al. used activation energies derived from TG measurements to compare the cracking properties of ZSM-5, HY, and MCM-41.³⁵ Coking was most significant for HY and MCM-41 exhibited the lowest HDPE cracking activation energy. In a similar study, Fernandes et al. compared the TG derived activation energy for HDPE

thermal decomposition with that for HZSM-5 catalytic cracking and found that the catalyst reduced the activation energy by more than a factor of two.³⁶⁻³⁷

Dufaud and Basset employed a zirconium hydride Ziegler-Natta catalyst to crack PE in a hydrogen atmosphere.³⁸ Ding et al. compared the catalytic activities of HZSM-5 and TiCl_3 for HDPE cracking.³⁹ TiCl_3 , which is an HDPE polymerization catalyst, yielded more n-alkanes than HZSM-5 and appeared to work via a radical mechanism. The same group also studied the hydroconversion of HDPE with sulfided Ni and NiMo silica-alumina and compared these catalysts to HZSM-5.⁴⁰ They found that Ni/silica-alumina produced better quality liquid products than commercial gasoline (i.e. more isoparaffins and fewer aromatics).

Park et al. compared the effectiveness of a natural zeolite (clinoptilolite structure, HNZ) and nickel-loaded HNZ (Ni/HNZ) to silica-alumina and HZSM-5.⁴¹ All four catalytically cracked PE, but volatile product slates were significantly different. For example, the gas yields for the Ni/HNZ and HNZ samples were found to be 64% and 35%, respectively. Uemichi et al. employed sequential catalyst beds (silica-alumina followed by HZSM-5) to crack PE into gasoline-range hydrocarbons.⁴² Optimum reactor conditions produced a 58.8% yield of RON = 94 gasoline. Manos and coworkers reported that carbon number distributions for products formed during HDPE cracking in a semi-batch reactor varied with cracking catalyst.⁴³⁻⁴⁴ They found that product size distributions were dependent on catalyst pore size and that USY, HY and β -zeolite formed more alkane products and HZSM-5 and MOR formed more alkene products. In a similar study, Serrano et al. compared HDPE cracking products for HZSM-5, HMCM-41 and H β and found that HZSM-5 formed the highest gas yield (50% wt.), whereas H β and

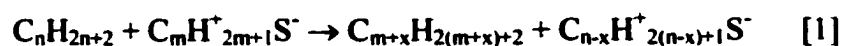
HMCM-41 formed higher liquid yields 60% and 54% wt., respectively.⁴⁵ Van Grieken et al. compared HZSM-5, HY, silica-alumina, MCM-41, PdMCM-41, and Pd/charcoal powder for LDPE and HDPE cracking between 360 to 420 °C. Product distributions suggested a random scission mechanism.⁴⁶⁻⁴⁷

Walendziewski et al. studied thermal cracking, catalytic cracking, and hydrocracking of PE in closed autoclaves and reported that the addition of hydrocracking catalysts decreased the boiling range and unsaturation of liquid products compared to thermal and catalytic cracking.⁴⁸⁻⁴⁹ Lin and coworkers used combined kinetic and mechanistic modeling of fluidized bed reactions to predict the production rates and product selectivity when HDPE was cracked by HZSM-5, MOR, USY, MCM-41, and silica-alumina catalysts.⁵⁰⁻⁵² Satsuma et al. reported the gas, liquid, and residue yields obtained under semi-batch conditions for various HDPE/catalyst (10:1 wt/wt) samples.⁵³ Manos and coworkers performed similar experiments with lower HDPE/catalyst ratios (1:1 or 2:1 wt/wt) and with different fresh and regenerated catalysts.⁵⁴⁻⁵⁶ They found that natural zeolites, saponite and montorillonite gave higher liquid yields (70%) compared to USY catalyst (50%). Aguado et al. compared cracking results for a polyolefin mixture (25% HDPE, 46.5 LDPE, and 28.5% PP wt.) obtained with varying polymer/catalyst (HZSM-5 and MCM-41) ratios and found that lower polyolefin/catalyst ratios resulted in increased conversion.⁵⁷⁻⁵⁸ The polyolefin/HZSM-5 combination yielded C₃-C₆ products whereas the polyolefin/MCM-41 combination yielded larger products (C₅-C₁₂ and C₁₃-C₂₂). Catalytic cracking of HDPE by silica MCM-41 has also been demonstrated.⁵⁹ Cracking activity was reported to increase with increased catalyst crystallinity and carbenium ion-mediated mechanisms were proposed.

1.3 Acid Catalyzed Chain Reaction Cracking Mechanisms

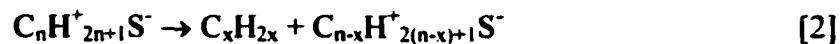
The chain reaction mechanisms for acid catalytic cracking proposed by Wojciechowski can be used to explain all of the phenomena observed in catalytic cracking.⁶⁰ These mechanisms are based on the following three postulates. First, all catalytic cracking reactions proceed via surface-resident ions. Second, ions undergo only two types of reactions, bimolecular (disproportionation) or unimolecular (decomposition), which produce all major gas phase products. The final postulate states that all major processes occur at Brønsted acid sites (H^+S^-) present on the catalyst.

Volatile products derived from small molecule cracking with solid acid catalysts can be rationalized by carbenium ion mechanisms. Zeolite cracking catalysts possess different pore structures and acid strengths that can influence the formation of volatile cracking products. Under steady-state (low conversion) conditions, hydrocarbon chain reaction cracking processes that yield volatile products can be represented by initiation, disproportionation, β -scission, and termination reactions.⁶⁰ By the chain reaction mechanism for hydrocarbon cracking, volatile paraffin products are formed by bimolecular disproportionation reactions on acid catalysts (Reaction [1]). Hydride abstraction and hydrogen transfer are disproportionation reactions where a hydride ion is exchanged between a feed molecule and a surface carbenium ion ($x = 0$).



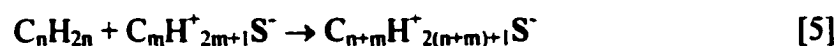
Wojciechowski states that disproportionation reactions are favored by carbenium ions formed at strong acid sites unless catalyst pore size restricts the bimolecular reaction (i.e. carbenium ions act as strong Lewis acids for disproportionation).⁶⁰ The rates of disproportionation reactions are thus dependent on catalyst acidity and pore size.

Volatile olefins can be formed by two different mechanisms on acid catalysts, β -scission [2] and desorption (i.e. termination) [3].



Like disproportionation, the rates of β -scission and desorption reactions are dependent on catalyst acidity and pore size. β -scission and desorption reactions are favored processes for the more stable carbenium ions on catalyst surfaces. Conjugate acid/base theory suggests that weak conjugate base sites result when strong acid sites are deprotonated. Weak conjugate base sites inhibit carbenium ions from undergoing β -scission and desorption and facilitate disproportionation reactions. However, the effect of a strong acid site can be overcome by a small pore structure. When catalyst pore size will not allow bimolecular disproportionation reactions, unimolecular reactions such as β -scission and desorption are the favored mechanisms for product formation from carbenium ions.

Reactions between product olefins and acid sites [4] or reactive carbenium ions [5] may occur when cracking at high conversion. Carbenium ions formed in reactions [4] and [5] may produce volatile products through Reactions [1-3]. Reaction [5] is a chain transfer reaction that can lead to a more diversified volatile product slate.



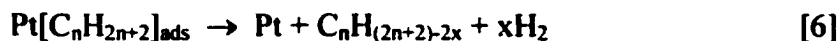
The chain reaction mechanism describes how paraffin and olefin cracking products are formed, but does not explain non-volatile residue or volatile aromatic product formation. However, like other cracking reactions, aromatic product and residue formation reactions involve surface carbenium ions.⁶⁰ Conjugated unsaturated residue

that forms on catalyst surfaces during catalytic cracking is believed to lead to the formation of volatile aromatic species. Carbenium ion thermal cracking can result in olefin ions that may undergo dehydrogenation and cyclization reactions to form aromatic species. Volatile aromatic products are formed at higher temperatures than volatile paraffin and/or olefin products because conjugated unsaturation is a precursor for aromatization. When unsaturated ions are protonated, di-carbenium ions are produced. Doubly charged ions can also be formed by disproportionation reactions between adjacent surface carbenium ions. Multiply charged carbenium ions are strongly bound to surface conjugate base sites and are less likely to participate in cracking reactions than singly charged carbenium ions. Non-volatile surface residue is believed to include these multiply charged species.

1.3.1 Bifunctional Catalyst Cracking Mechanisms

Four active sites must be considered for the isomerization and hydrocracking of alkanes on bifunctional catalysts comprised of platinum and a shape-selective zeolite: 1) platinum clusters on the external surface 2) platinum inside zeolite pores 3) acid sites on external surfaces 4) acidic sites inside pores. The classical bifunctional hydrocracking/hydroconversion mechanism attributes hydrogenation to the platinum and isomerization and cracking to the acid sites.⁶¹ However, when reactions of small hydrocarbons take place on bifunctional catalysts in the absence of hydrogen, the functionality of the metal can be altered. Dehydrogenation, cracking, and hydrogenolysis reactions can occur on the metal surface.⁶¹⁻⁶³ Two types of dehydrogenation reactions exist: dehydroisomerization and dehydrocyclization (Reaction [6]).

Dehydroisomerization reactions of small paraffin feed molecules result in the formation of olefins and molecular hydrogen.



Dehydrocyclization reactions form cyclic and aromatic species. Dehydrogenation reactions may occur at temperatures as low as -20 to 80 °C.⁶²⁻⁶³

When a paraffin molecule undergoes cracking on a metal surface, a shorter olefin is released and an ionic fragment remains on the metal surface.



An increase in volatile olefin yield in hydrogen deficient atmospheres may not be observed for bifunctional catalysts because electron-rich olefins are reactive towards Brønsted acid sites. In this case, secondary reactions occur at nearby acid sites.⁶⁰

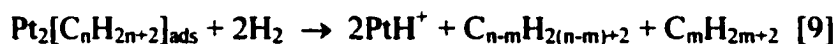
In hydrogen rich environments, volatile paraffins are favored over olefins due to platinum catalyzed hydrogenation.⁶¹⁻⁶³ Platinum catalyzed hydrogenation has been suggested to occur via a mechanism known as hydrogen spillover.⁶⁴⁻⁶⁷ During bifunctional hydrocracking reactions, molecular hydrogen activated on platinum sites (PtH_2^\bullet) migrates (i.e. hydrogen spillover) to another metal or acid site to participate in hydrogenation reactions. Reaction [8] represents hydrogen spillover from platinum to a carbenium ion occupied acid site.



The exact form of activated hydrogen species is unknown, but hydrogen spillover has been proposed to occur by both gas phase and surface transfer mechanisms.⁶⁵⁻⁶⁷ According to the classical bifunctional mechanism, if sufficient platinum sites are

available for reaction, hydrogenation reactions should offset all olefin forming reactions.⁶¹

Paraffins can also form on platinum by hydrogenolysis reactions. Hydrogenolysis is a paraffin cracking mechanism on the metal in which a pair of shortened paraffin products are formed.⁶²⁻⁶³ It has been proposed that multiple platinum sites are required for hydrogenolysis.⁶⁴ Reaction [9] illustrates platinum catalyzed hydrogenolysis on two platinum sites.



Hydrogenolysis reactions are important when sufficient molecular hydrogen is present. Hydrogen may be obtained from hydrogen-rich hydrocarbon species through dehydrogenation or from the reaction atmosphere.⁶⁸ When there is insufficient hydrogen available in the reaction atmosphere, platinum catalyzed cracking is more likely than hydrogenolysis. Carbon-carbon bond rupture is the rate-limiting step (RLS) in the platinum catalyzed cracking mechanism.⁶⁹⁻⁷⁰ However, hydrogenolysis and cracking reactions on platinum are less significant than dehydrogenation reactions.^{61,71-73}

The chain reaction cracking and bifunctional reaction mechanisms were proposed based on results obtained for small hydrocarbon reactions. Long chain polymer cracking and hydrogenation reactions may follow different mechanisms. Volatile products obtained by polymer cracking may vary with conversion because accessibility of polymer fragments to catalytic sites can change with conversion.

Polymer cracking mechanisms may begin at the external acid sites of zeolite catalysts. Manos et al. reported a decrease in gel-permeation chromatography (GPC) molecular weight of polyethylene mixed with USY catalyst after heating to 150 °C.⁷⁴ By

scanning electron microscope (SEM) studies of the polymer/catalyst interface. S. Maegaard⁷⁵ found that melted high density polyethylene (HDPE) was drawn into the spaces between particles of zeolite catalysts (external surfaces) and into the larger pores of amorphous materials at 300 °C. It was suggested that surface reactions formed lower molecular weight species that could diffuse into the catalyst structure for further reaction.⁷⁵⁻⁷⁶ Behrsing et al. have reported that acid catalyzed reactions of olefins were not confined to the internal sites of zeolite particles, but that external catalyst surfaces were also active.⁷⁷ Furthermore, catalyst particle size was reported to affect volatile product distributions when polymers were cracked.⁷⁸⁻⁷⁹ Therefore, accessible external acid sites are likely responsible for polymer cracking until the molecular weight (or size) of polymer fragments becomes small enough to diffuse into catalyst pores, which may directly influence volatile product formation mechanism(s).

1.4 Project Description

Although there have been many studies of PE cracking and hydrocracking, most have been performed by heating reactor vessels containing catalyst and polymer and subsequently collecting and analyzing the products with no attempt to minimize secondary reactions. This batch processing approach provides no information regarding the order of product formation. In our research, volatile cracking and/or hydrocracking products were removed from catalysts with helium or hydrogen purge gas and then analyzed on-line by using repetitive injection thermal analysis gas chromatography mass spectrometry (TA-GC/MS). Results obtained by TA-GC/MS were used to determine the temperature dependence of volatile product slates obtained by cracking/hydrocracking of PE by HZSM-5, HY, HMCM-41, and their platinum loaded analogs. Volatile product

slates derived from monofunctional (acid) and bifunctional (metal-acid) catalyzed PE cracking/hydrocracking can differ significantly with temperature and catalyst characteristics (i.e. pore size and acidity). The catalytic chain reaction cracking mechanisms proposed by Wojciechowski and the commonly accepted metal catalyzed cracking reactions will be used to explain change in product slate and effective activation energy.

Activation energies for hydrocarbon cracking reactions can be influenced by many variables. For example, changes in catalyst properties (e.g. pore size and acidity) may independently affect cracking reaction kinetics.⁶⁰ The model-free isoconversion method for calculating activation energies provides a means for detecting reaction mechanism changes during the course of polymer cracking. When TA-GC/MS results are combined with thermal analysis mass spectrometry (TA-MS) measurements, activation energy (E_a) values can be calculated for specific classes of volatile products detected during PE cracking/hydrocracking. Trends in E_a value versus temperature plots can be used to assess contributions from specific reaction mechanism(s) to the formation of volatile products. A better understanding of PE cracking/hydrocracking mechanisms may lead to development of improved plastic waste tertiary recycling processes.

1.5 References

- 1. Municipal Solid Waste in the United States: 2000 Facts and Figures; EPA530-R-02-001; U.S. Environmental Protection Agency, Office of Solid Waste and Emergency Response (5305W), U.S. Government Printing Office; Washington, D.C. June 2002**
- 2. WasteWise 7th Year Annual Report; EPA530-R-01-019; U.S. Environmental Protection Agency, Office of Solid Waste and Emergency Response (5305W), U.S. Government Printing Office; Washington, D.C. November 2001**
- 3. Resource Conservation Challenge What Can You Save Today?; EPA530-F-02-031; U.S. Environmental Protection Agency, Office of Solid Waste and Emergency Response (5305W), U.S. Government Printing Office; Washington, D.C. September 2002**
- 4. Aguado, J.; Serrano, D.P.; Feedstock Recycling of Plastic Wastes; Royal Society of Chemistry; Cambridge, UK, 1999**
- 5. Ding, W.; Liang, J.; Anderson, L.L.; Energy Fuels 1997, 11, 1219-1224 "Hydrocracking and Hydroisomerization of High-Density Polyethylene and Waste Plastic over Zeolite and Silica-Alumina-Supported Ni and Ni-Mo Sulfides"**
- 6. Plastics resource[®] Information on Plastics in the Environment
www.plasticresource.com/recycling/index.html (accessed September 2002)**
- 7. American Plastics Council[®] Plastics and the Environment
<http://www.americanplasticscouncil.org/apcorg/environment/environment.html>
(accessed September 2002)**
- 8. Ayame, A.; Uemichi, Y.; Yoshida, T.; Kanoh, H.; J. Jpn. Petrol. Inst. 1979, 22, 280-287 "Gasification of Polyethylene over Solid Acid Catalyst. Part 3. Gasification over Calcium X Zeolite in a Fixed Bed Tubular Flow Reactor"**
- 9. Uemichi, Y.; Ayame, A.; Yoshida, T.; Kanoh, H.; J. Jpn. Petrol. Inst. 1980, 23, 35-43 "Gasification of Polyethylene over Solid Acid Catalyst. Part 4. Gasification over Sodium X Zeolite and Silica-Alumina in a Fixed Bed Tubular Flow Reactor"**
- 10. Uemichi, Y.; Ayame, A.; Kashiwaya, Y.; Kanoh, H.; J. Chromatogr. 1983, 259, 69-77 "Gas Chromatographic Determination of the Products of Degradation of Polyethylene over a Silica-Alumina Catalyst"**
- 11. Uemichi, Y.; Kashiwaya, Y.; Ayame, A.; Kanoh, H.; Chem. Lett. 1984, 41-44 "Formation of Aromatic Hydrocarbons in Degradation of Polyethylene over Activated Carbon Catalyst"**

12. Nanbu, H.; Ishihara, Y.; Honma, H.; Takesue, T.; Ikemura, T.; Chem. Soc. Jpn. 1987, 765-770 "Synthesis of Branched Polyethylene by Catalytic Degradation-Isomerization of High Density Polyethylene in the Presence of Silica-Alumina Catalyst"
13. Ishihara, Y.; Nanbu, H.; Saido, K.; Ikemura, T.; Takesue, T.; Bull. Chem. Soc. Jpn. 1991, 64, 3585-3592 "Back Biting Reactions During the Catalytic Decomposition of Polyethylene"
14. Nanbu, H.; Sakuma, Y.; Ishihara, Y.; Takesue, T.; Ikemura, T.; Polym. Deg. Stab. 1987, 19, 61-76 "Catalytic Degradation of Polystyrene in the Presence of Aluminum Chloride Catalyst"
15. Ishihara, Y.; Nanbu, H.; Ikemura, T.; Takesue, T.; J. Appl. Polym. Sci. 1989, 38, 1491-1501 "Effect of Branching of Polyolefin Backbone Chain on Catalytic Gasification Reaction"
16. Ishihara, Y.; Nanbu, H.; Ikemura, T.; Takesue, T.; Fuel 1990, 69, 978-984 "Catalytic Decomposition of Polyethylene using a Tubular Flow Reaction System"
17. Ishihara, Y.; Nanbu, H.; Saido, K.; Ikemura, T.; Takesue, T.; Polymer 1992, 33, 3482-2486 "Mechanism for Gas Formation in Polyethylene Decomposition"
18. Beltrame, P.; Carniti, P.; Polym. Deg. Stab. 1989, 26, 209-220 "Catalytic Degradation of Polymers: Part II - Degradation of Polyethylene"
19. Ivanova, S.R.; Gumerova, E.F.; Berlin, A.A.; Minsker, K.S.; Zaikov, G.E.; Russ. Chem. Rev. 1991, 60, 225-234 "Catalytic Degradation of Polyolefins - A Promising Method for the Regeneration of Monomers"
20. Songip, A.R.; Masuda, T.; Kuwahara, H.; Hashimoto, K.; Appl. Catal. B 1993, 2, 153-164 "Test to Screen Catalysts for Reforming Heavy Oil from Waste Plastics"
21. Ng, S.H.; Seoud, H.; Stanciulescu, M.; Sugimoto, Y.; Energy Fuels 1995, 9, 735-742 "Conversion of Polyethylene to Transportation Fuels through Pyrolysis and Catalytic Cracking"
22. Ohkita, H.; Nishiyama, R.; Tochiwara, Y.; Mizushima, T.; Kakuta, N.; Morioka, Y.; Ueno, A.; Namiki, Y.; Tanifuji, S.; Katoh, H.; Sunazuka, H.; Nakayama, R.; Kuroyanagi, T.; Ind. Eng. Chem. Res. 1993, 32, 3112-3116 "Acid Properties of Silica-Alumina Catalysts and Catalytic Degradation of Polyethylene"
23. Ng, S.H.; Energy Fuels 1995, 9, 216-224 "Conversion of Polyethylene Blended with VGO to Transportation Fuels by Catalytic Cracking"

24. Liu, K.; Meuzelaar, H.C.L.; Fuel Proc. Tech. 1996, 49, 1-15 "Catalytic Reactions in Waste Plastics, HDPE, and Coal Studied by High-Pressure Thermogravimetry with On-line GC/MS"
25. Ding, W.B.; Tuntawiroon, W.; Liang, J.; Anderson, L.L.; Fuel Proc. Tech. 1996, 49, 49-63 "Depolymerization of Waste Plastics with Coal over Metal-Loaded Silica-Alumina Catalysts"
26. Joo, H.K.; Curtis, C.W.; Fuel Proc. Tech. 1998, 53, 197-214 "Catalytic Coprocessing of LDPE with Coal and Petroleum Resid Using Different Catalysts"
27. Ochoa, R.; Van Woert, H.; Lee, W.H.; Subramanian, R.; Kugler, E.; Eklund, P.C.; Fuel Proc. Tech. 1996, 49, 119-136 "Catalytic Degradation of Medium Density Polyethylene over Silica-Alumina Supports"
28. Aguado, J.; Serrano, D.P.; Romero, M.D.; Escola, J.M.; Chem. Comm. 1996, 725-726 "Catalytic Conversion of Polyethylene into Fuels over Mesoporous MCM-41"
29. Aguado, J.; Sotelo, J.L.; Serrano, D.P.; Calles, J.A.; Escola, J.M.; Energy Fuels 1997, 11, 1225-1231 "Catalytic Conversion of Polyolefins into Liquid Fuels over MCM-41: Comparison with ZSM-5 and Amorphous $\text{SiO}_2\text{-Al}_2\text{O}_3$ "
30. Sakata, Y.; Uddin, M.A.; Muto, A.; Kanada, Y.; Koizumi, K.; Murata, K.; J. Anal. Appl. Pyrol. 1997, 43, 15-25 "Catalytic Degradation of Polyethylene into Fuel Oil over Mesoporous Silica (KFS-16) Catalyst"
31. Sakata, Y.; "Catalytic Degradation of Polyethylene and Polypropylene into Fuel Oil," Recycling of Polymers, Ed. Kahovec, J.; Wiley-VCH, Weinheim, Germany, 1998, 7-18
32. Sharratt, P.N.; Lin, Y-H.; Garforth, A.A.; Dwyer, J.; Ind. Eng. Chem. Res. 1997, 36, 5118-5124 "Investigation of the Catalytic Pyrolysis of High Density Polyethylene over a HZSM-5 Catalyst in a Laboratory Fluidized-Bed Reactor"
33. Garforth, A.A.; Lin, Y-H.; Sharratt, P.N.; Dwyer, J.; Appl. Catal. A 1998, 169, 331-342 "Production of Hydrocarbons by Catalytic Degradation of High Density Polyethylene in a Laboratory Fluidized-Bed Reactor"
34. Lin, Y-H.; Sharratt, P.N.; Garforth, A.A.; Dwyer, J.; Thermochim. Acta 1997, 294, 45-50 "Deactivation of US-Y Zeolite by Coke Formation during the Catalytic Pyrolysis of High Density Polyethylene"
35. Garforth, A.; Fiddy, S.; Lin, Y-H.; Ghanbari-Siakhali, A.; Sharratt, P.N.; Dwyer, J.; Thermochim. Acta 1997, 294, 65-69 "Catalytic Degradation of High Density Polyethylene: An Evaluation of Mesoporous and Microporous Catalysts using Thermal Analysis"

36. Fernandes Jr., V.J.; Araujo, A.S.; Fernandes, G.J.T.; *J. Thermal Anal.* 1997, 49, 355-260 "Catalytic Degradation of Polyethylene Evaluated by TG"
37. Fernandes Jr., V.J.; Araujo, A.S.; Fernandes, G.J.T.; *J. Thermal Anal. Calorim.* 1999, 56, 275-285 "Thermal Analysis Applied to Solid Catalysts - Acidity, Activity, and Regeneration"
38. Dufaud, V.; Basset, J.M.; *Angew. Chem. Int. Ed.* 1998, 37, 806-810 "Catalytic Hydrogenolysis at Low Temperature and Pressure of Polyethylene and Polypropylene to Diesels or Lower Alkanes by a Zirconium Hydride Supported on Silica-Alumina: A Step Toward Polyolefin Degradation by the Microscopic Reverse Ziegler-Natta Polymerization"
39. Ding, W.; Liang, J.; Anderson, L.L.; *Fuel Proc. Tech.* 1997, 51, 47-62 "Thermal and Catalytic Degradation of High Density Polyethylene and Commingled Post-Consumer Plastic Waste"
40. Ding, W.; Liang, J.; Anderson, L.L.; *Energy Fuel* 1997, 11, 1219-1224 "Hydrocracking and Hydroisomerisation of High-Density Polyethylene and Waste Plastic over Zeolite and Silica-Alumina-Supported Ni and Ni-Mo Sulfides"
41. Park, D.W.; Hwang, E.Y.; Kim, J.R.; Choi, J.K.; Kim, Y.A.; Woo, H.C.; *Polym. Deg. Stab.* 1999, 65, 193-198 "Catalytic Degradation of Polyethylene over Solid Acid Catalysts"
42. Uemichi, Y.; Nakamura, J.; Itoh, T.; Sugioka, M.; Garforth, A.A.; Dwyer, J.; *Ind. Eng. Chem. Res.* 1999, 38, 385-390 "Conversion of Polyethylene into Gasoline-Range Fuels by Two-Stage Catalytic Degradation using Silica-Alumina and HZSM-5 Zeolite"
43. Manos, G.; Garforth, A.; Dwyer, J.; *Ind. Eng. Chem. Res.* 2000, 39, 1198-1202 "Catalytic Degradation of High-Density Polyethylene over Different Zeolitic Structures"
44. Manos, G.; Garforth, A.; Dwyer, J.; *Ind. Eng. Chem. Res.* 2000, 39, 1203-1208 "Catalytic Degradation of High-Density Polyethylene on an Ultrastable-Y Zeolite. Nature of Initial Polymer Reactions, Pattern of Formation of Gas and Liquid Products, and Temperature Effects"
45. Serrano, D.P.; Aguado, J.; Escola, J.M.; *Ind. Eng. Chem. Res.* 2000, 39, 1177-1184 "Catalytic Cracking of a Polyolefin Mixture over Different Acid Solid Catalysts"
46. Van Grieken, R.; Serrano, D.P.; Aguado, J.; Garcia, R.; Rojo, C.; *J. Anal. Appl. Pyrol.* 2001, 58-59, 127-142 "Thermal and Catalytic Cracking of Polyethylene under Mild Conditions"

47. Serrano, D.P.; Van Grieken, R.; Aguado, J.; Garcia, R.A.; Rojo, C.; Temprano, F.; *Stud. Surf. Sci. Catal.* 2000, 130, 1589-1594 "Study on the Initial Steps of the Polyethylene Cracking over Different Acid Catalysts"
48. Walendziewski, J.; Steininger, M.; *Catal. Today* 2002, 65, 323-330 "Thermal and Catalytic Conversion of Waste Polyolefins"
49. Walendziewski, J.; *Fuel* 2002, 81, 473-481 "Engine Fuel Derived from Waste Plastics by Thermal Treatment"
50. Lin, Y-H.; Hwu, W-H.; Ger, M-D.; Yeh, T-F.; Dwyer, J.; *J. Molec. Catal. A* 2001, 171, 143-151 "A Combined Kinetic and Mechanistic Modeling of the Catalytic Degradation of Polymers"
51. Lin, Y-H.; Sharratt, P.N.; Garforth, A.A.; Dwyer, J.; *Energy Fuel* 1998, 12, 767-774 "Catalytic Conversion of Polyolefins to Chemicals and Fuels over Various Cracking Catalysts"
52. Garforth, A.; Lin, Y-H.; Sharratt, P.; Dwyer, J.; *Stud. Surf. Sci. Catal.* 1999, 121, 197-202 "Catalytic Polymer Degradation for Producing Hydrocarbons over Zeolites"
53. Satsuma, A.; Ebigase, T.; Inaki, Y.; Yoshida, H.; Kobayashi, S.; Uddin, M.A.; Sakata, Y.; Hattori, T.; *Stud. Surf. Sci. Catal.* 2001, 135, 4001-4008 "Catalytic Sites of Mesoporous Silica in Degradation of Polyethylene"
54. Gobin, K. Koumantaropoulos, D.; Manos, G.; *Stud. Surf. Sci. Catal.* 2001, 135, 4989-4994 "One Stage Catalytic Cracking of Plastic Waste on Zeolite-Based Catalysts"
55. Manos, G.; Yusof, I.Y.; Papayannakos, N.; Gangas, N.H.; *Ind. Eng. Chem. Res.* 2001, 40, 2220-2225 "Catalytic Cracking of Polyethylene over Clay Catalysts. Comparison with Ultrastable Y Zeolite"
56. Manos, G.; Yusof, I.Y.; Gangas, N.H.; Papayannakos, N.; *Energy Fuel* 2002, 16, 485-489 "Tertiary Recycling of Polyethylene to Hydrocarbon Fuel by Catalytic Cracking over Aluminum Pillared Clays"
57. Aguado, J.; Serrano, D.P.; Van Grieken, R.; Escola, J.M.; Garagorri, E.; *Stud. Surf. Sci. Catal.* 2001, 135, 3915-3922 "Catalytic Properties of Micelle Templated Microporous and Mesoporous Materials for the Conversion of Low-Density Polyethylene"
58. Aguado, J.; Serrano, D.P.; Sotelo, J.L.; Van Grieken, R.; Escola, J.M.; *Ind. Eng. Chem. Res.* 2001, 40, 5696-5704 "Influence of the Operating Variables on the Catalytic Conversion of a Polyolefin Mixture over HMCM-41 and Nanosized HZSM-5"

59. Seddegi, Z.S.; Budrthumal, U.; Al-Arfaj, A.A.; Al-Amer, A.M.; Barri, S.A.I.; Appl. Catal. A 2002, 225, 167-176 "Catalytic Cracking of Polyethylene over All-Silica MCM-41 Molecular Sieve"
60. Wojciechowski, B.W.; Catal. Rev. - Sci. Eng. 1998, 40, 209-328 "The Reaction Mechanism of Catalytic Cracking: Quantifying Activity, Selectivity, and Catalyst Decay"
61. Weisz, P.B.; Swegler, E.W. Science 1957, 126, 31-32 "Stepwise Reaction on Separate Catalytic Centers: Isomerization of Saturated Hydrocarbons"
62. Paal, Z.; Menon, P.G. Catal. Rev. - Sci. Eng. 1983, 25, 229-324 "Hydrogen Effects in Metal Catalysis"
63. Weisz, P.B.; Adv. Catal. 1962, 13, 137-190 "Polyfunctional Heterogeneous Catalysis"
64. Paal, Z.; Hydrogen Effects in Catalysis: Fundamentals and Practical Applications. Eds. Paal, Z.; Menon, P.G.; Marcel Dekker, Inc.. New York, 1988, Ch. 17
65. Baumgarten, E.; Niemeyer, I.; React. Kinet. Catal. Lett. 2000, 70, 371-377 "On the Role of Surfaces in Hydrogenation Reactions with Gas Phase Spillover Hydrogen"
66. Baumgarten, E.; Maschke, L.; Appl. Catal. A 2000, 202, 171-177 "Hydrogen Spillover through the Gas Phase Reaction with Graphite and Activated Carbon"
67. Roessner, F.; Roland, U.; J. Mol. Catal. A 1996, 112, 401-412 "Hydrogen Spillover in Bifunctional Catalysis"
68. Thomas, C.L.; J. Am. Chem. Soc. 1944; 66, 1586-1594 "Hydrocarbon Reactions in the Presence of Cracking Catalysts. II. Hydrogen Transfer"
69. Leclercq, G.; Leclercq, L.; Maurel, R.; J. Catal. 1977, 50, 87-97 "Hydrogenolysis of Saturated Hydrocarbons III. Selectivity in Hydrogenolysis of Various Aliphatic Hydrocarbons on Platinum/Alumina"
70. Cimino, A.; Boudart, M.; Taylor, H.; J. Phys. Chem. 1954, 58, 796-800 "Ethane Hydrogenation-Cracking on Iron Catalysts With and Without Alkali"
71. Leclercq, G.; Leclercq, L.; Maurel, R.; J. Catal. 1977, 50, 87-97 "Hydrogenolysis of Saturated Hydrocarbons III. Selectivity in Hydrogenolysis of Various Aliphatic Hydrocarbons on Platinum/Alumina"
72. Paal, Z.; Tetenyi, T.; J. Catal. 1973, 29, 176-179 "Isomerization of Hydrocarbons in the Presence of Platinum Black"

73. Carter, J.L.; Cusumano, J.A.; Sinfelt, J.H.; *J. Catal.* 1971, 20, 223-229
"Hydrogenolysis of n-Heptane over Unsupported Metals"
74. Manos G.; Garforth, A.; Dwyer, J.; *Ind. Eng. Chem. Res.* 2000, 39, 1203-1208
"Catalytic degradation of High-Density Polyethylene on an Ultrastable-Y Zeolite. Nature of Initial Polymer Reactions, Pattern of Formation of Gas and Liquid Products, and Temperature Effects"
75. Maegaard, S.; M.Sc. dissertation, University of Manchester Institute of Science and Technology, 1997 "Studies of the interface between zeolite catalysts and degrading polymer"
76. Lin, Y.-H.; Hwu, W.-H.; Ger, M.-D.; Yeh, T.-F.; Dwyer, J.; *J. Molec. Catal. A* 2001, 171, 143-151 "A combined kinetic and mechanistic modeling of the catalytic degradation of polymers"
77. Behrsing, T.; Jaeger, H.; Mole, T.; *Appl. Catal.* 1989, 47, 67-73 "Hydroisomerization of Branched-Chain Olefins over Pt/HZSM-5 Zeolite"
78. Triantafillidis, C.S.; Evmirdis, N.P.; *Ind. Eng. Chem. Res.* 1999, 38, 916-927
"Performance of ZSM-5 as a Fluid Catalytic Cracking Catalyst Additive: Effect of the Total Number of Acid Sites and Particle Size"
79. Sotelo, J.L.; Van Grieken, R.; Aguado, J.; Serrano, D.P.; Escola, J.M.; Menendez, J.M.; *Proc. 12th Int. Zeolite Conf.*, Baltimore, Maryland, July 1998, Eds. Treacy, M.M.J.; Marcus, B.K.; Bisher, M.E.; Higgins, J.B.; Materials Research Society, Warrendale, PA 1999

CHAPTER 2 - EXPERIMENTAL

2.1 Introduction

Low molecular weight poly(ethylene) (LPE) was cracked by using three solid acid catalysts and their bifunctional platinum loaded analogs: HZSM-5, HY, HMCM-41, PtHZSM-5, PtHY, and PtHMCM-41. Thermogravimetry (TG) was employed to measure sample mass changes as a function of temperature and the weight percent of residue deposited on each catalyst. Thermal analysis coupled with mass spectrometry (TA-MS) was used to characterize the acidic properties of the catalysts by temperature programmed desorption (TPD) of ammonia. TA-MS was also used to calculate class-specific effective isoconversion activation energies for polymer decomposition, which will be discussed separately in Chapter 3. Thermal analysis coupled with gas chromatography - mass spectrometry (TA-GC/MS) was used to separate and identify volatile cracking products. Data analysis methods developed in our laboratory were used to obtain species-specific evolution profiles for volatile cracking products. The instrumental and data analysis methods that were used to characterize catalytic polymer cracking in inert and reducing atmospheres (e.g. helium and hydrogen, respectively) are described in this chapter.

2.2 Materials

Low molecular weight poly(ethylene) (LPE) with a reported average molecular weight of 700 g/mol and melting temperature range of 80-90 °C was purchased from Polysciences Inc. (Warrington, PA). The hydrogen form of ZSM-5 (Zeolite Socony Mobil – Five or HZSM-5) was obtained from Mobil Oil (Paulsboro, NJ). The framework of HZSM-5 was reported to contain 1.5% by weight alumina.¹ The 3-dimensional MFI (ZSM-Five) type

crystal structure (5.3 x 5.6 Å and 5.1 x 5.5 Å intersecting channels) was confirmed by Mobil Oil. An example of the pore framework of HZSM-5 is shown at the top of Figure 2-1.³

The sodium Y-54 form of the Faujasite (FAU) structure zeolite Y was kindly donated by Universal Oil Products (UOP), a division of Allied Signal or formerly Union Carbide (Danbury, CT). The SiO₂/Al₂O₃ for this catalyst was reported to be 5.30. Sodium ions were removed from the catalyst by ion exchange with 1.0 M ammonium nitrate solution. About 1.0 g of catalyst was placed in 250 mL of NH₄NO₃ and the mixture was refluxed with constant stirring overnight. The NH₄Y was dried at 110 °C and then calcined at 550 °C for 3 hours to produce HY. HY zeolite has a FAU pore framework with a 3-dimensional pore structure having a 7.4 Å channel diameter and 12.3 Å channel intersections (super-cages) as shown in the middle of Figure 2-1.^{3,4}

MCM-41 is one of the most investigated mesoporous sieves in the M41S family. MCM-41 has an amorphous silica or alumino-silicate framework, which possesses a honeycomb-like structure with uniform, parallel pores (see bottom of Figure 2-1). MCM-41 was first synthesized by a group of scientists at Mobil Oil Corporation in 1992.⁵ Mesoporous (15 – 150 Å pore size range) MCM-41 was synthesized in our laboratory by using procedures described in the literature. Dodecyltrimethyl-ammonium bromide (DTMABr) and tetramethyl-ammonium hydroxide pentahydrate (TMAH) were used as template molecules.⁵⁻⁷

⁷ A solution containing 11.47 g LUDOX[®] (30% wt. SiO₂) and 10.0 g of TMAH in 16.4 mL of distilled water was prepared and then allowed to age for 2 days. Then, 20.0 g of DTMABr and 0.296 g of Al₂O₃ were added to the aged solution with thorough mixing. A second solution was prepared by dissolving 1.29 g of NaOH in 5.46 mL of distilled water and then 2.5 g of SiO₂ was added.

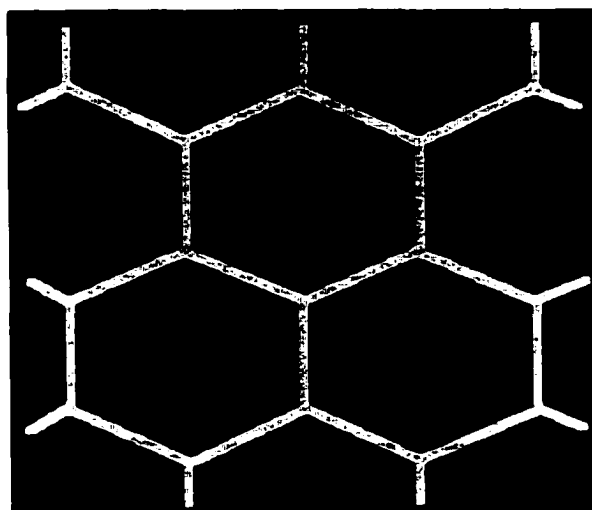
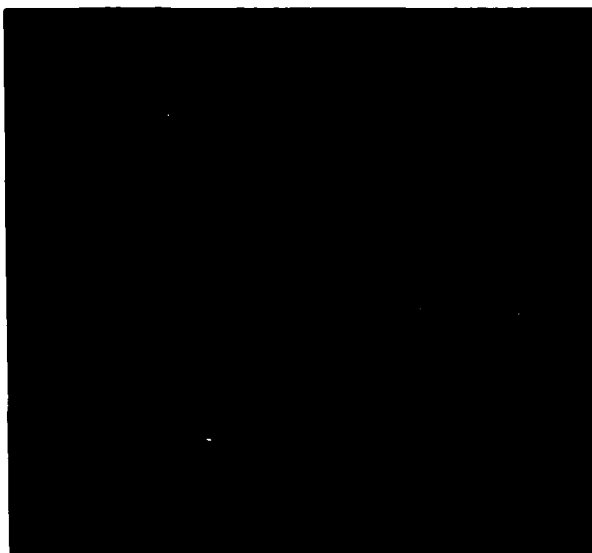
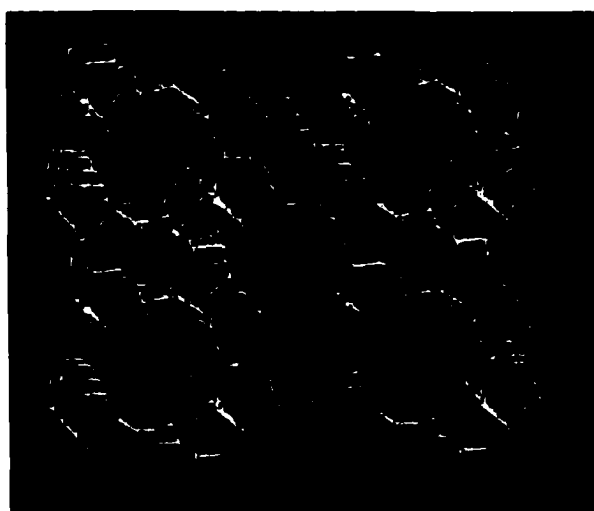


Fig 2-1: Acid catalyst framework structures
Top – HZSM-5^a, Middle – HY^a, Bottom – HMCM-41
[*Reprinted with permission from Ch. Baerlocher, Atlas of Zeolite Framework Types, 2001]

The two solutions were combined and the resulting mixture was autoclaved at 140 °C for 4 days. The resulting solid was filtered, rinsed with distilled water, and dried at 110 °C. The dried powder was calcined at 600 °C for 4 hours to remove the organic templates from the silica-alumina framework. The resulting NaMCM-41 was ion-exchanged as described previously to remove sodium ions and then dried and calcined for six hours at 540 °C to obtain HMCM-41. Electron microprobe analysis revealed that the Al₂O₃ content of this catalyst was about 17% by weight.

Each catalyst had been stored under ambient conditions over an extended period. Therefore, each catalyst was calcined at 400 °C to remove volatile impurities. Once calcined, each catalyst was ion exchanged following the process described previously with 1.0 M ammonium nitrate. This ion exchange process was done to ensure that each catalyst attained maximum protonation prior to use. All catalysts were then dried and calcined at 500 °C for 4 hours before platinum was added or mixed with the polymer. Bifunctional catalysts were prepared by adding approximately 1% by weight platinum to the solid acid catalysts by an incipient wetness method described by Jacobs et al.⁸ Hydrogen hexachloroplatinate(IV) hydrate (H₂PtCl₆·xH₂O) of 99.9% purity and 38-40% wt. platinum was obtained from Aldrich Chemical Company (Milwaukee, WI). The platinum solution was made by adding 0.0418 g H₂PtCl₆ to 1.0 mL of distilled water. About 100 mg of catalyst was mixed with 0.63 mL of the platinum solution and the slurry was then stirred on a Buchner Instruments VV-mini (Kansas City, Mo) roto-evaporation apparatus at ambient conditions for several hours. The slurry was then dried at 110 °C for 2 hours followed by calcination at 400 °C for two hours. Each bifunctional catalyst sample was heated in flowing hydrogen (25 mL/min) for 2 hours at 500 °C to reduce the platinum.

2.3 Sample Preparation

Catalyst and polymer powders were combined to prepare samples. Small particles were used to maximize contact between the polymer and catalysts. Three different sieves were used to select particle sizes: 150, 180, and 250 μm . The HY particle sizes used for preparing samples were less than 180 μm , whereas HZSM-5 and HMCM-41 particles were less than 250 μm . Larger particle sizes were employed for the HZSM-5 and HMCM-41 catalysts because they did not grind as well as HY. Polymer powders used for sample preparation consisted of particles that were less than 150 μm . Polymer/catalyst samples were prepared by mechanically mixing $\approx 10\%$ by weight (1:9 wt. ratio) polymer with catalyst in a sample vial. Samples contained more catalyst than polymer to ensure that polymer decomposition occurred by catalytic processes.

2.4 Thermogravimetric Analysis (TGA)

TGA is an important analytical tool for preliminary material characterization.⁹ TGA is a technique in which changes in sample mass are measured as a function of temperature. The thermogravimetric analyzer used for studies described here was a DuPont model 951 equipped with Thermal Analyst 2000[®] software (Wilmington, DE). Solid samples of approximately 10-100 mg were placed in a platinum sample pan that hung from a balance arm, as shown in Figure 2-2.¹⁰ The balance arm slid into a quartz tube that was positioned inside a 500 W furnace that could be heated from ambient to over 1000 $^{\circ}\text{C}$.

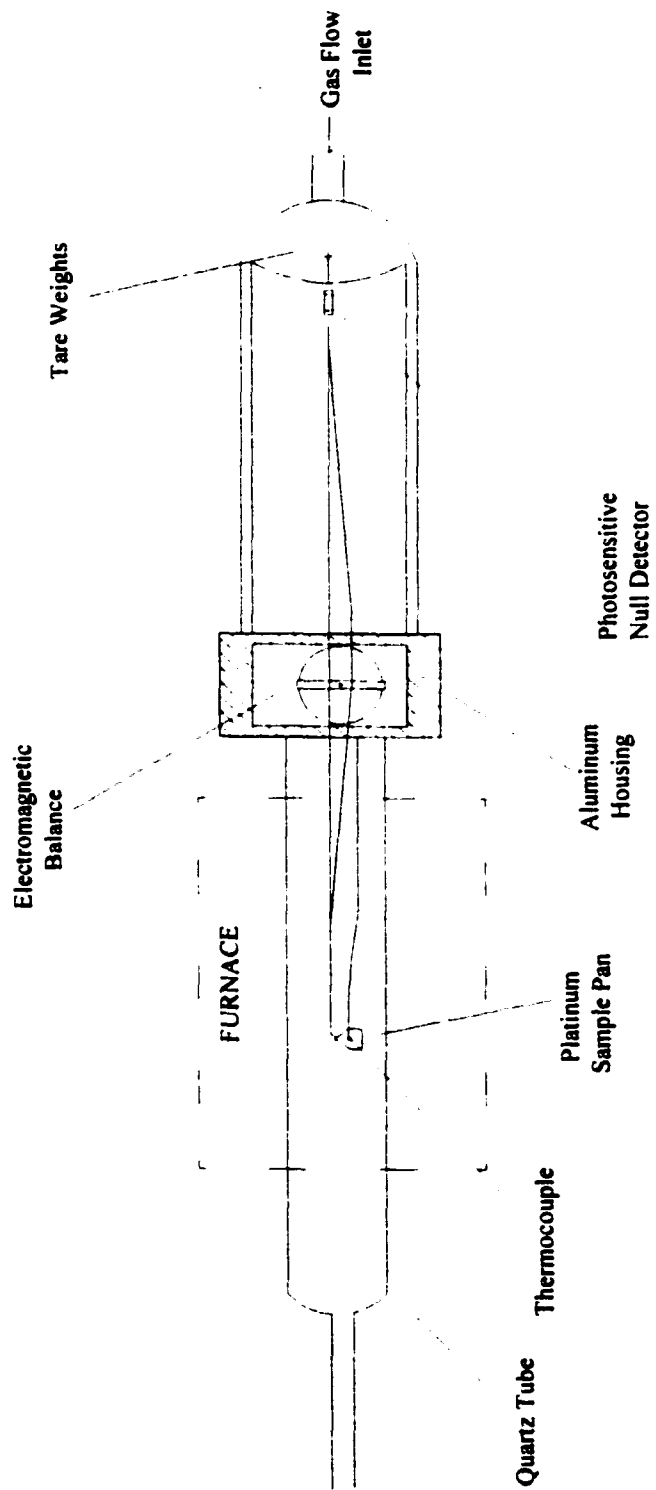


Figure 2-2: Diagram of the thermogravimetric balance
 [Reprinted with permission from E. Bonnet, Ph.D. Dissertation, University of Oklahoma, 2000]

An Omega Engineering, Inc. CHAL-010 thermocouple (Stamford, CT) was placed close to the platinum pan to measure the sample temperature. The electromagnetic balance mechanism was encased inside an aluminum housing. Tare weights and a photosensitive null detector incased in a sealed glass housing were used to zero the instrument. The glass casing and quartz tube were purged with gas to provide the desired environment for thermal decomposition. For the studies described here, helium, hydrogen, and air supplied by Airgas (Radnor, PA) were used as purge gases. The 25 mL/min purge gas flow rate was set by using a NUPRO needle valve. Helium provided an inert atmosphere, hydrogen was used as a reducing or hydrocracking atmosphere, and air was used to oxidize polymer residues left on the catalyst surfaces after first heating in helium or hydrogen. The balance baseline variance was measured to be ± 0.015 mg with an empty sample pan (≈ 150 mg) in flowing helium (25 mL/min) at temperatures ranging from 50-100 °C over a 1 hr time period.

Figure 2-3 is a TGA weight loss curve obtained by heating 6.664 mg of neat LPE at 10 °C/min with a purge gas flow of 25 mL/min helium. No significant weight loss was observed until the temperature exceeded 200 °C. The polymer was completely volatilized by 475 °C. In the example shown in Figure 2-3, LPE was completely volatilized and there was no hydrocarbon residue measured. However, when polymers are cracked in the presence of a catalyst, residues may remain on catalyst surfaces.

Carbon burn-off (CBO) measurements were employed to determine the mass of hydrocarbon residue remaining on the catalysts after polymer cracking. The polymer/catalyst samples were heated at 10 °C/min to 400 °C in a non-oxidative purge gas (25 mL/min) and allowed to cool to below 100 °C. The purge gas flow was then switched to air and the sample was heated again at 10 °C/min to 700 °C to burn off the residue.

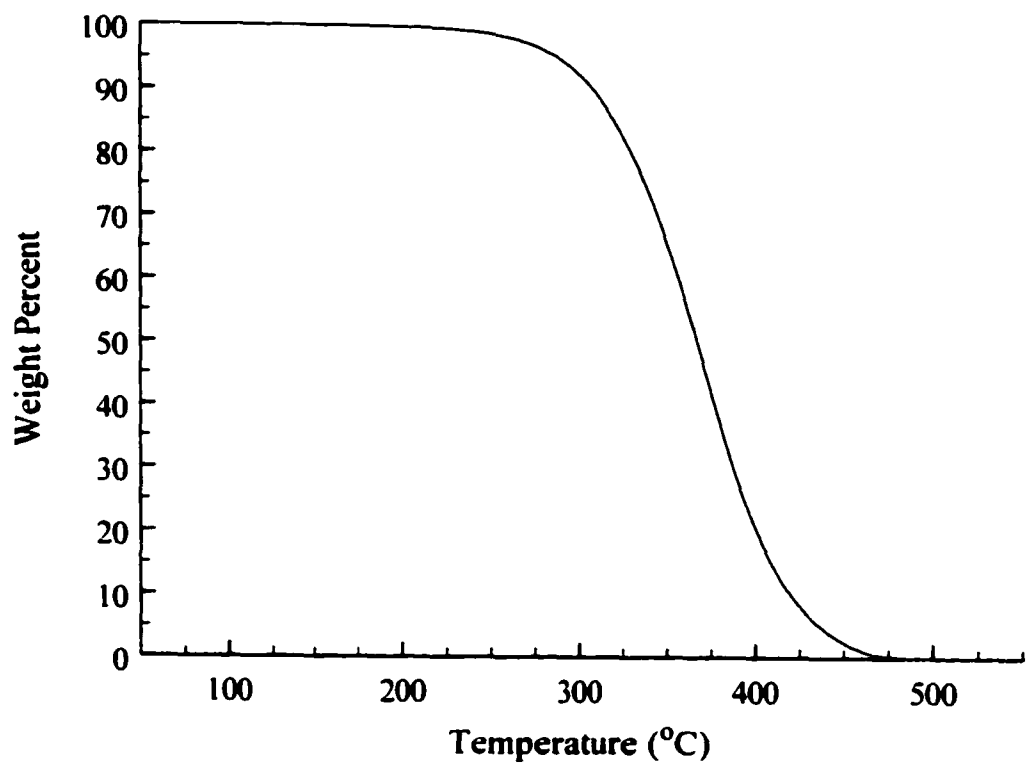


Figure 2-3: TGA of neat LPE heated in helium

The amount of oxidizable residue was measured by using the step transition function of the Thermal Analyst 2000[®] software and was reported as a percentage of the initial polymer weight. The first point on the CBO curve was chosen between 300-350 °C and the second point was chosen between 600-650 °C. The software plotted two lines tangent to the CBO curve at the temperatures chosen (dashed lines in Figure 2-4b) and then calculated the change in percent weight between the tangent lines at the point of maximum rate loss. Calculations of the relative percent residue for each sample varied by less than 1% when using the step transition function for two different points along the CBO curves. An example of the a) TGA and b) CBO curves obtained for the LPE/PtHY sample are shown in Figure 2-4. Figure 2-4a shows that the primary weight loss from polymer degradation occurred between 175 and 300 °C when the sample was heated in helium. Approximately 18% weight loss was observed due to desorption of water and therefore the initial weight loss of the polymer was observed to begin at $\approx 82\%$ percent weight (Figure 2-4a). The amount of carbon residue was then calculated from the percent weight loss between 300 and 600 °C after heating the sample in air (Figure 2-4b). The initial weight loss of approximately 2.5% due to desorption of water was not shown (Figure 2-4b).

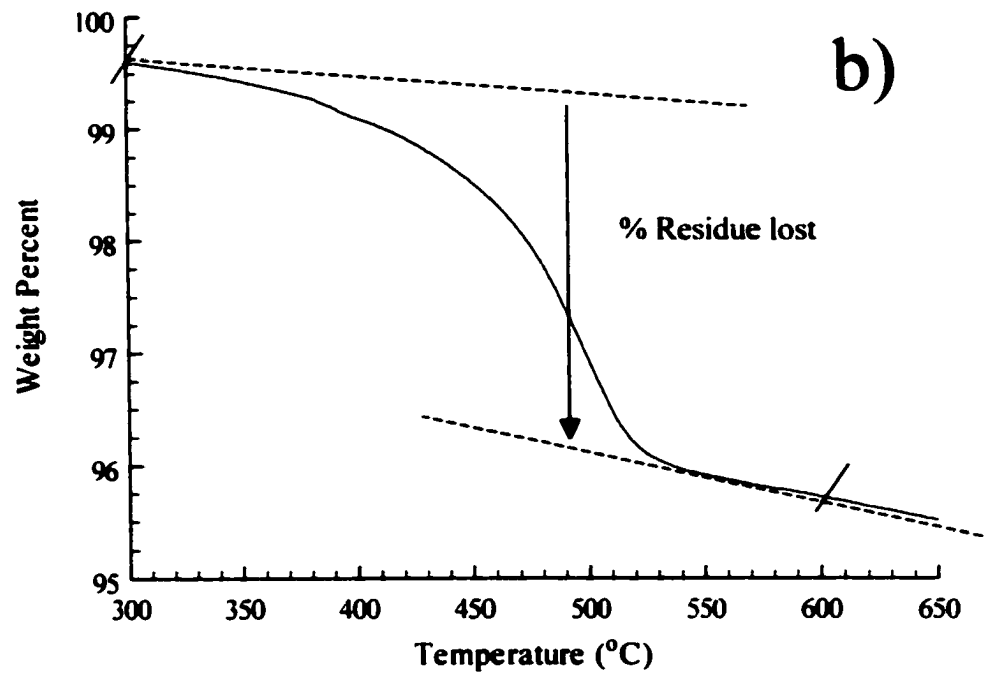
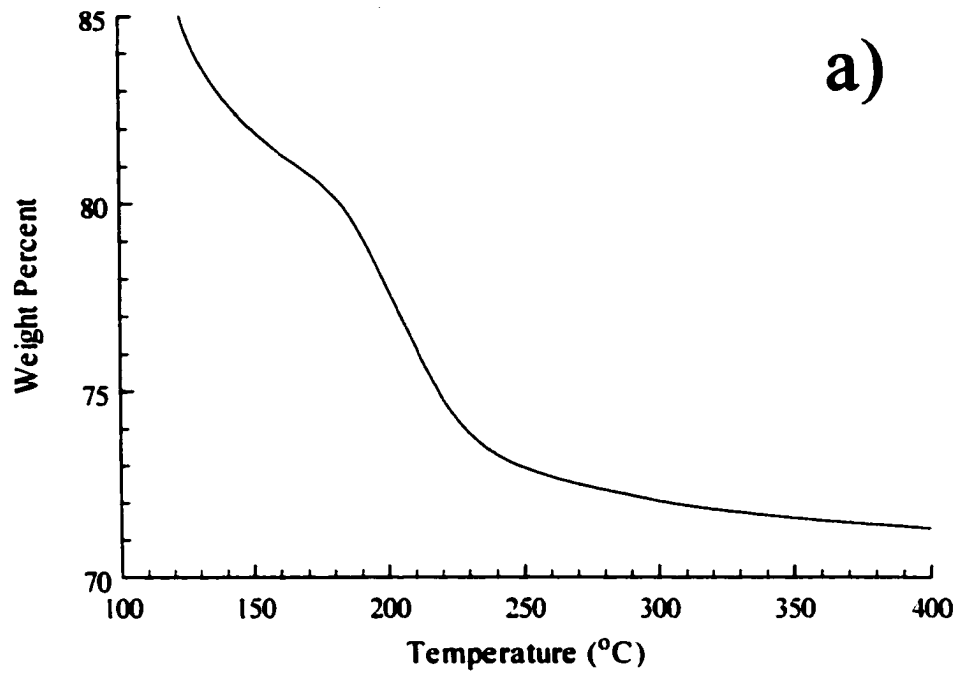


Figure 2-4: TGA and CBO curves of LPE/PtHY a) weight loss curve obtained by heating the sample to 400°C in helium b) CBO weight loss curve

2.5 Thermal Analysis coupled with Mass Spectrometry (TA-MS)

Although TGA methods can be used to determine the temperature range over which weight loss occurs and volatile products evolve, no information regarding the composition of volatile product mixtures can be obtained by this method. However, by combining thermal analysis (TA) with evolved gas (EG) analysis, volatile product structure information can be obtained. TGA weight loss information is often augmented with information from EG analyzers attached to the thermal analysis purge gas exit. Mass spectrometry and infrared spectroscopy are commonly employed EG analyzers.¹¹⁻¹⁵ Many examples of using TA-MS for polymer related studies have been published.¹⁶⁻²⁷ Our TA-MS studies were performed by connecting a 400 W Carbolite model MTF tube furnace (Watertown, WI) and a Hewlett Packard (Palo Alto, CA) 5985 quadrupole MS through a heated interface. The MS was controlled by an IBM compatible computer equipped with Technivent Vector/One[®] (revised version 3.01) software. A diagram of our TA-MS system is shown in Figure 2-5.¹⁰ There are multiple paths to follow through the interface, which allow the instrument to be utilized in different modes. Paths that are relevant only to the TA-MS mode are described here.

The TA purge gas flow was controlled by an Edwards High Vacuum (Grand Island, NY) type 825 mass flow controller and adjusted by using a Model 1605 controller unit with digital display. Inlet gas flow was introduced into the tube furnace through 1/8 in. copper tubing connected to a 1/8-1/4 in. Swagelok (Solon, OH) reducer and union tee. Another 1/8-1/4 in. Swagelok reducer was attached to the union tee through which an 18 in. long, 1/8 in. o.d. Omega K-type (KMQSS-125E-18) thermocouple was passed.

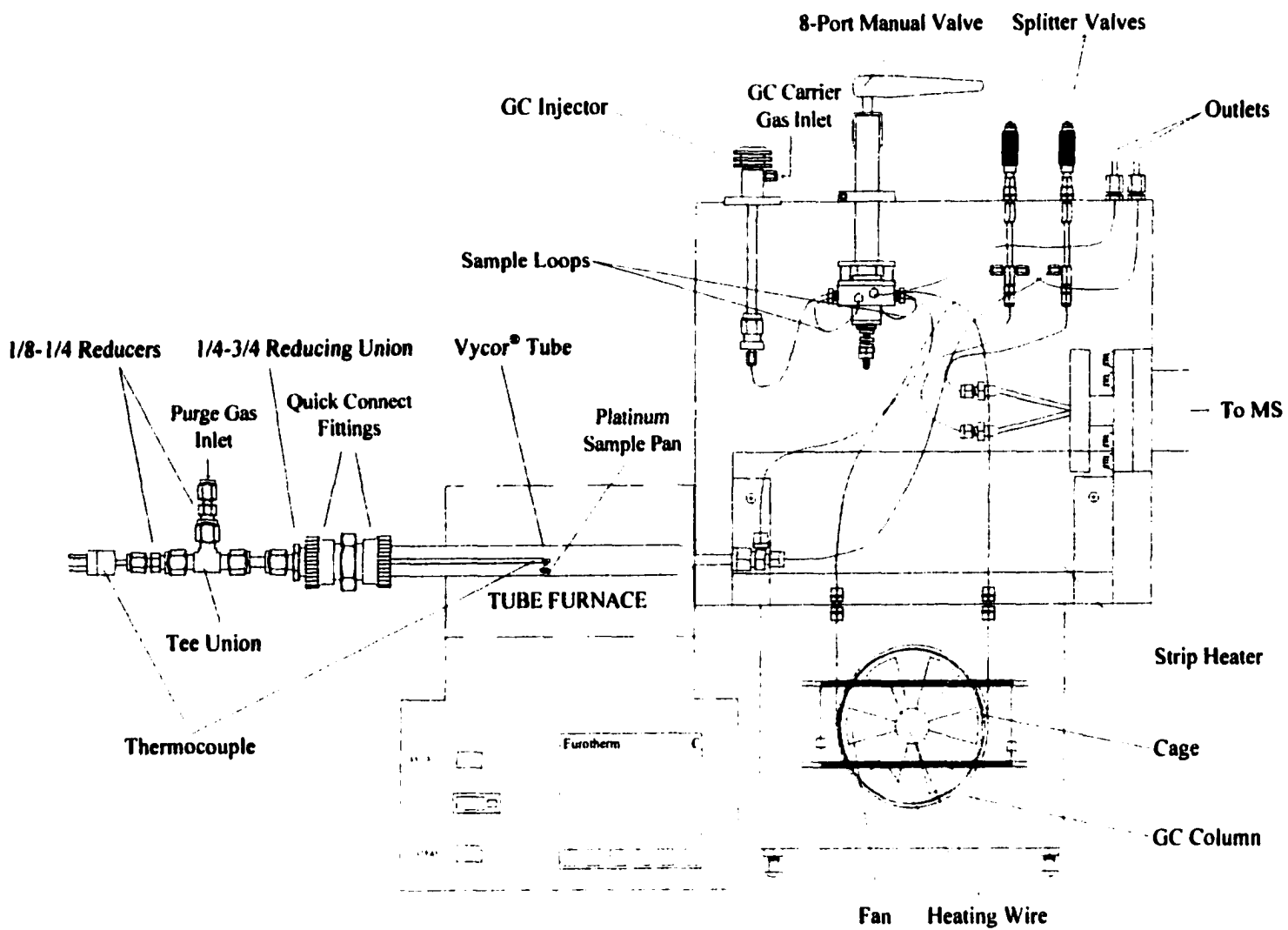


Figure 2-5: Diagram of the TA-GC/MS system
 [Reprinted with permission from E. Bonnet, Ph.D. Dissertation, University of Oklahoma, 2000]

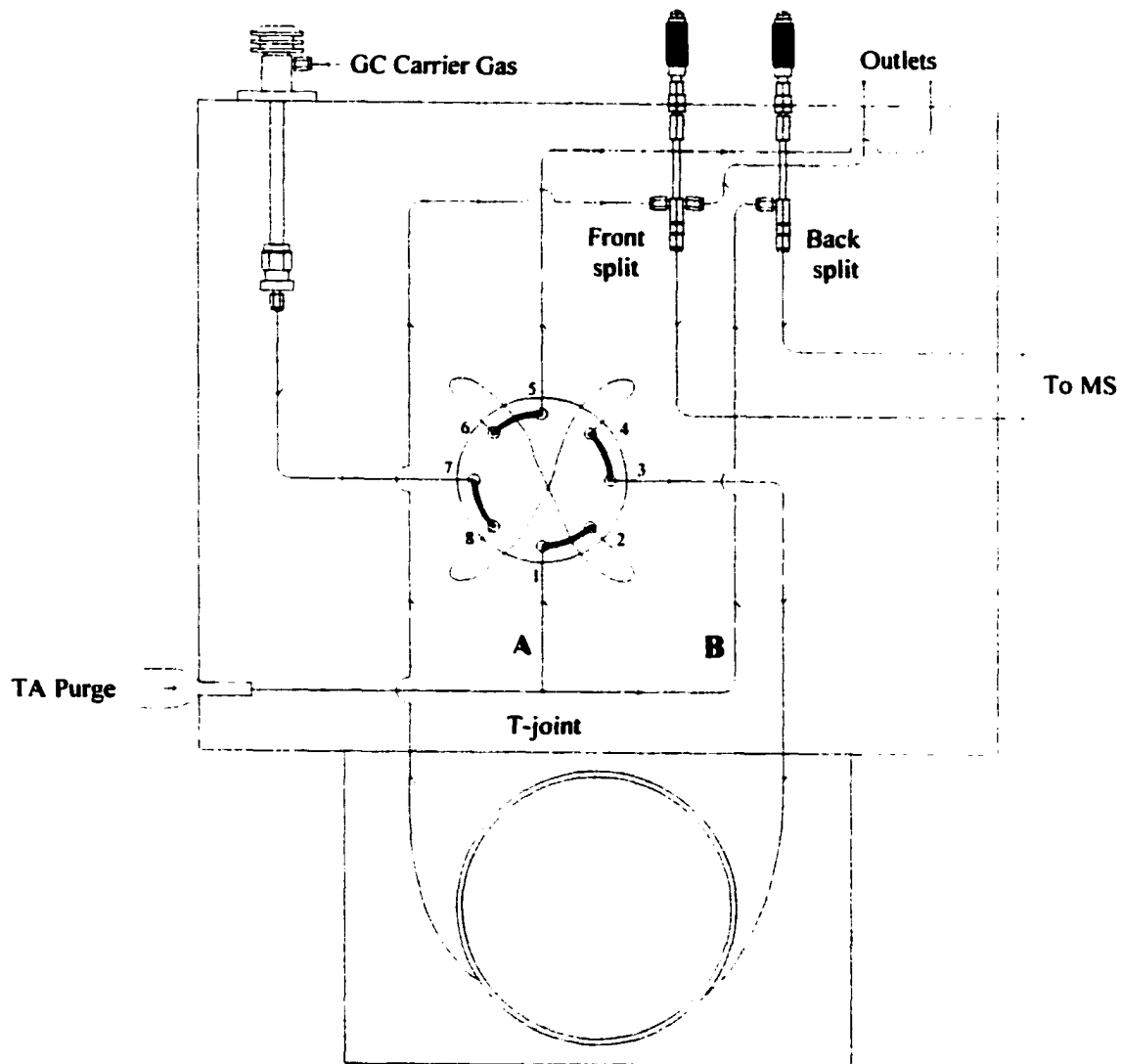


Figure 2-6: Flow Diagram of TA-GC/MS System
 [Reprinted with permission from E. Bonnet, Ph.D. Dissertation, University of Oklahoma, 2000]

The remaining union tee fitting was connected to an 8 in. long, 3/4 in. o.d. Vycor[®] tube by a 1/4-3/4 in. Swagelok reducer and a 3/4 in. quick connect Cajon (Macedonia, OH) union. Rubber o-rings were used without grease in the Cajon quick connect fitting to seal the system. The outlet end of the Vycor[®] tube was a 1.5 in. long, 1/4 in. o.d. quartz tube that was connected to a union tee located inside the heated interface. Path "B" in Figure 2-6 shows the TA-MS path inside of the heated interface.¹⁰ The interface was contained within an insulated 12 in. × 10 in. × 6 in. aluminum oven. Connecting tubing within the heated interface was either 1/16 in. stainless steel or 0.332 mm o.d. uncoated silica and all connections were made with appropriate size graphite ferrules. A Scientific Glass Engineering Inc. (Austin, TX) model MCV-1-50 splitter valve (labeled back split in Figure 2-6) was used to adjust the flow of TA purge gas into the MS. The interface was heated by a pair of 500 W (3 in. × 10 in.) strip heaters purchased from Thermal Corporation (Madison, AL). The interface temperature was maintained at 200 °C (unless stated otherwise) by an Omega CN76000 programmable temperature controller.

Solid samples were placed inside the Vycor[®] tube on a platinum sample pan hanging from the end of the thermocouple (Figure 2-5). The sample temperature was measured with this exposed junction thermocouple by a Eurotherm (Sussex, England) 902 temperature controller. The thermocouple was calibrated to 0 °C with ice/water and to 100 °C with boiling water. The temperature of the furnace was controlled manually or through software provided by Eurotherm (IPSC version 2.04) to ramp the sample temperature up to as high as 1000 °C. The sample temperature was found to vary with the position of the thermocouple inside the furnace. Figure 2-7 illustrates the sample position within the tube furnace. A plot of the temperature versus sample position is shown in Figure 2-8.

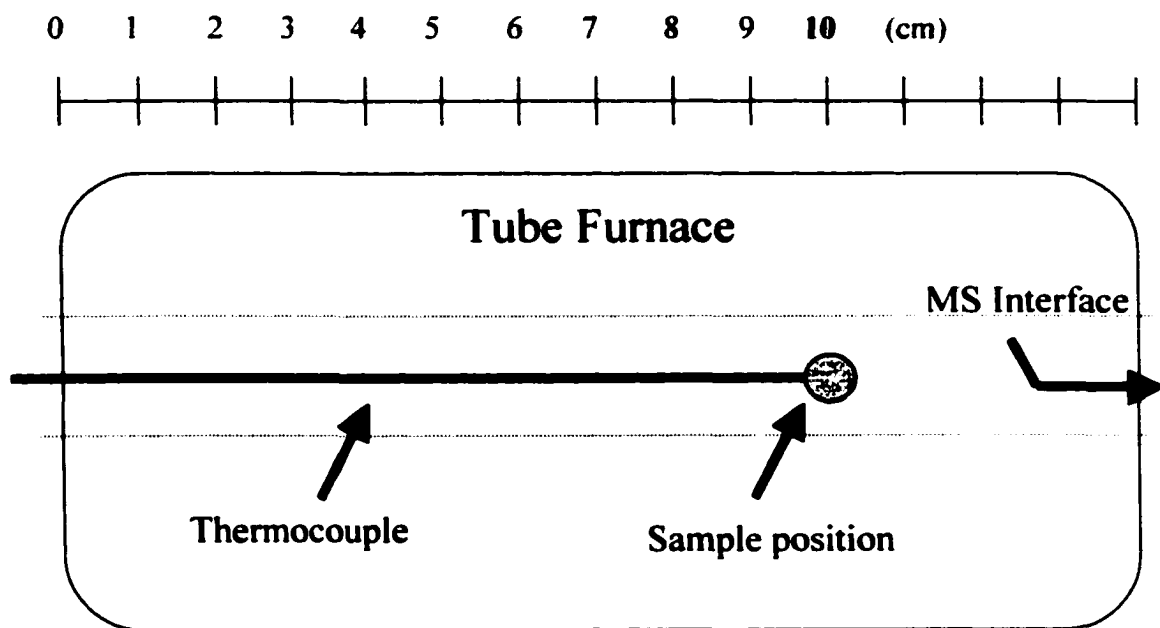


Figure 2-7: Diagram of sample location inside tube furnace

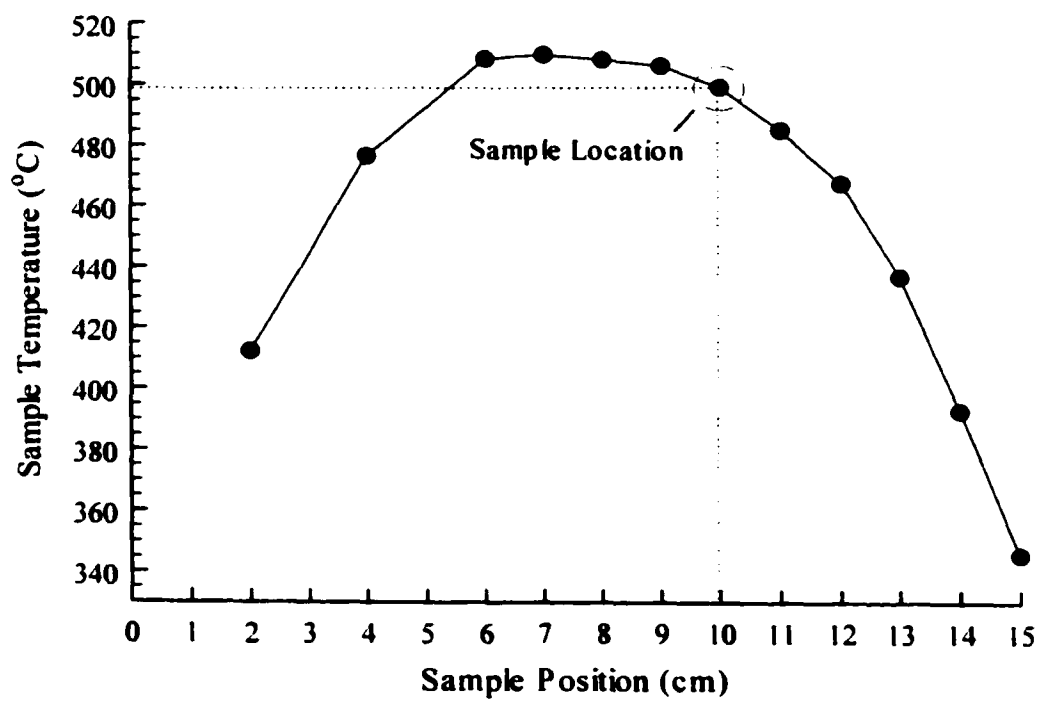


Figure 2-8: Sample temperature with respect to location inside tube furnace

Temperature measurements shown in Figure 2-8 were acquired with the furnace temperature controller set to 500 °C and a helium flow rate of 25 mL/min. The sample position of 10 cm was chosen because the sample temperature matched the set point temperature at the selected conditions. In retrospect, the 10 cm sample position was probably not the best position in the furnace. Placement of the sample between 6 cm and 9 cm would have resulted in a more reproducible sample temperature because there was less temperature variation between these positions. In order to minimize temperature variations, samples were placed at the same position (10 cm) for all experiments.

2.5.1 TA coupled with Gas Chromatography/Mass Spectrometry (TA-GC/MS)

In order to facilitate species-specific analysis when unique spectroscopic features are unavailable, gas chromatographic separations²⁸⁻³⁴ and tandem mass spectrometry³⁵ can be employed as EG analyzers. Detection of volatile products in previous catalytic polymer degradation studies have been accomplished by cryogenically trapping volatiles, which are subsequently analyzed.³⁶⁻⁴¹ Species-specific evolution profiles of volatile reaction products cannot be obtained by this method. The TA-GC/MS apparatus described here is unique and was specifically developed to aid in in-situ characterization of volatile cracking products.⁴²⁻⁴³ McClennen et al. described TA-GC/MS and TA-GC/IR analysis systems that incorporated automated vapor sampling and short chromatographic columns, which provided both satisfactory gas chromatographic separations and species-specific TA evolution profiles.⁴⁴ Isothermal chromatographic separations could be repeated at one minute intervals during TA analysis by using their systems. These hyphenated systems represented a significant advance in EG analysis. However, they were limited to isothermal GC conditions. Jakab et al.⁴⁵ and Liu et al.⁴⁶ briefly described a repetitive injection reactor-GC/MS system that they used for

studies of the decomposition of wood, cellulose, waste plastics, and coal. Their system, unlike that described by McClennen et al. employed automated sample injections and GC heating ramps. Our TA-GC/MS analysis system overcomes the limitation of slow heating rates from these instruments and facilitates rapid, repetitive temperature programmed gas chromatographic analyses. Multiple species-specific evolution profiles can be readily generated by using our TA-GC/MS apparatus.

The TA-GC/MS analysis system consists of the same furnace, interface, and mass spectrometer described earlier (Section 2.5) plus the addition of a small volume gas chromatograph. A diagram of the TA-GC/MS system is shown in Figure 2-5. Figure 2-6 displays the flow diagram of the system. Two gas flows enter the interface oven, TA purge and GC carrier gas. For the TA-GC/MS mode of operation, the TA purge enters the heated interface from the Vycor[®] tube described earlier and follows path "A" (Figure 2-6), which is connected to a Valco Instruments (Houston, TX) 4C8WT eight port injection valve (port 1). Connections to the injection valve employed stainless steel ferrules, except for the GC inlet (port 3), which employed a vespel[®]/graphite ferrule. Following path "A" of Figure 2-6, effluent flows from port 1 to port 2, where a 100 μ L sample loop connects port 2 to port 6. Port 6 is connected to port 5, where a 1/16 in. stainless steel tube serves as the outlet.

Helium GC carrier gas passes through a Scientific Glass Engineering, Inc. UNI-K10 on-column capillary GC injector, which was mounted to the top of the interface oven (Figure 2-5). The injection valve was connected to the GC injector (Figure 2-6). Helium flow entered port 7 of the injection valve, passed through a 100 μ L stainless steel sample loop via ports 8 and 4, and then passed into the capillary GC column connected to port 3. The capillary GC column exit was connected to the mass spectrometer ion source by a Scientific

Glass Engineering, Inc. MCVT-1-50 effluent splitter (front split in Fig. 2-6). A 1/16 in. stainless steel tube served as the GC carrier gas outlet.

Figure 2-9 shows the two positions of the eight port injection valve. A 100 μL aliquot of TA effluent was injected into the GC each time the valve was rotated. By rotating the injection valve, the 100 μL of TA effluent (A) contained in sample loop 1 (Figure 2-9 top) is injected into the GC (Figure 2-9 bottom). The next valve rotation injects TA effluent (A) contained in sample loop 2 (Figure 2-9 bottom) into the GC (Figure 2-9 top). The eight port injection valve was replaced by a Valco Instruments 4C6WT six port injection valve midway through sample analyses because of a leak that had developed. The six-port valve had two positions, load (top) and inject (bottom) (Figure 2-10). In the load position, TA effluent entered the injection valve, passed through a 100 μL sample loop, and then exited through a 1/16 in. stainless steel outlet. When the valve was rotated to the injection position, the sample effluent trapped in the sample loop was introduced into the GC column. After the injection of the sample effluent into the GC column (injection position), the valve was returned to the load position to fill the sample loop with TA effluent before the next injection. The valve was returned to the load position during the 45 s period during which the GC oven was cooled. The rotation back to the load position typically resulted in a small air peak at the end of each repetitive injection chromatogram.

A 10 meter long AT-1 capillary column with 0.25 μm stationary phase thickness and 0.25 mm i.d. purchased from Alltech Assoc. Inc. (Deerfield, IL) was used for separations. The stationary phase was 100% dimethylpolysiloxane. Helium was used as the carrier gas at a flow rate of 2 mL/min. The capillary column was contained within an 8 in. x 6 in. x 6 in. oven that was placed underneath the heated interface (Figure 2-5).

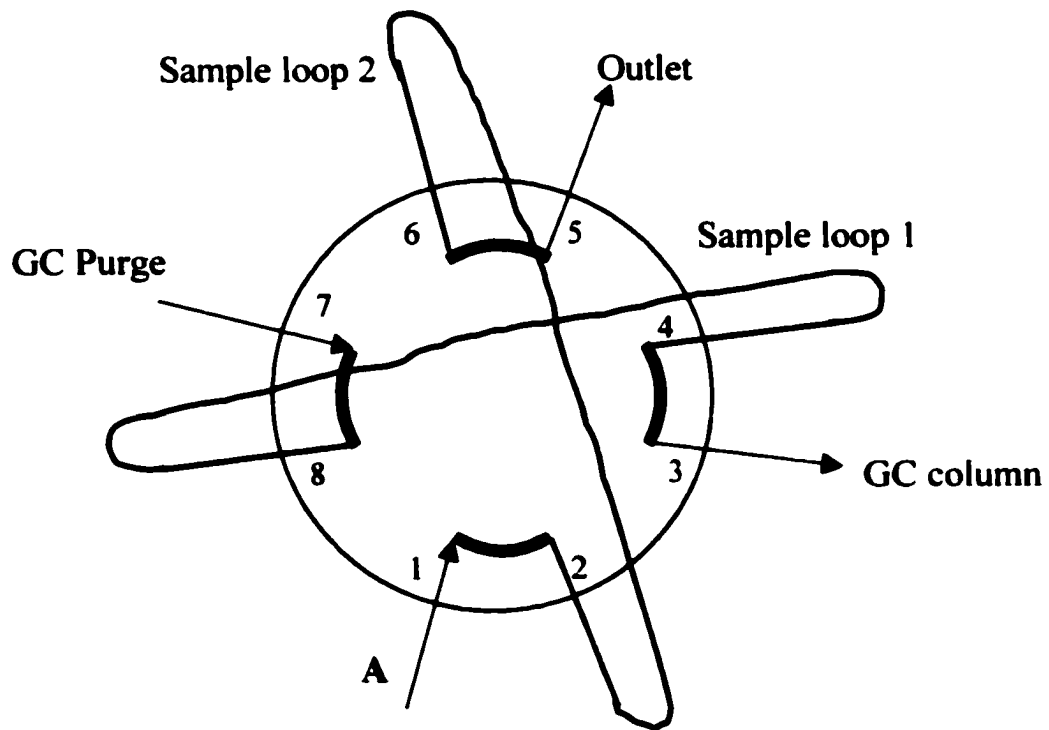
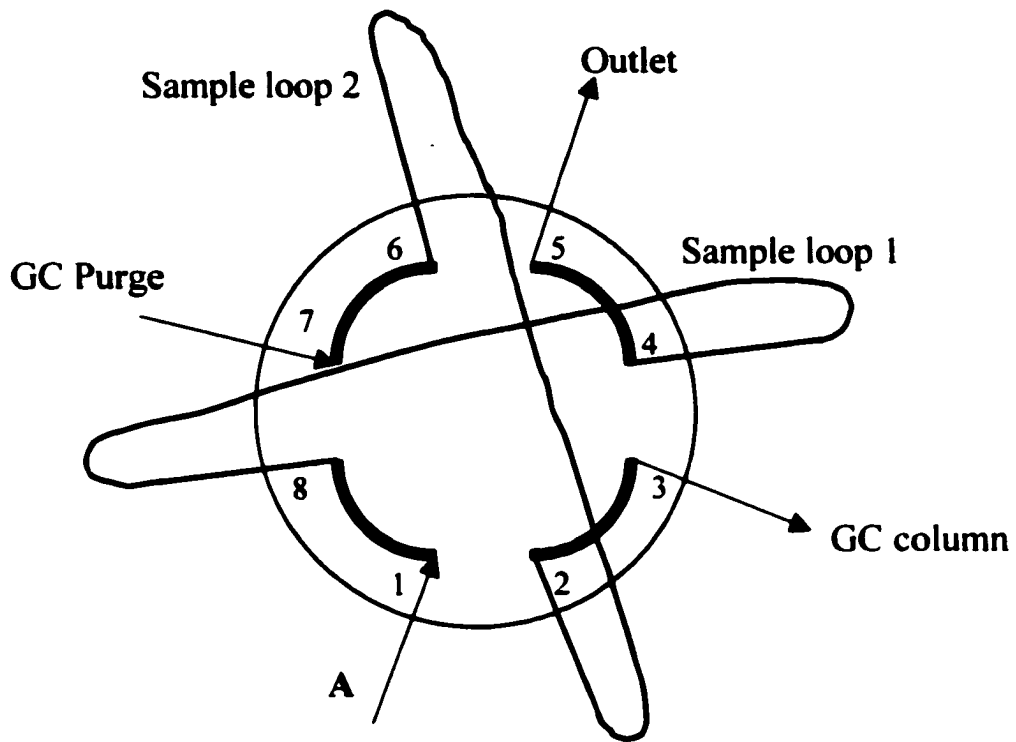


Figure 2-9: Eight port injection valve positions

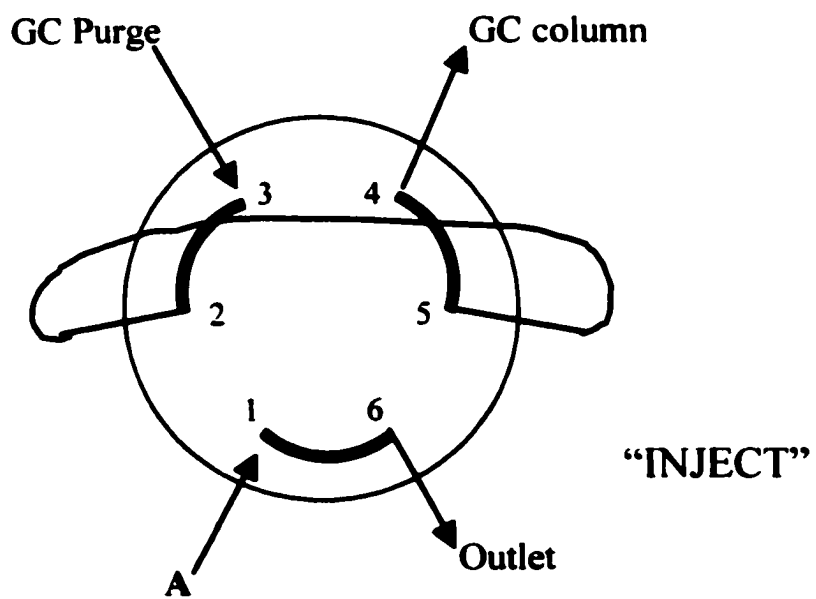
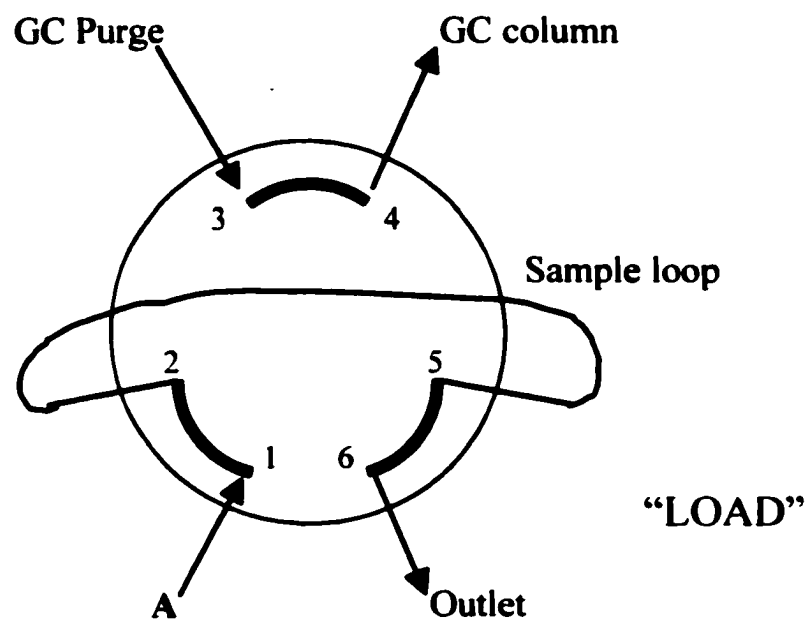


Figure 2-10: Six port injection valve positions

The GC oven also contained two 11-12 ohm coils of Chromel A heating wire obtained from Hoskins Mfg. Co. (Hamburg, MI), which were connected in parallel and used as resistive heaters. Heater current was controlled by an Omega CN3202TC1-8 temperature controller connected to an Omega solid state relay (SSR2400C25). A Dayton 4M078A fan obtained from Grainger (Oklahoma City, OK) was used to circulate the heated air and temperatures were measured with an Omega CHAL-010 thermocouple connected to the temperature controller and placed in the center of the GC oven. Heating rates of approximately 200 °C/min could be attained inside the GC oven.

To allow for rapid cooling after temperature programmed separations, a solenoid valve (not shown in Figure 2-5) purchased from Grainger was used to permit the introduction of liquid nitrogen into the GC oven. The solenoid valve was mounted to the chromatograph oven front panel and was controlled by the Omega CN3202TC1-8 temperature controller. The solenoid valve was attached to a 25 L liquid nitrogen Dewar by insulated 1/4 in. o.d. copper tubing. The Dewar was pressurized by a regulated in-house dry air line. When the Dewar pressure was $\approx 7 \text{ lb/in}^2$, the GC oven could be cooled from 200 °C to -50 °C in less than 30 s.

Identical heating and MS conditions were used for all LPE/catalyst samples in this study. LPE/catalyst samples weighing 15 mg ($\pm 5 \text{ mg}$) were heated in the tube furnace at 2 °C/min from 100 to 400 °C. For sample analyses in an inert atmosphere, the tube furnace was purged in helium (25 mL/min) for 30 min prior to heating. For analyses in a hydrogen atmosphere, a helium purge was followed by a 30 min purge of hydrogen (25 mL/min) prior to sample heating. Total ion current (TIC) chromatograms were obtained by injecting TA effluent into the GC at 5 min intervals or every 10 °C increase in sample temperature in the

tube furnace beginning at 120 °C for LPE/HZSM-5 samples and 180 °C for LPE/HY and LPE/HMCM-41 samples. The GC oven temperature was held at -50 °C for 0.3 min followed by a ramp to 80 °C at 50 °C/min and a second ramp to 200 °C at 109 °C/min. After the final temperature was reached, the GC oven was made ready for another injection within 45 s by cooling with liquid N₂ to -50 °C. The mass spectrometer was set to integrate for 1 ms over the mass range between 15 and 160 (3.425 scans/s). The MS ion source temperature was maintained at 200 °C and an ionization potential of 70 eV was used for all GC/MS measurements. Calibration of the MS was done daily by using direct probe insertion of perfluorotributylamine (PFTBA) to achieve a source pressure of 6×10^{-6} Torr, then the GC valve (front split) was opened to achieve a source pressure of 1×10^{-5} Torr. Chromatographic eluents were identified by library search with 38,000 spectra with the Technivent software.

Figure 2-11 shows the repetitive injection chromatogram for LPE/PtHZSM-5 heated in helium as an illustration of the TA-GC/MS apparatus performance. The y-axis in Figure 2-11 represents the total ion current (TIC) detected by the MS and the x-axis represents the sample temperature. Each tic mark on the x-axis indicates the sample temperature at which an injection was made (every 10 °C). Note that volatile product distributions changed with sample temperature resulting in chromatogram shape variations. Chromatograms obtained when the sample temperature reached 150, 240, and 300 °C are shown at the top of Figures 2-12, 2-13, and 2-14, respectively. Few volatile products, most with retention times (R_t) less than 2.25 min were detected for the 150 °C injection (Figure 2-12a). When the sample temperature reached 240 °C (Figure 2-13a), an increase in the total number of volatile products was detected, including an increase in the amount of volatile products with R_t less than 1.5 min.

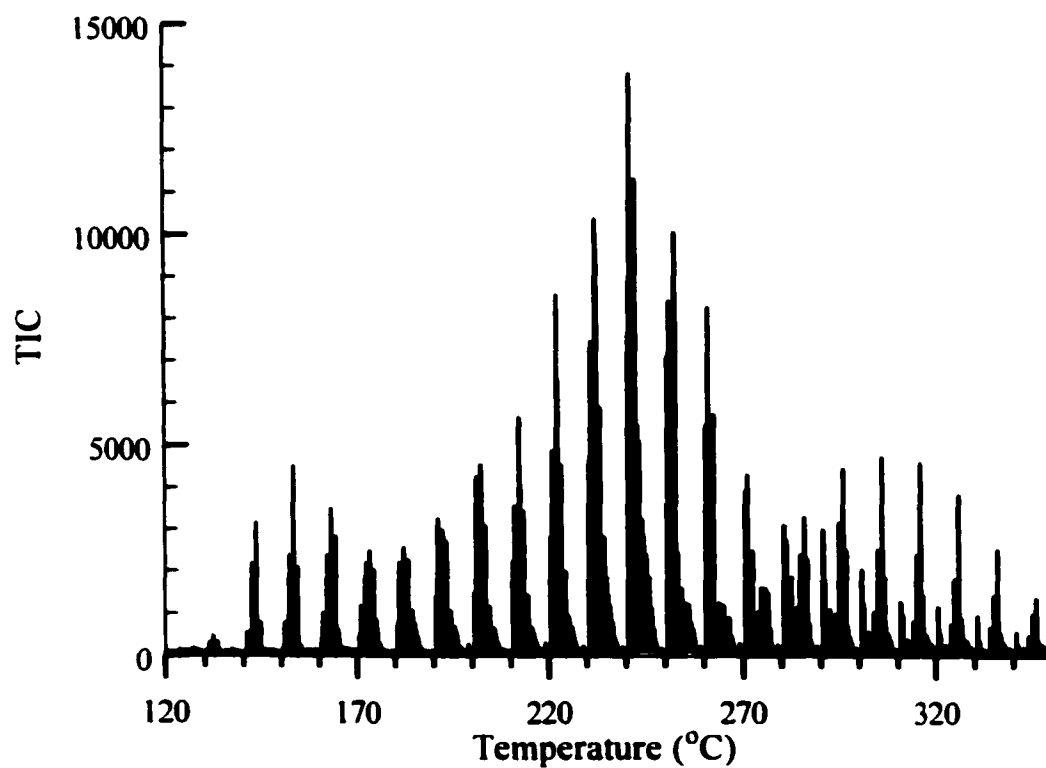


Figure 2-11: Repetitive injection chromatograms from LPE/PtHZSM-5 heated in helium

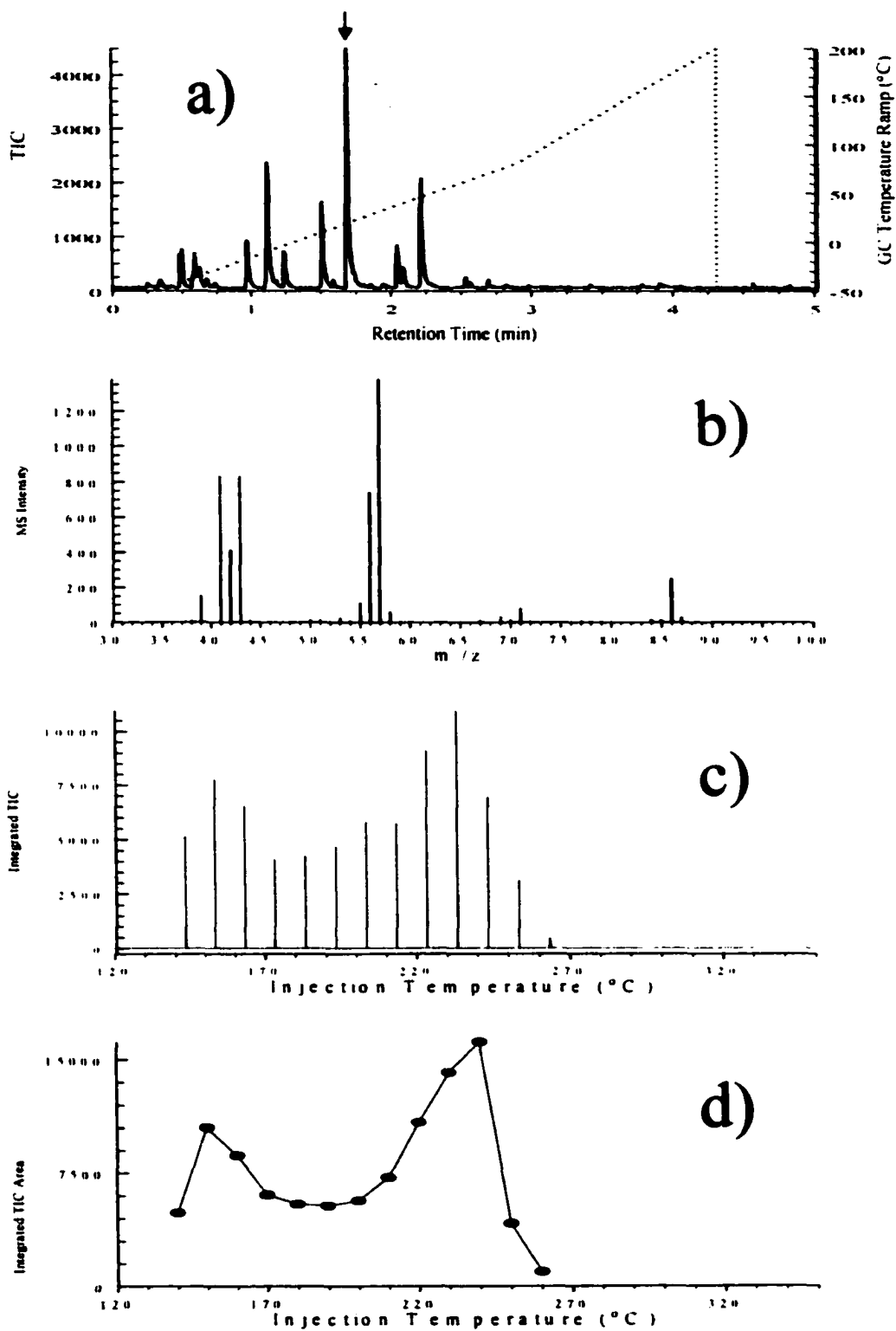


Figure 2-12: a) Repetitive injection chromatogram of volatile TA effluent at 150°C from LPE/PtHZSM-5 heated in helium b) Mass spectrum for n-hexane c) Repetitive injection chromatograms for n-hexane d) Species-specific evolution profile for n-hexane

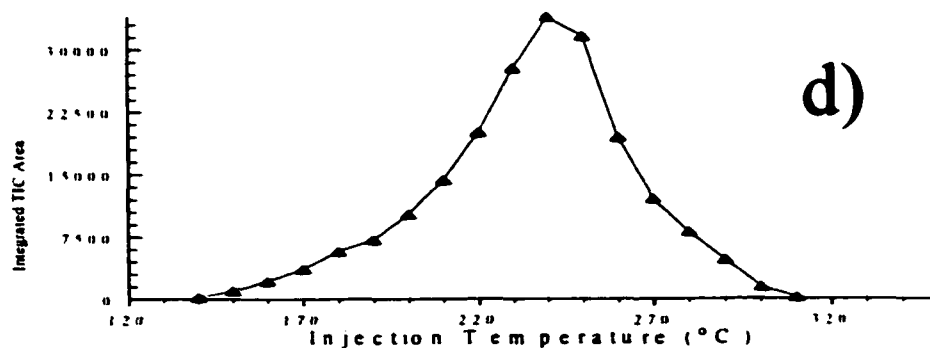
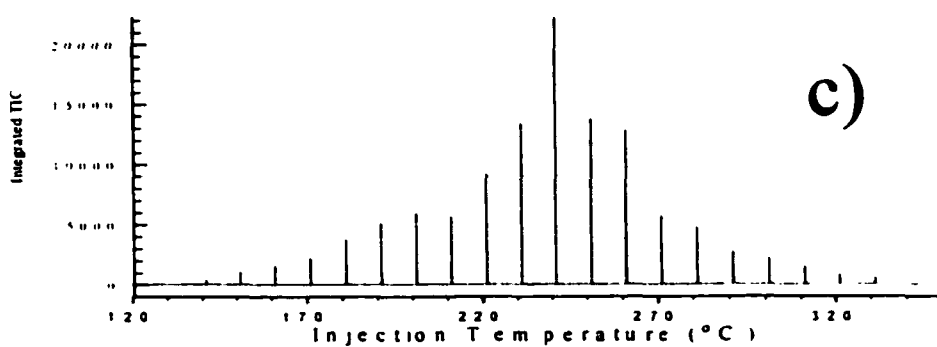
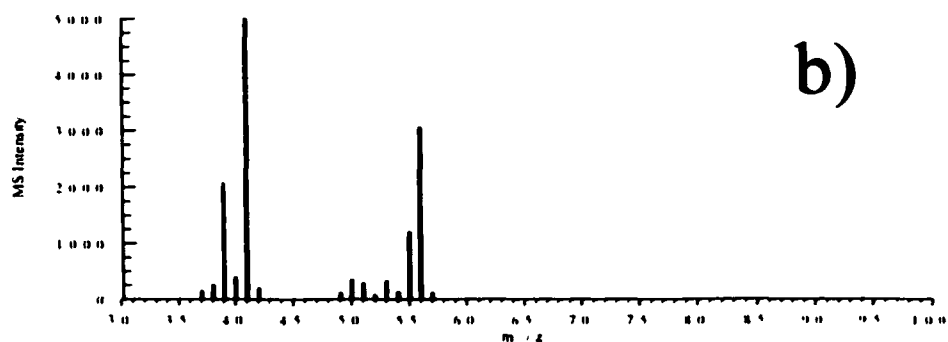
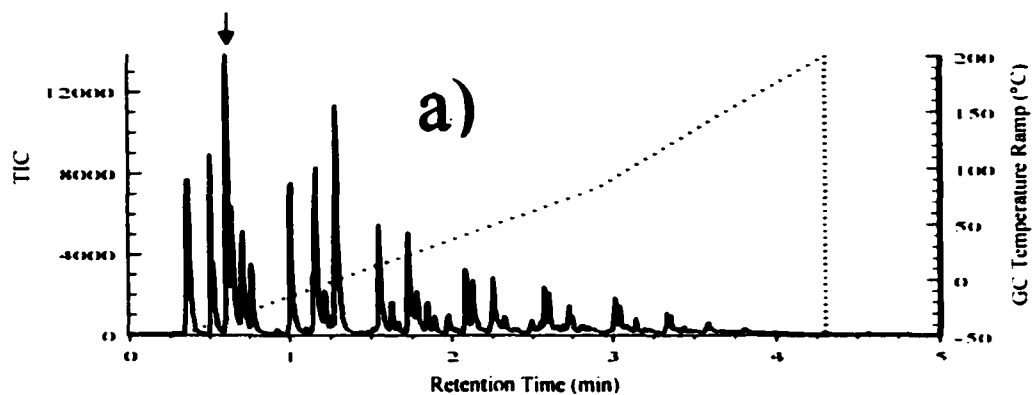


Figure 2-13: a) Repetitive injection chromatogram of volatile TA effluent at 240°C from LPE/PtHZSM-5 heated in helium b) Mass spectrum for iso-butene c) Repetitive injection chromatograms for iso-butene d) Species-specific evolution profile for iso-butene

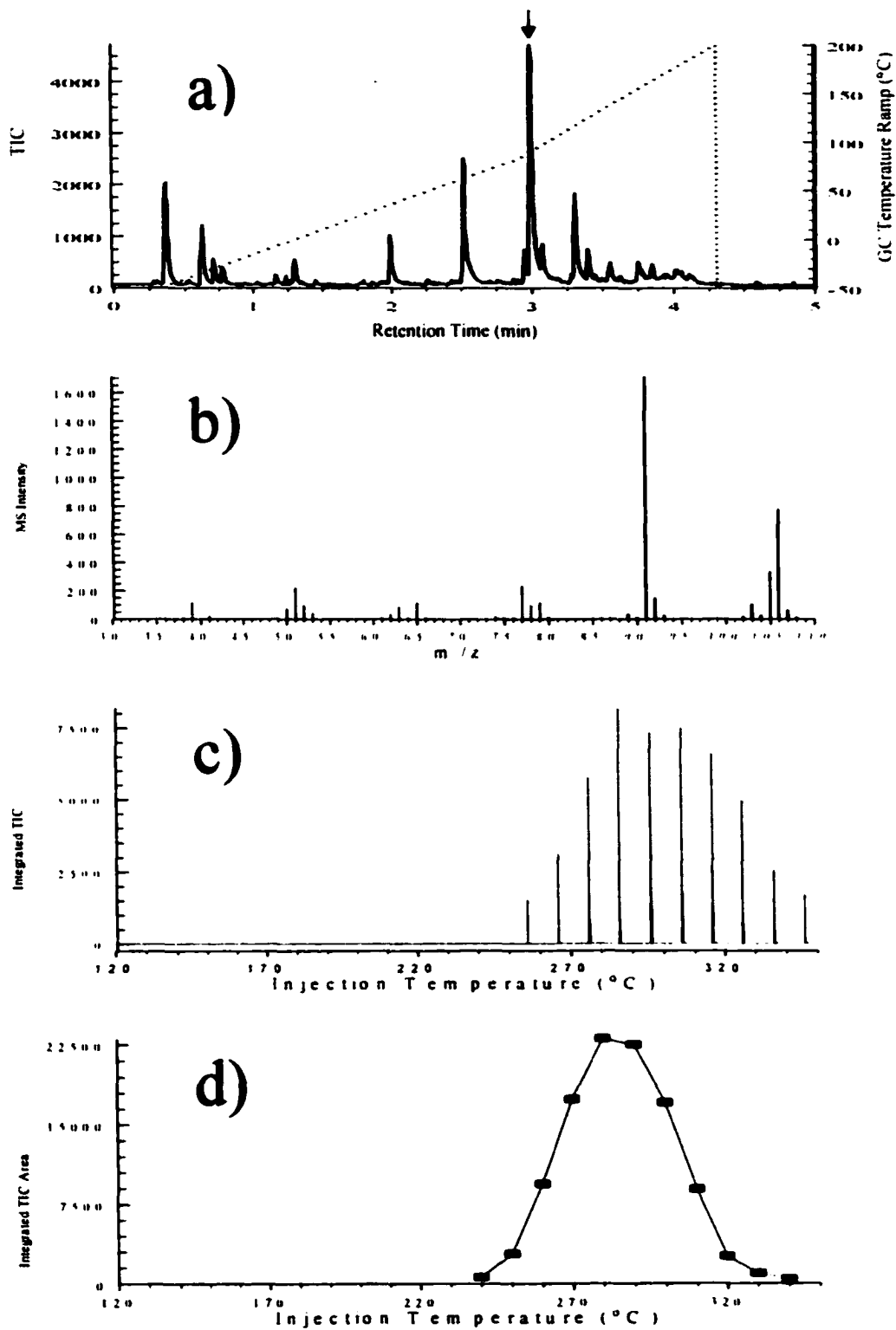


Figure 2-14: a) Repetitive injection chromatogram of volatile TA effluent at 300 °C from LPE/PtHZSM-5 heated in helium b) Mass spectrum for a C₂-phenyl isomer (xylene or ethyl benzene) c) Repetitive injection chromatograms for C₂-Phenyl d) Species-specific evolution profile for C₂-Phenyl

At 300 °C (Figure 2-14a), few volatiles were detected and the majority of them evolved with R_t greater than 2.5 min. The method used to generate the species-specific temperature profiles for selected volatile products from TA-GC/MS chromatograms will be described next.

Because of the large amount of data generated by TA-GC/MS, methods for simplifying data analysis were developed. Software was created to permit extraction of chromatographic peaks representing the same substance from each chromatogram recorded during a TA-GC/MS analysis. A computer program was used to compare a selected mass spectrum with all other mass spectra collected during the TA-GC/MS analysis to identify those that represent the same substance. This was done by representing mass spectra as vectors in n -dimensional space (where n = mass range scanned) and computing dot products between a selected spectrum vector and the rest of the TA-GC/MS spectrum vectors. The program calculated the cosines of the angles between the selected mass spectrum vector and those derived from all of the mass spectra collected for the TA-GC/MS chromatograms. When the cosine value was equal to or greater than an operator selected threshold value (e.g. 0.95), a satisfactory match was assumed between the mass spectra. The total ion current (TIC) value and retention time for the mass spectrum was saved to create a species-specific chromatogram. If the cosine value was less than the threshold value, the chromatogram point was not extracted. In this manner, those points (or peaks) which represented volatile products that yielded the selected mass spectrum were extracted from the TA-GC/MS chromatograms to produce species-specific chromatograms. The program also calculated species-specific chromatogram peak areas. These integrated peak areas were used to

generate species-specific evolution profiles and to calculate relative percent yields for volatile products.

Examples of how this program was used to create temperature dependent species-specific evolution profiles from an LPE/PtHZSM-5 sample heated in helium are shown in Figures 2-12 to 2-14. The TIC chromatogram (solid line) and the GC oven temperature ramp (dotted line, right y-axis scale) are shown in Figure 2-12a. Although the GC oven temperature did not decrease linearly from 200 to -50 °C as shown in Figure 2-12a, the oven temperature was returned to -50 °C within the 0.75 minutes shown. Figure 2-11a shows that within the first 2 minutes of the chromatogram, about 15 volatile products were separated. Figures 2-12b to 2-12d illustrate how species-specific chromatograms and evolution profiles were created. An arrow at 1.7 min in Figure 2-12a marks the chromatographic peak for the product to be profiled. This product was identified by the mass spectrum in Figure 2-12b as n-hexane. Using the program described, species-specific chromatograms for n-hexane were obtained as shown in 2-12c. The y-axis of Figure 2-12d represents the integrated n-hexane peak area (from Figure 2-12c). Figure 2-12d represents the n-hexane temperature dependent evolution profile.

Iso-butene is the product selected at 0.6 min in Figure 2-13a. The corresponding mass spectrum is shown in Figure 2-13b. The species-specific chromatogram for iso-butene is shown in Figure 2-13c and the evolution profile for iso-butene is shown in Figure 2-13d. Figure 2-14 depicts the species-specific profile for a C₂-phenyl (alkyl aromatic) isomer. The species-specific profiles depicted in Figures 2-12, 2-13, and 2-14 show the temperature dependence of individual volatile products formed when heating LPE/PtHZSM-5 in helium.

Evolution profiles for individual (or a group of related) product(s) obtained by TA-GC/MS can be useful for elucidation of the degradation mechanism(s). Figures 2-12 to 2-14 show evolution profiles for the formation of n-hexane, iso-butene, and C₂-phenyl (alkyl aromatics) volatile products detected when heating LPE/PtHZSM-5 in helium. Initial n-hexane production was favored at low temperatures, followed by a second maximum at which iso-butene and n-hexane were produced together. Therefore, at low temperatures, catalytic mechanism(s) that form n-hexane are favored on the PtHZSM-5 surface. As the sample temperature increases, mechanism(s) that form iso-butene become important. Alkyl aromatic products (C₂-Phenyl) were formed at higher sample temperatures. The delay in production of alkyl aromatics can be explained by the need for conjugated unsaturated species. The unsaturated residue that collects on the catalyst surface at high temperatures may cyclize and desorb as volatile aromatic species. A reproducibility of approximately 2% in total integrated TIC area was calculated for profiles created from separate analyses of the same sample.

2.6 Ammonia Temperature Programmed Desorption (NH₃-TPD)

Temperature programmed desorption (TPD) of small, basic probe molecules are typically used to characterize solid acid catalysts. Small amines such as isopropyl-amine⁴⁷⁻⁴⁸, ammonia⁴⁹⁻⁵⁴, and pyridine⁵⁵⁻⁵⁶ are commonly employed basic probe molecules. TA-MS was used to characterize the acidity of each catalyst by NH₃-TPD.

Approximately 30 mg (± 5 mg) samples were loaded into the TA-MS platinum sample pan for NH₃-TPD experiments. Samples were then purged for at least 30 min in a flow of helium. After purging, samples were heated to 500 °C and held at this temperature for 2 hrs to remove adsorbed water from the catalysts. Samples were then cooled to 100 °C.

With the helium flow turned off, a pulse of NH₃ (10-12 psi) was passed through the sample tube. After approximately 5 min, the helium flow was turned back on and the sample was purged for 3 hrs to remove excess and physisorbed NH₃. After purging, sample temperatures were increased from 100-600 °C at 10 °C/min. The back split valve in Figure 2-6 was adjusted to achieve a mass spectrometer ion source pressure of 1x10⁻⁵ Torr during analysis. The TA-MS apparatus provided mass spectral information for water (m/z 18) and ammonia (m/z 17). The MS was set to integrate for 100 ms and signal average 100 times for a 20.002 s/scan rate. The m/z 17 NH₃⁺ ion signal was corrected for the contribution from OH⁺ from water by:

$$\text{Corrected m/z 17 signal} = \text{Total m/z 17 signal} - (1/3 \times \text{m/z 18 signal}) \quad [1]$$

The m/z 17 (OH⁺) ion signal intensity is 1/3 of the intensity of m/z 18 (H₂O⁺) in the water vapor mass spectrum. Correction for the contribution of water in equation [1] must be done to calculate the total ion intensity of m/z 17 resulting from NH₃⁺ alone. Figure 2-15 shows results from NH₃-TPD analysis of an HZSM-5 catalyst. The number of acid sites found on the catalyst surface is proportional to the corrected m/z 17 ion signal area. The combination of temperature and distribution of corrected m/z 17 ion signal area represents the acid strength profile of catalyst sites.

NH₃-TPD experimental reproducibility is depicted in Figures 2-16 to 2-18 for HZSM-5, HY, and HMCM-41 catalysts. In these figures, the corrected m/z 17 ion signals were normalized and plotted against catalyst temperature.

$$\text{Normalized m/z 17 signal} = \frac{(\text{corrected m/z 17 signal} - \text{minimum corrected m/z 17 signal})}{(\text{maximum corrected m/z 17 signal} - \text{minimum corrected m/z 17 signal})} \quad [2]$$

The solid and dashed lines in Figures 2-16 to 2-18 represent duplicated NH₃-TPD curves for all catalyst samples.

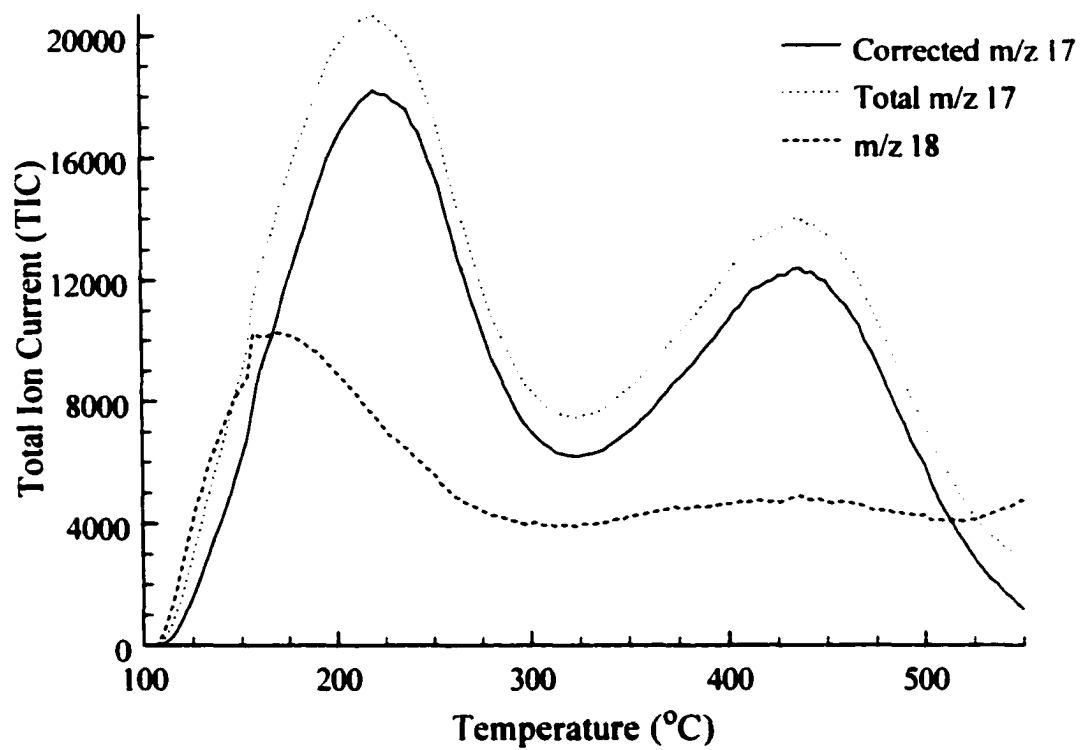


Figure 2-15: Correction for water in the HZSM-5 NH₃-TPD curve

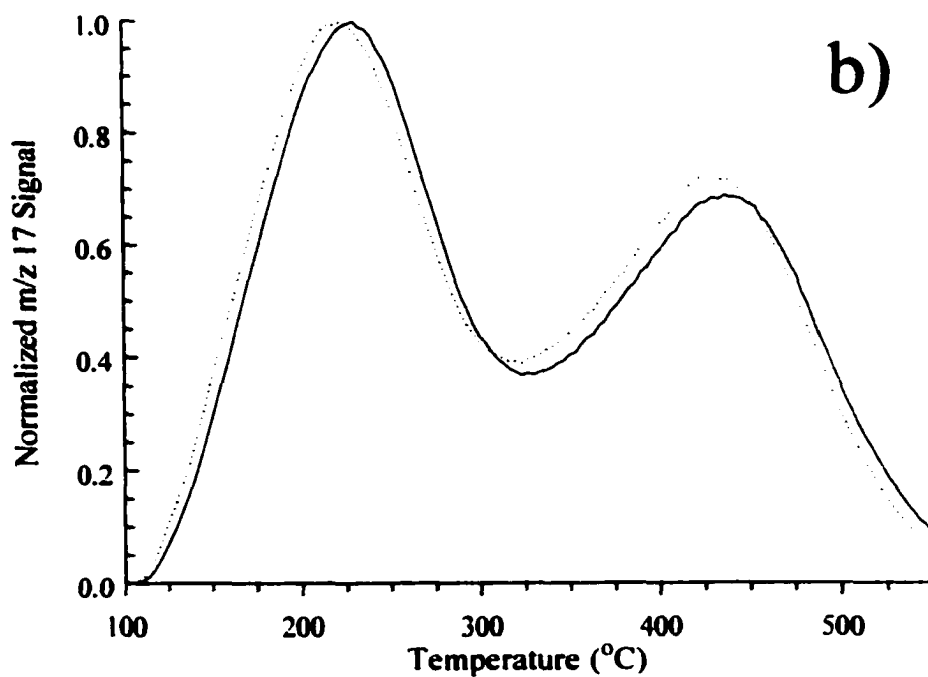
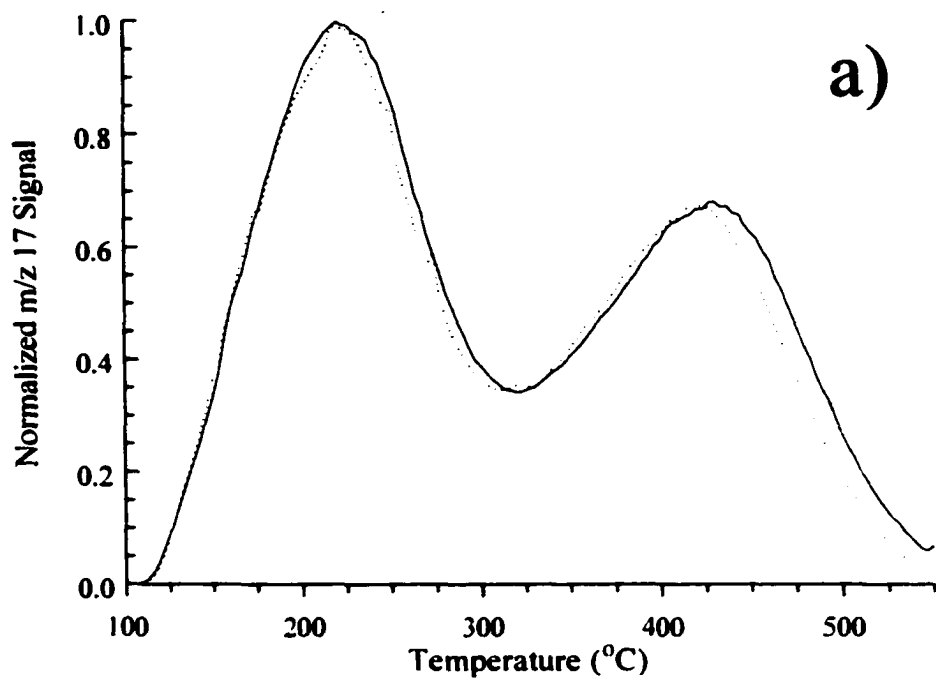


Figure 2-16: Normalized NH_3 -TPD curves for a) HZSM-5 b) PtHZSM-5

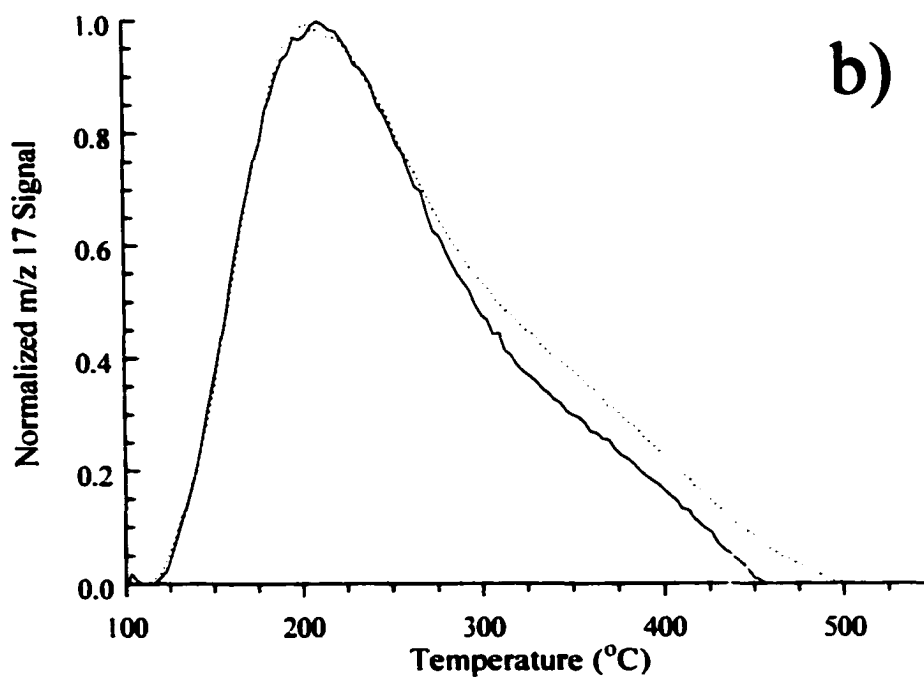
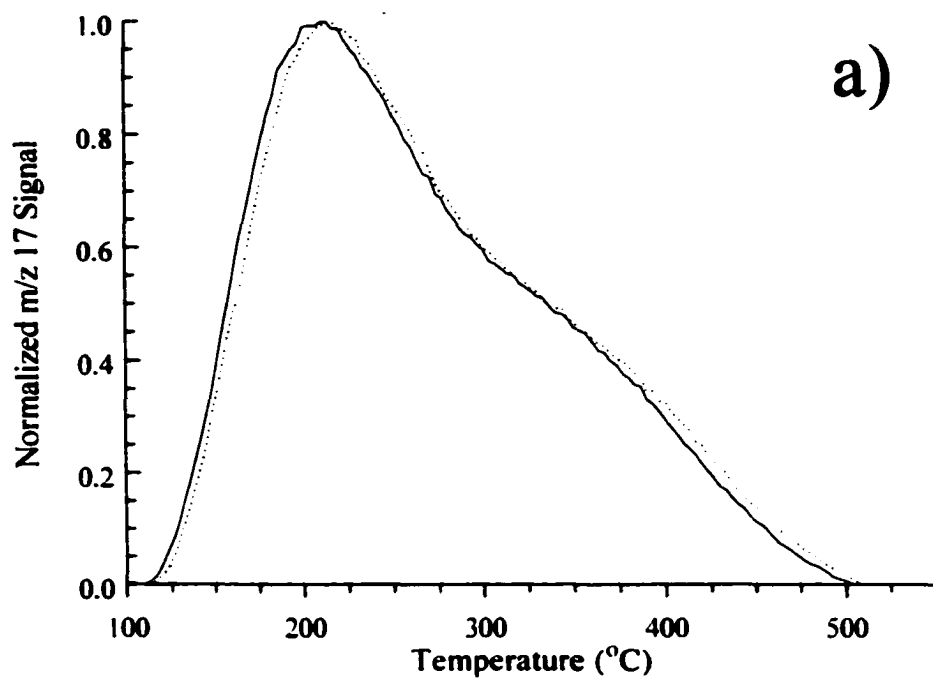


Figure 2-17: Normalized NH_3 -TPD curves for a) HY b) PtHY

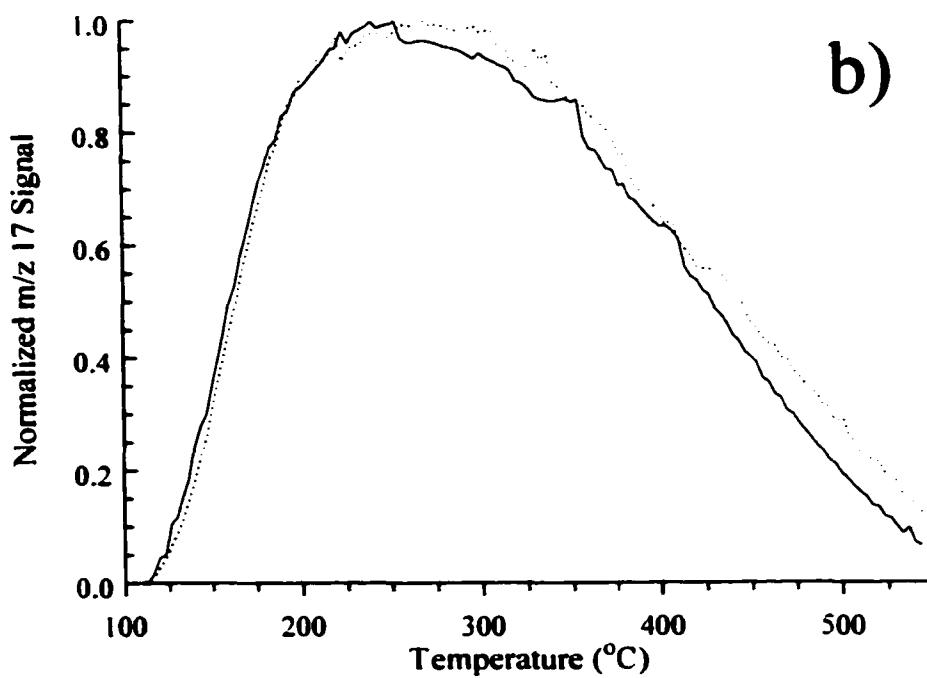
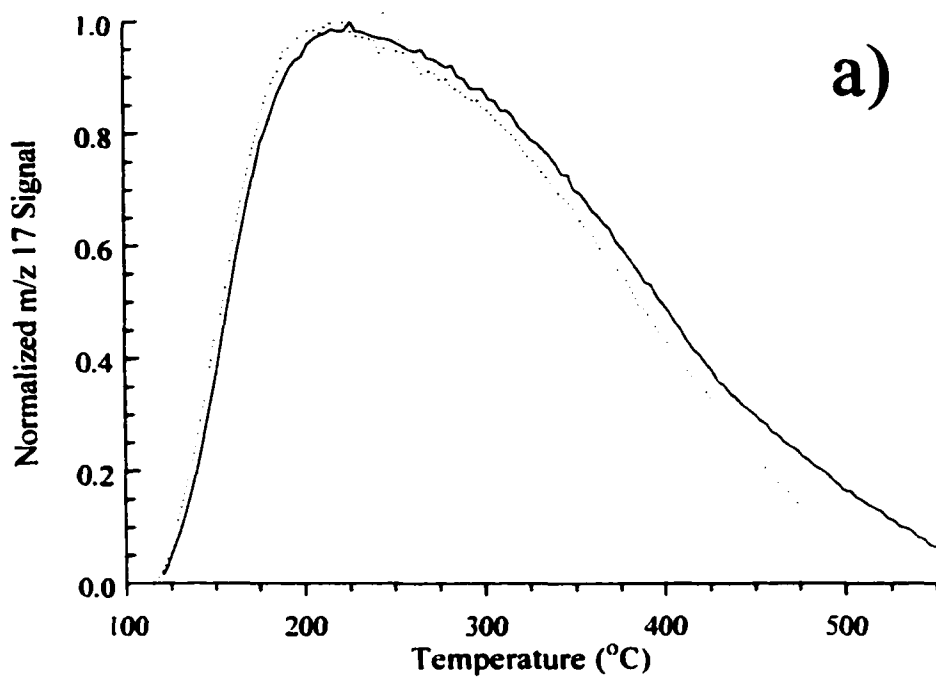


Figure 2-18: Normalized NH_3 -TPD curves for a) HMC41 b) PtHMC41

For all catalyst samples, TPD curves obtained for replicate samples were very similar. The largest temperature deviation (≈ 30 °C) was observed for the HMCM-41 catalyst (Figure 2-18a) at high temperatures. Typically, the largest deviations were observed at high temperatures (>400 °C) when ammonia ion signals were low.

The NH_3 -TPD curves for HZSM-5 and PtHZSM-5 (Figure 2-16) consisted of two characteristic peaks, which is consistent with previous literature.^{51,57} Maxima were observed for both catalysts at approximately 220 °C and 440 °C (Figure 2-16). Figures 2-17 and 2-18 show the replicate NH_3 -TPD curves for both (a) neat and (b) platinum containing HY and HMCM-41 catalysts, respectively. The TPD curve shapes obtained for the HY and HMCM-41 catalysts represent a broad tailing acid strength distribution, which reached a maximum at approximately 210 °C. Similar results are found in the literature for NH_3 -TPD acid site characterizations of HY and HMCM-41 catalysts.⁵⁸⁻⁶¹

The addition of platinum did not significantly affect the overall acidity of the catalysts (Figures 2-16b to 2-18b). The relative temperature range and shape of each TPD distribution for each catalyst was very similar with and without platinum. Analogous TPD characterization studies on various zeolite acid catalysts have shown that the addition of metals (i.e. platinum) does not affect the overall acidity of the catalysts.⁶²⁻⁶⁶ For relative comparisons it can be shown that the HY catalyst absorbed the most ammonia and HMCM-41 adsorbed the least (Figure 2-19). The HY catalysts showed the narrowest temperature distribution with no NH_3 desorbed over 500 °C and both the HZSM-5 and HMCM-41 catalysts did not show complete NH_3 desorption by 550 °C. The overall acid strength of the catalysts used in decreasing order can be given as: PtHZSM-5 \cong HZSM-5 > PtHY \cong HY > PtHMCM-41 \cong HMCM-41.

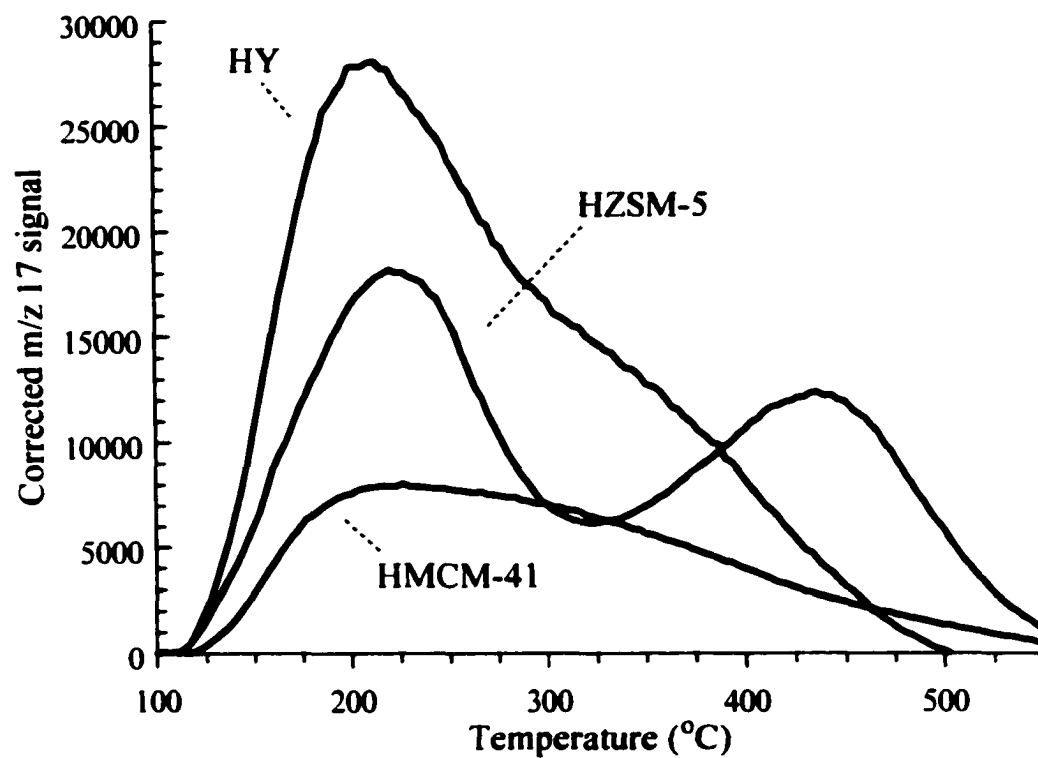


Figure 2-19: NH₃-TPD curves for all metal-free catalysts used

2.7 References

1. Lin, R.; Ph.D. Dissertation, University of Oklahoma, 1997 "Catalytic Cracking of Poly(ethylene) and Poly(styrene) by Silica-Alumina, HZSM-5 Zeolite, and Sulfated Zirconia"
2. Argauer, R. J.; Kensington, M.; Landolt, G.R.; U.S. Patent 3702886 (1972) "Crystalline Zeolite ZSM-5 and Method of Preparing the Same"
3. Baerlocher, Ch.; Meier, W.M.; Olson, D.H.; Atlas of Zeolite Framework Types, 5th ed., Elsevier: Amsterdam, The Netherlands, 2001 (or <http://www.iza-structure.org>)
4. Mostad, H.B.; Appl. Catal. A 1996, 144, 305-316 "Comparison of the Isostructural H-SAPO-37 and H-Faujasite as Catalysts for the Isobutane / 2-Butene Alkylation"
5. Kresge, C.T.; Leonowicz, M.E.; Roth, W.J.; Vartuli, J.C.; Beck, J.S.; Nature 1992, 359, 710-712 "Ordered Mesoporous Molecular Sieves Synthesized by a Liquid-Crystal Template Mechanism"
6. Schmidt, R.; Akporiaye, D.; Stocker, M.; Ellstad, O.H.; J. Chem. Soc. Chem. Comm. 1994, 1943-1494 "Synthesis of a Mesoporous MCM-41 Material with High Levels of Tetrahedral Aluminum"
7. Beck, J.S.; Vartuli, J.C.; Roth, W.J.; Leonowicz, M.E.; Kresge, C.T.; Schmitt, K.D.; Chu, C.T.W.; Olson, D.H.; Sheppard, E.W.; McCullen, S.B.; Higgins, J.B.; Schlenker, J.L.; J. Am. Chem. Soc. 1992, 114, 10834-10843 "A New Family of Mesoporous Molecular Sieves Prepared with Liquid Crystal Templates"
8. Jacobs, G.; Ghadiali, F.; Pisanu, A.; Borgna, A.; Alvarez, W.A.; Resasco, D.E.; Appl. Catal. A. 1999, 188, 79-98 "Characterization of the Morphology of Pt Clusters Incorporated in a KL Zeolite by Vapor Phase and Incipient Wetness Impregnation. Influence of Pt Particle Morphology on Aromatization Activity and Deactivation"
9. Earnest, C.M. Anal. Chem. 1984, 56, 1471A-1486A "Modern Thermogravimetry"
10. Bonnet, E.; Ph.D. Dissertation, University of Oklahoma, 2000 "A Fixed Bed Catalytic Microreactor with Repetitive Injection Gas Chromatographic/Mass Spectrometric Analysis"
11. Raemaekers, K.G.H.; Bart, J.C.J; Thermochim Acta 1997, 295, 1-58 "Applications of Simultaneous Thermogravimetry-Mass Spectrometry in Polymer Analysis"
12. Materazzi, S.; Curini, R.; Appl. Spec. Rev. 2001, 36, 169-180 "The Coupling of Mass Spectrometry with Thermoanalytical Instruments: Applications of Evolved Gas Analysis"
13. Statheropoulos, M.; Kyriakou, S.; Pappa, A.; Thermochim. Acta, 329, 83-88 "Repetitive Pulsed Sampling Interface for Combined Thermogravimetry/Mass Spectrometry"

14. Price, D.M.; Reading, M.; Hammiche, A.; Pollock, H.M.; *J. Therm. Anal. Calorim.* 2000, 60, 723-733 "New Adventures in Thermal Analysis"
15. Xie, W.; Pan, W.-P.; *J. Therm. Anal. Calorim.* 2000, 65, 669-685 "Thermal Characterization of Materials Using Evolved Gas Analysis"
16. Kaisersberger, E.; Post, E.; Opfermann, J.; Emmerich, W.-D.; *Thermochim. Acta* 1999, 325, 25-34 "Combined Thermal Analysis and Gas-analysis Methods and Software Simulations for the Investigation of the Potential Endangerment to the Environment through Production and Recycling Processes"
17. Reggers, G.; Ruysen, M.; Carleer, R.; Mullens, J.; *Thermochim. Acta* 1997, 295, 107-117 "TG-GC-MS, TG-MS and TG-FTIR Applications on Polymers and Waste Products"
18. Matuschek, G.; Milanov, N.; Kettrup, A.; *Thermochim. Acta* 2000, 361, 77-84 "Thermoanalytical Investigations for the Recycling of PVC"
19. Breen, C.; Last, P.M.; Taylor, S.; Komadel, P.; *Thermochim. Acta* 2000, 363, 93-104 "Synergic Chemical Analysis – The Coupling of TG with FTIR, MS, GC-MS 2. Catalytic Transformation of the Gases Evolved During the Thermal Decomposition of HDPE Using Acid-Activated Clays"
20. Zitomer, F.; *Anal. Chem.* 1968, 40, 1091-1095 "Thermogravimetric – Mass Spectrometric Analysis"
21. Mitchell, J.; Chiu, J.; *Anal. Chem.* 1973, 45, 273R-332R "Analysis of High Polymers"
22. Baumgartner, E.; Nachbaur, E.; *Thermochim. Acta* 1977, 19, 3-12 "Thermogravimetry Combined with Chemical Ionization Mass Spectrometry – A New Technique in Thermal Analysis"
23. Chiu, J.; Beattie, A. J.; *Thermochim. Acta* 1980, 40, 251-259 "Techniques for Coupling Mass Spectrometry to Thermogravimetry"
24. Yuen, H.K.; Mappes, G.W.; Grote, W.A.; *Thermochim. Acta* 1982, 52, 143-153 "An Automated System for Simultaneous Thermal Analysis and Mass Spectrometry. Part I"
25. Holdiness, M.R.; *Thermochim. Acta* 1984, 75, 361-399 "Evolved Gas Analysis by Mass Spectrometry: A Review"
26. Matuschek, G.; *Thermochim. Acta* 1995, 263, 59-71 "Thermal Degradation of Different Fire Retardant Polyurethane Foams"
27. McEuen, D.J.; Lee, W.R.; Swarin, S.J.; *Thermochim. Acta* 1985, 86, 251-256 "Combined Thermogravimetric and Infrared Analysis of Polymers"

28. Kaiserberger, E.; Post, E.; *Thermochim. Acta* 1997, 295, 73-93 "Practical Aspects for the Coupling of Gas Analytical Methods with Thermal-Analysis Instruments"
29. Chiu, J.; *Anal. Chem.* 1968, 40, 1516-1520 "Polymer Characterization by Coupled Thermogravimetry – Gas Chromatography"
30. Whiting, L.F.; Langvardt, P.W.; *Anal. Chem.* 1984, 56, 1755-1758 "On-Column Sampling Device for Thermogravimetry/Capillary Gas Chromatography/Mass Spectrometry"
31. Chiu, J.; *Anal. Calorim.* 1984, 5, 197-207 "A Combined TG-GC/MS System for Materials Characterization"
32. Chung, H.L.; Aldridge, J.C.; *Anal. Instrum. (N.Y.)* 1992, 20, 123-135 "On-Line Thermogravimetry/Gas Chromatography/Mass Spectrometry"
33. Arai, T.; Senda, T.; Fujii, N.; *Thermochim. Acta* 1995, 267, 209-221 "A Combined Thermogravimetric-Gas Chromatographic/Mass Spectrometric Analysis (TG-GC/MS) Using a High Resolution Technique"
34. Prime, R.B.; Shushan, B.; *Anal. Chem.* 1989, 61, 1195-1201 "Thermogravimetric Analyzer/Atmospheric Pressure Chemical Ionization Tandem Triple Quadrupole Mass Spectrometer System for Evolved Gas Analysis"
35. Chang, T.; Mead, T.E.; *Anal. Chem.* 1971, 43, 534-538 "Tandem Thermogravimetric Analyzer – Gas Chromatograph - High Resolution Mass Spectrometer System"
36. Seddegi, Z.S.; Budrthumal, U.; Al-Arfaj, A.A.; Al-Amer, A.M.; Barri, S.A.I.; *Appl. Catal. A* 2002, 225, 167-176 "Catalytic Cracking of Polyethylene over All-Silica MCM-41 Molecular Sieve"
37. Manos, G.; Yusof, I.Y.; Gangas, N.H.; Papayannakos, N.; *Energy Fuels* 2002, 16, 485-489 "Tertiary Recycling of Polyethylene to Hydrocarbon Fuel by Catalytic Cracking over Aluminum Pillard Clays"
38. Walendziewski, J.; Steininger, M.; *Catal. Today* 2001, 65, 323-330 "Thermal and Catalytic Conversion of Waste Polyolefins"
39. Manos, G.; Garforth, A.; Dwyer, J.; *Ind. Eng. Chem. Res.* 2000, 39, 1198-1202 "Catalytic Degradation of High-Density Polyethylene over Different Zeolitic Structures"
40. Serrano, D.P.; Aguado, J.; Escola, J.M.; *Ind. Eng. Chem. Res.* 2000, 39, 1177-1184 "Catalytic Cracking of a Polyolefin Mixture over Different Acid Solid Catalysts"

41. Lin, Y.-H.; Sharratt, P.N.; Garforth, A.A.; Dwyer, J.; *Energy Fuels* 1998, 12, 767-774 "Catalytic Conversion of Polyolefins to Chemicals and Fuels over Various Cracking Catalysts"
42. Negelein, D.; Bonnet, E.; White, R.L.; *J. Chromatogr. Sci.* 1999, 37, 263-269 "Effluent Monitoring by Repetitive Injection Gas Chromatography – Mass Spectrometry"
43. Sikabwe, E.C.; Negelein, D.L.; Lin, R.; White, R.L.; *Anal. Chem.* 1997, 69, 2606-2609 "A Thermogravimetry-Capillary Gas Chromatography/Mass Spectrometry Interface"
44. McClennen, W.H.; Buchanan, R.M.; Arnold, N.S.; Dworzanski, J.P.; Meuzelaar, H.L.C.; *Anal. Chem.* 1993, 65, 2819-2823 "Thermogravimetry/Gas Chromatography/Mass Spectrometry and Thermogravimetry/Gas Chromatography/ Fourier Transform Infrared Spectroscopy: Novel Hyphenated Methods in Thermal Analysis"
45. Jakab, E.; Liu, K.; Meuzelaar, H.L.C.; *Ind. Eng. Chem. Res.* 1997, 36, 2087-2095 "Thermal Decomposition of Wood and Cellulose in the Presence of Solvent Vapors"
46. Liu, K.; Jakab, E.; Zmierczak, W.; Shabtai, J.; Meuzelaar, H.L.C.; *Prepr. Pap. Am. Chem. Soc., Div. Fuel Chem.* 1994, 39, 576-580 "Studies of Thermal and Catalytic Hydro liquefaction of Model Compounds, Waste Polymers, and Coal by High Pressure TG/GC/MS"
47. Yiu, H.H.P.; Brown, D.R.; Barnes, P.A.; *Catal. Lett.* 1999, 59, 207-211 "Mesoporous Solid Acid Catalysts: Relationship between Amine TPD Data and Catalytic Activities"
48. Daniell, W.; Topsoe, N.-Y.; Knoezinger, H.; *Langmuir* 2001, 17, 6233-6239 "An FTIR Study of the Surface Acidity of USY Zeolites. Comparison of CO, CD₃CN, and C₅H₅N Probe Molecules"
49. Brueva, T.R.; Mishin, I.V.; Kapustin, G.I.; *Thermochim. Acta* 2001, 379, 15-23 "Distribution of Acid-site Strengths in Hydrogen Zeolites and Relationships between Acidity and Catalytic Activity"
50. Sikabwe, C.E.; Coelho, M.A.; Resasco, D.E.; White, R.L.; *Catal. Lett.* 1995, 34, 23-30 "Catalyst Decomposition during Temperature Programmed Desorption of Bases from Promoted Sulfated Zirconias"
51. Bagnasco, G.; *J. Catal.* 1996, 159, 249-252 "Improving the Selectivity of NH₃ TPD Measurements"
52. Post, J.G.; van Hooff, J.H.C.; *Zeolites* 1984, 4, 9-14 "Acidity and Activity of H-ZSM-5 Measured with NH₃-T.P.D. and n-Hexane Cracking"

53. Hidalgo, C.V.; Itoh, H.; Hattori, T.; Niwa, M.; Murakami, Y.; *J. Catal.* 1984, 85, 362-369 "Measurement of the Acidity of Various Zeolites by Temperature-Programmed Desorption of Ammonia"
54. Kuehne, M.A.; Babitz, S.M.; Kung, H.H.; Miller, J.T.; *Appl. Catal. A* 1998, 166, 293-299 "Effect of Framework Al Content on HY Acidity and Cracking Activity"
55. Lee, C.; Parrillo, D.J.; Gorte, R.J.; Farneth, W.E.; *J. Am. Chem. Soc.* 1996, 118, 3262-3268 "Relationship between Differential Heats of Adsorption and Brønsted Acid Strengths of Acidic Zeolites: H-ZSM-5 and H-Mordenite"
56. Parrillo, D.J.; Biaglow, A.; Gorte, R.J.; White, D.; *Stud. Surf. Sci. Catal.* 1994, 84, 701-708 "Quantification of Acidity in H-ZSM-5"
57. Post, J.G.; van Hoof, J.H.C.; *Zeolites* 1984, 4, 9-14 "Acidity and Activity of H-ZSM-5 Measured with NH₃-TPD and n-Hexane Cracking"
58. Hidalgo, C.V.; Itoh, H.; Hattori, T.; Niwa, M.; Murakami, Y.; *J. Catal.* 1984, 85, 362-369 "Measurement of the Acidity of Various Zeolites by Temperature Programmed Desorption of Ammonia"
59. Weglarski, J.; Datka, J.; He, H.; Klinowski, J.; *J. Chem. Soc., Faraday Trans.* 1996, 92, 5161-5164 "IR Spectroscopic Studies of the Acidic Properties of the Mesoporous Molecular Sieve MCM-41"
60. Kosslick, H.; Landmesser, J.; Fricke, R.; *J. Chem. Soc. Faraday Trans.* 1997, 93, 1849-1854 "Acidity of Substituted MCM-41-type Mesoporous Silicates Probed by Ammonia"
61. Chakraborty, B.; Viswanathan, B.; *Catal. Today* 1999, 49, 253-260 "Surface Acidity of MCM-41 by the in situ IR Studies of Pyridine Adsorption"
62. Chupin, J.; Gnep, N.S.; Lacombe, S.; Guisnet, M.; *Appl. Catal. A* 2001, 206, 43-56 "Influence of the Metal and of the Support on the Activity and Stability of Bifunctional Catalysts for Toluene Hydrogenation"
63. Pirmgruber, G.D.; Zinck-Stagno, O.P.E.; Seshan, K.; Lercher, J.A.; *J. Catal.* 2000, 190, 374-386 "The Effect of the Pore Structure of Medium-Pore Zeolites on the Dehydroisomerization of n-Butane: A Comparison of Pt-FER, Pt-TON, and Pt-ZSM-5"
64. Pirmgruber, G.D.; Seshan, K.; Lercher, J.A.; *J. Catal.* 1999, 186, 188-200 "Dehydroisomerization on n-Butane over Pt-ZSM-5 (I): Effect of the Metal Loading and Acid Site Concentration"

65. Jentys, A.; Lugstein, A.; Kinger, G.; Vinek, H.; Proceedings of the International Zeolite Conference, 12th, Baltimore, July 5-10, 1998 (1999), 2817-2824 "Hydroconversion of Heptane and Octane over Bifunctional Zeolites; Influence of Structure and Metal Distribution on Activity and Selectivity"

66. Alvarez, F.; Ribeiro, F.R.; Perot, G.; Thomazeau, C.; Guisnet, M.; J. Catal. 1996, 162, 179-189 "Hydroisomerization and Hydrocracking of Alkanes 7. Influence of the Balance between Acid and Hydrogenating Functions on the Transformation of n-Decane on PtHY Catalysts"

CHAPTER 3 - ISOCONVERSION EFFECTIVE ACTIVATION ENERGY

3.1 Introduction

Kinetic studies are often useful for understanding the steps by which a chemical reaction takes place. Activation energy is a kinetic term defined as the minimum energy required to form a reaction transition state. The activation energies of hydrocarbon cracking reactions can be influenced by many variables such as: reaction atmosphere, reactant and product concentrations (or pressures), and selection of catalyst. Manipulations of the reaction mechanism by altering the reaction conditions can lead to formation of select reaction products.

The importance of the petroleum industry in today's society has led to research in catalytic cracking, hydrocracking, and conversion of small hydrocarbon molecules under various conditions. Many studies have shown that the choice of catalyst, size of hydrocarbon feed, hydrogen pressure, and temperature affect the kinetics of cracking reactions.¹⁻²² Typically, kinetic measurements for small hydrocarbon cracking reactions are made at very low conversions (steady state) or with low concentrations of reactant feed. In order to relate volatile products to cracking mechanisms, each step of the mechanism must be known. The effects of various conditions on each reaction step can then be determined. Simple kinetic reaction models have been developed to facilitate calculation of rate constants and activation energies.

Polymer catalytic cracking is a high conversion reaction in which polymer residue constantly changes and secondary reactions result in a wide range of volatile products. Our studies attempt to determine activation energy values for volatile LPE cracking products and to correlate changes in these kinetic values with the chain reaction cracking

and bifunctional catalyst cracking mechanisms for small molecules. Calculated activation energies represent multiple reaction processes and are termed “effective” activation energies (E_a). Our research is focused on understanding polymer catalytic cracking mechanisms and the effects of zeolite acidity and pore size and reaction conditions (i.e. helium and hydrogen) on cracking reactions.

3.2 Theory/Background

Various theoretical methods have been proposed for calculating kinetic constants from thermogravimetric analysis (TGA) results.²³⁻²⁶ Each method assumes that a single reaction occurs that generates a product slate that is independent of sample temperature. The methods of Freeman and Carroll²³, Friedman²⁴, and Doyle²⁵ all assume that the degradation reaction model can be explained by the following equation:

$$\frac{-dW}{dt} = A \exp\left(\frac{-\Delta E}{RT}\right) W^n \quad [1]$$

where W is the fractional residual weight of the sample, T is the absolute temperature, R is the gas constant, t is time, and A , ΔE , and n are the frequency factor, activation energy, and the order of the reaction, respectively. Freeman and Carroll²³ have shown that activation energy can be calculated from a single decomposition curve, but similar values can be calculated from results obtained at different heating rates. However, simultaneous adjustments of E , A , and W^n can often be made to fit any W^n to the data, leading to wide variations in kinetic parameters.²⁷

The Ozawa method avoids these problems by using multiple measurements at different linear heating rates to calculate the activation energy of a decomposition reaction without the use of a reaction model (model-free isoconversion method).²⁶

Ozawa found this method to be particularly useful for calculating activation energies when two or more parallel processes occur.²⁶ E_a calculations for multi-step reaction mechanisms using simulated data have shown that model-free isoconversion methods are more consistent than single thermal analysis curve fitting.²⁷⁻³¹ Khanna et al. employed the methods developed by Freeman-Carroll and Ozawa for studies of the thermal degradation of aromatic polyamides and found that the model-free Ozawa method was more consistent for calculating E_a values of reactions with varying reaction order (n).³² Therefore, we will investigate the kinetics of LPE cracking mechanisms by using the model-free isoconversion method.

Many studies using TGA for kinetic analysis of polyethylene degradation have been documented.³³⁻⁴⁷ The kinetic parameters of the catalytic cracking of PE with acid catalysts have been calculated for the simple decomposition model shown in equation [1].³³⁻³⁹ Similar TGA studies have been used to explore the kinetics of PE catalytic cracking by using the model-free method proposed by Ozawa.⁴⁰⁻⁴⁷ Reported PE cracking activation energies for various catalysts range between 13-43 kcal/mol.^{34,37,39,43-44,47-48} These values are similar to those reported for small molecule catalyzed reactions: β -scission (18-36 kcal/mol)¹⁷, hydrogen transfer (i.e. disproportionation) (ca. 10 kcal/mol)⁶², acid catalyzed hydrocracking (9.5-16.7 kcal/mol), and bifunctional catalyzed hydrocracking (21.7-43.5 kcal/mol).^{11-12,63} All of the PE cracking reports were based on degradation studies that involved calculating a single E_a value for the entire cracking process. Volatile product slates derived from the catalytic cracking of LPE can differ significantly with temperature (Chapter 4). Therefore, rather than reporting a single E_a value, E_a values that represent the formation of individual products would be more useful.

By using TGA, it is impossible to obtain mechanistic information regarding specific products. However, TA-MS results can be used to calculate kinetic parameters for specific volatile products formed during polymer decomposition.⁴⁸⁻⁵¹ Vyazovkin developed methods for interpreting changes in isoconversion kinetic parameters derived from Ozawa's equations.⁵¹⁻⁶⁰ This approach was used here to calculate kinetic parameters for the formation of specific volatile product classes during LPE catalytic cracking.

Effective activation energies (E_a) were calculated from TA-MS results by using a modification of the isoconversion method developed by Ozawa.⁵¹⁻⁶⁰ The isoconversion method is based on the assumption that the state of a system at an arbitrary conversion (C) is independent of heating rate. The method assumes that a single process is responsible for the physical change, but does not require a specific reaction model (model-free).⁵¹⁻⁵² Based on the Arrhenius equation, the kinetics of solid sample reactions can be described by:⁵⁴⁻⁵⁵

$$d(C)/dt = k(T)f(C) = A \exp(-E_a/RT)f(C) \quad [2]$$

where $f(C)$ is the reaction model in terms of the conversion, $k(T)$ is the rate constant, T is the absolute temperature, t is time, R is the gas constant (1.987 cal/mol·K). A is the frequency (pre-exponential) factor, and E_a is the activation energy. Vyazovkin⁵⁴ states that if a measured physical value is proportional to the extent of conversion (e.g. mass loss, pressure and/or volume of a released gas), numerical differentiation can be used to estimate Arrhenius parameters by equation [2]. However, numerical differentiation considerably lowers the signal-to-noise ratio of experimental data. Integration of

equation [2] provides another basis for evaluating Arrhenius parameters from experimentally derived data.

$$g(C) \equiv \int_0^C [1/f(C)]d(C) = A \int_0^t \exp[-E_a/RT(t)]dt \quad [3]$$

In equation [3], $g(C)$ is the integral form of the reaction model and $T(t)$ is a function that represents the variation of temperature during a given measurement. The variation in temperature during the experiment must be known in order to integrate equation [3]. If a constant heating rate is applied, then $T(t) = T_0 + Ht$, where T_0 is the initial temperature and H is the heating rate (dT/dt). Substitution into equation [3] leads to equation [4], which has no analytical solution.⁵⁴

$$g(C) = A/H \int_0^t \exp[-E_a/RT]dT = (A/H)I(E_a, T) \quad [4]$$

From the assumption in the isoconversion method that the integrated reaction model $g(C)$ depends on conversion but not heating rate, $g(C)$ is constant at a given conversion. The integral of [4] ($I(E_a, T)$) can be replaced by Doyle's approximation⁶¹ when $E_a/RT \geq 20$ (Equation [5]). Linear equations of $\ln(H)$ with respect to $1/T$ at a given conversion can then be obtained by equation [6], or more simply by equation [7].

$$I(E_a, T) \approx (E_a/R) \exp(-5.331 - 1.052E_a/RT) \quad [5]$$

$$\ln(H) = -1.052E_a/RT + \ln[(AE_a/g(C)R) - 5.331] \quad [6]$$

$$\ln(H) = -1.052E_a/RT + B \quad [7]$$

The isoconversion method derivation assumes that the E_a value calculated at a given conversion represents a single reaction process. Guidelines for the interpretation of

isoconversion E_a vs. conversion plots have been described by Vyazovkin et al.⁵¹ and have been applied in our laboratory by Bonnet et al.⁴⁰⁻⁴¹ When a single process is responsible for a temperature dependent physical change, calculated E_a values are constant with respect to conversion.⁵⁶ However, when contributions from multiple processes change with conversion, E_a values change. An increase in E_a value with respect to conversion results from increased contribution from a parallel reaction with higher E_a . E_a values decrease with respect to conversion when there is a change in the rate limiting step (RLS) or a decreased contribution from a higher E_a process.

LPE cracking consists of complex parallel processes. Therefore, calculated effective activation energies do not represent a single reaction, but rather multiple processes can contribute to the formation of a specific product. Thus, effective activation energies will be used only to characterize changes in reaction mechanisms. It will not be possible to relate effective activation energy changes to specific reaction mechanism parameters.

3.3 Experimental

TA-MS provides structural information regarding volatiles generated during thermal analysis and is therefore very useful for studies where multiple volatiles are produced. Previous work in our laboratory has demonstrated the use of the isoconversion method with TA-MS data for calculating E_a values for specific volatile products formed during calcium oxalate and poly(vinylbutyral) decompositions.⁴⁰⁻⁴¹ However, lack of species-specific ions precludes calculation of E_a values for the formation of individual cracking products. Vyazovkin⁵¹ has shown that the E_a values calculated for the m/z 41-43 ions detected by using TA-MS during the thermal degradation of polypropylene

followed similar trends with respect to polymer conversion. No information was given on the mechanism of formation of each ion, but it was stated that shape similarities between the E_a vs. polymer conversion plots meant that these three ions were formed by similar mechanisms.⁵¹

Isoconversion experiments were performed by using the TA-MS combination previously described in Chapter 2. The MS interface temperature was set to 250 °C. Approximately 5 mg (± 1 mg) of LPE/catalyst sample was analyzed in flowing (50 mL/min) helium or hydrogen. The MS was set to scan at 7.686 sec intervals by integrating for 5 ms and signal averaging 25 times over a mass range of 35-95. The MS ion source pressure was maintained between $1-1.2 \times 10^{-5}$ Torr by adjusting the back split valve (Figure 2-6). The sample was purged for at least 30 min and then the MS ion source was allowed to stabilize by collecting background spectra for 10-20 min prior to analysis. The sample temperature ramp was initiated after a level baseline was achieved in the MS. Separate samples were subjected to linear heating ramps of 5, 10, 15, and 25 °C/min under the same reaction conditions. When the sample temperature reached 80-110 °C, MS scanning was stopped for 1-2 min prior to analysis of the sample, which was initiated at sample temperatures between 100-120 °C. This procedure was utilized to insure the initial linearity of the temperature ramp and for stabilization (thermal equilibrium) of the MS ionization chamber. MS data collection was initiated after the sample temperature reached 100 °C for the LPE/HZSM-5 samples and 120 °C for the LPE/HY and LPE/HMCM-41 samples. Sample temperatures were measured and ion signals were collected by using the IPS and Technivent software described in Chapter 2.

A computer program was written to integrate selected ion signal profiles and to calculate effective E_a values. E_a values were calculated by equation [7] for selected ions at 0.01 increments from 0.01 to 0.99 fractional integrated ion signal (i.e. conversion). The standard deviations of the slopes of $\ln(H)$ vs. $1/T$ plots (equation [7]) were used as error estimates. E_a value errors were found to be less than 5% between 0.05 and 0.95 fractional integrated ion signal for all samples except the LPE/PtHZSM-5 (He) and LPE/HMCM-41 (He) samples. Vyazovkin reported that errors of 5% or less are commonly accepted in E_a value measurements by using the model-free isoconversion method.⁵⁶ Large errors were observed at low fractional integrated ion signal for the LPE/PtHZSM-5 (He) (m/z 57) and LPE/HMCM-41 (He) (m/z 55) samples. The large errors for these two samples may be due to a combination of effects. One effect could be due to variation in the product slate when the sample was heated. The product slate changed at low temperature (low fractional integrated ion signal) for the LPE/PtHZSM-5 (He) sample (Chapter 4). A second effect could be due to methods by which temperature and fractional integrated ion signals were calculated by the program. Low ion signal signal-to-noise may result in large errors in temperatures associated with small fractional integrated ion signals.

Figures 3-1 to 3-3 depict the process by which E_a values were calculated for the m/z 57 ion signal detected from the LPE/HY (He) sample. Figure 3-1 shows the effect of heating rate (H) on the integrated ion signal profiles for m/z 57. Results for eight samples, two for each heating rate of 5, 10, 15, 25 °C/min are shown. Experimental reproducibility is reflected by the nearly overlapping plots in Figure 3-1.

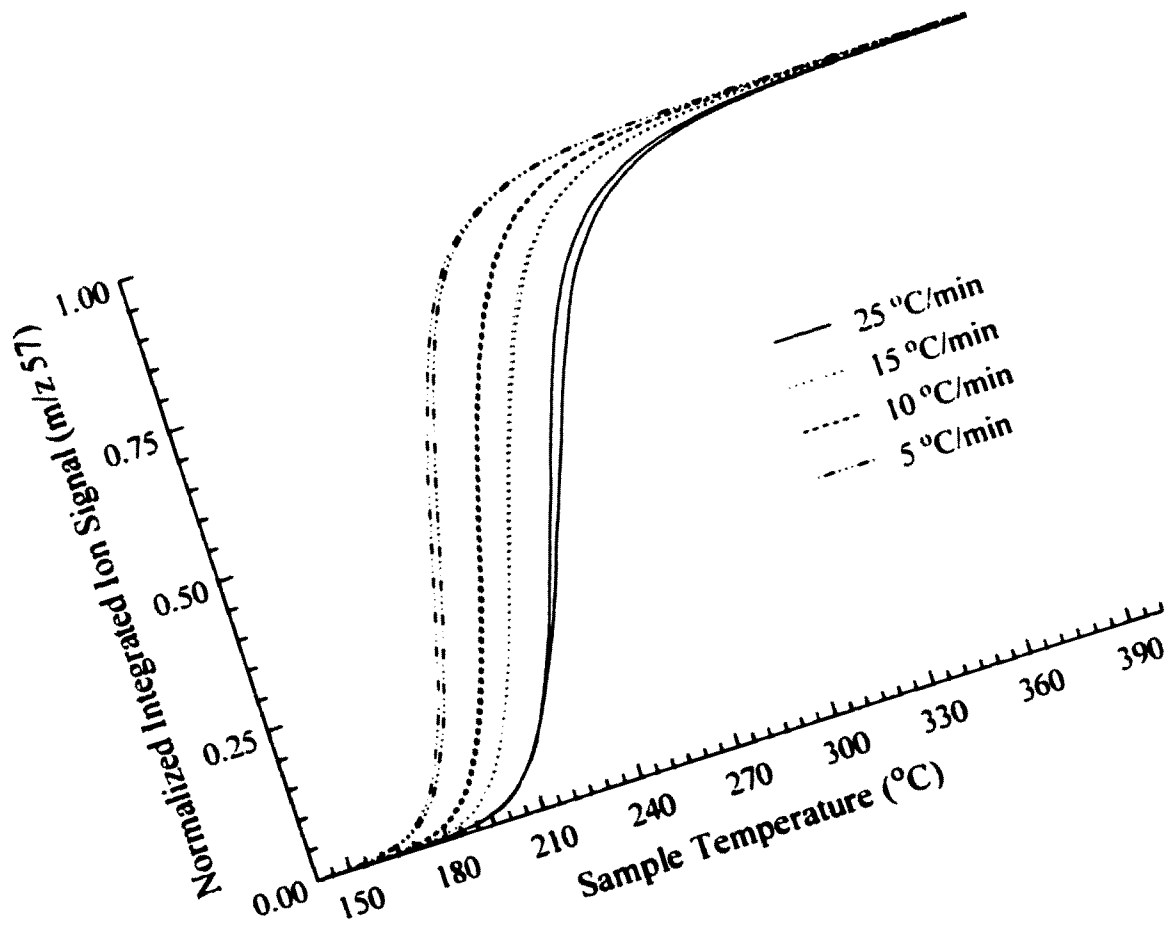


Figure 3-1: Normalized integrated m/z 57 ion signal versus sample temperature for LPE/HY heated in helium

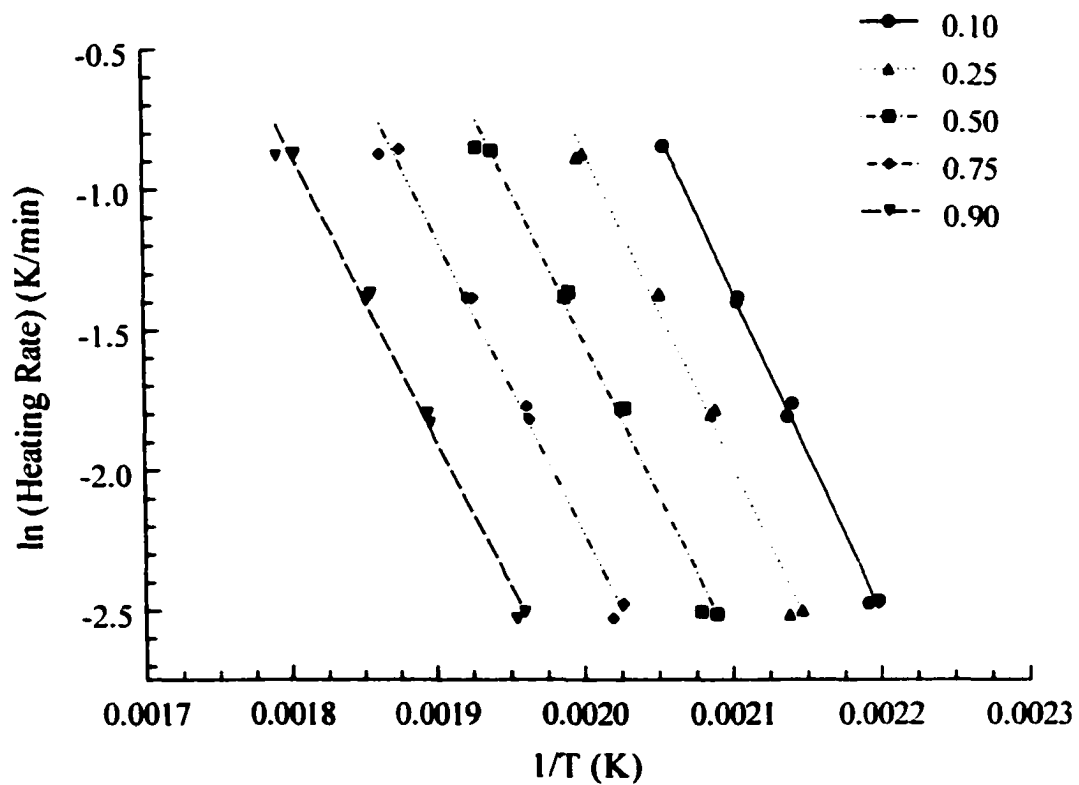


Figure 3-2: Natural log of heating rate versus inverse absolute temperature at 0.10, 0.25, 0.50, 0.75, and 0.90 fractional integrated m/z 57 ion signal for LPE/HY heated in helium

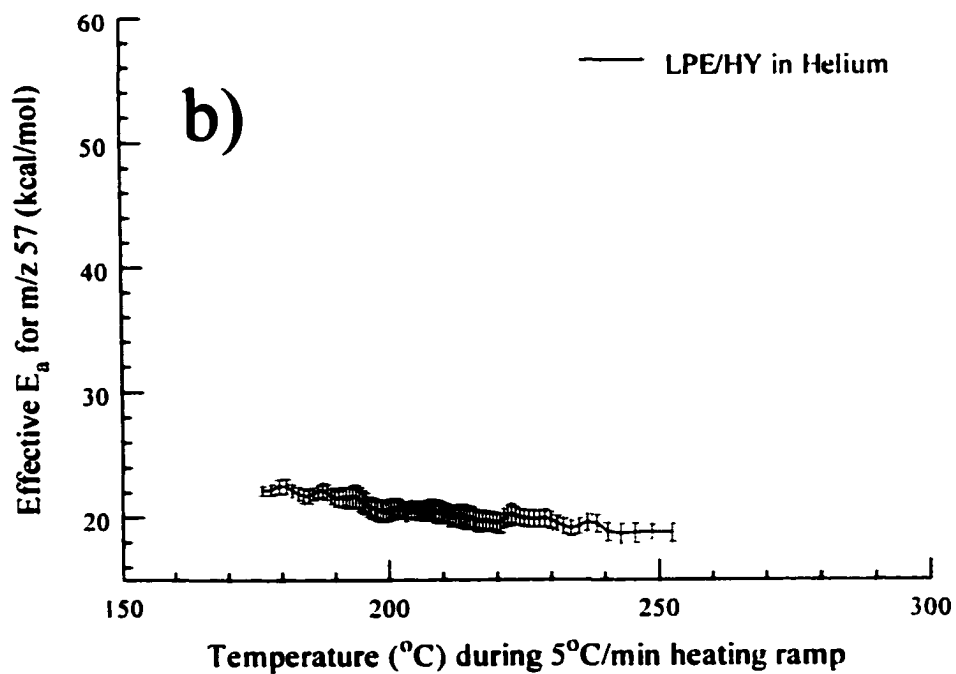
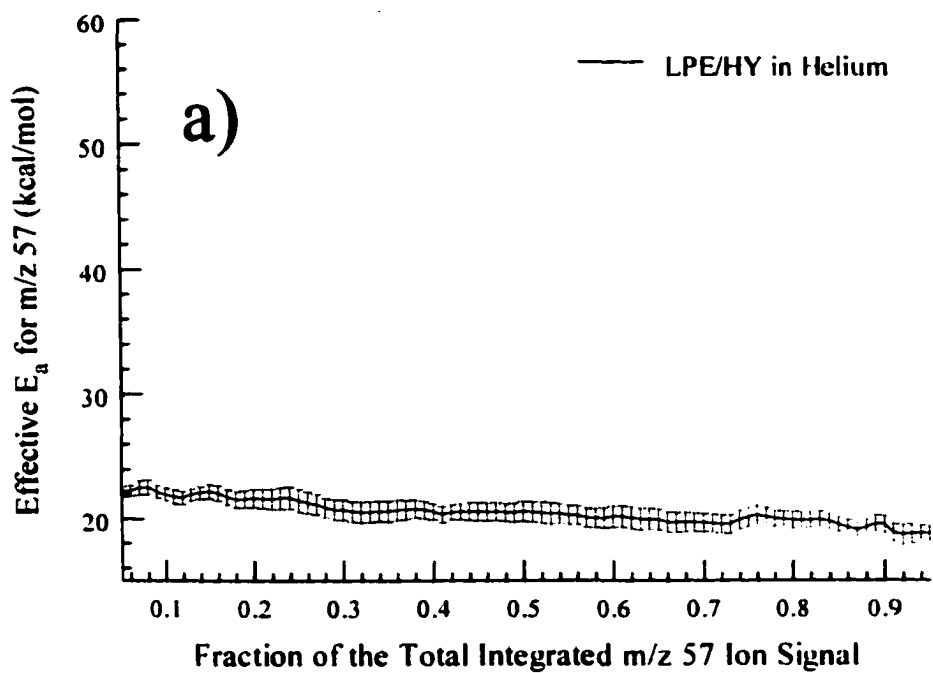


Figure 3-3: a) E_a vs. Fractional integrated ion signal plot for the m/z 57 ion from LPE/HY heated in helium b) E_a vs. Temperature plot for the m/z 57 ion from LPE/HY heated in helium

From this data, linear plots of $\ln(H)$ vs. $1/T$ (Equation [7]) for specified fractional integrated ion signal values were made. E_a values were calculated from the slopes of these lines at 0.01 fractional integrated ion signal intervals. Figure 3-2 shows linear plots of all eight points (one for each curve in Figure 3-1) at 0.10, 0.25, 0.50, 0.75, and 0.90 fractional integrated ion signal. Plots of a) E_a versus fractional integrated ion signal and b) E_a versus temperature are shown in Figure 3-3. E_a versus temperature plots are important for comparing profiles representing substances with different evolution temperatures. Because evolution profiles (and fractional integrated ion signal) depend on sample heating rate, a specified heating rate is required for the generation of E_a versus temperature plots. The x-axes in Figure 3-3 show the range of fractional integrated ion signal (0.05-0.95) and the corresponding sample temperature at the calculated fractional integrated ion signal when heating the sample at 5 °C/min.

Many different volatile products are evolved during LPE catalytic cracking. Because volatile products consisted mainly of homologues, no species-specific ions were found by TA-MS. Mass spectrometer ions at m/z 55 ($C_4H_7^+$) and 57 ($C_4H_9^+$) were found to be representative of volatile olefins and paraffins, respectively. Volatile alkyl aromatics were represented by the m/z 91 tropylium ion ($C_7H_7^+$). However, the degree to which these ions were representative of these volatile products varied. Figures 3-4 to 3-6 depict how the selectivity of m/z 55 for volatile olefin formation was calculated from TA-GC/MS repetitive injection chromatograms for the LPE/HZSM-5 (He) sample. Figures 3-4a and 3-4b show the repetitive injection TIC chromatogram and the m/z 55 ion signal chromatogram obtained when the LPE/HZSM-5 (He) sample temperature reached 150 °C.

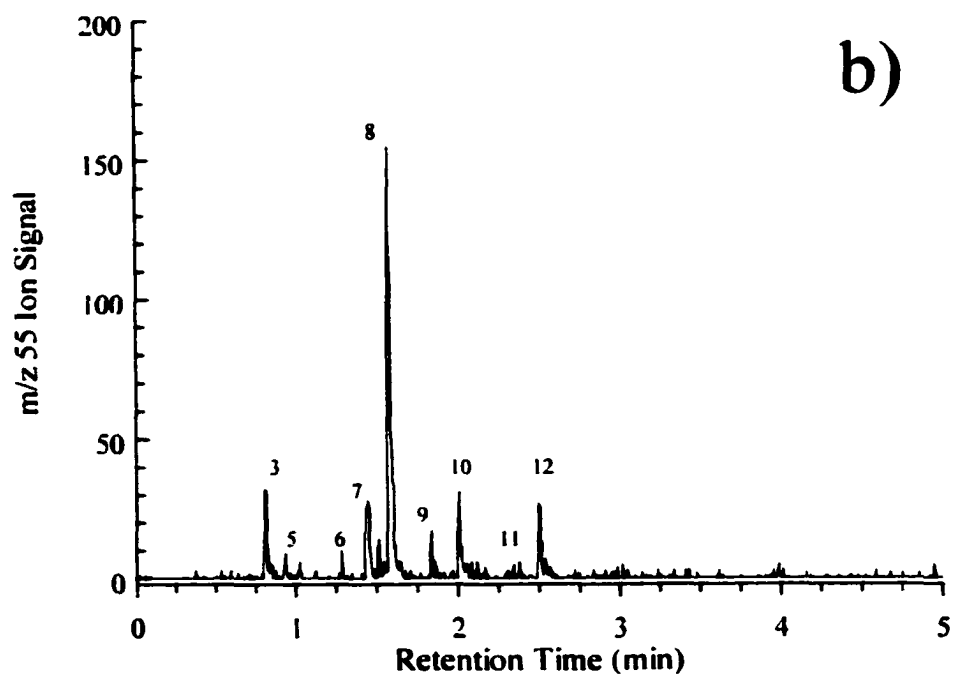
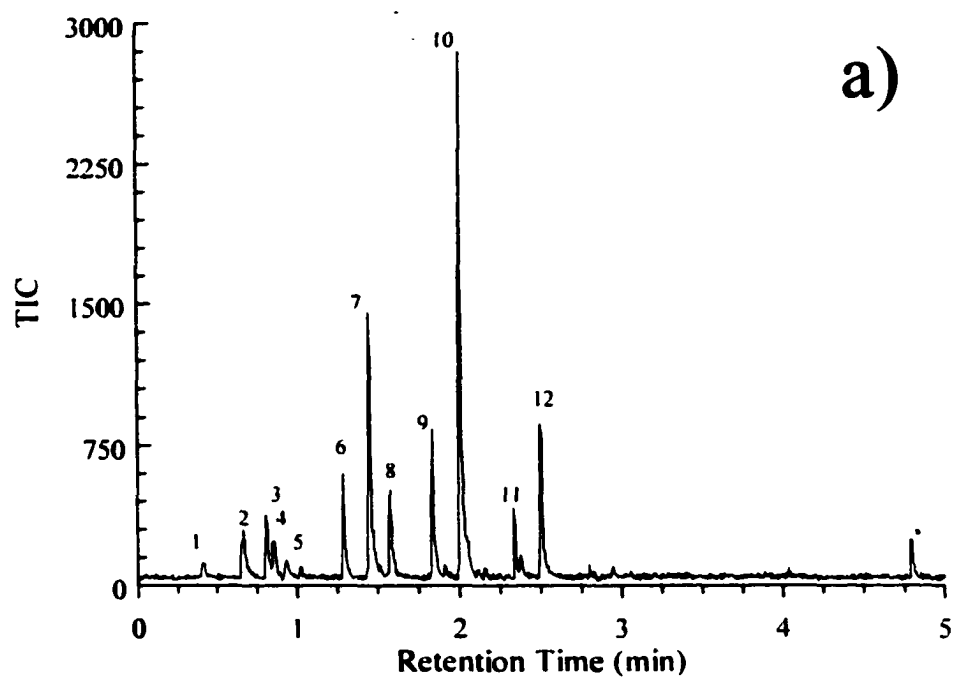


Figure 3-4: Demonstrates the selectivity of m/z 55 for olefin formation by heating the LPE/HZSM-5 sample in helium a) TIC chromatogram from volatiles formed at 150°C b) m/z 55 signal chromatogram from volatiles formed at 150°C (see Table 3-1)

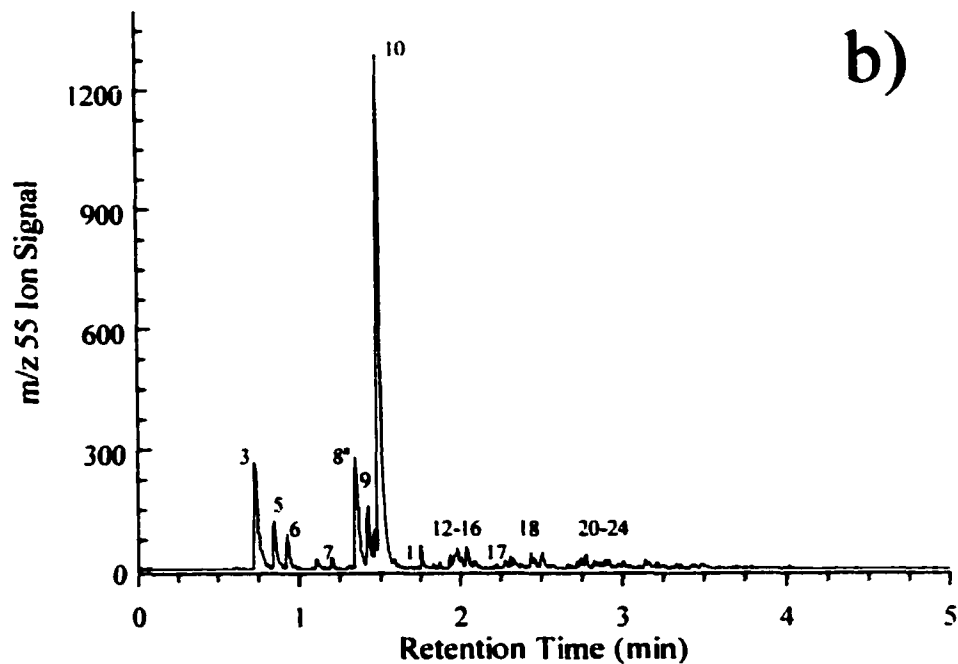
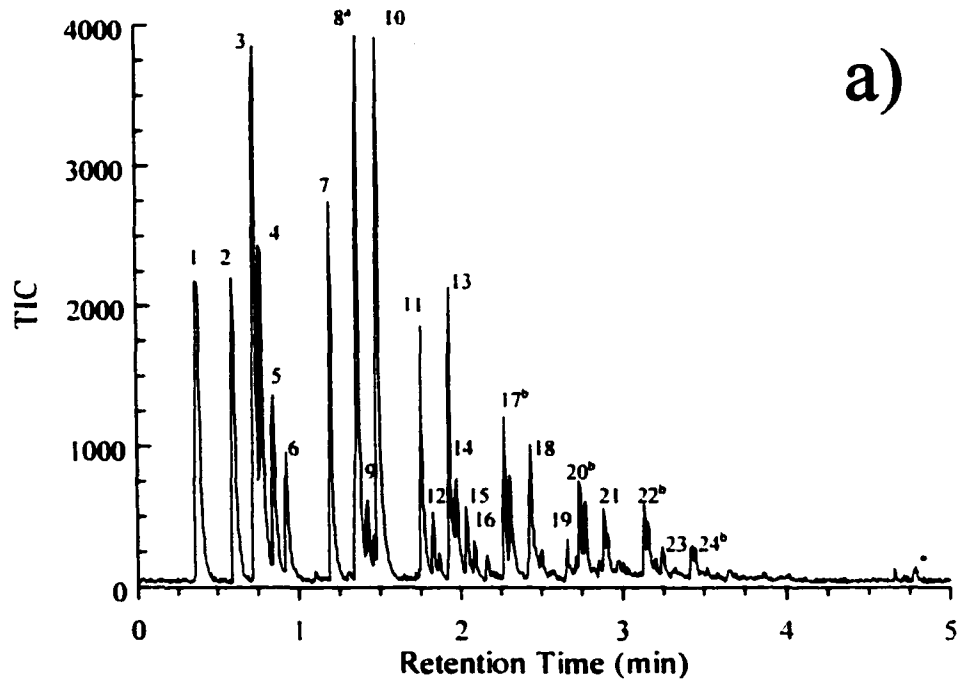


Figure 3-5: Demonstrates the selectivity of m/z 55 for olefin formation by heating the LPE/HZSM-5 sample in helium a) TIC chromatogram from volatiles formed at 230°C b) m/z 55 signal chromatogram from volatiles formed at 230°C ^a C_3 -alkene product identified in front shoulder of peak ^bPeaks are not baseline separated, but are product isomers (see Table 3-1)

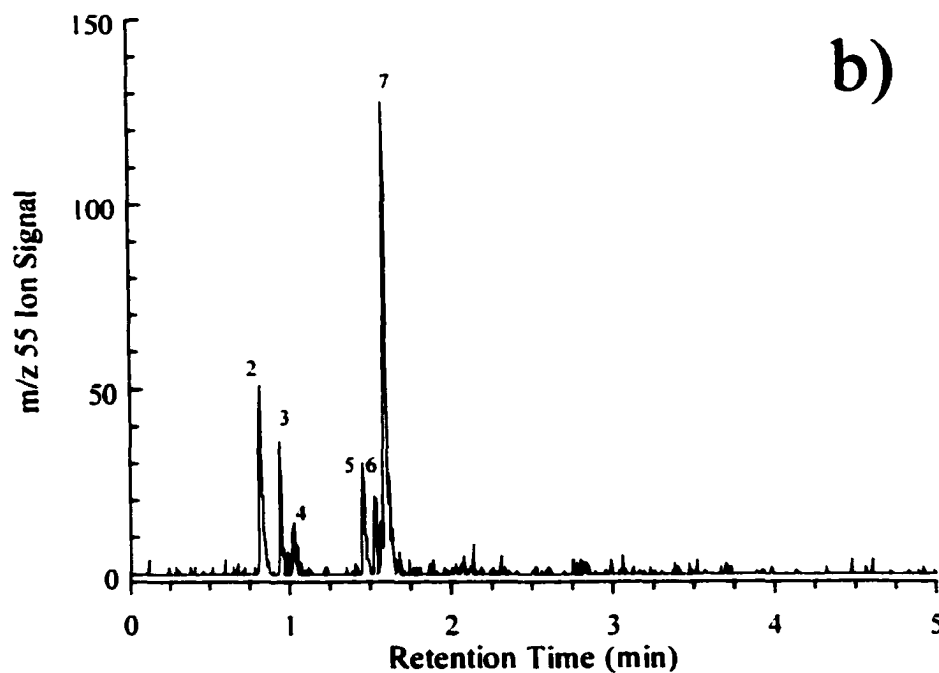
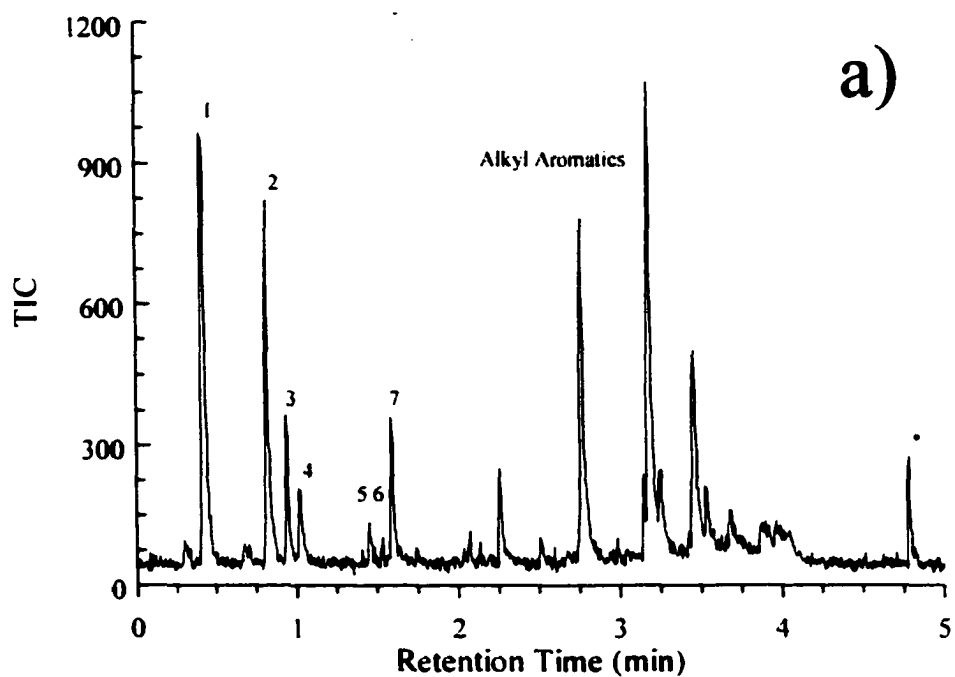


Figure 3-6: Demonstrates the selectivity of m/z 55 for olefin formation by heating the LPE/HZSM-5 sample in helium a) TIC chromatogram from volatiles formed at 290°C b) m/z 55 signal chromatogram from volatiles formed at 290°C (see Table 3-1)

Each peak in the chromatograms was identified by using the methods described in Chapter 2. A listing of the peaks and their identities are given in Table 3-1. Peak numbers 1, 3, 5, and 8 were identified as C₃-C₅ olefins. However, only olefins ≥C₄ can be represented by m/z 55. The percentage of the integrated m/z 55 peak area obtained for olefin products (peaks 3, 5, and 8) identified in Figure 3-4b was divided by the total m/z 55 integrated area (peaks 3-12) to calculate the m/z 55 selectivity for olefin formation as illustrated by equation [8].

$$\text{m/z 55 Olefin Selectivity} = \frac{\text{Integrated m/z 55 peak area (Olefins only)}}{\text{Total integrated m/z 55 peak area}} \times 100 \quad [8]$$

The selectivity for m/z 55 for the formation of olefins at 150 °C was calculated to be 58%. Low selectivity for olefin formation resulted because a large fraction of the total m/z 55 ion signal (peaks 6, 7, and 9-12 in Figure 3-4b) was contributed by paraffin products. Therefore, E_a values calculated for m/z 55 ion signals may not accurately represent olefin formation at this temperature. As the sample temperature increased, the amount of volatile olefins also increased. Figure 3-5 shows the TIC and m/z 55 chromatograms obtained from the sample injection at 230 °C for the LPE/HZSM-5 (He) sample. Many of the peaks in Figure 3-5b were due to olefins (Table 3-1, 230 °C). A higher m/z 55 selectivity (80%) for olefins at 230 °C was calculated by using equation [8]. The higher selectivity suggests that the 230 °C E_a value may be more accurate than the 150 °C E_a value. All of the peaks (1-7) in Figure 3-6b for the 290 °C sample injection were identified as olefin products from the LPE/HZSM-5 (He) sample (Table 3-1). Volatile products detected with R_t ≥2.0 min (Figure 3-6a) were identified as alkyl aromatics (not listed in Table 3-1).

Figure 3-4: Sample Injection at 150 °C*

Peak #	R _t (min)	Identity	Peak #	R _t (min)	Identity
1	0.40	C ₃ -alkene	7	1.45	C ₅ -alkane
2	0.70	C ₄ -alkane	8	1.60	C ₅ -alkene/ane
3	0.80	C ₄ -alkene	9	1.85	C ₆ -alkane
4	0.85	C ₄ -alkane	10	2.05	C ₆ -alkane
5	0.95	C ₄ -alkene	11	2.35	C ₇ -alkane
6	1.30	C ₅ -alkane	12	2.50	C ₇ -alkane

Figure 3-5: Sample Injection at 230 °C*

Peak #	R _t (min)	Identity	Peak #	R _t (min)	Identity
1	0.40	C ₃ -alkene	13	1.90	C ₆ -alkane
2	0.65	C ₄ -alkane	14	1.95	C ₆ -alkene
3	0.75	C ₄ -alkene	15	2.05	C ₆ -alkene
4	0.80	C ₄ -alkane	16	2.10	C ₆ -alkene
5	0.85	C ₄ -alkene	17	2.30	C ₇ -alkane
6	0.95	C ₄ -alkene	18	2.45	C ₇ -alkane
7	1.20	C ₅ -alkane	19	2.65	C ₇ -diene
8 ^a	1.35	C ₅ -alkane	20	2.75	C ₈ -alkane
9	1.40	C ₅ -alkene	21	2.90	C ₈ -alkane
10	1.50	C ₅ -alkene	22	3.20	N/A
11	1.75	C ₆ -alkane	23	3.25	N/A
12	1.80	C ₆ -alkene	24	3.45	N/A

Figure 3-6: Sample Injection at 290 °C*

Peak #	R _t (min)	Identity	Peak #	R _t (min)	Identity
1	0.40	C ₃ -alkene	5	1.45	C ₅ -alkene
2	0.80	C ₄ -alkene	6	1.55	C ₅ -alkene
3	0.95	C ₄ -alkene	7	1.65	C ₅ -alkene
4	1.05	C ₄ -alkene			

*Peak at ≈4.75 min. in each chromatogram was identified as an air leak

Table 3-1: Identities of the numbered peaks from Figures 3-4 to 3-6

The m/z 55 selectivity for volatile olefins at 290 °C was calculated to be $\geq 99\%$ because no other products contributed to the m/z 55 ion signal. Thus, E_a values should provide an accurate representation of olefin formation mechanisms at this temperature. The TA-GC/MS chromatograms for the LPE/HZSM-5 (He) sample are shown in Figure 3-7a. The volatile product evolution profile for C_4 olefins is shown in Figure 3-7b. The TA-MS m/z 55 ion signal profile is shown in Figure 3-7c. The low selectivity for m/z 55 for olefin formation below 200 °C can be correlated to the difference in shapes of Figures 3-7b and 3-7c. In general, when E_a value selectivities were low (e.g. 75%), activation energy accuracies were considered questionable and the data was not incorporated into temperature profiles shown in Chapter 4 and 5.

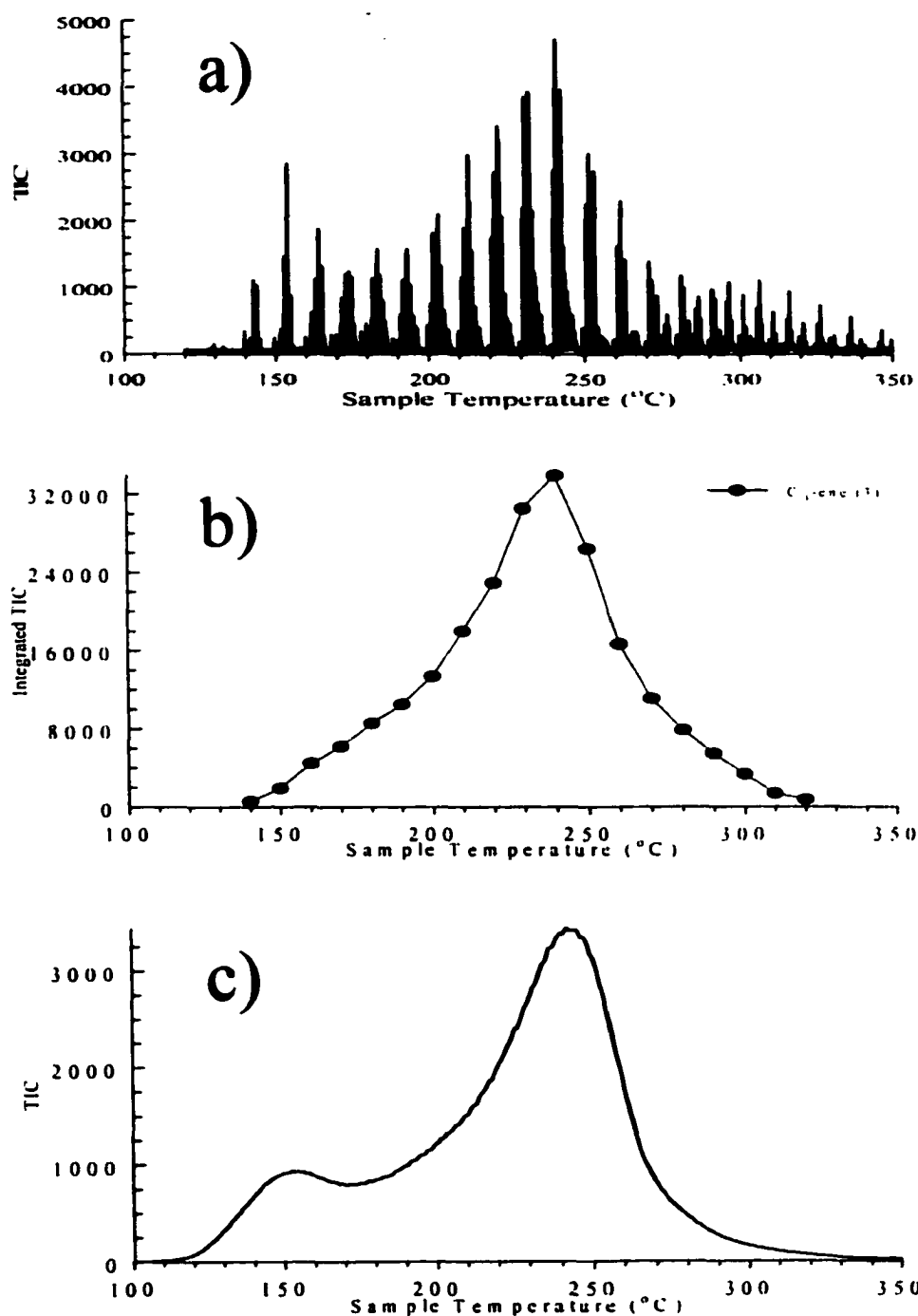


Figure 3-7: a) TA-GC/MS repetitive injection chromatograms obtained from LPE/HZSM-5 heated in helium (2 °C/min) b) Volatile product evolution profile calculated for C₄ olefins c) TA-MS profile for m/z 55 obtained from heating LPE/HZSM-5 in helium (5 °C/min)

3.4 References

1. Jentoft, F.C.; Gates, B.C.; *Top. Catal.* 1997, 4, 1-13 "Solid-Acid-Catalyzed Alkane Cracking Mechanisms: Evidence from Reactions of Small Probe Molecules"
2. Shimizu, K.; Sunagawa, T.; Vera, C.R.; Ukegawa, K.; *Appl. Catal. A* 2001, 206, 79-86 "Catalytic Activity for Synthesis of Isomerized Products from Benzene over Platinum-Supported Sulfated Zirconia"
3. Tromp, M.; van Bokhoven, J.A.; Garriga Oostenbrink, M.T.; Bitter, J.H.; de Jong, K.P.; Koningsberger, D.C.; *J. Catal.* 2000, 190, 209-214 "Influence of the Generation of Mesopores on the Hydroisomerization Activity and Selectivity of n-Hexane over Pt/Mordenite"
4. Pieterse, J.A.Z.; Seshan, K.; Lercher, J.A.; *J. Catal.* 2000, 195, 326-335 "Structure-Activity Correlations for TON, FER, and MOR in the Hydroisomerization on n-Butane"
5. Raybaud, P.; Patriceon, A.; Toulhoat, H.; *J. Catal.* 2001, 197, 98-112 "The Origin of the C₇-Hydroconversion Selectivities on Y, β, ZSM-22, ZSM-23, and EU-1 Zeolites"
6. Denayer, J.F.; Baron, G.V.; Vanbutsele, G.; Jacobs, P.A.; Martens, J.A.; *J. Catal.* 2000, 190, 469-473 "Evidence of Alkylcarbenium Ion Reaction Intermediates from Intrinsic Reaction Kinetics of C₆-C₉ n-Alkane Hydroisomerization and Hydrocracking on Pt/H-Y and Pt/USY Zeolites"
7. Degnan, T.F.; Kennedy, C.R.; *AIChE J.* 1993, 39, 607-614 "Impact of Catalyst Acid/Metal Balance in Hydroisomerization of Normal Paraffins"
8. Martens, G.G.; Marin, G.B.; Martens, J.A.; Jacobs, P.A.; Baron, G.V.; *J. Catal.* 2000, 195, 253-267 "A Fundamental Kinetic Model for Hydrocracking of C₈ to C₁₂ Alkanes on Pt/US-Y Zeolites"
9. Chevalier, F.; Guisnet, M.; Maurel, R.; *Proc. Int. Congr. Catal.* 6th 1977, 1, 478-487 "Tracer Study of the Isomerization of Paraffins on Bifunctional Catalysts"
10. Bond, G.C.; *Catal. Today* 1999, 49, 41-48 "Kinetics of Alkane Reactions on Metal Catalysts: Activation Energies and the Compensation Effect"
11. Perrotin, L.; Finiels, A.; Fajula, F.; Cholly, T.; *Stud. Surf. Sci. Catal.* 2001, 135, 3838-3845 "Peculiarities in the Hydroconversion of n-Hexadecane over Bifunctional Catalysts"
12. de Gauw, F.J.M.M.; van Grondelle, J.; van Santen, R.A.; *J. Catal.* 2002, 206, 295-304 "The Intrinsic Kinetics of n-Hexane Hydroisomerization Catalyzed by Platinum-Loaded Solid-Acid Catalysts"

13. Guisnet, M.; Fouche, V.; Appl. Catal. 1991, 71, 295-306 "Isomerization of n-Hexane on Platinum Dealuminated Mordenite Catalysts"
14. Allain, J.F.; Magnoux, P.; Schulz, Ph.; Guisnet, M.; Appl. Catal. A 1997, 152, 221-235 "Hydroisomerization of n-Hexane over Platinum Mazzite and Platinum Mordenite Catalysts Kinetics and Mechanism"
15. van de Runstraat, A.; Kamp, J.A.; Stobbelaar, P.J., van Grondelle, J.; Krijnen, S.; van Santen, R.A.; J. Catal. 1997, 171, 77-84 "Kinetics of Hydro-Isomerization of n-Hexane over Platinum Containing Zeolites"
16. Noordhoek, N.J.; Schuring, D.; de Gauw, F.J.M.M.; Anderson, B.G.; de Jong, A.M.; de Voight, J.A.; van Santen, R.A.; Ind. Eng. Chem. Res. 2002, 41, 1973-1985 "In Situ Study of Alkane Conversion on Pt-Loaded Acidic Zeolites"
17. Lukyanov, D.B.; Shtral, V.I.; Khadzhiev, S.N.; J. Catal. 1994, 146, 87-92 "A Kinetic Model for the Hexane Cracking over H-ZSM-5"
18. Frash, M.V.; Kazansky, V.B.; Rigby, A.M.; van Santen, R.A.; J. Phys. Chem. B 1998, 102, 2232-2238 "Cracking of Hydrocarbons on Zeolites Catalysts: Density Functional and Hartee-Fock Calculations on the Mechanisms of the β -Scission Reaction"
19. Aberuagba, F.; React. Kinet. Catal. Lett. 2000, 70, 243-249 "Aromatization of Heptene-2 on Pt/Al₂O₃ Catalysts"
20. Wootsch, A.; Paal, Z.; J. Catal. 1999, 185, 192-198 "n-Hexane Reactions on EUROPT-1 at Different Hydrogen Pressures: The Possibility of Calculating Kinetic Parameters"
21. Wootsch, A.; Paal, Z.; J. Catal. 2002, 205, 96-96 "Reactions of n-Hexane on Pt Catalysts: Reaction Mechanism as Revealed by Hydrogen Pressure and Compensation Effect"
22. Lane, G.S.; Modica, F.S.; Miller, J.T.; J. Catal. 1991, 129, 145-158 "Platinum/Zeolite Catalyst for Reforming n-Hexane: Kinetic and Mechanistic Considerations"
23. Freeman, E.S.; Carroll, B.; J. Phys. Chem. 1958, 62, 394-397 "The Application of Thermoanalytical Techniques to Reaction Kinetics. The Thermogravimetric Evaluation of the Kinetics of the Decomposition of Calcium Oxalate Monohydrate"
24. Friedman, H.L.; J. Polym. Sci.: Part C 1963, n.6, 183-195 "Kinetics of Thermal Degradation of Char-forming Plastics from Thermogravimetry. Application to a Phenolic Plastic"
25. Doyle, C.D.; J. Appl. Polym. Sci. 1961, 5, 285-292 "Kinetic Analysis of Thermogravimetric Data"

26. Ozawa, T.; *Bull. Chem. Soc. Jpn.* 1965, 38, 1881-1886 "A New Method of Analyzing Thermogravimetric Data"
27. Vyazovkin, S.; *Anal. Chem.* 2002, 74, 2749-2762 "Thermal Analysis"
28. Brown, M.E.; Maciejewski, M.; Vyazovkin, S.; Nomen, R.; Sempere, J.; Burnham, A.; Opfermann, J.; Strey, R.; Anderson, H.L.; Kemmler, A.; Keuleers, R.; Janssens, J.; Desseyn, H.O.; Li, C-R.; Tang, T.B.; Roduit, B.; Malek, J.; Mitsuhashi, T.; *Thermochim. Acta* 2000, 355, 125-143 "Computational Aspects of Kinetic Analysis Part A: The ICTAC Kinetics Project-Data Methods and Results"
29. Maciejewski, M.; *Thermochim. Acta* 2000, 355, 145-154 "Computational Aspects of Kinetic Analysis Part B: The ICTAC Kinetics Project - The Decomposition Kinetics of Calcium Carbonate Revisited, or Some Tips on Survival in the Kinetic Minefield"
30. Burnham, A.; *Thermochim. Acta* 2000, 355, 165-170 "Computational Aspects of Kinetic Analysis Part D: The ICTAC Kinetics Project - Multi-Thermal-History Model-fitting Methods and Their Relation to Isoconversional Methods"
31. Roduit, B.; *Thermochim. Acta* 2000, 355, 171-180 "Computational Aspects of Kinetic Analysis Part E: The ICTAC Kinetics Project - Numerical Techniques and Kinetics of Solid State Processes"
32. Khanna, Y.P; Pearce, E.M.; *J. Thermal Anal.* 1983, 26, 107-116 "Aromatic Polyamides VIII. Kinetic Analysis of the Thermal- and Thermo-Oxide Degradation"
33. Carniti, P.; Gervasini, A.; *Thermochim. Acta* 2001, 379, 51-58 "Thermogravimetric Study of the Kinetics of Degradation of Polypropylene with Solid Catalysts"
34. Garforth, A.; Lin, Y-H.; Sharratt, P.; Dwyer, A.; *Stud. Surf. Sci. Tech.* 1999, 121, 197-202 "Catalytic Polymer Degradation for Producing Hydrocarbons over Zeolites"
35. Lin, Y-H.; Hwu, W-H.; Ger, M-D.; Yeh, T-F.; Dwyer, J.; *J. Molec. Catal. A* 2001, 171, 143-151 "A Combined Kinetic and Mechanistic Modeling of the Catalytic Degradation of Polymers"
36. Lin, R.; Ph.D. Dissertation, University of Oklahoma, 1997 "Catalytic Cracking of Poly(ethylene) and Poly(styrene) by Silica-Alumina, HZSM-5 Zeolite, and Sulfated Zirconia"
37. Lin, R.; White, R.L.; *J. Appl. Polym. Sci.* 1995, 58, 1151-1159 "Effects on Catalyst Acidity and HZSM-5 Channel Volume on the Catalytic Cracking of Poly(ethylene)"

38. Lin, R.; Negelein, D.L.; White, R.L.; Preprint Papers - Am. Chem. Soc., Div. Fuel Chem. 1997, 42, 982-986 "Effects of Catalyst Acidity and Structures on Polymer Cracking Mechanisms"
39. Beltrame, P.L.; Carniti, P.; Polym. Deg. Stab. 1989, 26, 209-220 "Catalytic Degradation of Polymers: Part II - Degradation of Polyethylene"
40. Bonnet, E.; M.S. Thesis, University of Oklahoma, 1997 "Effects of Water Vapor on the Thermal Decomposition Mechanisms of Poly(vinyl butyral) Coated on Silica, Mullite, α -Alumina, δ -Alumina"
41. Bonnet, E.; White, R.L.; Thermochim. Acta 1998, 311, 81-86 "Species-Specific Isoconversion Effective Activation Energies Derived by Thermogravimetry-mass Spectrometry"
42. Fernandes Jr., V.J.; Araujo, A.S.; Fernandes, G.J.T.; Matos, J.R.; Ionashiro, M.; J. Thermal Anal. Calorim. 2001, 64, 585-589 "Kinetic Parameters of Polymer Degradation by SAPO-37"
43. Fernandes Jr., V.J.; Araujo, A.S.; Medeiros, R.A.; Matos, J.R.; Mercuri, L.P.; Silva, A.O.; Melo, D.M.A.; J. Thermal Anal. Calorim. 1999, 56, 1279-1282 "Kinetic Parameters of Polyethylene degradation by the Natural Zeolite Chabazite"
44. Fernandes Jr., V.J.; Araujo, A.S.; Fernandes, G.J.T.; J. Thermal Anal. Calorim. 1999, 56, 275-285 "Thermal Analysis Applied to Solid Catalysts - Acidity, Activity, and Regeneration"
45. Fernandes Jr., V.J.; Araujo, A.S.; Fernandes, G.J.T.; J. Thermal Anal. 1997, 49, 355-260 "Catalytic Degradation of Polyethylene Evaluated by TG"
46. Garforth, A.; Fiddy, S.; Lin, Y-H.; Ghanbari-Siakhali, A.; Sharratt, P.; Dwyer, J.; Thermochim. Acta 1997, 294, 65-69 "Catalytic Degradation of High Density Polyethylene: An Evaluation of Mesoporous and Microporous Catalysts Using Thermal Analysis"
47. Lin, Y-H.; Sharratt, P.N.; Garforth, A.A.; Dwyer, J.; Thermochim. Acta 1997, 294, 45-50 "Deactivation of US-Y Zeolite by Formation During the Catalytic Pyrolysis of High Density Polyethylene"
48. Ballistreri, A.; Montaudo, G.; Puglisi, C.; J. Therm. Anal. 1984, 29, 237-241 "Reliability of the Volatilization Method for Determination of the Activation Energy in the Thermal Decomposition of Polymers"
49. Risby, T.H.; Yergey, J.A.; Anal. Chem. 1982, 54, 2228-2233 "Linear Programmed Thermal Degradation Mass Spectrometry of Polystyrene and Poly(vinyl chloride)"

50. Risby, T.H.; Yergey, J.A.; *Anal. Chem.* 1978, 50, 326A-334A "Linear Programmed Thermal Degradation Mass Spectrometry"
51. Vyazovkin, S.; Goryachko, V.; Bogdanova, V.; Guslev, V.; *Thermochim. Acta* 1993, 215, 325-328 "Thermolysis Kinetics of Polypropylene on Rapid Heating"
52. Vyazovkin, S.; Linert, W.; *J. Solid State Chem.* 1995, 114, 392-398 "The Application of Isoconversional Methods for Analyzing Isokinetic Relationships Occurring at Thermal Decomposition of Solids"
53. Vyazovkin, S.V.; Lesnikovich, A.I.; *Thermochim. Acta* 1990, 165, 11-15 "Error in Determining Activation Energy Caused by the Wrong Choice of Process Model"
54. Vyazovkin, S.; *J. Comp. Chem.* 1997, 18, 393-402 "Evaluation of Activation Energy of Thermally Stimulated Solid-State Reactions under Arbitrary Variation of Temperature"
55. Hatakeyama, T.; Quinn, F.X.; *Thermal Analysis - Fundamentals and Applications to Polymer Science*, 2nd Ed.. John Wiley & Sons, Chichester, England 1999
56. Vyazovkin, S.; *Int. J. Chem. Kinet.* 1996, 28, 95-101 "A Unified Approach to Kinetic Processing of Nonisothermal Data"
57. Kelsey, M.S.; *Am. Lab.* 1996, 1, 13-18 "Applications of Model-free Kinetics"
58. Ozawa, T.; Kanari, K.; *Thermochim. Acta* 1994, 234, 41-51 "A Method for Kinetic Analysis of Thermoanalytical Data of Competitive Reactions"
59. Ozawa, T.; *Thermochim. Acta* 1992, 203, 159-165 "Estimation of Activation Energy by Isoconversion Methods"
60. Vyazovkin, S.V.; Lesnikovich, A.I.; *Thermochim. Acta* 1990, 165, 273-280 "An Approach to the Solution of the Inverse Kinetic Problem in the Case of Complex Processes. Part 1. Methods Employing a Series of Thermoanalytical Curves"
61. Doyle, C.D.; *J. Appl. Polym. Sci.* 1962, 6, 639-642 "Estimating Isothermal Life from Thermogravimetric Data"
62. Gao, Y.; Zhang, J.; *Lianyou Sheji* 2000, 30, 34-38 "Study on Hydrogen Transfer Reaction in Catalytic Cracking"
63. Meusinger, J.; Liers, J.; Mosch, A.; Reschetilowski, W. *J. Catal.* 1994, 148, 30-35 "Cracking of n-Heptane on Metal-Free H-ZSM-5 Zeolite at High Hydrogen Pressure"

CHAPTER 4 - RESULTS OF LPE CRACKING AND ISOCONVERSION E_a EXPERIMENTS

4.1 Introduction

Catalytic cracking and hydrocracking of poly(ethylene) (PE) by various zeolite catalysts has been shown in many studies. Acid catalysts are used to reduce the product size distribution, which is dependent on the catalyst properties. Most PE catalytic cracking studies have been performed by heating reactor vessels containing catalyst and polymer and subsequently collecting and analyzing the products. This semi-batch processing approach provides no information regarding the order in which products form. In addition, if sealed reaction vessels are employed, initial reaction products may react with catalyst to form secondary products. Instead, volatile products can be removed from catalysts with an inert purge gas and then analyzed on-line. The three acid catalysts used in this study possess different acid strengths and pore structures. Therefore, information regarding the effects of pore structure and acid strength on cracking processes can be obtained by comparing volatile product evolution profiles and trends in isoconversion E_a values as a function of temperature.

4.2 Experimental Results

This chapter contains experimental results from TA-GC/MS and TA-MS analyses of LPE/catalyst samples heated in helium and hydrogen. Volatile product evolution profiles and isoconversion E_a values are given for each catalyst and reaction condition (i.e. purge gas). For clarity, sample names will be followed by the purge gas in parentheses [e.g. LPE/HZSM-5 (He)]. The effects of catalyst acidity and pore size, the presence of platinum, and reaction environment (He vs. H₂) on evolution profiles and E_a values will be discussed in Chapter 5.

4.2.1 LPE/HZSM-5 (He)

4.2.1a TA-GC/MS Results

Figure 4-1a shows the repetitive injection chromatograms obtained while heating the LPE/HZSM-5 (He) sample. The tic marks on the x-axis in Figure 4-1a denote sample temperatures at which evolved gases were injected into the gas chromatograph. Purge gas effluent was analyzed at 5 min intervals, which corresponded to 10 °C sample temperature increments at the 2 °C/min heating rate. The y-axis represents the total ion current (TIC) detected in the mass spectrometer over the selected mass range (15-160 amu). Volatile products were detected from 130-350 °C. Three volatile product evolution maxima were observed in the chromatograms at 150, 240, and 300 °C. Figure 4-1b shows the negative derivative ($-\Delta mg/\Delta^{\circ}C$) of the TGA weight loss curve for the LPE/HZSM-5 (He) sample. The sample temperature (x-axis) of the TGA curve (Figure 4-1b) was shifted slightly to correlate with the TA-GC/MS results (Figure 4-1a) because the TGA measurements were obtained at a different heating rate (10 °C/min). Three distinct regions of polymer weight loss rate were observed by using TGA. There is a shoulder in the TGA curve between 140-190 °C that corresponds to the first product evolution maximum (Figure 4-1b). Maximum weight loss is observed between 190-260 °C and another shoulder at 260-350 °C correlates with the third maximum in Figure 4-1a.

Figure 4-2 shows the repetitive injection chromatograms obtained at a) 150, b) 240, and c) 300 °C corresponding to the three volatile product evolution maxima. Relative amounts of volatile products can be compared based on the total ion current (TIC) represented by the left y-axis. The dotted line (right y-axis scale) shows the GC heating ramp used to separate the volatile products for each sample injection.

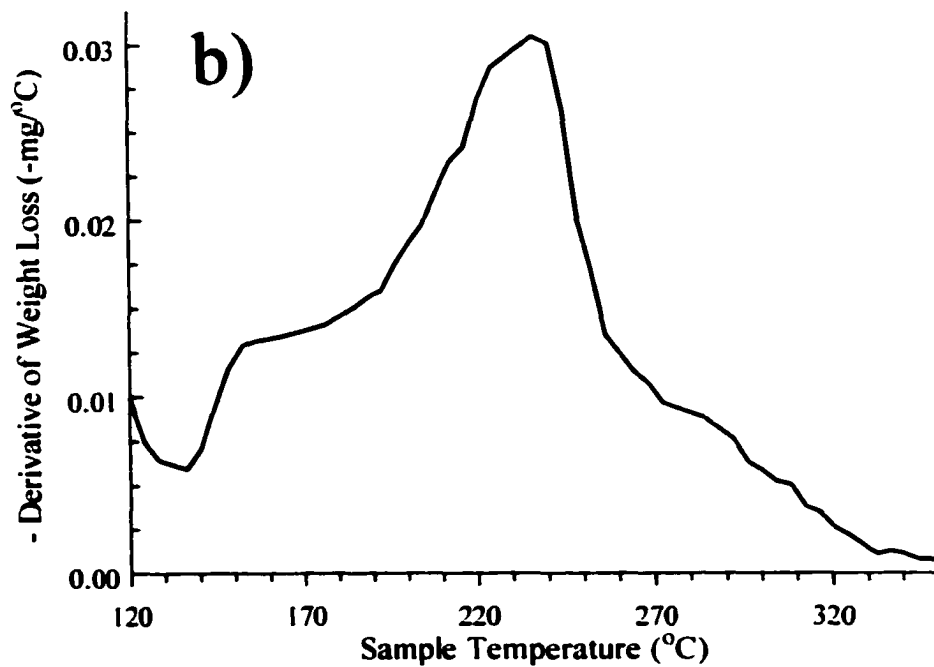
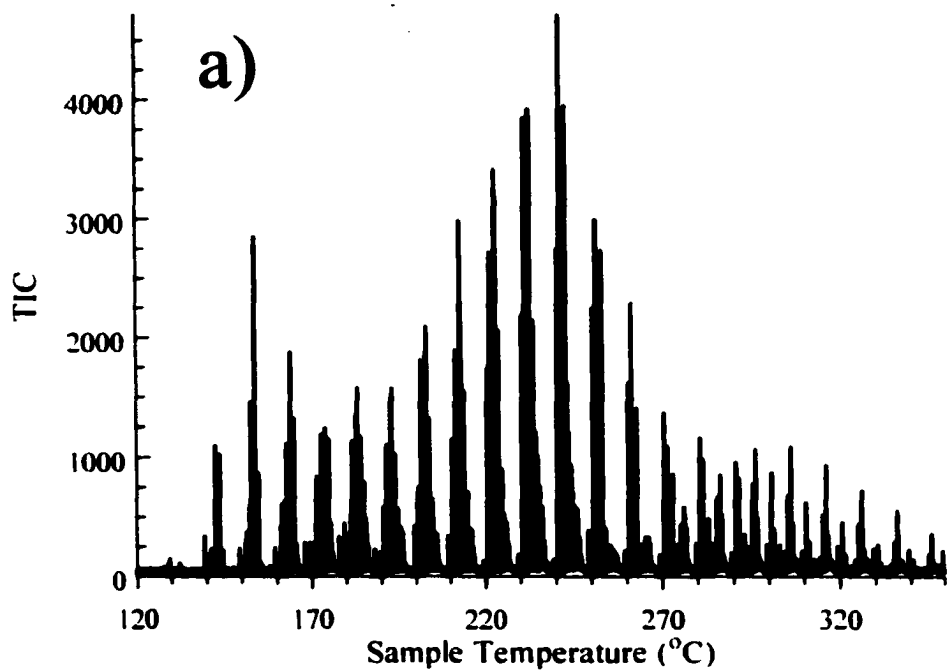


Figure 4-1: a) Repetitive injection chromatogram for LPE/HZSM-5 heated in helium b) Negative derivative of the weight loss obtained for LPE/HZSM-5 heated in helium by using TGA

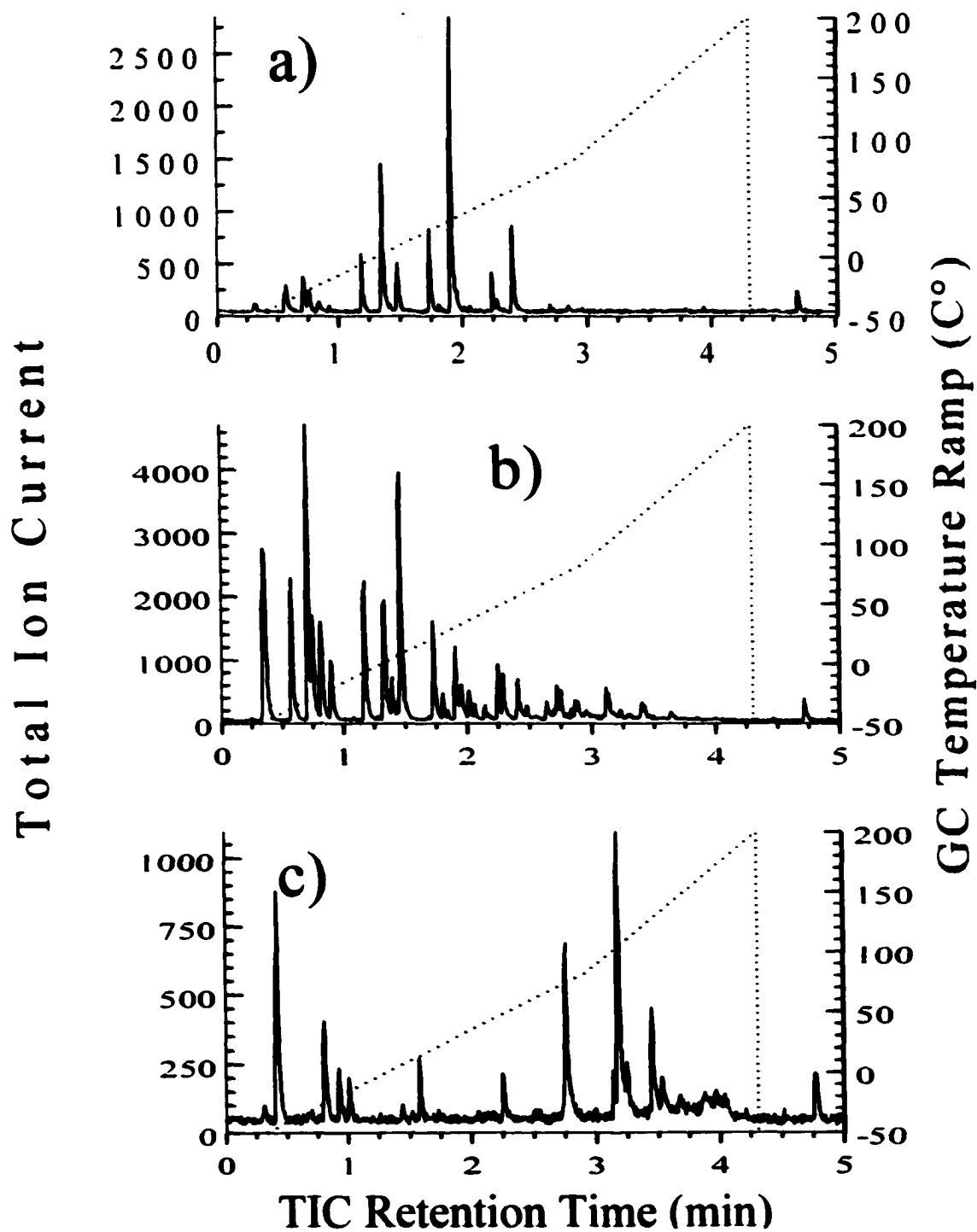


Figure 4-2: Repetitive injection chromatograms obtained from LPE/HZSM-5 heated in helium when the sample temperature reached a) 150 °C b) 240 °C c) 300 °C

The small air peak at $R_t \approx 4.75$ min in each Figure 4-2 chromatogram was caused by leakage of the six port injection valve when it was rotated back to the load position (Chapter 2). At 150 °C (Figure 4-2a), only 14 volatile hydrocarbons were detected, most of which were low molecular weight substances with retention times (R_t) less than 2.5 min. When the sample temperature reached 240 °C (Figure 4-2b), an increase in the total number of volatile products (27) was detected as well as the amount of volatile products formed with R_t of less than 1.5 min. Fewer volatile products (12) were detected at 300 °C (Figure 4-2c). Most volatiles that evolved at 300 °C had R_t values greater than 2.5 min.

The chromatographic resolution exhibited in Figure 4-2 was typical of all of the chromatograms obtained during analysis and was sufficient to permit calculation of species-specific evolution profiles. Figure 4-3 shows the species-specific evolution profiles calculated for a) paraffin, b) olefin, and c) alkyl aromatic volatile products. Separated volatile products were identified by using the mass spectral library search function of the MS software. Integrated total ion current (TIC) values were calculated by adding the TIC chromatographic peak areas for all species identified with the same number of carbons at each sample temperature (i.e. for the same chromatographic injection). The numbers in parentheses in Figure 4-3 denote the number of isomers detected. "Greater (3)" in Figure 4-3a denotes that three paraffin isomers with nine or more carbons ($\geq C_9$) were combined to generate the profile. The volatile product slate illustrated in Figure 4-3 shows that C_3 - C_{10} hydrocarbons were formed and that C_3 - C_6 hydrocarbons were the dominant volatile species. Below 200 °C, volatile product mixtures were composed mostly of C_4 - C_7 paraffins (Figure 4-3a).

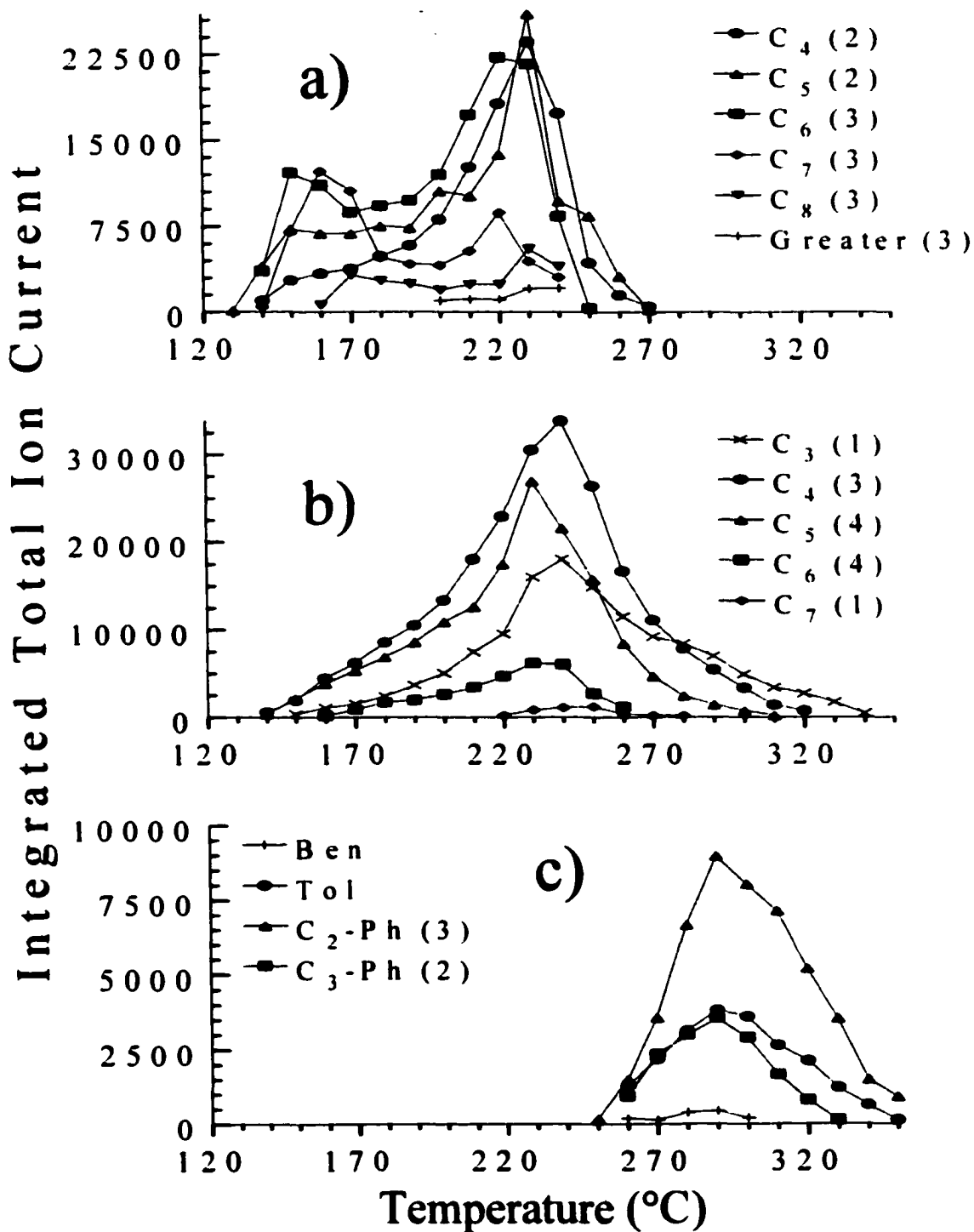


Figure 4-3: Volatile product evolution profiles for LPE/HZSM-5 heated in helium a) paraffins b) olefins c) alkyl aromatics [Values in parentheses represent the number of isomers detected]

As the sample temperature increased, C₃-C₅ olefins became the most abundant volatile products (Figure 4-3b). The temperature corresponding to the maximum paraffin and olefin evolution rates was 240 °C (Figures 4-3a and b). Paraffin products were not detected above 270 °C. Ben and Tol in Figure 4-3c represent benzene and toluene (methyl benzene) and C₂-Ph and C₃-Ph represent alkyl aromatic species with the indicated number of side chain carbons. Alkyl aromatic volatile products were detected initially at 250 °C and their evolution maximized at 310 °C (Figure 4-3c). Three C₂-Ph substituted phenyl isomers (xylenes and/or ethyl benzene) were the most abundant alkyl aromatic species detected (Figure 4-3c). The largest integrated TIC peak area calculated for volatile aromatic products was about 1/3 of the C₄-olefin area at their respective maximum temperatures. Substituted aromatic isomers with the same number of carbons could not be differentiated by the identification methods used in this study. These isomers had nearly identical mass spectra and GC standards were not used to identify them by R_t. However, the exact identities of these alkyl aromatics were not important for the conclusions drawn in this research.

4.2.1b TA-MS Results

Isoconversion E_a values for paraffin formation were calculated from the m/z 57 ion signal as described in Chapter 3. The triangle points (right y-axis scale) in Figure 4-4 represent the m/z 57 ion signal selectivity for volatile paraffin products with respect to the a) fraction of the total integrated m/z 57 ion signal and b) temperature. The temperature scale for the E_a vs. temperature plots was derived from the 5 °C/min heating ramp used during TA-MS measurements. The selectivity calculated from 0.01-0.50 fractional integrated ion signal was 85-99%.

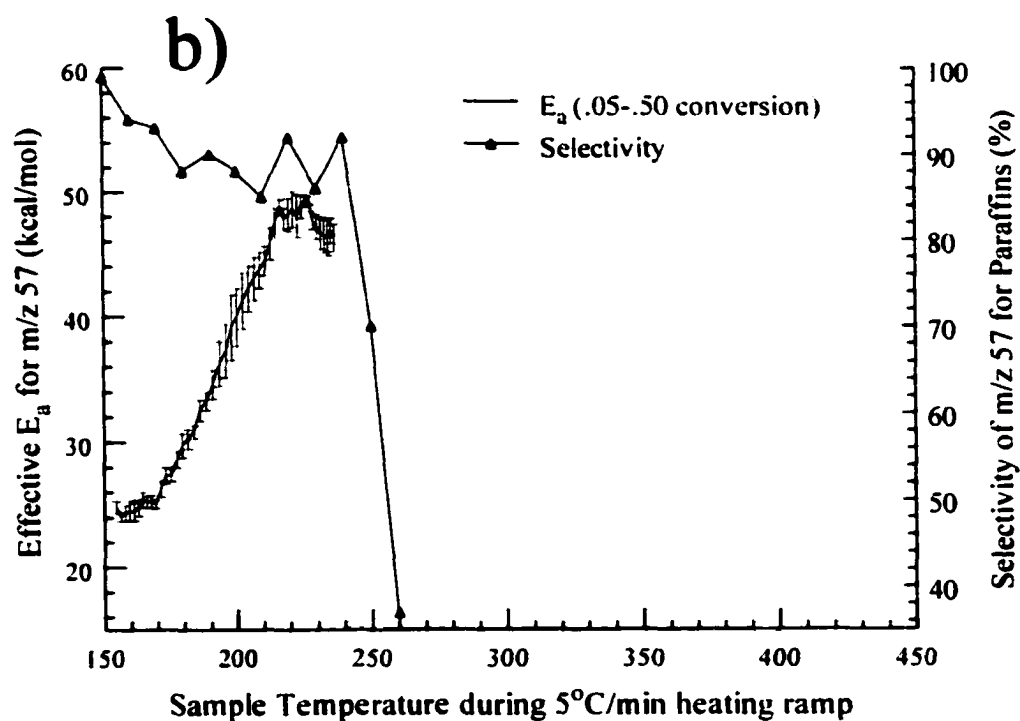
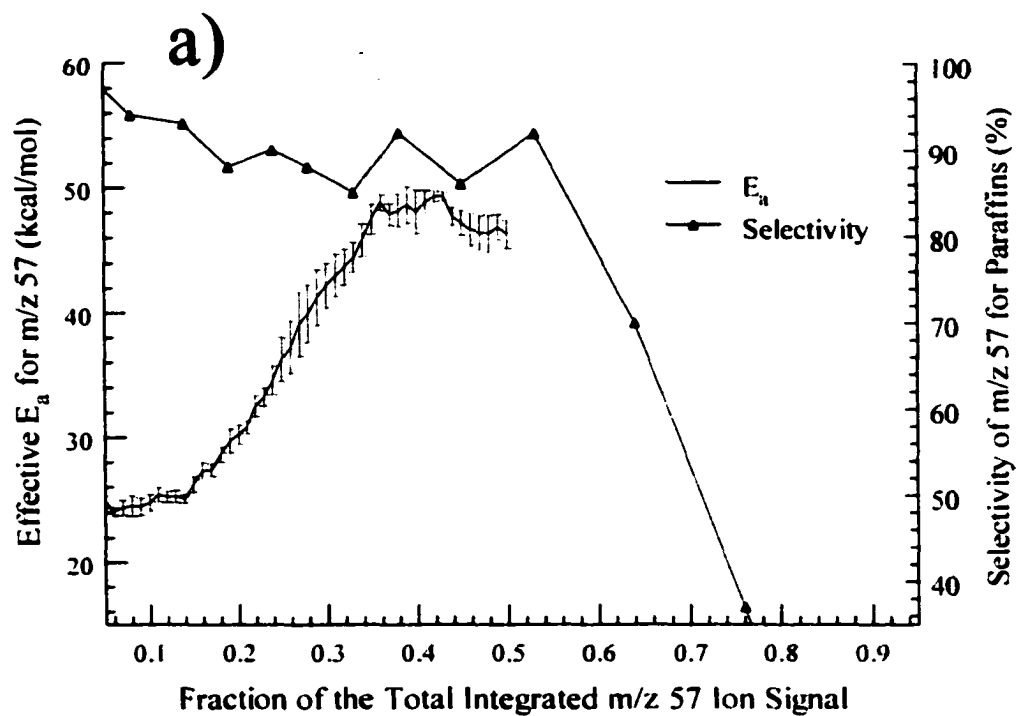


Figure 4-4: a) E_a vs. Fractional integrated ion signal b) E_a vs. Temperature plots for the formation of paraffins (m/z 57) from LPE/HZSM-5 heated in helium

The m/z 57 ion signal selectivity for volatile paraffins decreased drastically above 0.50 fractional integrated ion signal (250 °C) because little or no volatile paraffins were detected. The m/z 57 ion signal detected above 0.50 fractional integrated ion signal (250 °C) resulted primarily from volatile olefin products.

Figure 4-4 shows E_a (left y-axis scale) vs. a) fraction of the total integrated m/z 57 ion signal and b) temperature plots generated for the formation of paraffins (solid lines w/ error bars). The paraffin E_a plot has three distinct regions. The initial E_a value for paraffin formation was about 24 kcal/mol at 0.05 fractional integrated ion signal (155 °C) and remained relatively constant until 0.15 fractional integrated ion signal (170 °C). Isoconversion E_a values increased to approximately 48 kcal/mol by 0.35 fractional integrated ion signal (215 °C), and then decreased to 42 kcal/mol from 0.35-0.50 fractional integrated ion signal (240 °C).

The triangle points (right y-axis scale) in Figure 4-5 represent the calculated m/z 55 ion signal selectivity for volatile olefin products with respect to the a) fraction of the total integrated m/z 55 ion signal and b) temperature. The m/z 55 ion signal selectivity for olefins was 58-80% from 0.01-0.15 fractional integrated ion signal, 80-88% from 0.16-0.50 fractional integrated ion signal, and 99% above 0.50 fractional integrated ion signal. The low initial m/z 55 ion signal selectivity for olefins from 0.01-0.15 fractional integrated ion signal was due to the dominance of volatile paraffins that produced m/z 55 ion signals in their mass spectra. As the percentage of olefins increased in the volatile product slate, the m/z 55 selectivity for olefins increased.

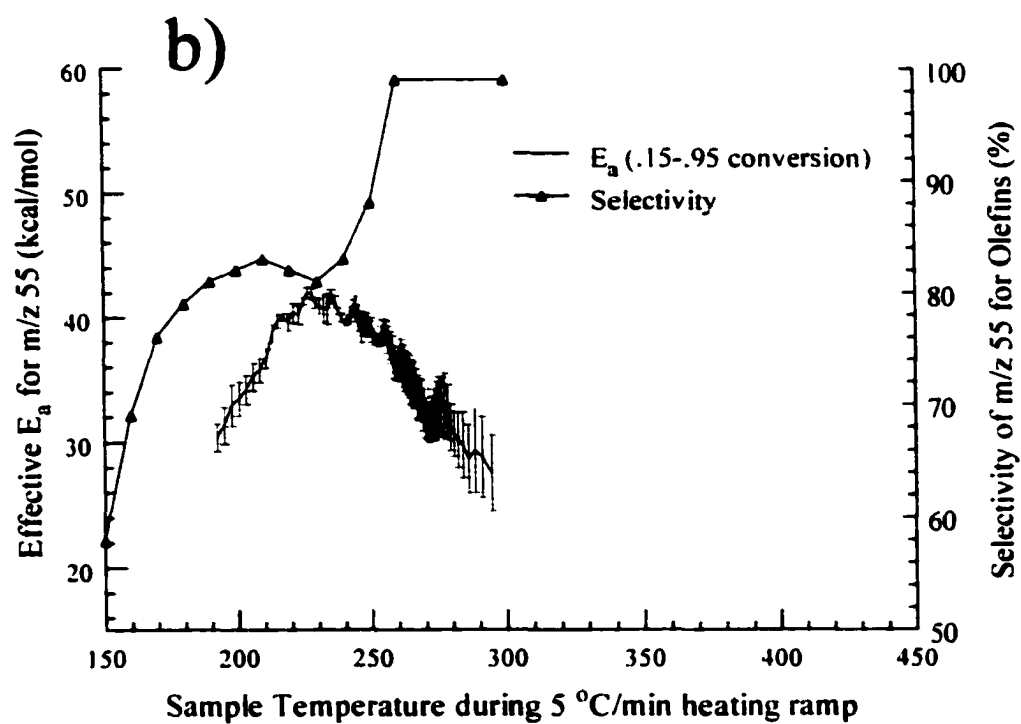
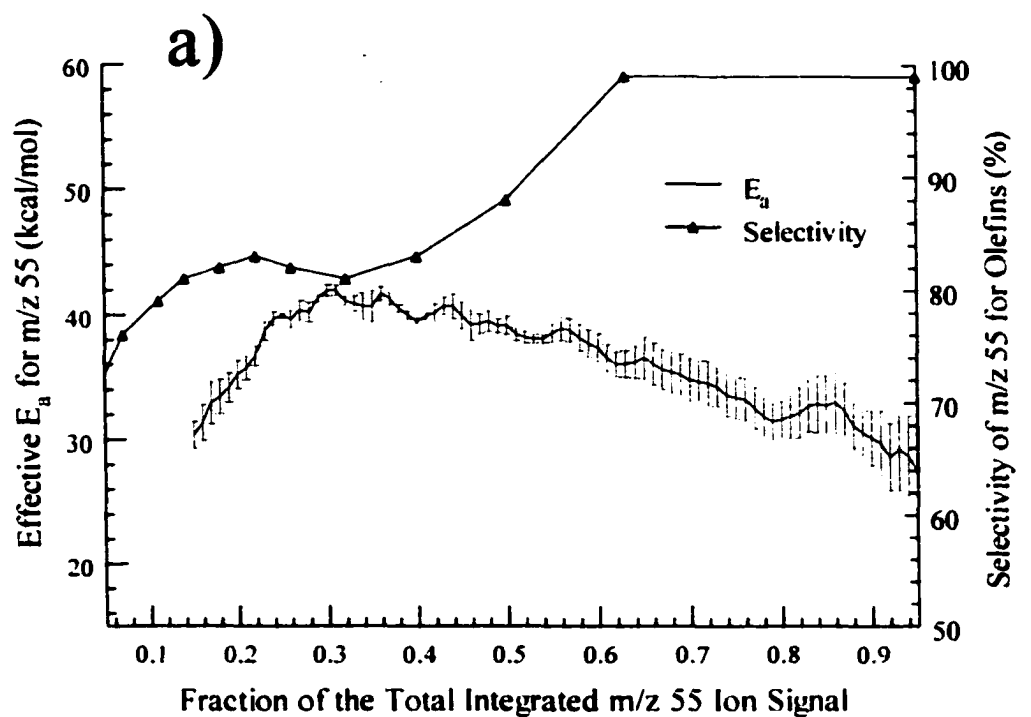


Figure 4-5: a) E_a vs. Fractional integrated ion signal b) E_a vs. Temperature plots for the formation of olefins (m/z 55) from LPE/HZSM-5 heated in helium

The m/z 55 olefin selectivity increased dramatically above 0.50 fractional integrated ion signal (250 °C) because the only volatile products detected beyond this point (temperature) were olefins and aromatics.

Volatile olefin formation E_a plots contained two different regions (Figure 4-5, solid line w/ error bars). An increase in E_a value between 0.15-0.30 fractional integrated ion signal (190-220 °C) was followed by a gradual decrease in E_a . The E_a value calculated at 0.15 fractional integrated ion signal (190 °C) was 30 kcal/mol. The olefin formation E_a value then increased to 41 kcal/mol at 0.30 fractional integrated ion signal (220 °C). Above 0.30 fractional integrated ion signal, the E_a value decreased to 28 kcal/mol by 0.95 fractional integrated ion signal (300 °C).

The m/z 91 ion signal selectivity was calculated to be greater than 99% for alkyl aromatic volatile products between 0.05-0.95 fractional integrated ion signal for the LPE/HZSM-5 (He) sample. Figure 4-6 shows the E_a vs. a) fraction of the total integrated ion signal and b) temperature plots generated for the formation of alkyl aromatics. Evolution profiles show that volatile aromatic product formation occurred over the 250-350 °C temperature range. The initial alkyl aromatic E_a value was 30 kcal/mol at 0.05 fractional integrated ion signal (270 °C) and remained relatively constant to 0.95 fractional integrated ion signal (430 °C).

4.2.2 LPE/HZSM-5 (H₂)

4.2.2a TA-GC/MS Results

Figure 4-7a shows the repetitive injection chromatograms obtained while heating the LPE/HZSM-5 (H₂) sample.

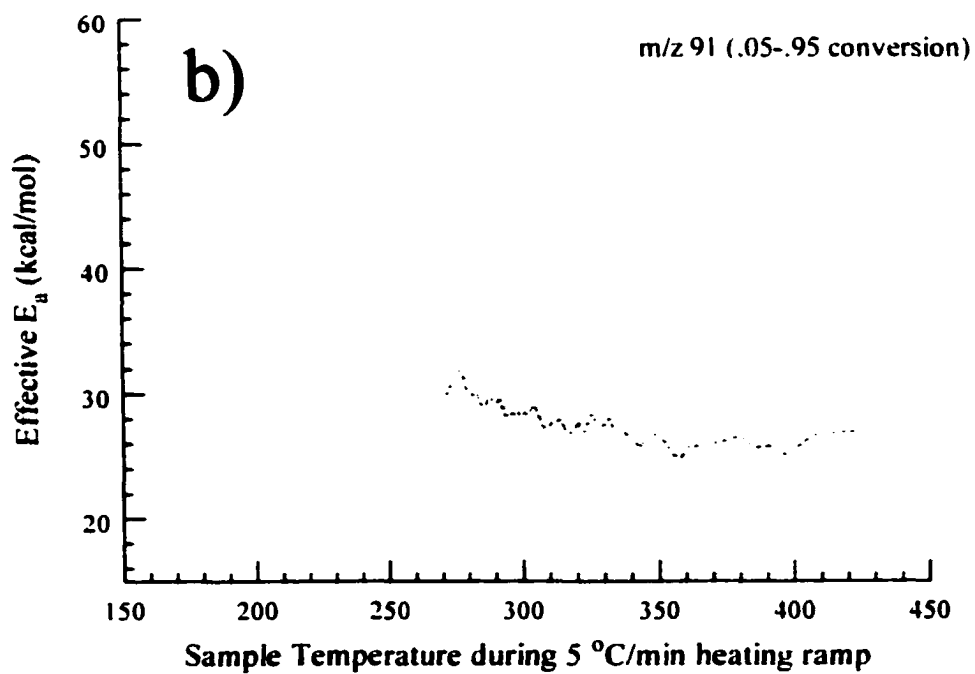
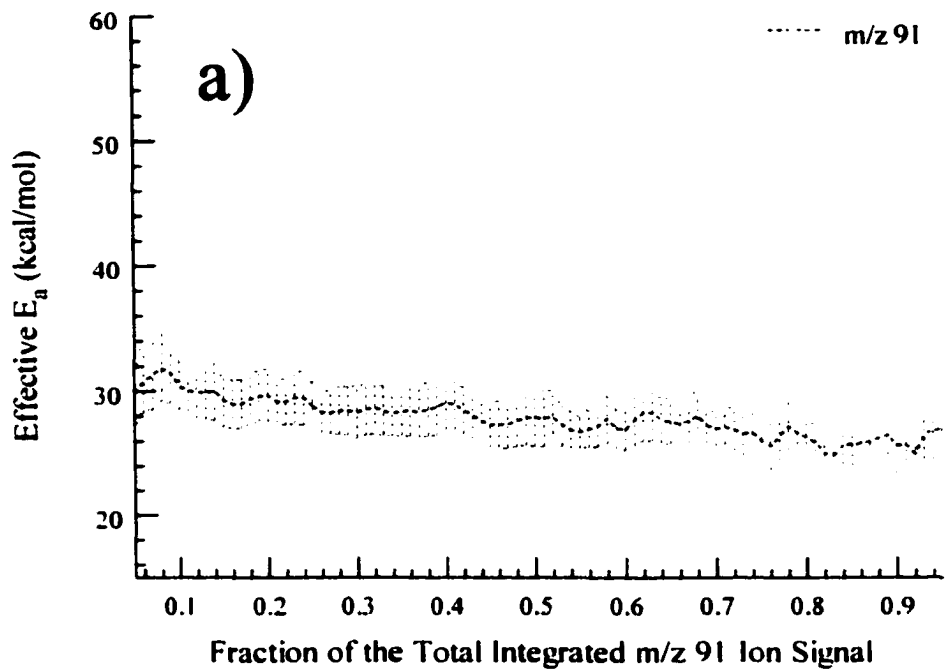


Figure 4-6: a) E_a vs. Fractional integrated ion signal b) E_a vs. Temperature plots for the formation of alkyl aromatics (m/z 91) from LPE/HZSM-5 heated in helium

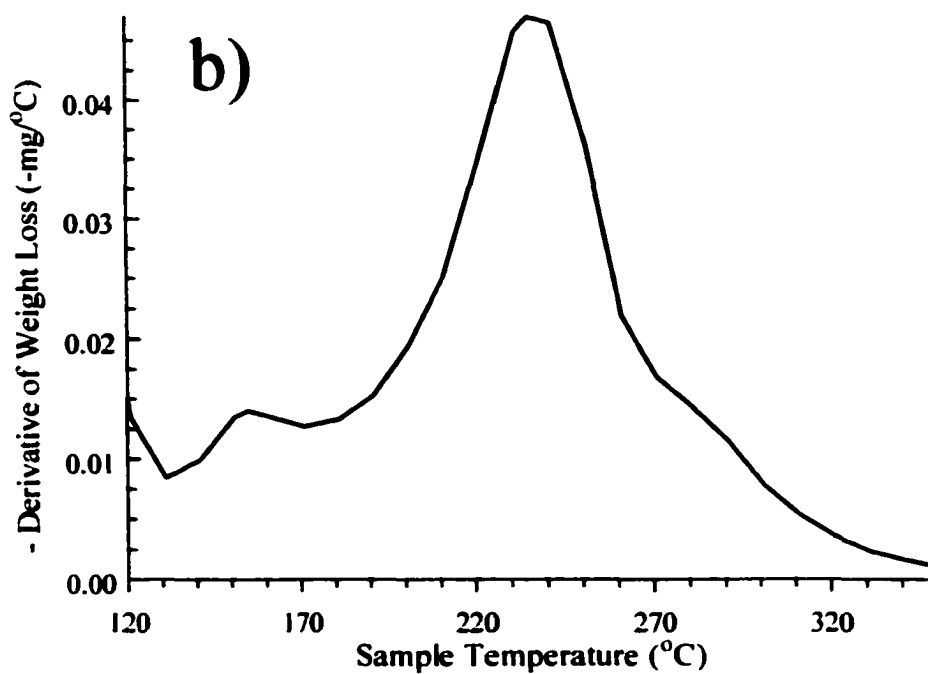
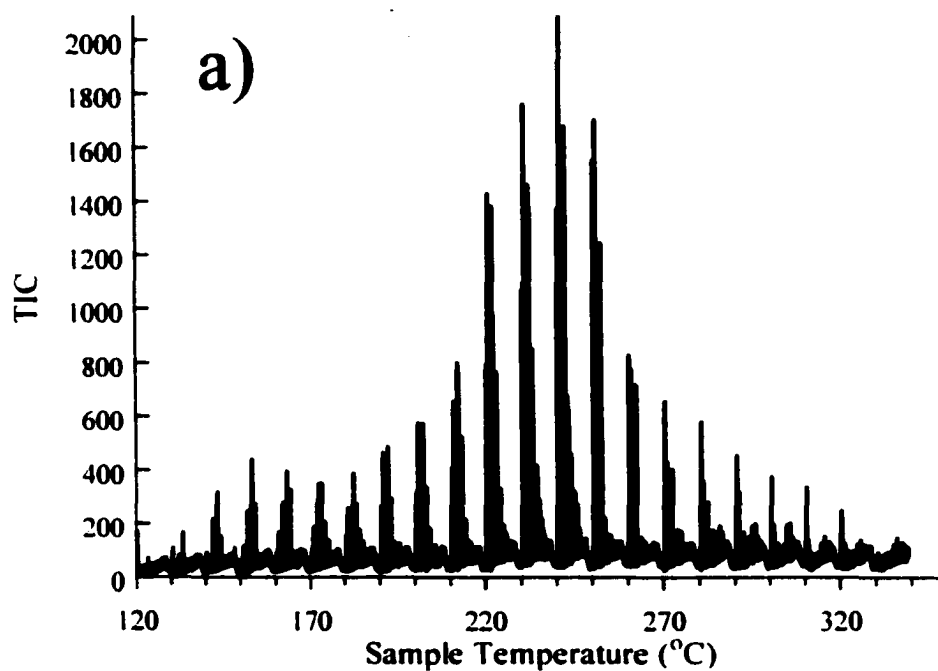


Figure 4-7: a) Repetitive injection chromatogram for LPE/HZSM-5 heated in hydrogen b) Negative derivative of the weight loss obtained for LPE/HZSM-5 heated in hydrogen by using TGA

Volatile products were detected over the same temperature range as for the LPE/HZSM-5 (He) sample (130-350 °C). Two volatile product evolution maxima were observed in the chromatograms at 150 and 240 °C. Figure 4-7b shows the negative derivative ($-\Delta\text{mg}/\Delta^\circ\text{C}$) of the TGA weight loss curve for the LPE/HZSM-5 (H₂) sample. Two distinct regions of polymer weight loss rate were observed by using TGA. A shoulder in the TGA curve (Figure 4-7b) from 130-180 °C corresponds to the first product evolution maximum. Maximum weight loss is observed between 180-260 °C.

Figure 4-8 shows the repetitive injection chromatograms obtained at a) 150, b) 240, and c) 300 °C. At 150 °C (Figure 4-8a), only 9-10 volatile hydrocarbons were detected, most of which were low molecular weight substances with retention times (R_t) less than 2.3 min. When the sample temperature reached 240 °C (Figure 4-8b), an increase in the total number of volatile products (25) was detected as well as the amount of volatile products formed with R_t of less than 1.5 min. Fewer volatile products (6) were detected at 300 °C (Figure 4-8c).

Figure 4-9 shows the species-specific evolution profiles calculated for a) paraffin, b) olefin, and c) alkyl aromatic volatile products. The volatile product slate illustrated in Figure 4-9 shows that C₃-C₁₀ hydrocarbons were formed and that C₃-C₆ hydrocarbons were the dominant volatile species. Below 200 °C, volatile product mixtures were composed mostly of C₅-C₇ paraffins (Figure 4-9a). Relatively fewer volatile paraffin products were detected below 200 °C from LPE/HZSM-5 (H₂) compared to the LPE/HZSM-5 (He) sample. As the sample temperature increased, C₃-C₅ olefins became the most abundant volatile products (Figure 4-9b).

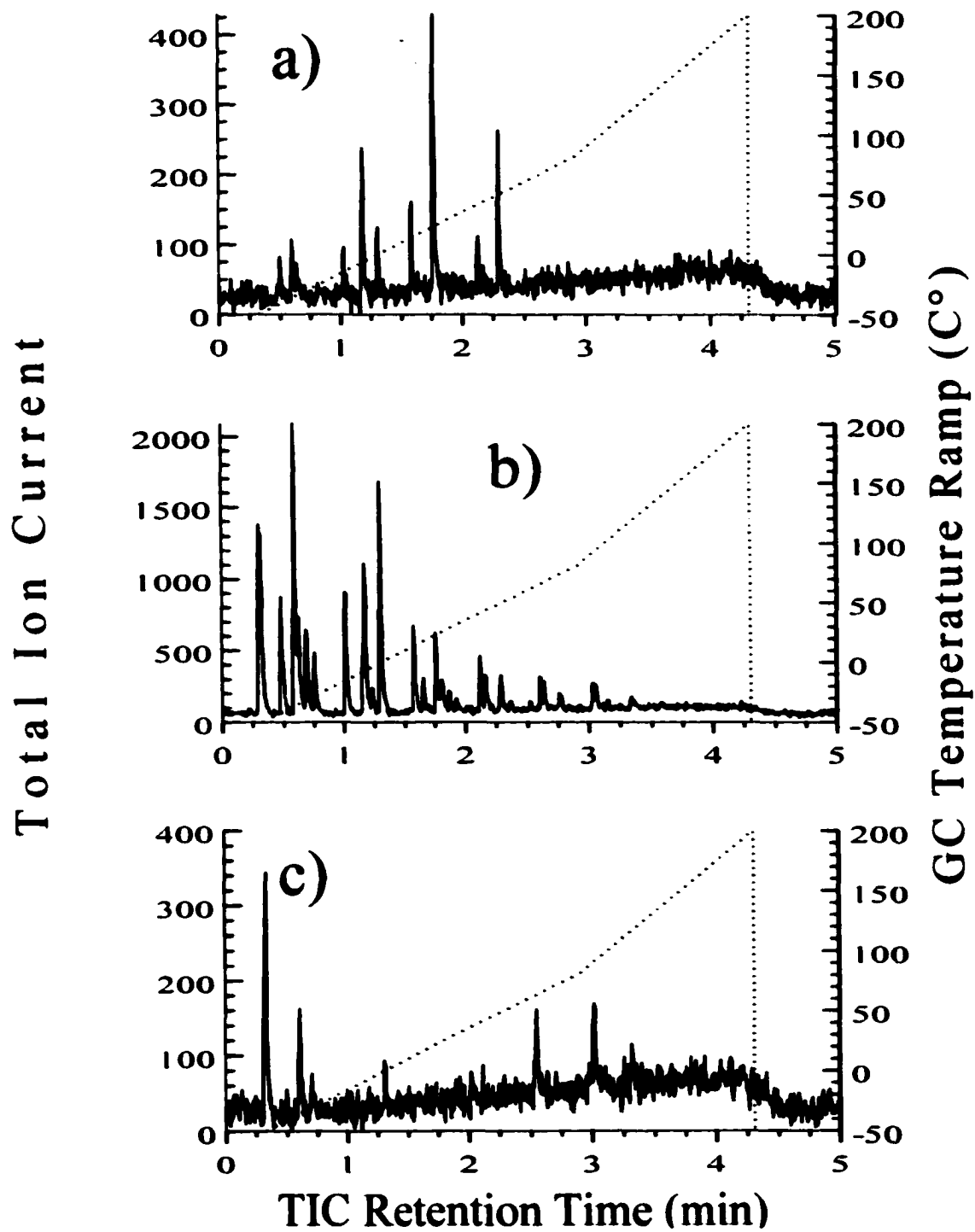


Figure 4-8: Repetitive injection chromatograms obtained from LPE/HZSM-5 heated in hydrogen when the sample temperature reached a) 150 °C b) 240 °C c) 300 °C

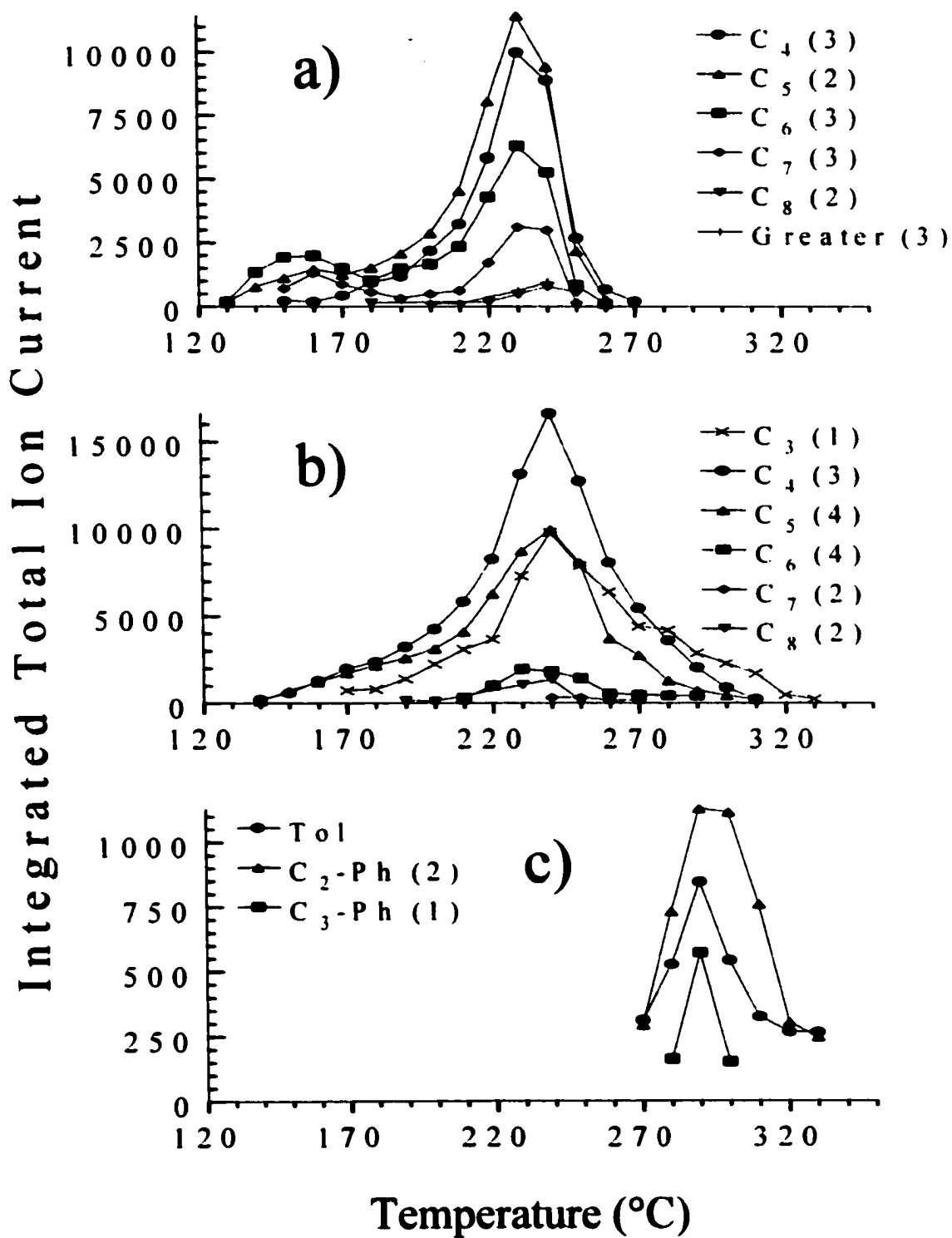


Figure 4-9: Volatile product evolution profiles for LPE/HZSM-5 heated in hydrogen a) paraffins b) olefins c) alkyl aromatics [Values in parentheses represent the number of isomers detected]

The temperature corresponding to the maximum paraffin and olefin evolution rates was 240 °C (Figures 4-9a and b). Paraffin products were not detected above 270 °C. Alkyl aromatic volatile products were detected initially at 270 °C and their evolution maximized at 290-300 °C (Figure 4-9c). Two C₂ substituted phenyl isomers (C₂-Ph) were the most abundant alkyl aromatic species detected (Figure 4-9c). The largest integrated TIC peak area calculated for the volatile aromatic products was about 1/15 of the C₄-olefin area at their respective maximum temperatures. The LPE/HZSM-5 (H₂) sample formed a smaller fraction of alkyl aromatic species than the LPE/HZSM-5 (He) sample.

4.2.2b TA-MS Results

The m/z 55 ion signal selectivity for the formation of olefins shown in Figure 4-10 varied with fractional integrated ion signal in a similar manner as for the LPE/HZSM-5 (He) sample. The m/z 55 ion signal selectivity for olefins was calculated to be 62-81% from 0.01-0.15 fractional integrated ion signal, 81-86% from 0.16-0.50 fractional integrated ion signal, and 99% above 0.50 fractional integrated ion signal for the LPE/HZSM-5 (H₂) sample. The low initial m/z 55 ion signal selectivity for olefins was due to the dominance of paraffins that produced m/z 55 ion signals in their mass spectra. As the percentage of olefins increased in the volatile product slate, the m/z 55 selectivity for olefins improved. The m/z 55 olefin selectivity increased dramatically above 0.50 fractional integrated ion signal (250 °C) because olefins and alkyl aromatics were the dominant volatile products detected beyond this point (temperature).

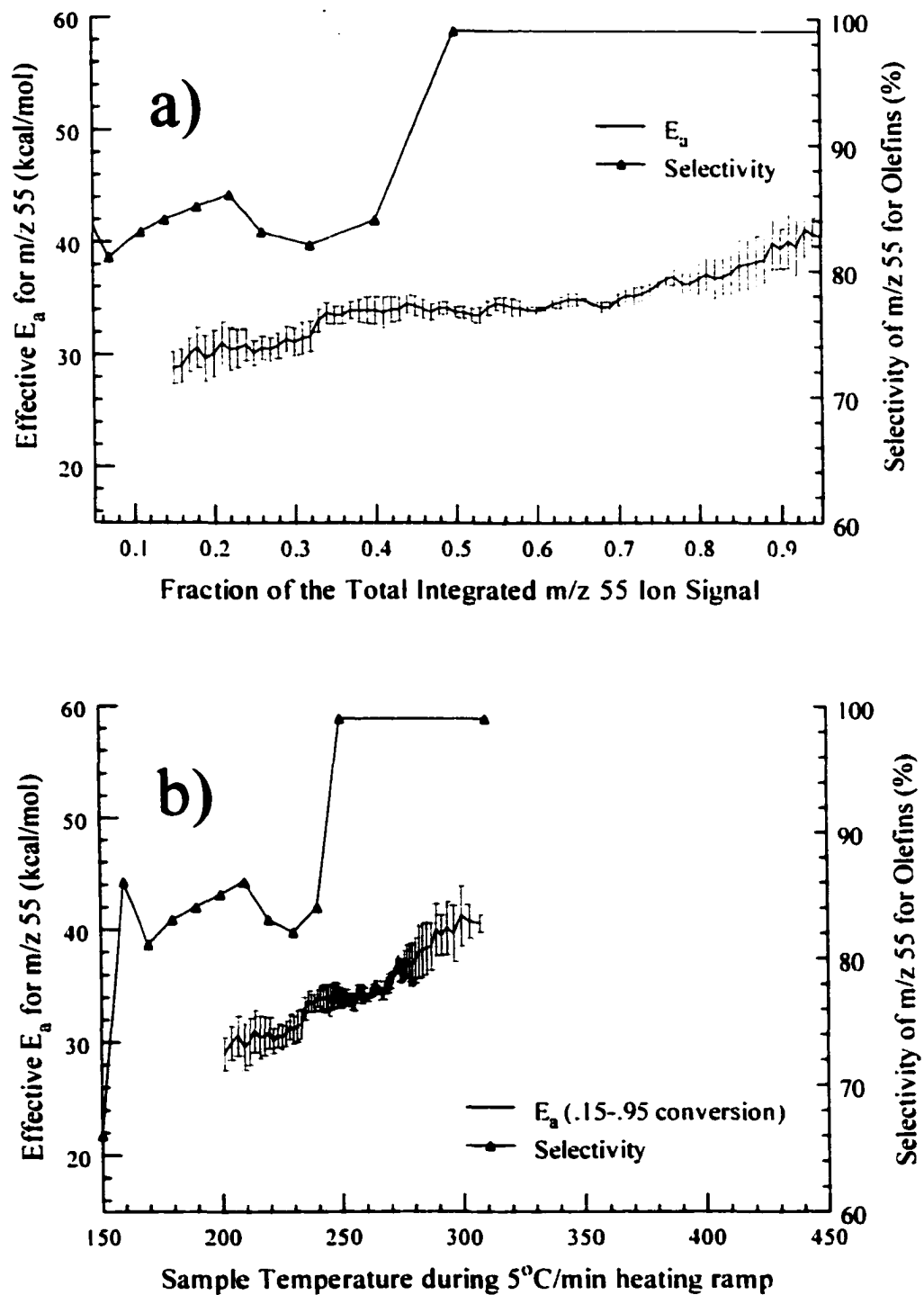


Figure 4-10: a) E_a vs. Fractional integrated ion signal b) E_a vs. Temperature plots for the formation of olefins (m/z 55) from LPE/HZSM-5 heated in hydrogen

Volatile olefin formation E_a values in Figure 4-10 exhibit a continuous increase from 0.15-0.95 fractional integrated ion signal. The initial E_a value was 29 kcal/mol. The olefin formation E_a value then increased to 40 kcal/mol by 0.95 fractional integrated ion signal (310 °C). The E_a plot representing olefin formation from LPE/HZSM-5 (H_2) was quite different than that shown for the LPE/HZSM-5 (He) sample (Figure 4-5).

The decrease of m/z 57 ion signal selectivity for the formation of paraffins with increasing fractional integrated ion signal shown in Figure 4-11 was similar to that observed for LPE/HZSM-5 (He). The m/z 57 ion signal selectivity calculated for paraffins was 80-99% from 0.01-0.50 fractional integrated ion signal. The m/z 57 ion signal selectivity for volatile paraffins decreased drastically above 0.50 fractional integrated ion signal (240 °C) because little or no volatile paraffins were detected. The m/z 57 ion signal detected above 0.50 fractional integrated ion signal (250 °C) resulted primarily from volatile olefin products.

The paraffin E_a plot has three distinct regions (Figure 4-11). The initial E_a value for paraffin formation was about 22 kcal/mol at 0.05 fractional integrated ion signal (155 °C) and remained relatively constant until about 0.15 fractional integrated ion signal (180 °C). Isoconversion E_a values increased to approximately 32 kcal/mol by 0.35 fractional integrated ion signal (210 °C), and then leveled off at 32 kcal/mol from 0.35-0.50 fractional integrated ion signal (210-240 °C). The paraffin E_a plot for the LPE/HZSM-5 (H_2) sample follows the same trends as for the LPE/HZSM-5 (He) sample (Figure 4-4), but the presence of hydrogen appeared to lower E_a values. Evolution profiles show that volatile alkyl aromatic formation occurred over the 270-350 °C temperature range.

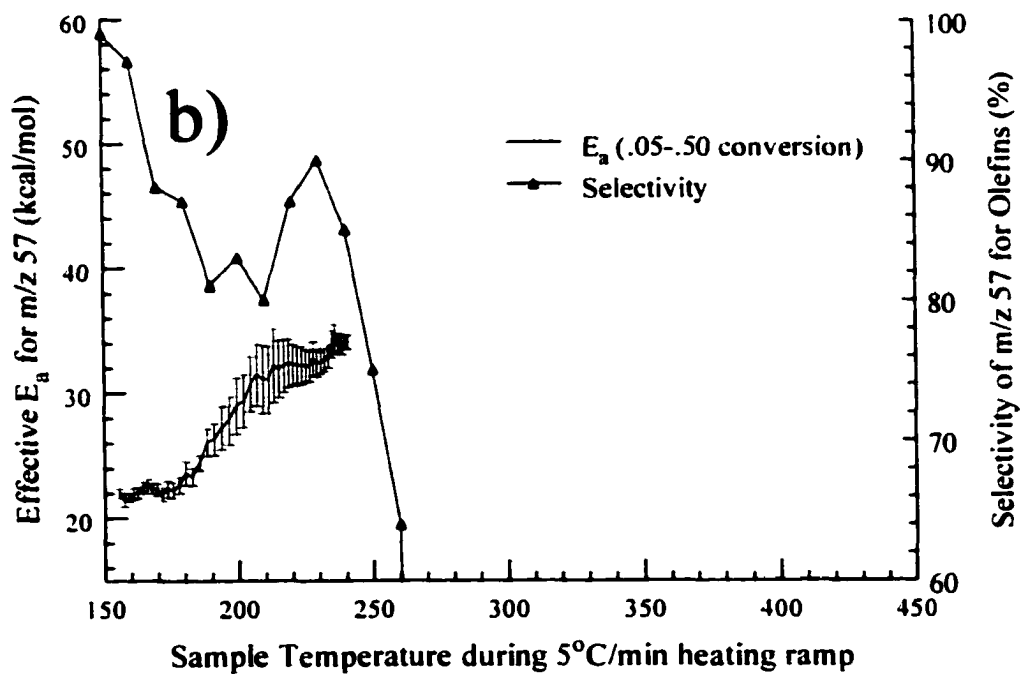
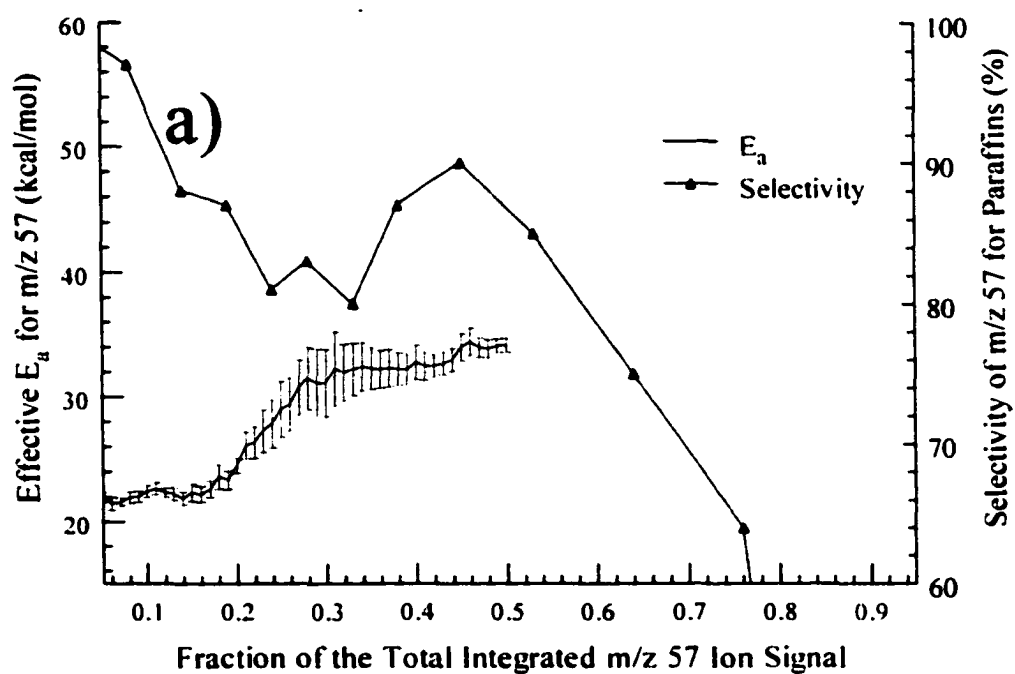


Figure 4-11: a) E_a vs. Fractional integrated ion signal b) E_a vs. Temperature plots for the formation of paraffins (m/z 57) from LPE/HZSM-5 heated in hydrogen

However, large E_a value errors were obtained because small amounts of volatile aromatic species (i.e. low m/z 91 ion signals) were detected from the LPE/HZSM-5 (H_2) sample. Consequently, the E_a vs. fractional integrated ion signal plot for alkyl aromatics is not included here.

4.2.3 LPE/PtHZSM-5 (He)

4.2.3a TA-GC/MS Results

Figure 4-12a shows the repetitive injection chromatograms obtained while heating the LPE/PtHZSM-5 (He) sample. Volatile products were detected over the same temperature range as for the LPE/HZSM-5 (He) and (H_2) samples (130-350 °C). Three volatile product evolution maxima were observed in the chromatograms at 150, 240, and 300 °C. Figure 4-12b shows the negative derivative ($-\Delta mg/\Delta^\circ C$) of the TGA weight loss curve for the LPE/PtHZSM-5 (He) sample. Two distinct regions of polymer weight loss rate were observed by using TGA. A shoulder in the TGA curve (Figure 4-12b) from 130-180 °C corresponds to the first product evolution maximum. Maximum weight loss is observed between 180-270 °C.

Figure 4-13 shows the repetitive injection chromatograms obtained at a) 150, b) 240, and c) 300 °C. At 150 °C (Figure 4-13a), only 16 volatile hydrocarbons were detected, most of which were low molecular weight substances with R_t less than 2.25 minutes. When the sample temperature reached 240 °C (Figure 4-13b), an increase in the total number of volatile products (29) was detected as well as the number of volatile products with R_t of less than 1.5 min. Fewer volatile products (18) were detected at 300 °C (Figure 4-13c).

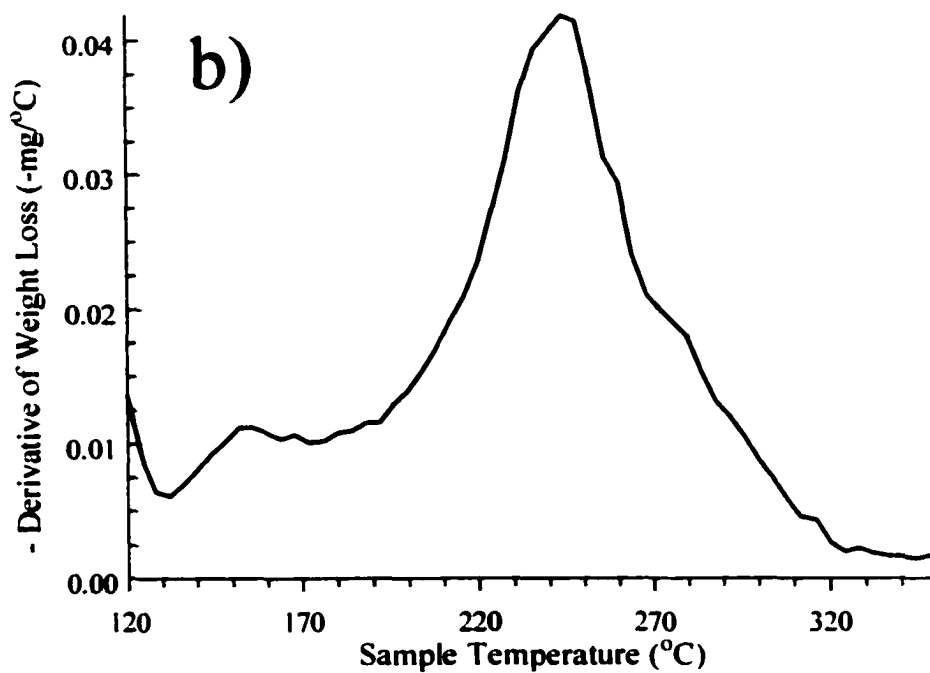
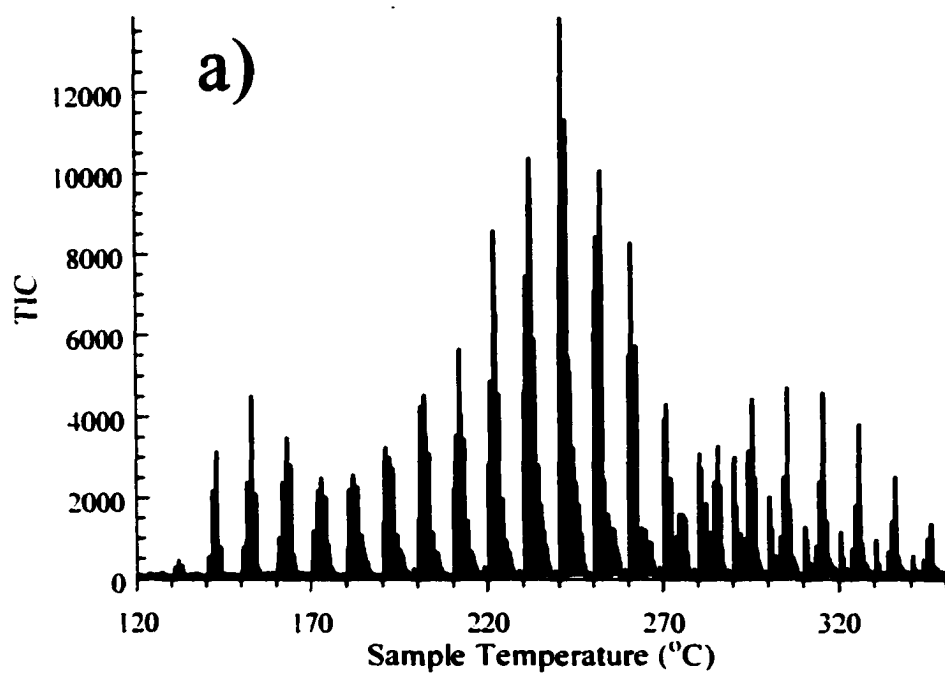


Figure 4-12: a) Repetitive injection chromatogram for LPE/PtHZSM-5 heated in helium b) Negative derivative of the weight loss obtained for LPE/PtHZSM-5 heated in helium by using TGA

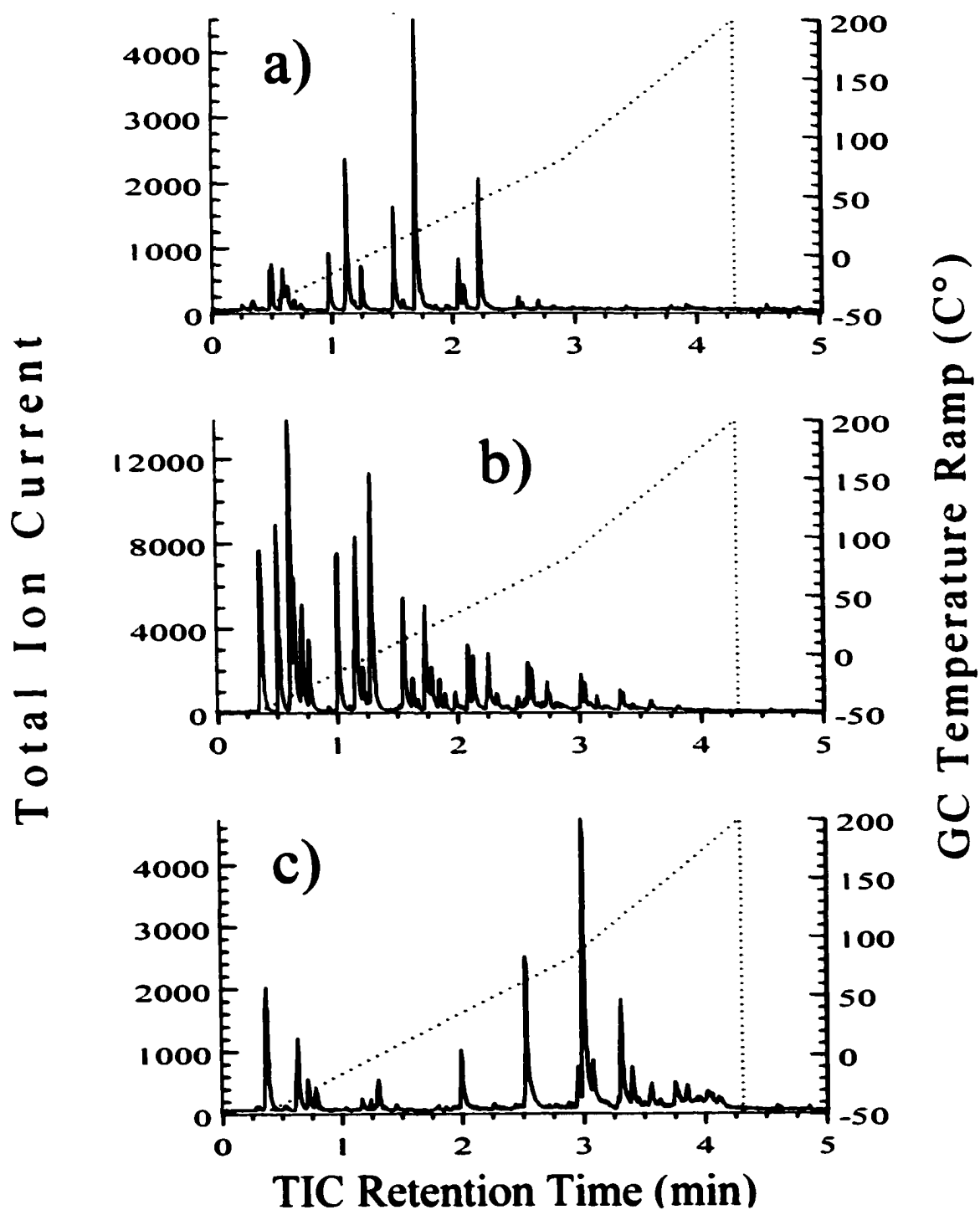


Figure 4-13: Repetitive injection chromatograms obtained from LPE/PtHZSM-5 heated in helium when the sample temperature reached a) 150 °C b) 240 °C c) 300 °C

Figure 4-14 shows the species-specific evolution profiles calculated for a) paraffin, b) olefin, and c) alkyl aromatic volatile products. The volatile product slate illustrated in Figure 4-14 shows that C₃-C₁₀ hydrocarbons were formed and that C₃-C₆ hydrocarbons were the dominant volatile species. Below 200 °C, volatile product mixtures were composed mostly of C₄-C₇ paraffins (Figure 4-14a). As the sample temperature increased, C₃-C₅ olefins became the most abundant volatile products (Figure 4-14b). The temperature corresponding to the maximum paraffin and olefin evolution rates was 240 °C (Figures 4-14a and b). Paraffin products were not detected above 280 °C. Alkyl aromatic volatile products were detected initially at 240 °C and their evolution maximized at 280-290 °C (Figure 4-14c). Two C₂ substituted phenyl isomers (C₂-Ph) were the most abundant volatile alkyl aromatic species (Figure 4-14c). The largest integrated TIC peak area calculated for the volatile aromatic products was about 2/3 of the C₄-olefin area at their respective maximum temperatures. Significantly more alkyl aromatics were derived from LPE/PtHZSM-5 (He) compared to the LPE/HZSM-5 (He) sample (Figure 4-3).

4.2.3b TA-MS Results

Figure 4-15 shows E_a vs. a) fraction of the total integrated ion signal and b) temperature plots generated for the formation of olefins (solid lines w/ error bars) and paraffins (dotted lines w/ error bars). The m/z 55 ion signal selectivity for the formation of olefins (solid) shown in Figure 4-15 varied with fractional integrated ion signal in a similar manner as for the LPE/HZSM-5 (He) sample.

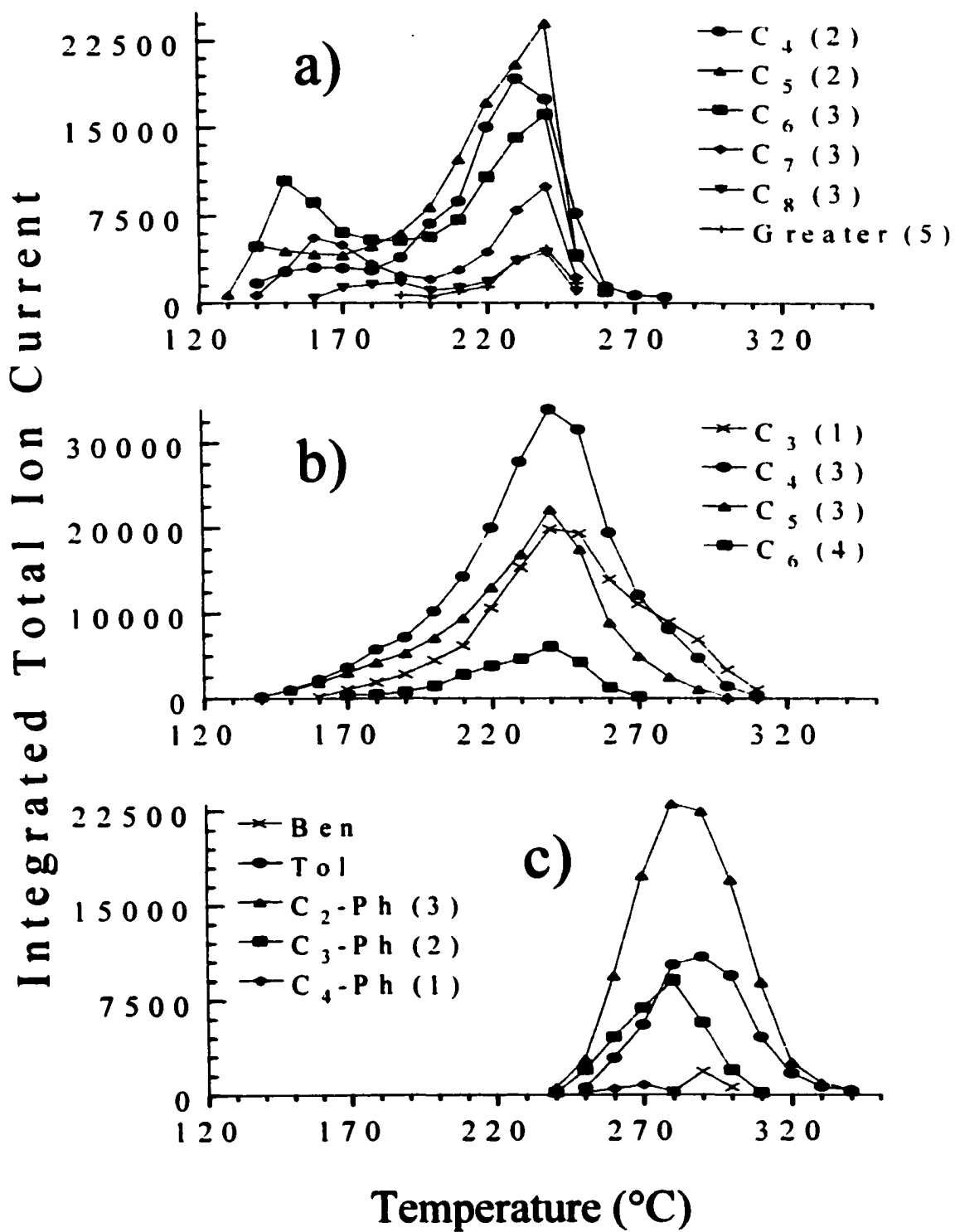


Figure 4-14: Volatile product evolution profiles for LPE/PtHZSM-5 heated in helium a) paraffins b) olefins c) alkyl aromatics
 [Values in parentheses represent the number of isomers detected]

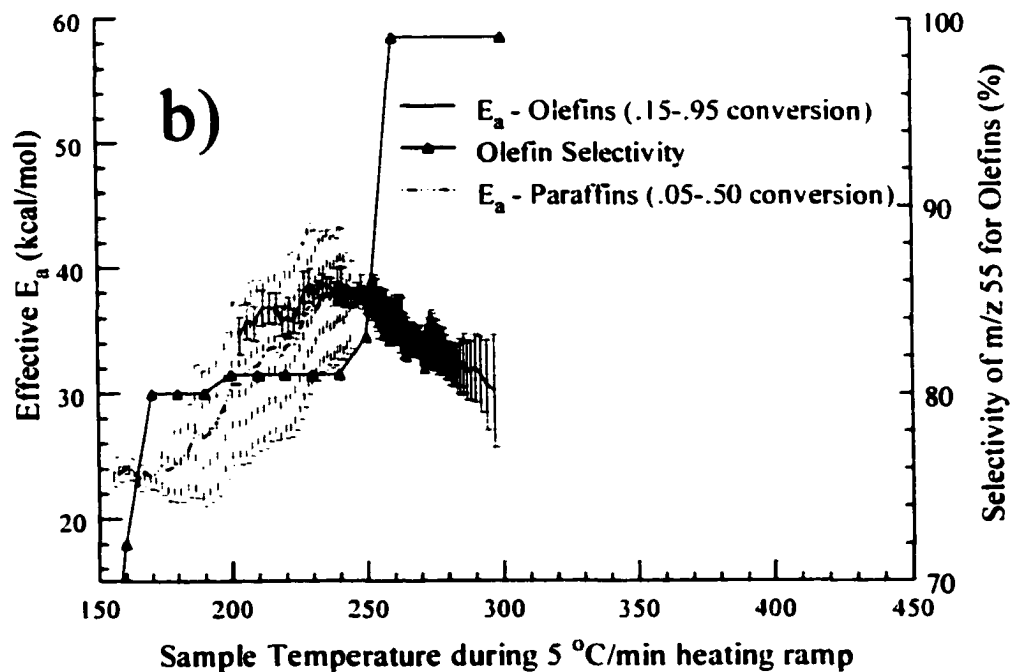
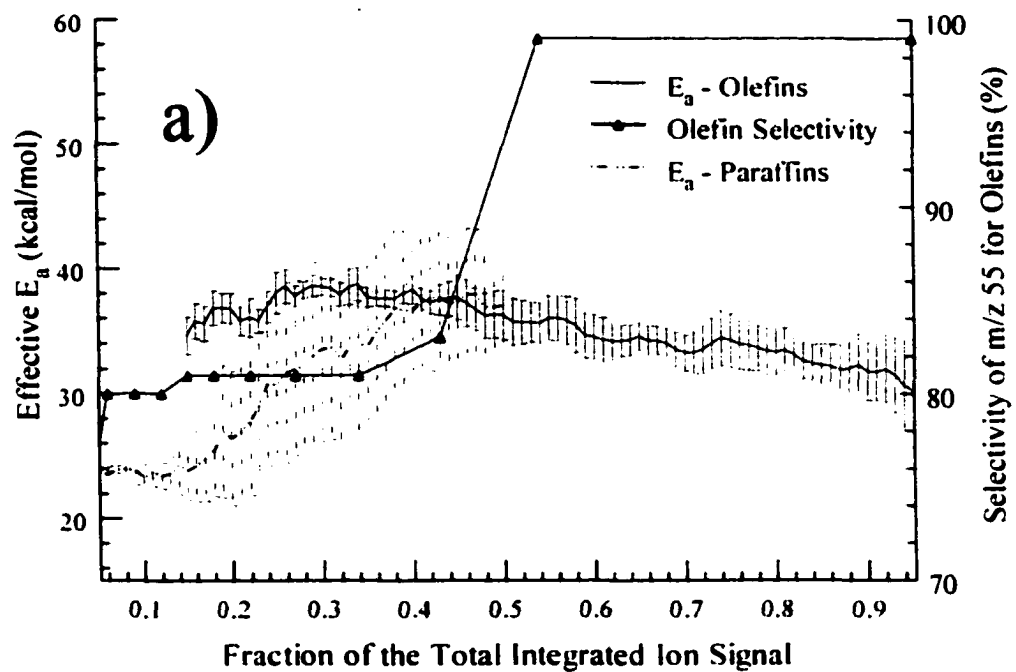


Figure 4-15: a) E_a vs. Fractional integrated ion signal b) E_a vs. Temperature plots for the formation of olefins (m/z 55) and paraffins (m/z 57) from LPE/PtHZSM-5 heated in helium

The m/z 55 ion signal selectivity for olefins was calculated to be 56-80% from 0.01-0.15 fractional integrated ion signal, 80-83% from 0.16-0.50 fractional integrated ion signal, and 99% above 0.50 fractional integrated ion signal for the LPE/PtHZSM-5 (He) sample. The low initial m/z 55 ion signal selectivity for olefins was due to the dominance of paraffins from 0.01-0.15 fractional integrated ion signal that produced m/z 55 ion signals in their mass spectra. As the percentage of olefins increased in the volatile product slate, the m/z 55 selectivity for olefins increased. The m/z 55 olefin selectivity increased dramatically above 0.50 fractional integrated ion signal (250 °C) because olefins and alkyl aromatics were the dominant volatile products detected beyond this point (temperature).

The m/z 57 ion signal selectivity for paraffins was 89-93% from 0.01-0.50 fractional integrated ion signal. The m/z 57 ion signal selectivity for volatile paraffins decreased drastically above 0.50 fractional integrated ion signal (250 °C) because little or no volatile paraffins were detected. The m/z 57 ion signal detected above 0.50 fractional integrated ion signal (250 °C) resulted primarily from volatile olefin products.

The paraffin E_a plot has three distinct regions (Figure 4-15, dotted line). The initial E_a value for paraffin formation was about 24 kcal/mol at 0.05 fractional integrated ion signal (155 °C) and remained relatively constant until 0.15 fractional integrated ion signal (180 °C). Isoconversion E_a values increased to approximately 36 kcal/mol by 0.40 fractional integrated ion signal (230 °C), and then remained constant at 36 kcal/mol from 0.40-0.50 fractional integrated ion signal (250 °C). The initial paraffin E_a value calculated for the LPE/PtHZSM-5 (He) sample was about the same as that calculated for the LPE/HZSM-5 (He) sample (24 kcal/mol). The maximum E_a value for paraffin

formation was lower for LPE/PtHZSM-5 (He) (36 kcal/mol) than for LPE/HZSM-5 (He) (48 kcal/mol).

Volatile olefin formation E_a plots contained two different regions (Figure 4-15, solid line w/ error bars). An increase in E_a value between 0.15-0.25 fractional integrated ion signal (200-230 °C) was followed by a gradual decrease in E_a . The E_a value calculated at 0.15 fractional integrated ion signal (200 °C) was 35 kcal/mol. The volatile olefin formation E_a value then increased to 38 kcal/mol at 0.25 fractional integrated ion signal (230 °C). Above 0.25 fractional integrated ion signal, the E_a value decreased to 30 kcal/mol by 0.95 fractional integrated ion signal (300 °C).

The m/z 91 ion signal selectivity was calculated to be greater than 99% for alkyl aromatic volatile products from 0.05-0.95 fractional integrated ion signal for the LPE/PtHZSM-5 (He) sample. Figure 4-16 shows the E_a vs. a) fraction of the total integrated ion signal and b) temperature plots generated for the formation of alkyl aromatics. Evolution profiles have shown that volatile aromatic product evolution occurred over the 240-340 °C temperature range. The initial alkyl aromatic E_a value was 34 kcal/mol at 0.05 fractional integrated ion signal (280 °C) and remained relatively constant until 0.95 fractional integrated ion signal (400 °C). E_a values for alkyl aromatic formation were about 4-6 kcal/mol higher for LPE/PtHZSM-5 (He) than for LPE/HZSM-5 (He) (Figure 4-6).

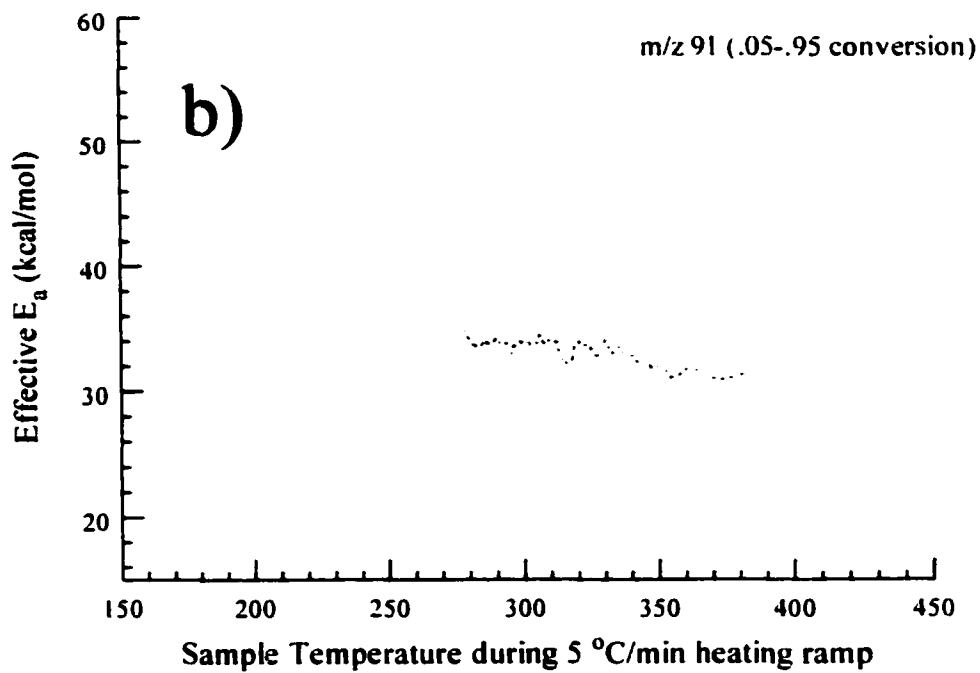
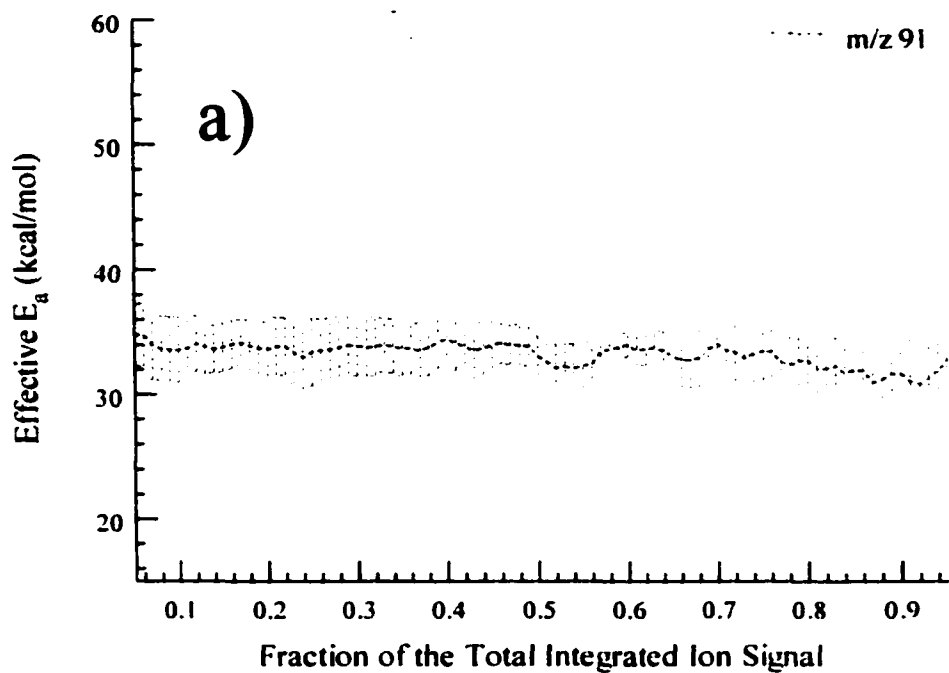


Figure 4-16: a) E_a vs. Fractional integrated ion signal b) E_a vs. Temperature plots for the formation of alkyl aromatics (m/z 91) from LPE/PtHZSM-5 heated in helium

4.2.4 LPE/PtHZSM-5 (H₂)

4.2.4a TA-GC/MS Results

Figure 4-17a shows the repetitive injection chromatograms obtained while heating the LPE/PtHZSM-5 (H₂) sample. Volatile products were detected over the same temperature range as for the LPE/HZSM-5 (He), (H₂), and LPE/PtHZSM-5 (He) samples (130-350 °C). Volatile product evolution maxima were observed in the chromatograms at 160 and 210 °C. Figure 4-17b shows the negative derivative ($-\Delta mg/\Delta^\circ C$) of the TGA weight loss curve for the LPE/PtHZSM-5 (H₂) sample. Two distinct regions of polymer weight loss rate were observed by TGA. The first peak in the TGA curve (Figure 4-17b) from 130-180 °C corresponds to the first product evolution maximum. Maximum weight loss is observed between 180-260 °C.

Figure 4-18 shows the repetitive injection chromatograms obtained at a) 150, b) 240, and c) 300 °C. At 150 °C (Figure 4-18a), only 9 volatile hydrocarbons were detected, most of which were low molecular weight substances with retention times (R_t) less than 2.25 minutes. When the sample temperature reached 240 °C (Figure 4-18b), an increase in the total number of volatile products (24) was detected as well as the amount of volatile products formed with R_t of less than 2.0 min. Fewer volatile products (14) were detected at 300 °C (Figure 4-18c).

Figure 4-19 shows the species-specific evolution profiles calculated for a) paraffin, b) olefin, and c) alkyl aromatic volatile products. The largest integrated TIC areas calculated for volatile olefin and aromatic products were about 1/6 and 1/12 of the maximum C₆-paraffin area at their respective maximum temperatures.

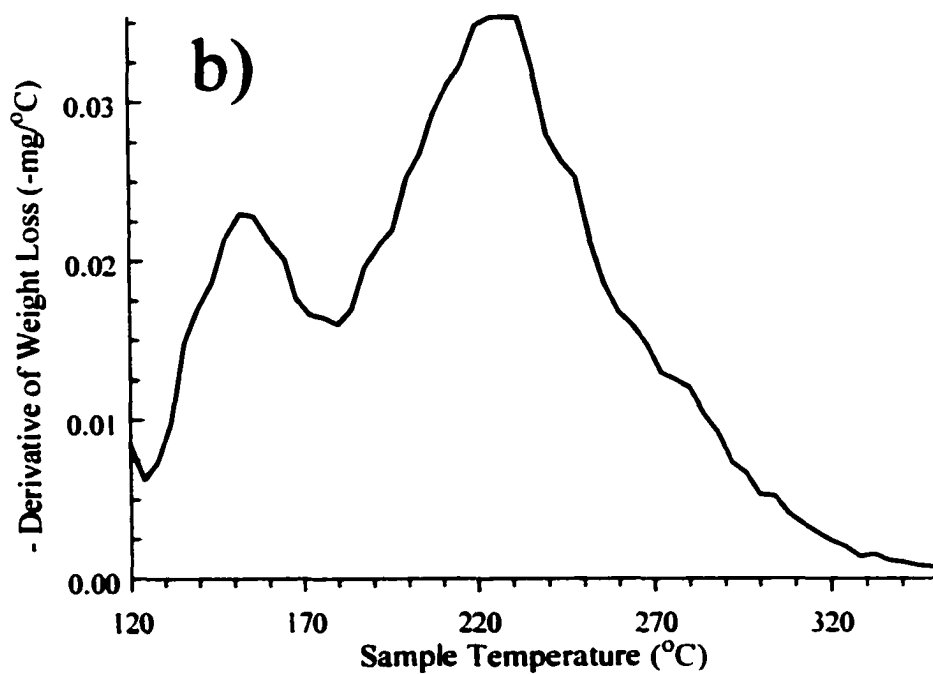
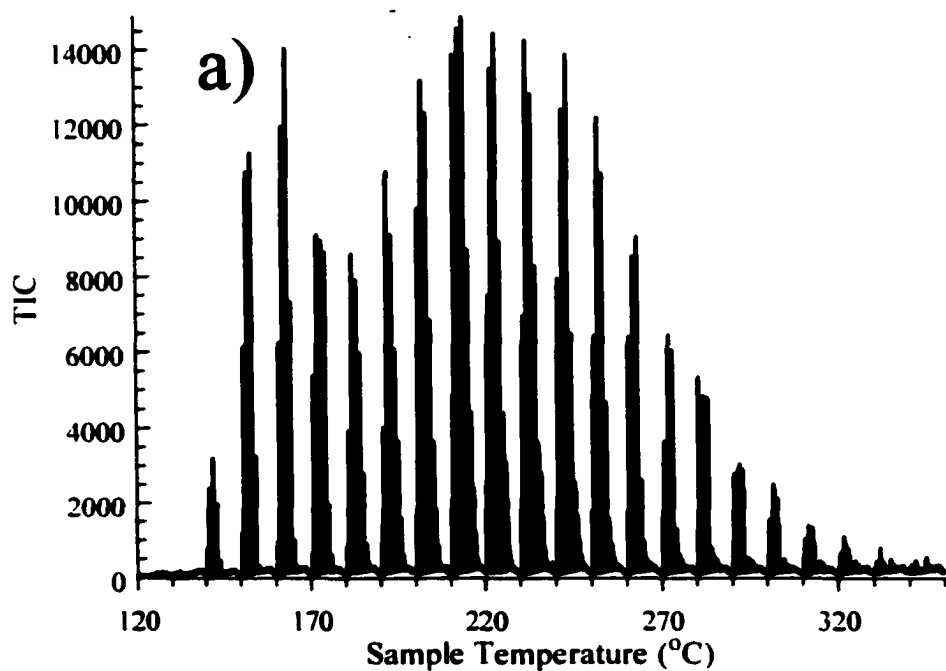


Figure 4-17: a) Repetitive injection chromatogram for LPE/PtHZSM-5 heated in hydrogen b) Negative derivative of the weight loss obtained for LPE/PtHZSM-5 heated in hydrogen by using TGA

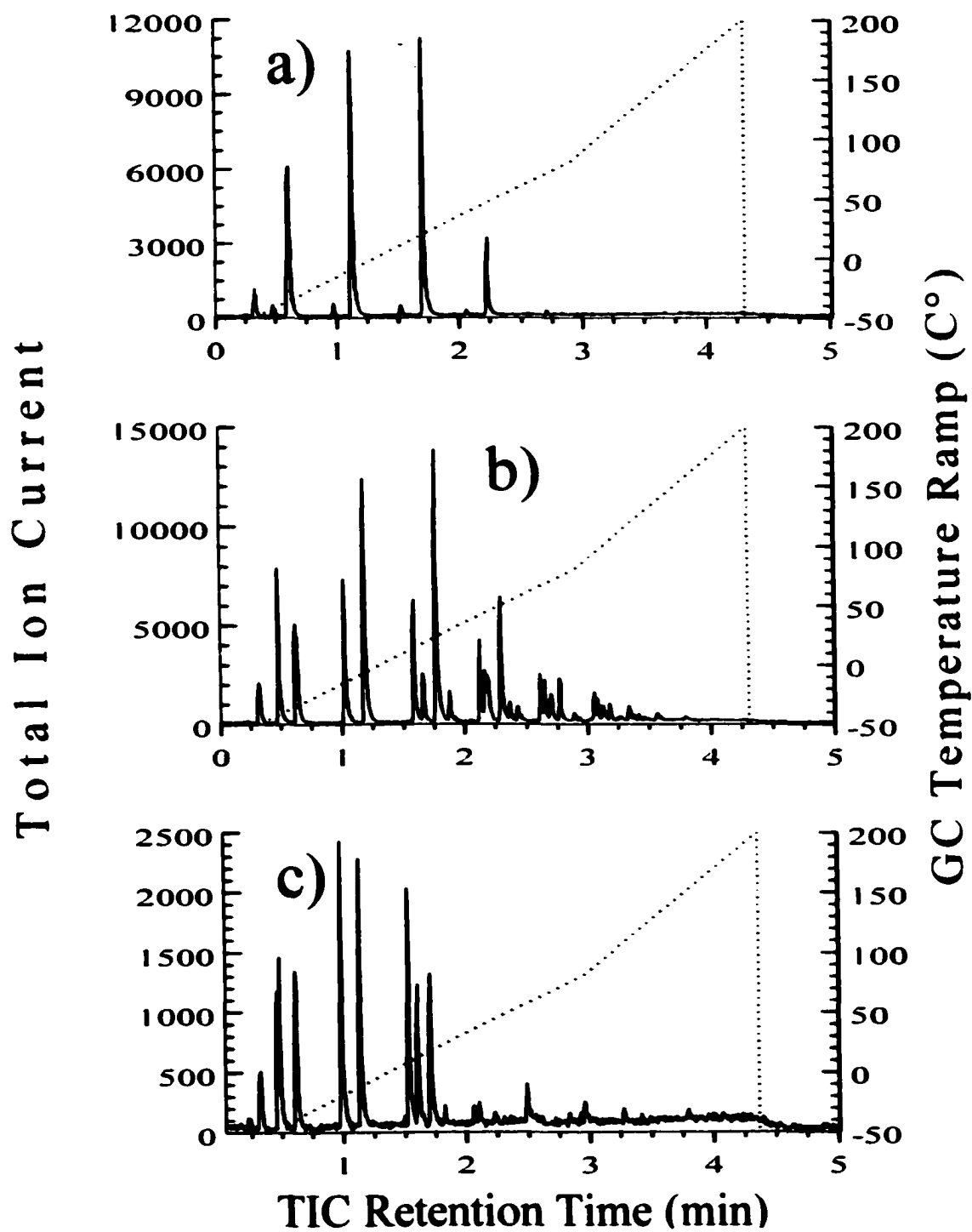


Figure 4-18: Repetitive injection chromatograms obtained from LPE/PtHZSM-5 heated in hydrogen when the sample temperature reached a) 150 °C b) 240 °C c) 300 °C

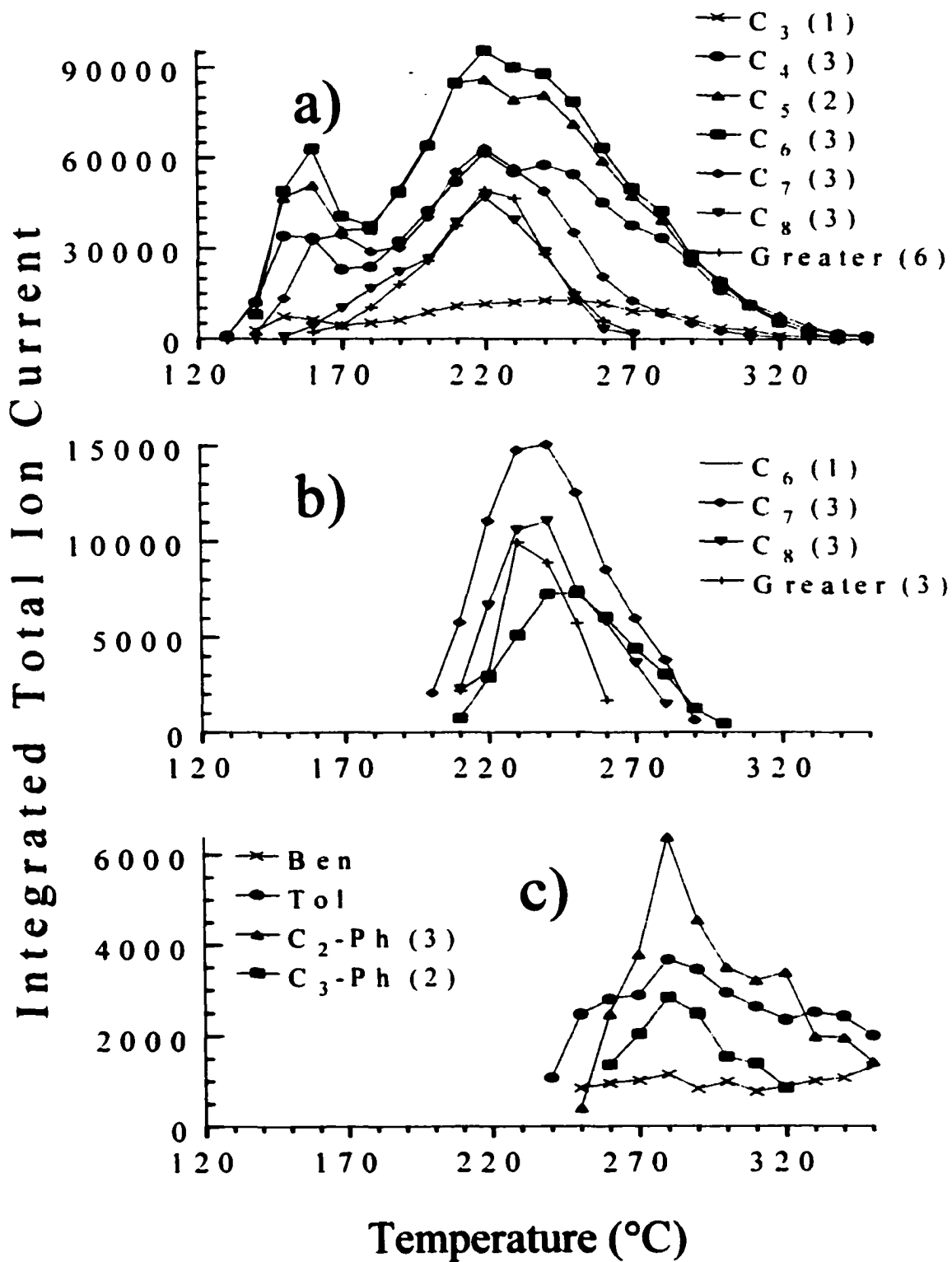


Figure 4-19: Volatile product evolution profiles for LPE/PtHZSM-5 heated in hydrogen a) paraffins b) olefins c) alkyl aromatics [Values in parentheses represent the number of isomers detected]

Below 200 °C, volatile product mixtures were composed entirely of paraffins (Figure 4-19a). More paraffins were detected below 200 °C from the LPE/PtHZSM-5 (H₂) sample than any of the other three LPE/HZSM-5 samples. As the sample temperature increased, a wide range of volatile paraffins C₃-C₁₀ were formed with C₅-C₆ paraffins being the most abundant volatile products detected (Figure 4-19a). Paraffin products dominated the volatile product slate, unlike the other HZSM-5 samples. The temperature corresponding to the maximum paraffin evolution rate was 220 °C (Figure 4-19a). Volatile olefins were not detected below 200 °C and the temperature corresponding to their maximum evolution was 230-240 °C (Figure 4-19b). Volatile olefin products consisted of C₆-C₉ molecules (Figure 4-19b). Alkyl aromatic volatile products were detected initially at 240 °C and their evolution maximized at 280 °C (Figure 4-19c). Two C₂ substituted phenyl isomers (C₂-Ph) were the most abundant volatile alkyl aromatic species detected (Figure 4-19c). The LPE/PtHZSM-5 (H₂) sample produced about the same relative amount of volatile alkyl aromatic species as the LPE/HZSM-5 (H₂) sample.

4.2.4b TA-MS Results

The m/z 57 ion signal selectivity for paraffins was 99% from 0.05-0.95 fractional integrated ion signal. This high selectivity resulted primarily from the dominance of volatile paraffin formation for the LPE/PtHZSM-5 (H₂) sample. The paraffin E_a plot has two distinct regions (Figure 4-20). The initial E_a value for paraffin formation was about 24 kcal/mol at 0.05 fractional integrated ion signal (190 °C) and increased to 40 kcal/mol by 0.30 fractional integrated ion signal (240 °C).

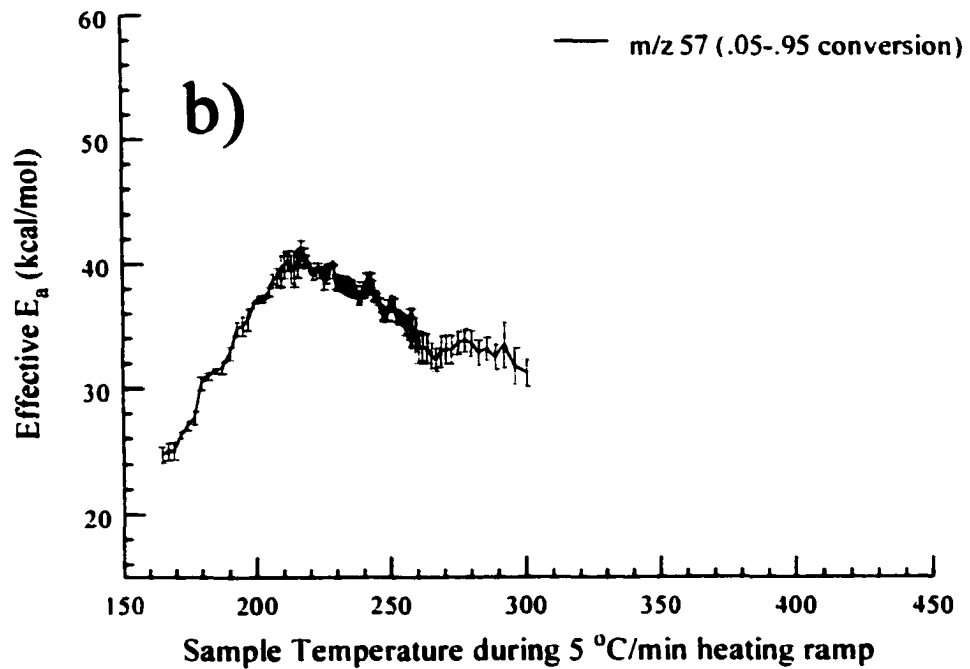
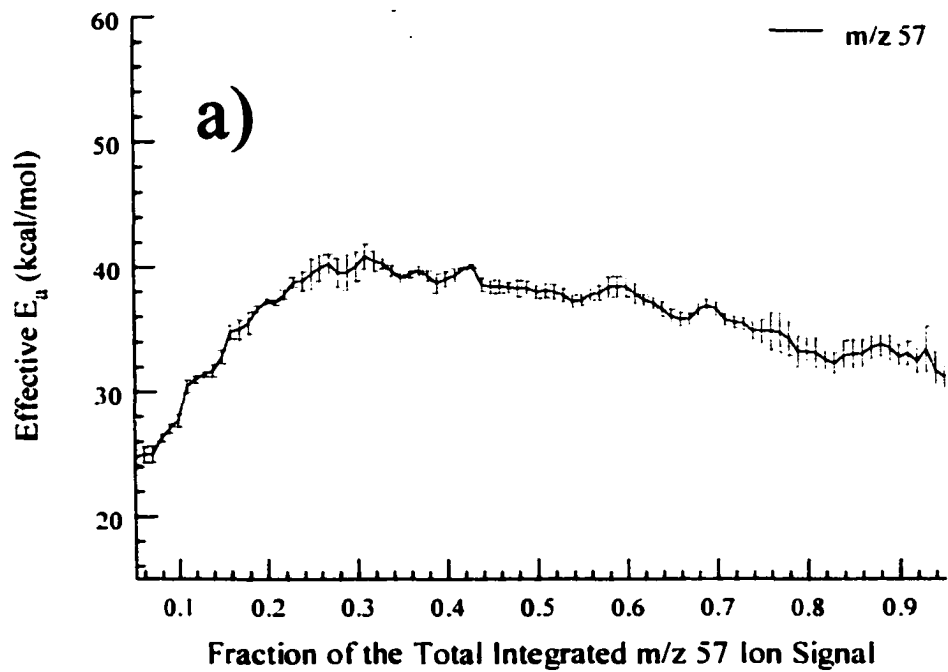


Figure 4-20: a) E_a vs. Fractional integrated ion signal b) E_a vs. Temperature plots for the formation of paraffins (m/z 57) from LPE/PtHZSM-5 heated in hydrogen

Isoconversion E_a values then decreased to approximately 34 kcal/mol by 0.95 fractional integrated ion signal (340 °C). The initial paraffin E_a value for the LPE/PtHZSM-5 (H_2) sample was similar to that for the LPE/PtHZSM-5 (He) sample. However, E_a values maximized at lower temperature compared to the LPE/PtHZSM-5 (He) sample (Figure 4-15). Evolution profiles show that olefin and alkyl aromatic formation occurred between 200-300 °C and 240-350 °C, respectively. The selectivity of m/z 91 for volatile alkyl aromatic formation was greater than 99%, but the maximum selectivity of m/z 55 for olefin formation was only 22%. Large errors in E_a values were attributed to small amounts of volatile olefin and aromatic species (low m/z 55 and 91 ion signals). Consequently, the E_a vs. fractional integrated ion signal plots for olefins and alkyl aromatics are not included here.

4.2.5 LPE/HY (He)

4.2.5a TA-GC/MS Results

Figure 4-21a shows the repetitive injection chromatograms obtained while heating the LPE/HY (He) sample. Volatile products were detected from 160-320 °C. The initial temperature of volatile product evolution was 30 °C higher than that for the LPE/HZSM-5 (He) sample. A single volatile product evolution maximum was observed in the chromatograms at 210 °C. Figure 4-21b shows the negative derivative ($-\Delta mg/\Delta^\circ C$) of the TGA weight loss curve for the LPE/HY (He) sample. The large initial decrease in the TGA plot between 120-160 °C was due to the desorption of water from the catalyst. A single polymer weight loss region was observed between 160-270 °C.

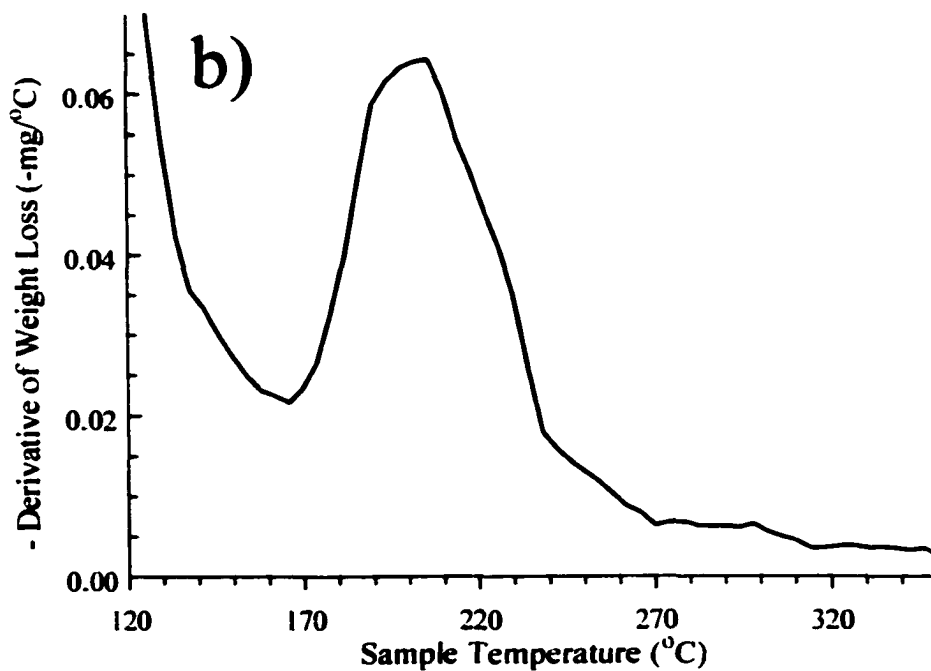
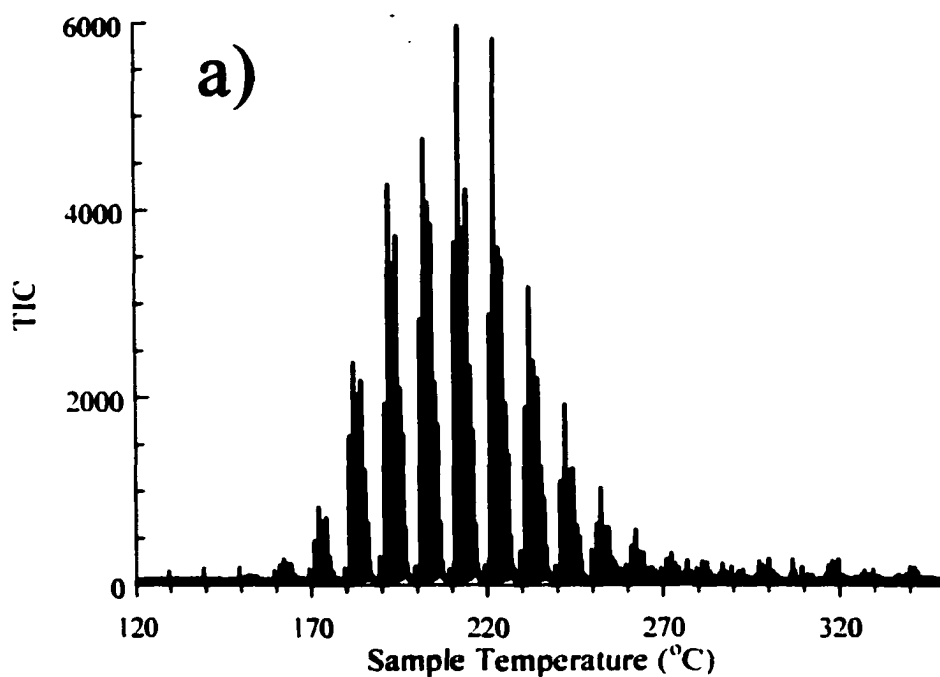


Figure 4-21: a) Repetitive injection chromatogram for LPE/HY heated in helium b) Negative derivative of the weight loss obtained for LPE/HY heated in helium by using TGA

Figure 4-22 shows the repetitive injection chromatograms obtained at a) 170, b) 210, and c) 260 °C. At 170 °C (Figure 4-22a), 15 volatile products were detected between 0 and 3.25 min and volatile product chromatograms did not change significantly as sample temperature increased (Figures 4-22b and 4-22c).

Figure 4-23 shows the species-specific evolution profiles calculated for a) paraffin, b) olefin, and c) alkyl aromatic volatile products. The shape of the volatile product evolution profiles for volatile paraffin and olefin products were very similar (Figure 4-23a and 4-23b), unlike those for LPE/HZSM-5 (He) (Figure 4-3). The temperature corresponding to the maximum paraffin evolution rate was 210 °C (Figure 4-23a). Alkyl aromatic volatile products were detected initially at 250 °C and their evolution maximized at 290-300 °C (Figure 4-23c). However, the largest integrated TIC peak area calculated for the volatile olefin and aromatic products were about 1/15 and 1/30 of the C₇-paraffin area at their respective maximum temperatures. The volatile product slate illustrated in Figure 4-23 shows that C₃-C₁₀ hydrocarbons were formed and C₅-C₈ paraffins (Figure 4-23a) were the dominant volatile species. Volatile alkyl aromatic products from the LPE/HY (He) sample contributed a smaller fraction of the total product slate relative to the LPE/HZSM-5 (He) sample.

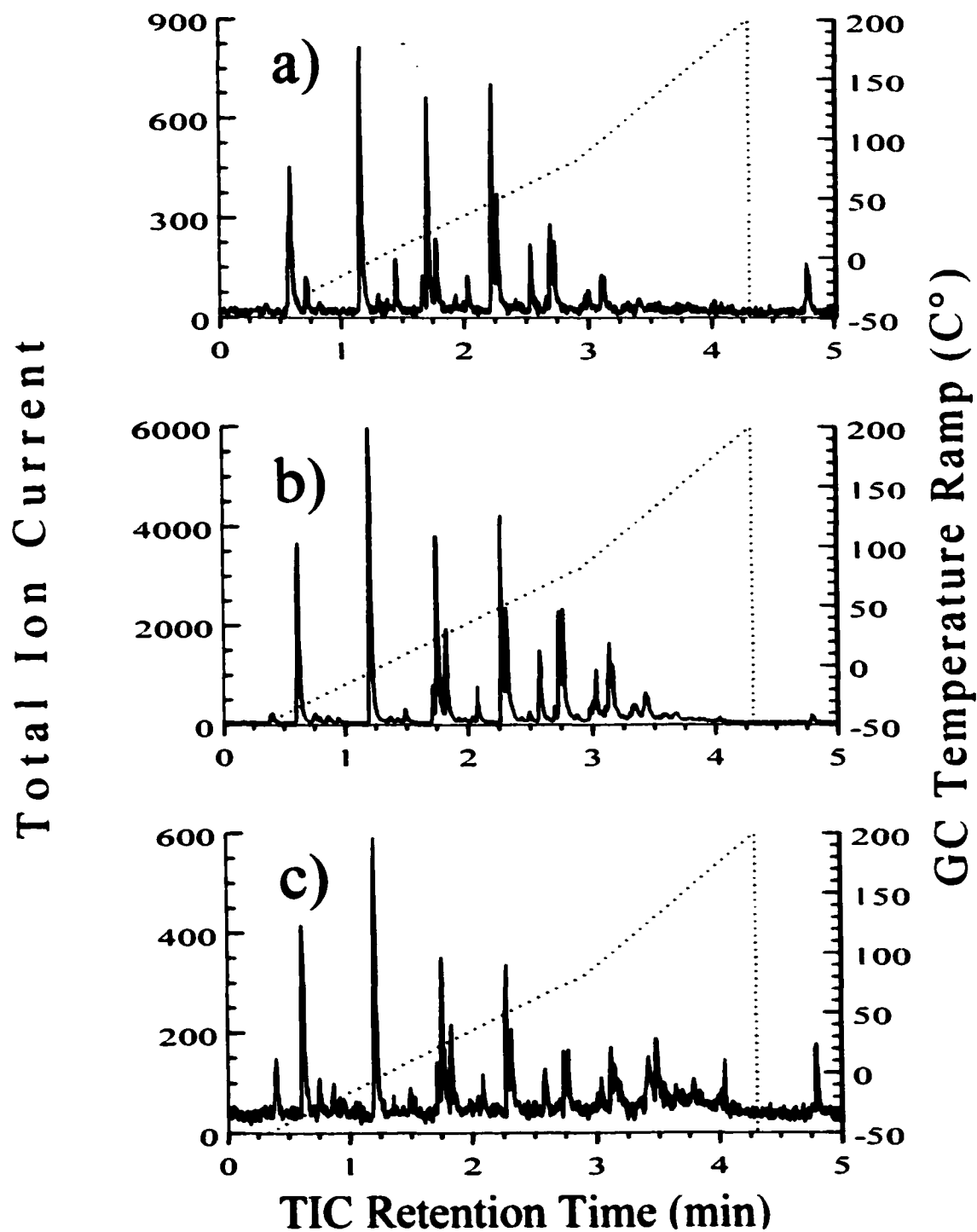


Figure 4-22: Repetitive injection chromatograms obtained from LPE/HY heated in helium when the sample temperature reached a) 170 °C b) 210 °C c) 260 °C

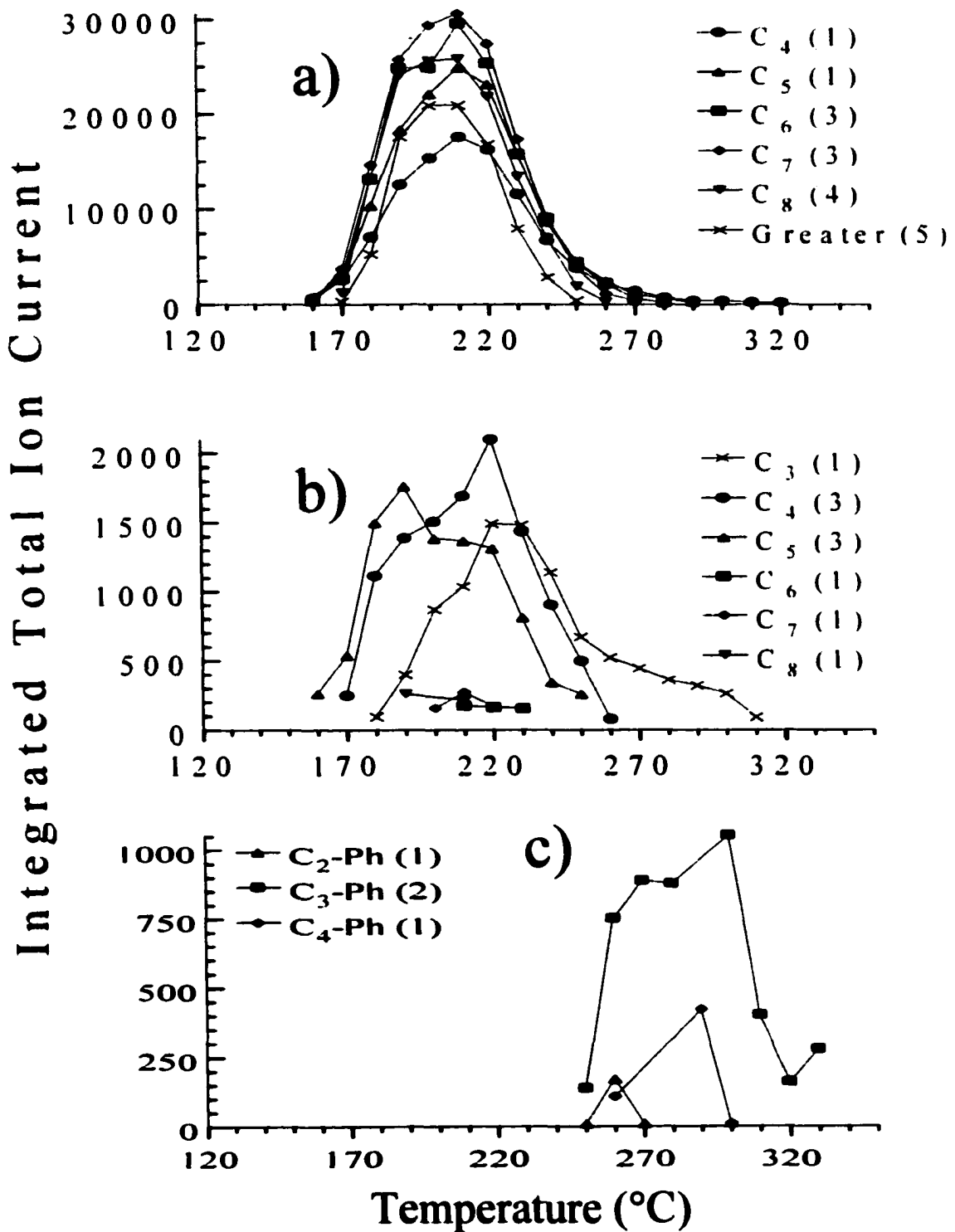


Figure 4-23: Volatile product evolution profiles for LPE/HY heated in helium
 a) paraffins b) olefins c) alkyl aromatics
 [Values in parentheses represent the number of isomers detected]

4.2.5b TA-MS Results

The m/z 57 ion signal selectivity for paraffins was 99% from 0.05-0.95 fractional integrated ion signal. The high selectivity resulted primarily from the dominance of volatile paraffin formation from the LPE/HY (He) sample. The initial E_a value for paraffin formation was about 22 kcal/mol at 0.05 fractional integrated ion signal (175 °C) and then decreased to approximately 19 kcal/mol by 0.95 fractional integrated ion signal (250 °C) (Figure 4-24). The initial paraffin E_a value was slightly lower than that for the LPE/HZSM-5 (He) sample (Figure 4-4) and the trend with respect to temperature (or fractional integrated ion signal) was clearly different. Evolution profiles show that volatile olefin and alkyl aromatic formation occurred between 160-310 °C and 250-330 °C, respectively.

The selectivity of m/z 91 for volatile alkyl aromatics formation was greater than 99%, but the maximum selectivity of m/z 55 for olefin formation was only 20%. Large errors in olefin E_a values were attributed to the small amounts of volatile olefin and aromatic species (low m/z 55 and 91 ion signals). Consequently, the E_a vs. fractional integrated ion signal plots for olefins and alkyl aromatics are not included here.

4.2.6 LPE/HY (H₂)

4.2.6a TA-GC/MS Results

Figure 4-25a shows the repetitive injection chromatograms obtained while heating the LPE/HY (H₂) sample. Volatile products were detected over the same temperature range as for the LPE/HY (He) sample (160-290 °C). A single volatile product evolution maximum was observed in the chromatograms at 210 °C.

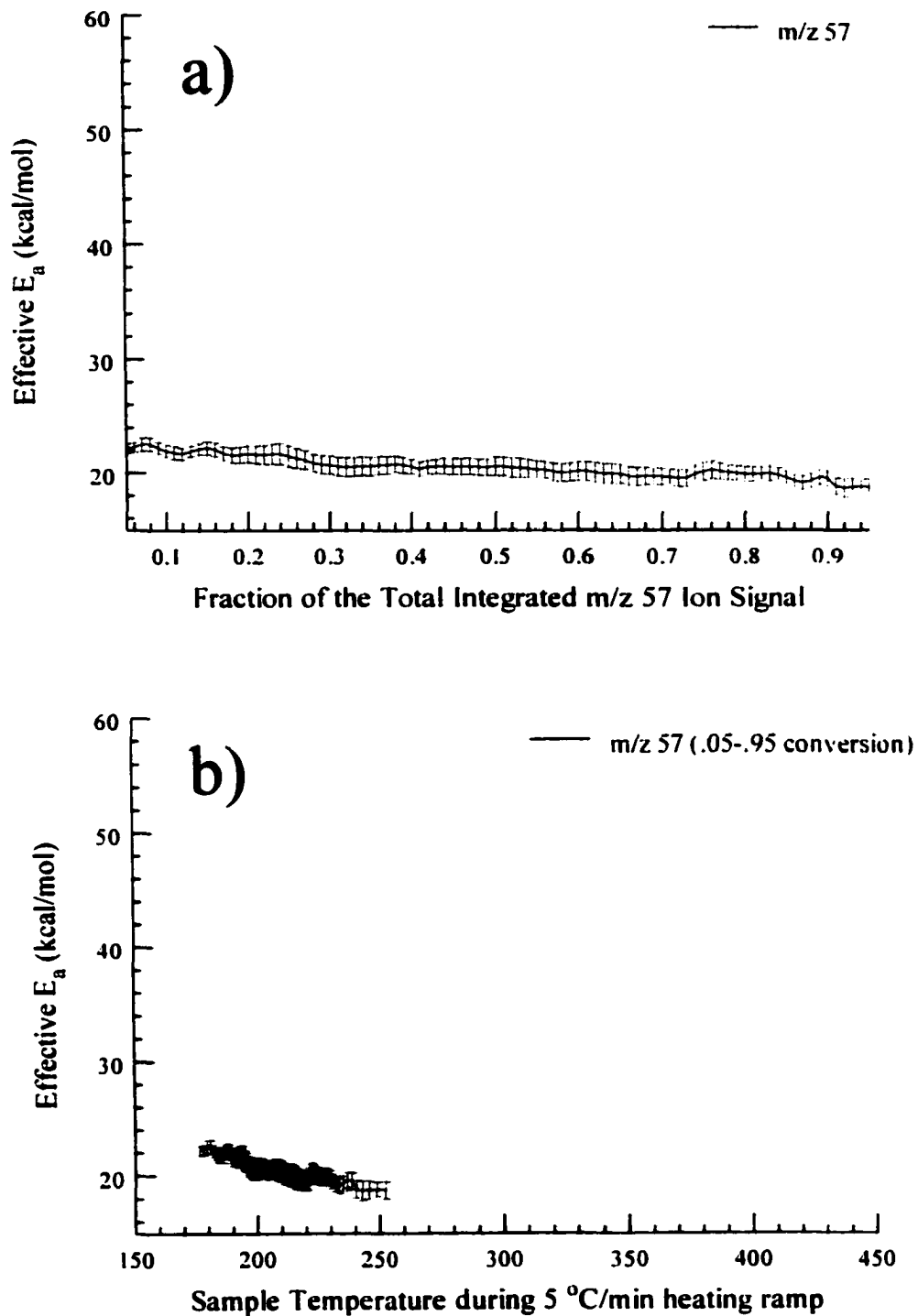


Figure 4-24: a) E_a vs. Fractional integrated ion signal b) E_a vs. Temperature plots for the formation of paraffins (m/z 57) from LPE/HY heated in helium

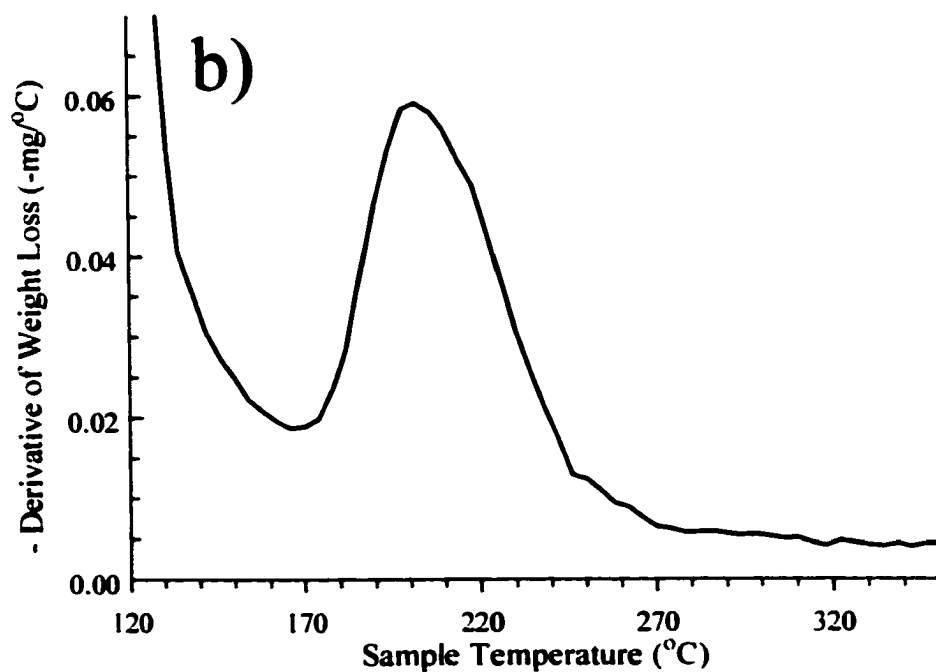
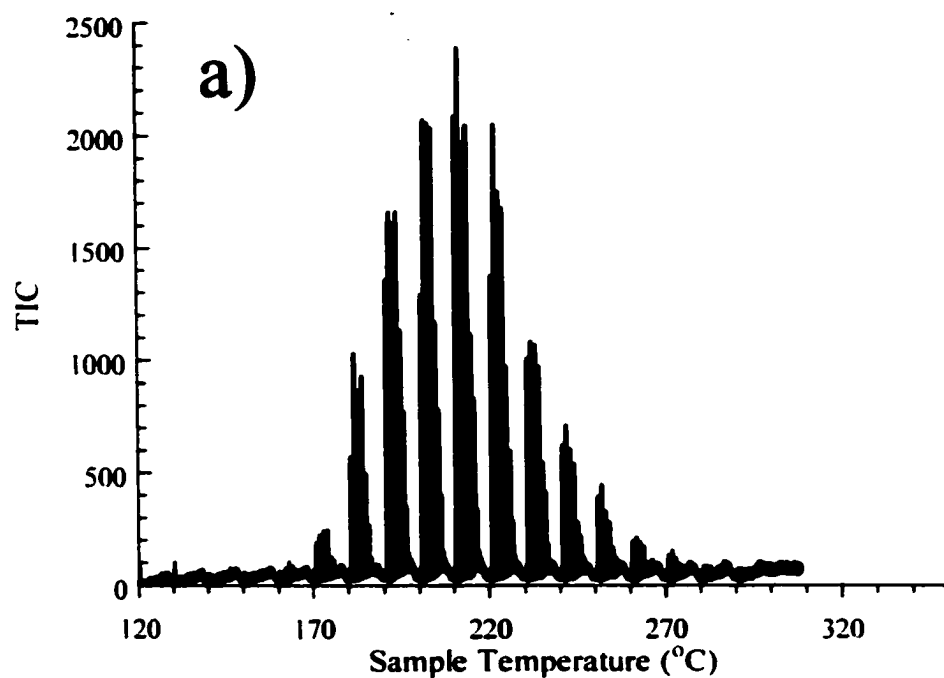


Figure 4-25: a) Repetitive injection chromatogram for LPE/HY heated in hydrogen b) Negative derivative of the weight loss obtained for LPE/HY heated in hydrogen by using TGA

Figure 4-25b shows the negative derivative ($-\Delta\text{mg}/\Delta^\circ\text{C}$) of the TGA weight loss curve for the LPE/HY (H_2) sample. The initial decrease in the TGA plot between 120-170 °C was due to water desorption from the catalyst. A single polymer weight loss region was observed between 170-270 °C.

Figure 4-26 shows the repetitive injection chromatograms obtained at a) 170, b) 210, and c) 260 °C. The chromatograms in Figure 4-26 show that relative volatile hydrocarbon product yields did not change significantly while the LPE/HY (H_2) sample was heated.

Figure 4-27 shows the species-specific evolution profiles calculated for a) paraffin and b) olefin volatile products. The shape of the volatile product evolution profiles versus temperature for volatile paraffin and olefin products were very similar (Figure 4-27a and b), much like those shown for the LPE/HY (He) sample (Figure 4-23). The largest integrated TIC peak area calculated for the volatile olefin products was less than 1/10 of the C_7 -paraffin area at their respective maximum temperatures. The volatile product slate illustrated in Figure 4-27 shows that C_3 - C_{10} hydrocarbons were formed and that C_6 - C_8 paraffins (Figure 4-27a) were the dominant volatile species. The temperature corresponding to the maximum paraffin evolution rate was 210 °C (Figure 4-27a). Volatile alkyl aromatic volatile products were detected in insufficient yield to be represented.

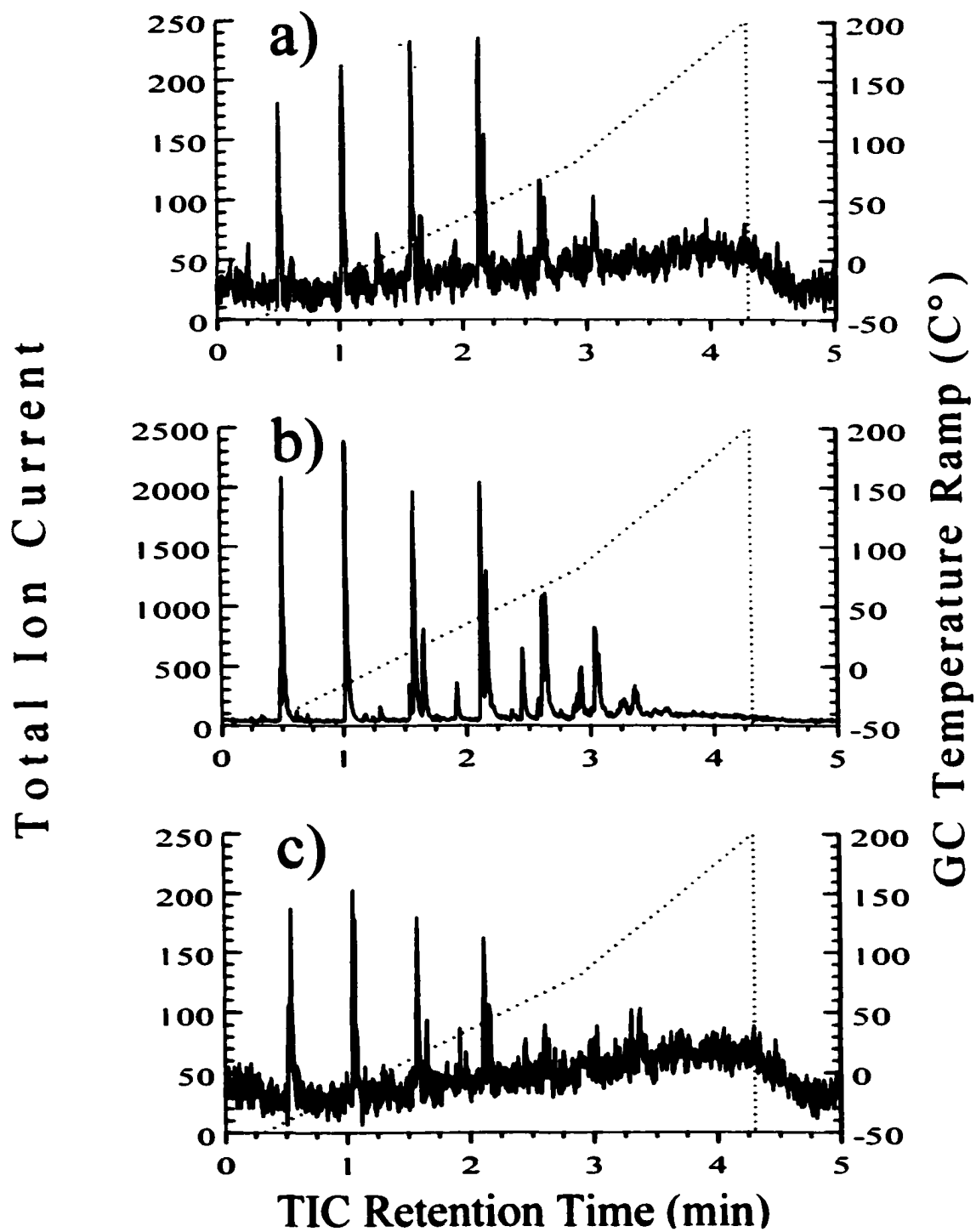


Figure 4-26: Repetitive injection chromatograms obtained from LPE/HY heated in hydrogen when the sample temperature reached a) 170 °C b) 210 °C c) 260 °C

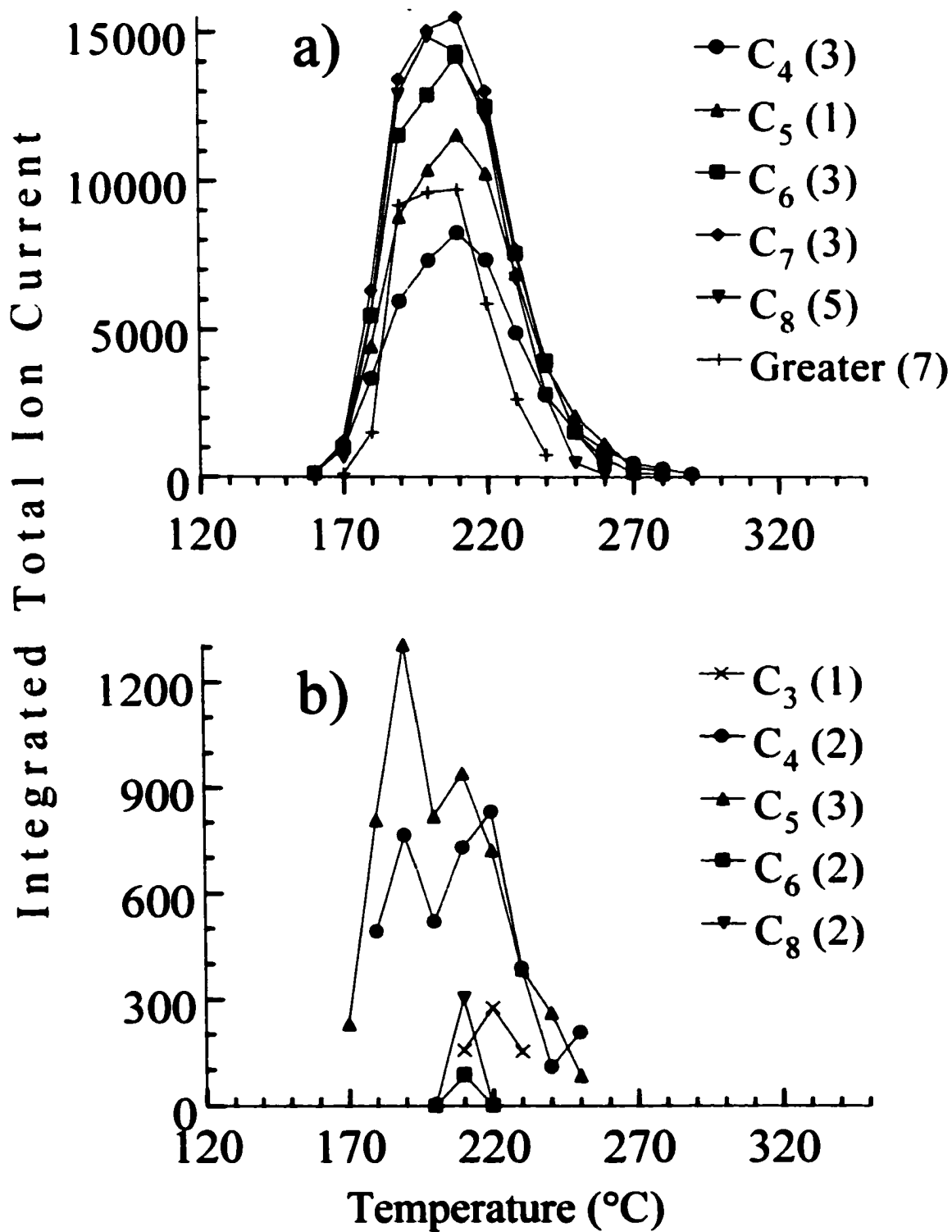


Figure 4-27: Volatile product evolution profiles for LPE/HY heated in hydrogen
 a) paraffins b) olefins
 [Values in parentheses represent the number of isomers detected]

4.2.6b TA-MS Results

The m/z 57 ion signal selectivity for paraffins was 99% from 0.05-0.95 fractional integrated ion signal. The E_a value remained relatively constant at 20-22 kcal/mol between 0.05-0.95 fractional integrated ion signal (180-260 °C) (Figure 4-28). The initial paraffin E_a value was slightly lower than that for the LPE/HY (He) (Figure 4-24) and the trend with respect to temperature (or fractional integrated ion signal) was different. Evolution profiles show that olefin formation occurred between 170-250 °C. The maximum selectivity of m/z 55 for olefin formation was less than 28% and E_a values had large errors due to the low volatile olefin yield. Consequently, the E_a vs. fractional integrated ion signal plot for olefins is not included here.

4.2.7 LPE/PtHY (He)

4.2.7a TA-GC/MS Results

Figure 4-29a shows the repetitive injection chromatograms obtained while heating the LPE/PtHY (He) sample. Volatile products were detected over the same temperature range as for the LPE/HY (He) and (H₂) samples (160-330 °C). Two volatile product evolution maxima were observed in the chromatograms at 210 and 280 °C. Figure 4-29b shows the negative derivative ($-\Delta mg/\Delta^\circ C$) of the TGA weight loss curve for the LPE/PtHY (He) sample. The TGA plot decrease between 120-170 °C was due to desorption of water from the catalyst. A single polymer weight loss region was observed from 170-265 °C.

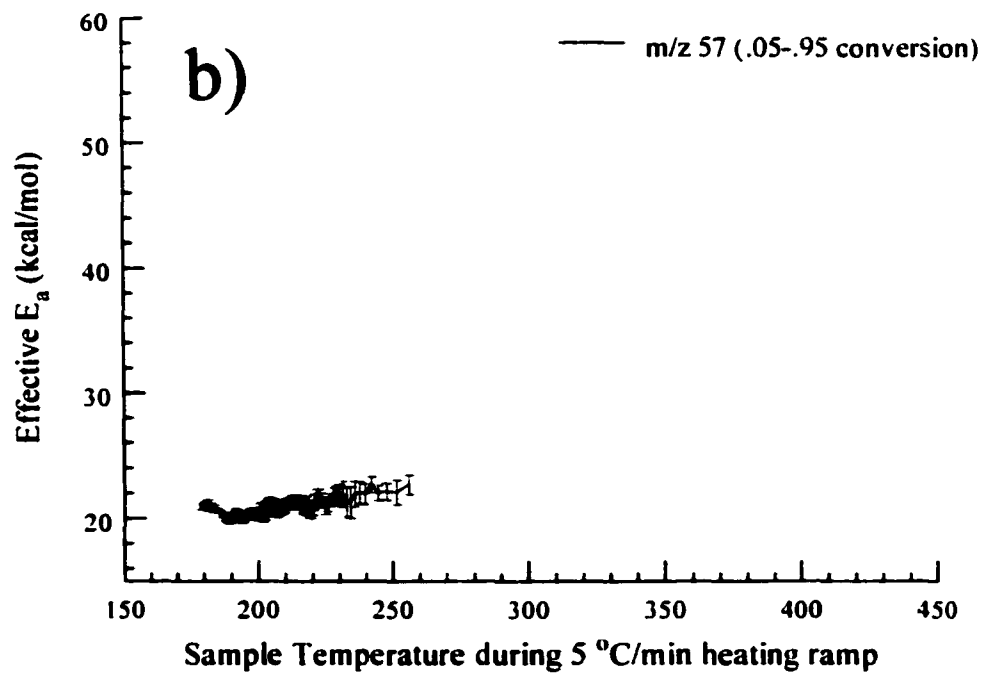
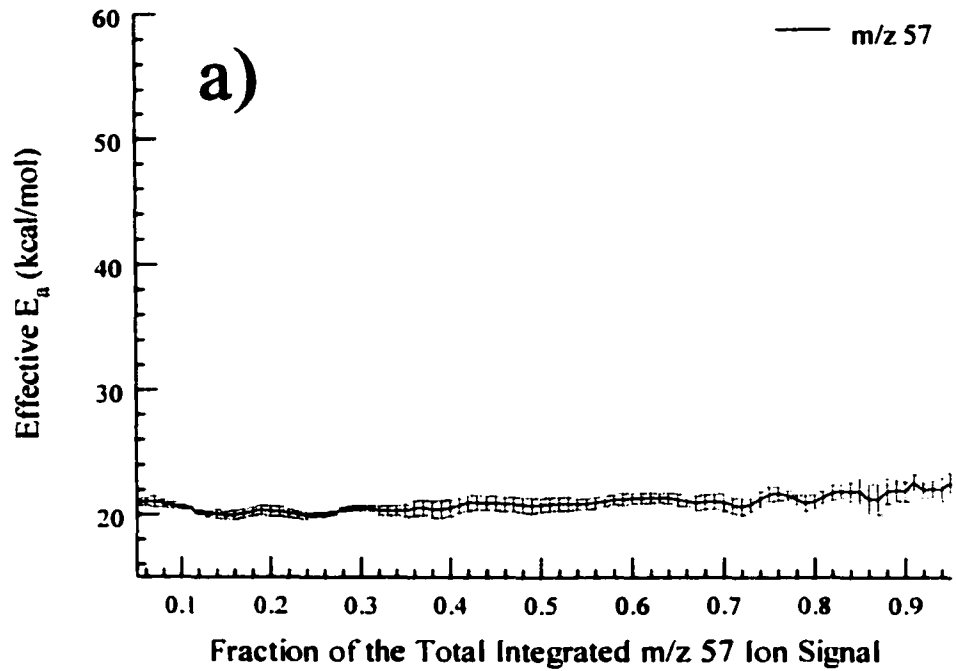


Figure 4-28: a) E_a vs. Fractional integrated ion signal b) E_a vs. Temperature plots for the formation of paraffins (m/z 57) from LPE/HY heated in hydrogen

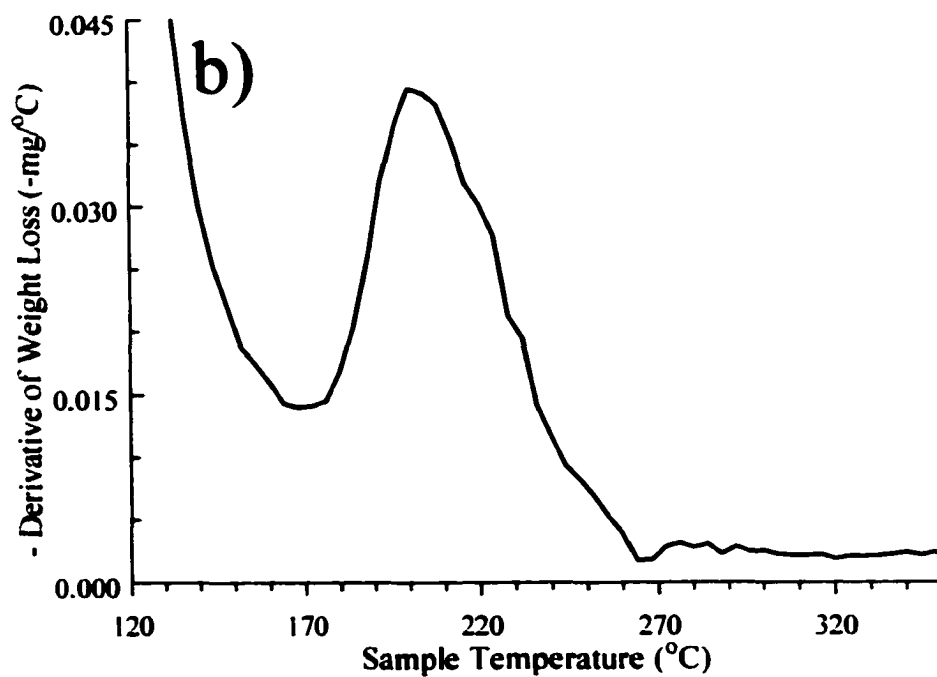
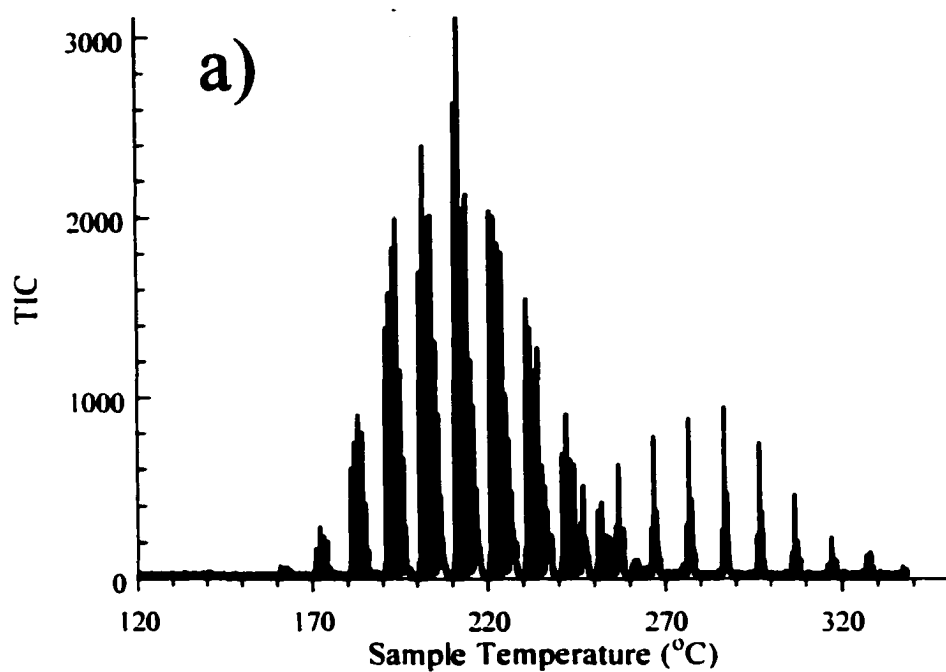


Figure 4-29: a) Repetitive injection chromatogram for LPE/PtHY heated in helium b) Negative derivative of the weight loss obtained for LPE/PtHY heated in helium by using TGA

Figure 4-30 shows the repetitive injection chromatograms obtained at a) 170, b) 210, and c) 260 °C. The majority of the volatile hydrocarbons detected at 150 and 240 °C (Figure 4-30a and 4-30b) had retention times (R_t) of less than 3.0 min. Volatile products with R_t of greater than 3.0 min were predominantly detected at 260 °C (Figure 4-30c).

Figure 4-31 shows the species-specific evolution profiles calculated for a) paraffin, b) olefin, and c) alkyl aromatic volatile products. The volatile product slate illustrated in Figure 4-31 shows that C_3 - C_{10} hydrocarbons were formed and that C_6 - $\geq C_9$ paraffins (Figure 4-31a) were the dominant volatile species. The shape of the volatile product evolution profiles versus temperature for volatile paraffin and olefin products were very similar (Figure 4-31a and b). The temperature corresponding to the maximum paraffin evolution rate was 210 °C (Figure 4-31a). The largest integrated TIC peak area calculated for the volatile olefin products was less than 1/9 of the $\geq C_9$ -paraffin area at their respective maximum temperatures. No volatile paraffin or olefin products were detected above 260 °C. Alkyl aromatic volatile products were detected initially at 230 °C and their evolution maximized at 270-280 °C (Figure 4-31c). More volatile alkyl aromatics evolved from the LPE/PtHY (He) sample compared to the LPE/HY (He) sample (Figure 4-23). The fraction of alkyl aromatics detected for LPE/PtHY (He) was similar to that for LPE/PtHZSM-5 (He) (Figure 4-14).

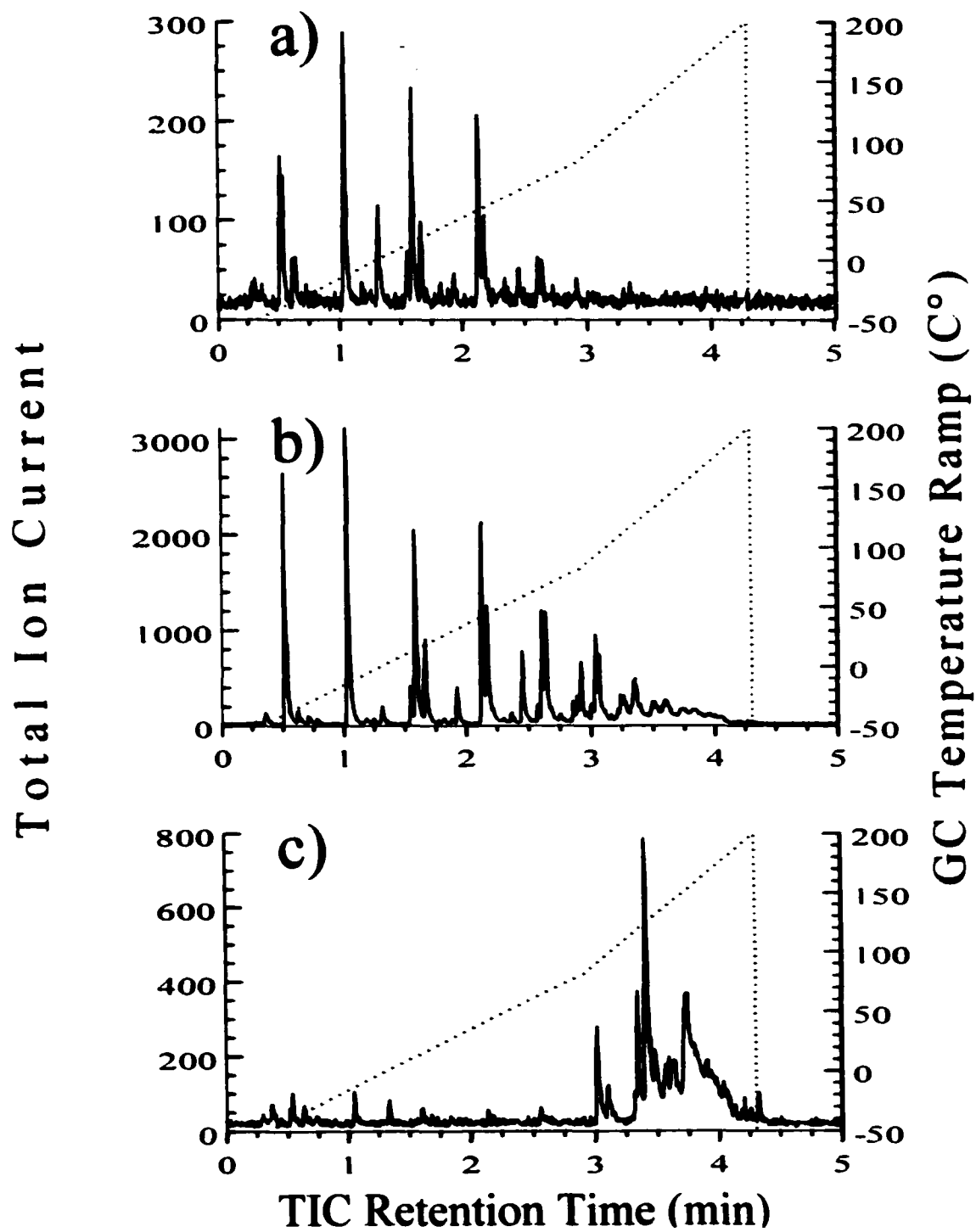


Figure 4-30: Repetitive injection chromatograms obtained from LPE/PtHY heated in helium when the sample temperature reached a) 170 °C
 b) 210 °C c) 260 °C

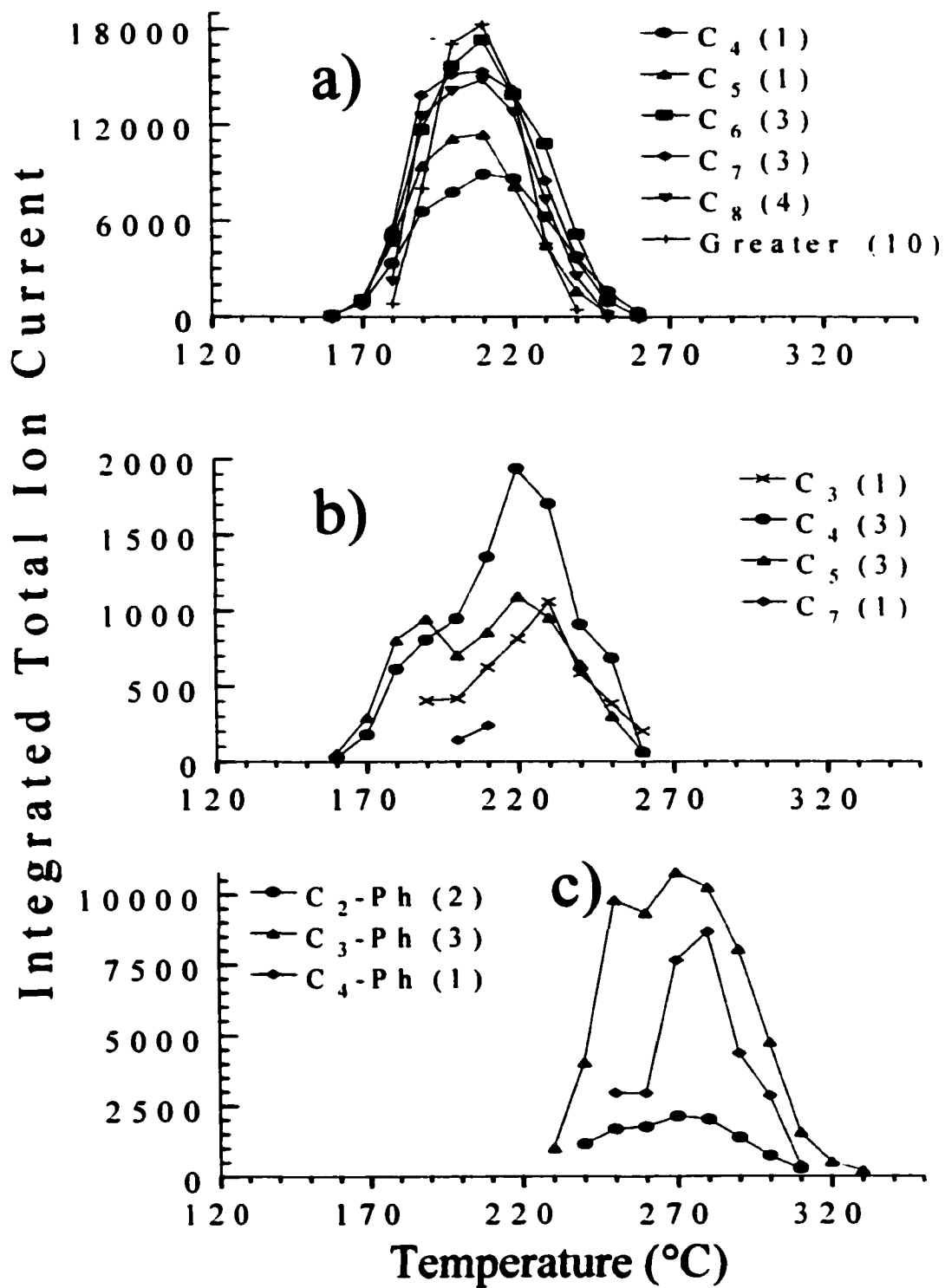


Figure 4-31: Volatile product evolution profiles for LPE/PtHY heated in helium a) paraffins b) olefins c) alkyl aromatics [Values in parentheses represent the number of isomers detected]

4.2.7b TA-MS Results

The m/z 57 and m/z 91 ion signal selectivities for paraffins and alkyl aromatics were both 99% from 0.05-0.95 fractional integrated ion signal. The initial E_a value for paraffin formation (solid line w/ error bars) was about 27 kcal/mol at 0.05 fractional integrated ion signal (175 °C) and then decreased to approximately 23 kcal/mol by 0.95 fractional integrated ion signal (255 °C) (Figure 4-32). The initial paraffin E_a value calculated for the LPE/PtHY (He) sample was 5 kcal/mol higher than that for the LPE/HY (He) sample (Figure 4-24). The initial E_a value for alkyl aromatic formation (dashed line w/ error bars) was about 23 kcal/mol at 0.05 fractional integrated ion signal (240 °C) and remained relatively constant (22-24 kcal/mol) until 0.95 fractional integrated ion signal (350 °C) (Figure 4-32). The alkyl aromatic E_a value calculated for the LPE/PtHY (He) sample was 10 kcal/mol lower than that for the LPE/PtHZSM-5 (He) sample (Figure 4-16). Evolution profiles show that volatile olefin evolution occurred between 160-260 °C. The maximum selectivity of m/z 55 for olefin formation was only 25%. Large errors in olefin E_a values were attributed to low volatile olefin yield and low m/z 55 olefin selectivity. Consequently, the E_a vs. fractional integrated ion signal plot for olefins is not included here.

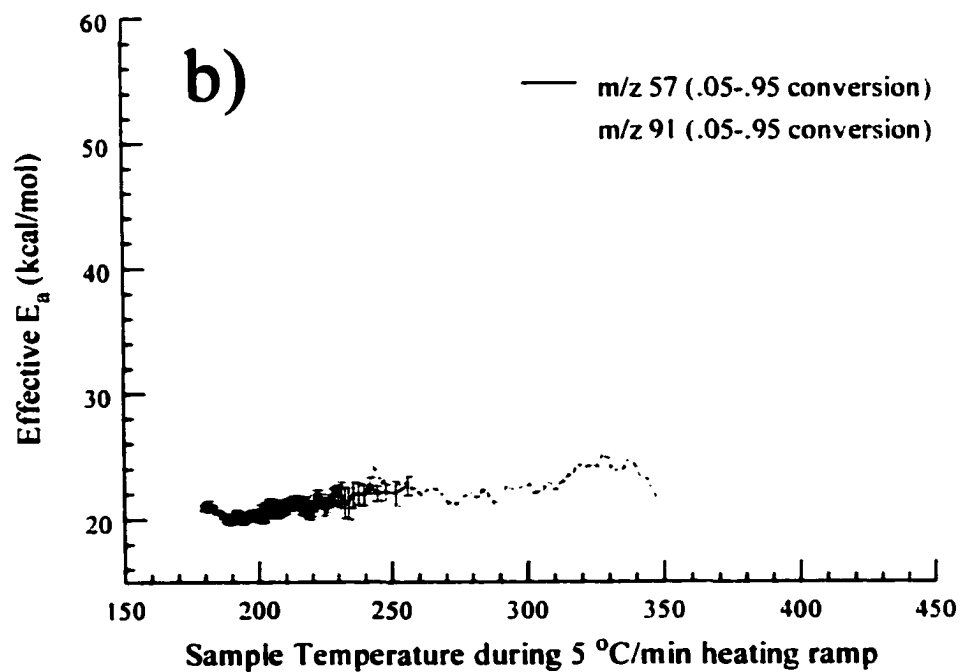
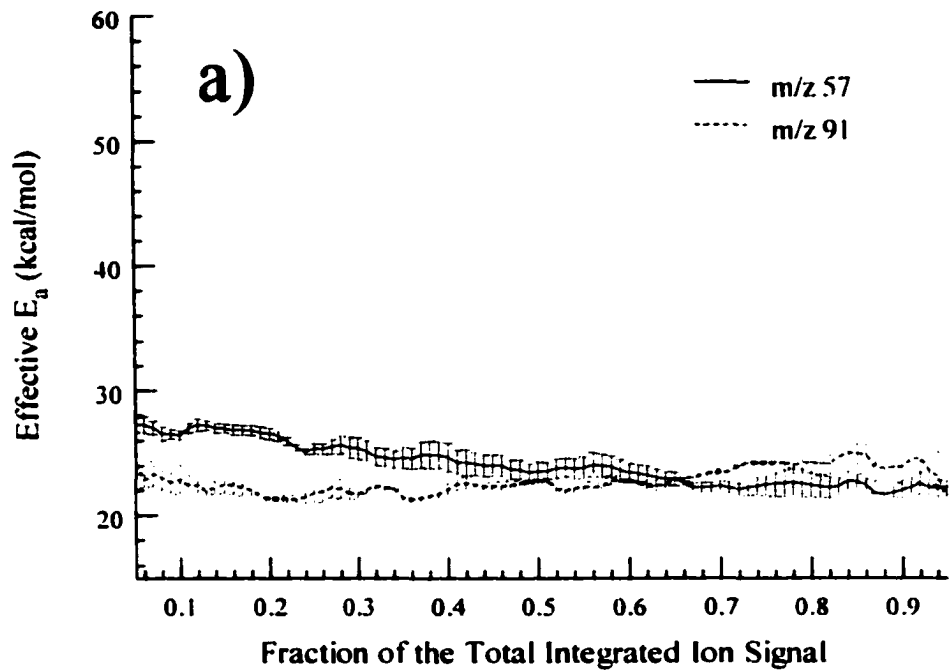


Figure 4-32: a) E_a vs. Fractional integrated ion signal b) E_a vs. Temperature plots for the formation of paraffins (m/z 57) and alkyl aromatics from LPE/PtHY heated in helium

4.2.8 LPE/PtHY (H₂)

4.2.8a TA-GC/MS Results

Figure 4-33a shows the repetitive injection chromatograms obtained while heating the LPE/PtHY (H₂) sample. Volatile products were detected between 220-320 °C. The initial temperature of volatile product evolution was 60 °C higher than for the LPE/PtHY (He) sample. A single volatile product evolution maximum at 260 °C was observed in the chromatograms. Figure 4-33b shows the negative derivative ($-\Delta\text{mg}/\Delta^\circ\text{C}$) of the TGA weight loss curve for the LPE/PtHY (H₂) sample. The TGA plot decrease between 120-210 °C was due to desorption of water from the catalyst. A single polymer weight loss region was observed from 210-300 °C.

Figure 4-34 shows the repetitive injection chromatograms obtained at a) 220, b) 260, and c) 300 °C. Over 20 volatile hydrocarbon products were detected and closely eluting volatile products with R_t values greater than 3.0 min caused the baseline increase.

Figure 4-35 shows the species-specific evolution profiles calculated for a) paraffin and b) olefin volatile products. The shapes of the volatile product evolution profiles versus temperature for volatile paraffins were very similar (Figure 4-35a). The largest integrated TIC peak area calculated for the volatile olefin products was less than 1/20 of the $\geq\text{C}_9$ -paraffin area at their respective maximum temperatures. The volatile product slate illustrated in Figure 4-35 shows that C_4 - $\geq\text{C}_9$ hydrocarbons were formed and that 17 isomers of $\geq\text{C}_9$ paraffins (Figure 4-35a) were the dominant volatile species. The C_8 and $\geq\text{C}_9$ paraffin isomer yield was significantly greater for the LPE/HY (H₂) sample than for the LPE/PtHY (He) sample (Figure 4-31).

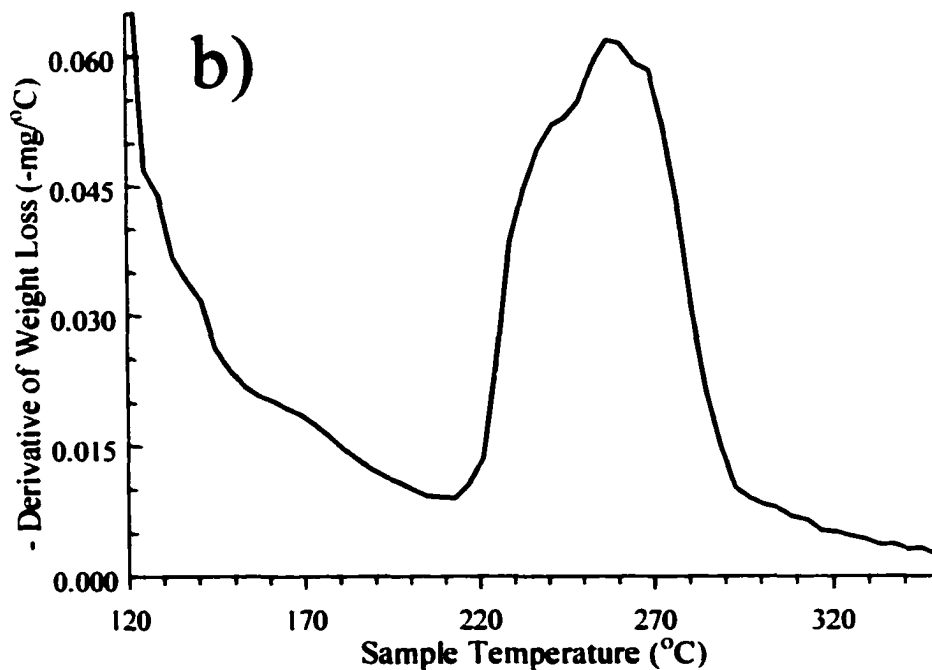
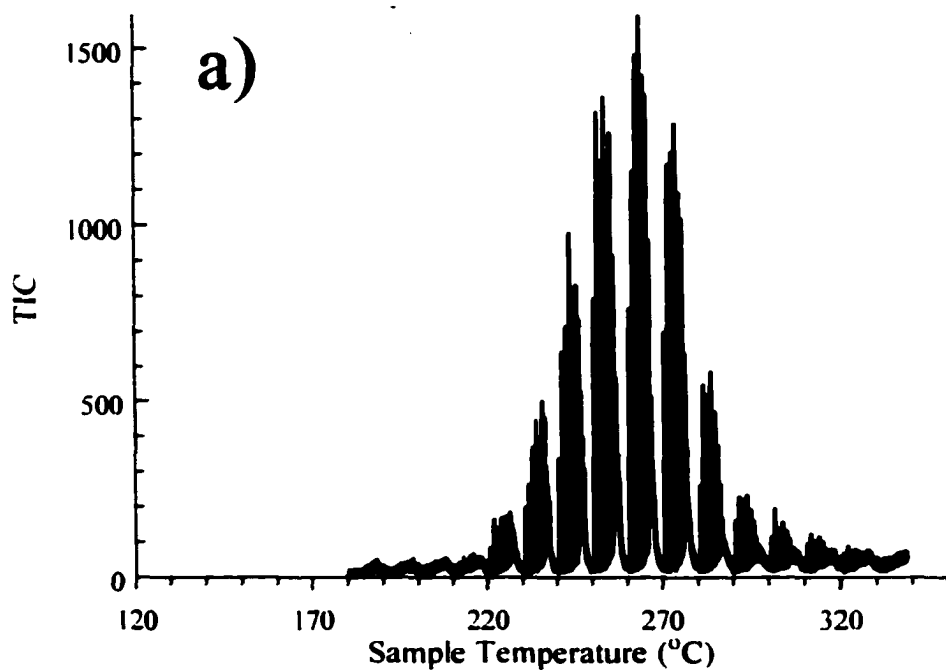


Figure 4-33: a) Repetitive injection chromatogram for LPE/PtHY heated in hydrogen b) Negative derivative of the weight loss obtained for LPE/PtHY heated in hydrogen by using TGA

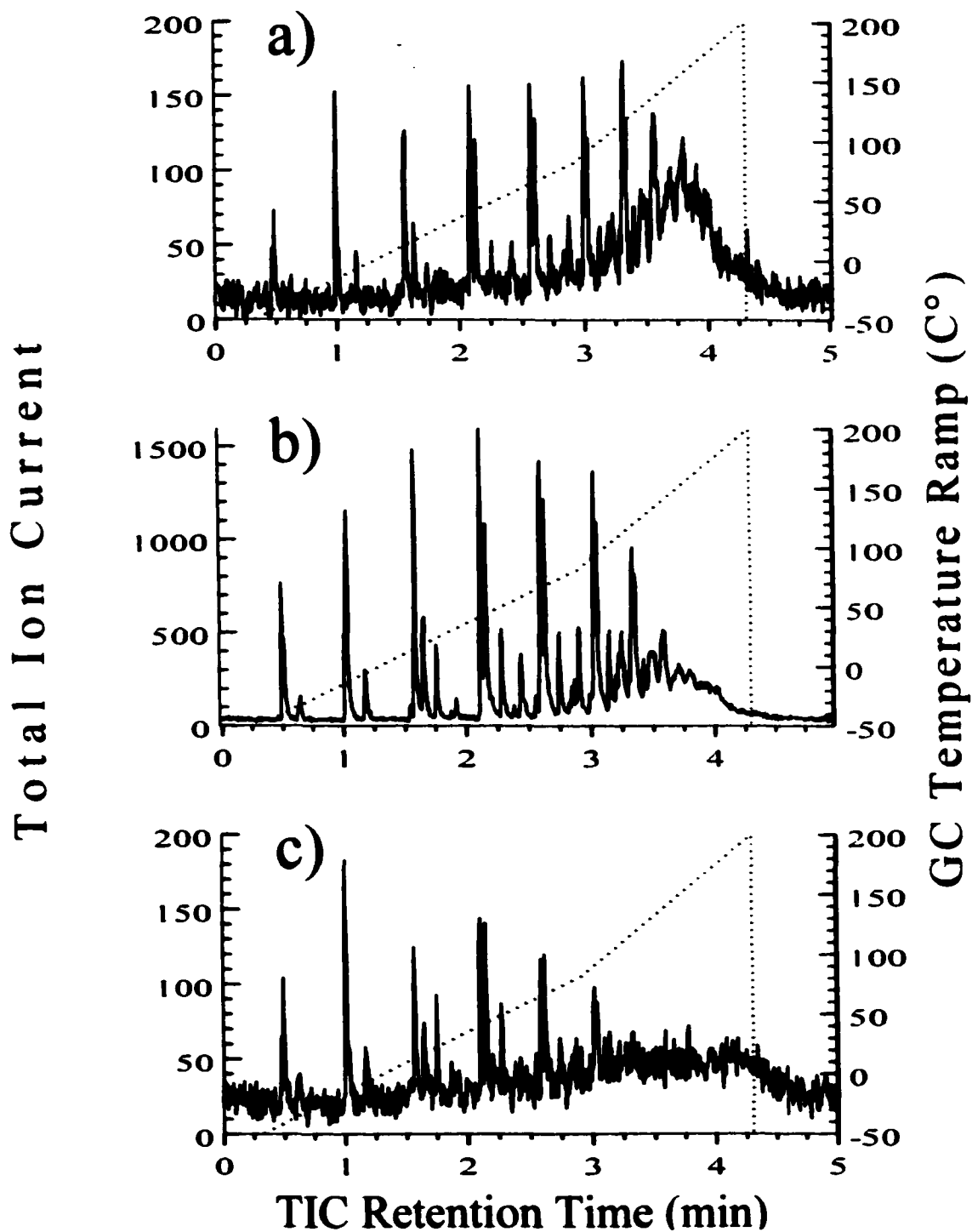


Figure 4-34: Repetitive injection chromatograms obtained from LPE/PtHY heated in hydrogen when the sample temperature reached a) 220 °C b) 260 °C c) 300 °C

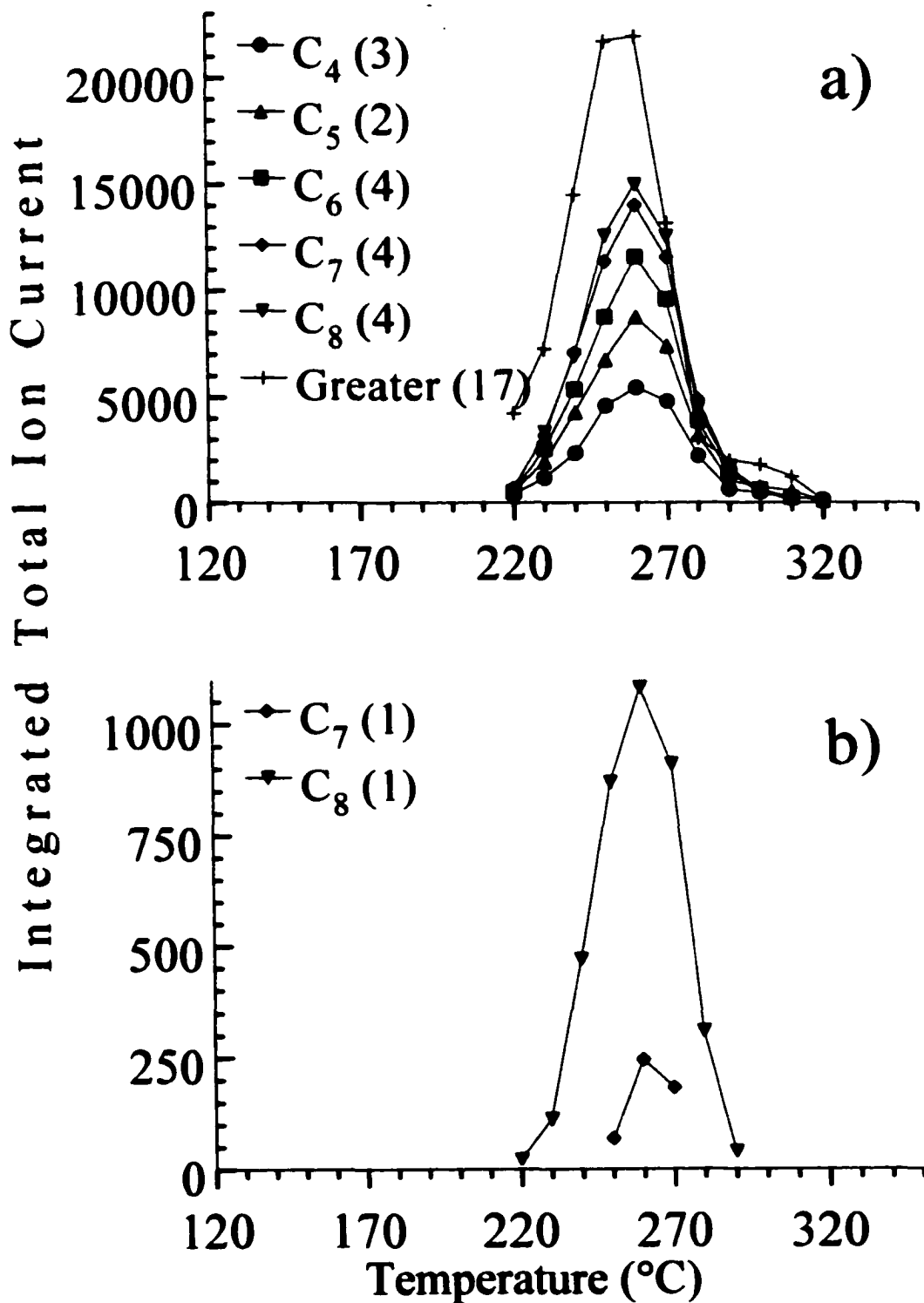


Figure 4-35: Volatile product evolution profiles for LPE/PtHY heated in hydrogen a) paraffins b) olefins
 [Values in parentheses represent the number of isomers detected]

The temperature corresponding to the maximum paraffin evolution rate was 260 °C (Figure 4-35a). Insufficient volatile alkyl aromatic volatile products were detected for them to be represented.

4.2.8b TA-MS Results

The m/z 57 ion signal selectivity calculated for paraffins was 99% from 0.05-0.95 fractional integrated ion signal. The E_a value for paraffin formation in Figure 4-36 was initially 38 kcal/mol at 0.05 fractional integrated ion signal (255 °C), but then decreased to 28 kcal/mol by 0.95 fractional integrated ion signal (345 °C). The initial E_a value for the LPE/PtHY (H₂) sample was 10 kcal/mol higher and occurred 40 °C higher than for the LPE/PtHY (He) sample (Figure 4-32). The initial E_a value for the LPE/PtHY (H₂) sample was about the same as that for the LPE/PtHZSM-5 (H₂) sample at 0.30 fractional integrated ion signal (Figure 4-20). Evolution profiles show that volatile olefin formation occurred between 220-290 °C. Large olefin E_a errors were attributed to low volatile olefin yields. Consequently, the E_a vs. fractional integrated ion signal plot for olefins is not included here.

4.2.9 LPE/HMCM-41 (He)

4.2.9a TA-GC/MS Results

Figure 4-37a shows the repetitive injection chromatograms obtained while heating the LPE/HMCM-41 (He) sample. Volatile products were detected from 220-340 °C. The initial temperature of volatile product evolution was 60 °C higher than that for the LPE/HY (He) sample. A single volatile product evolution maximum was observed at 270 °C in the chromatograms.

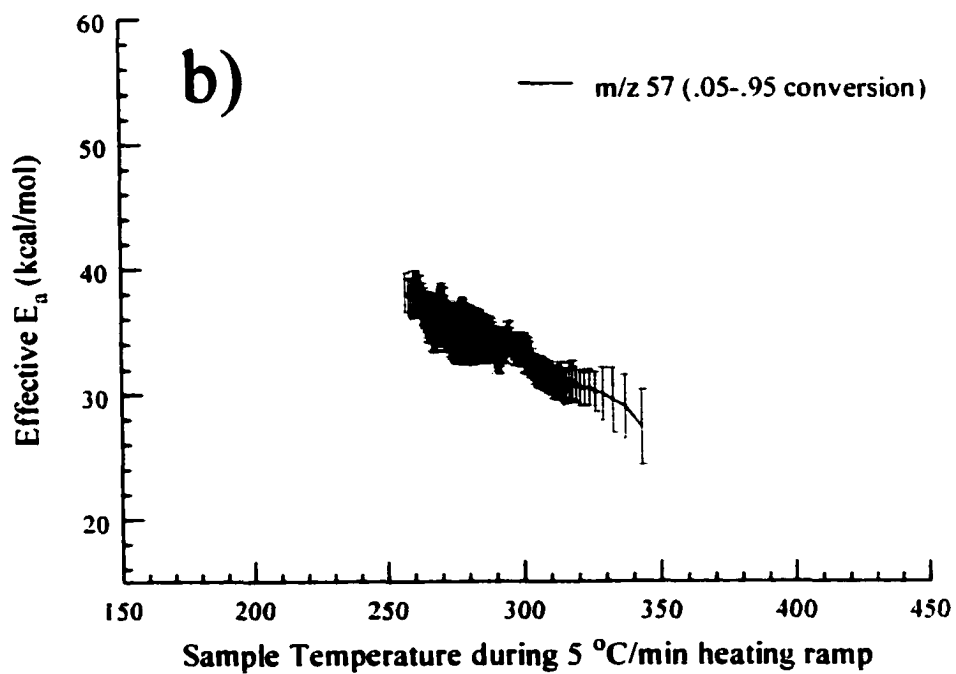
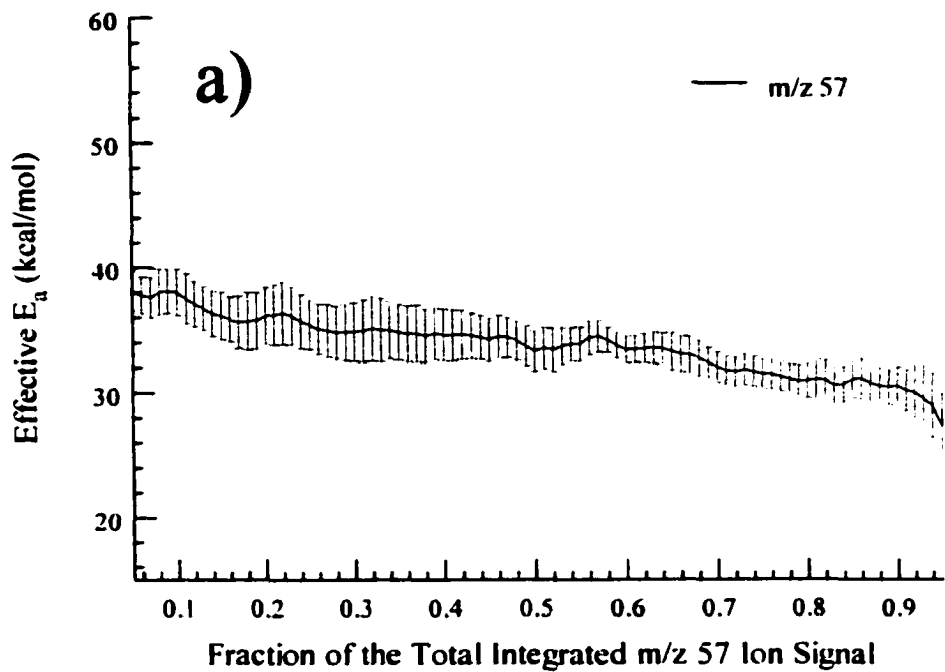


Figure 4-36: a) E_a vs. Fractional integrated ion signal b) E_a vs. Temperature plots for the formation of paraffins (m/z 57) from LPE/PtHY heated in hydrogen

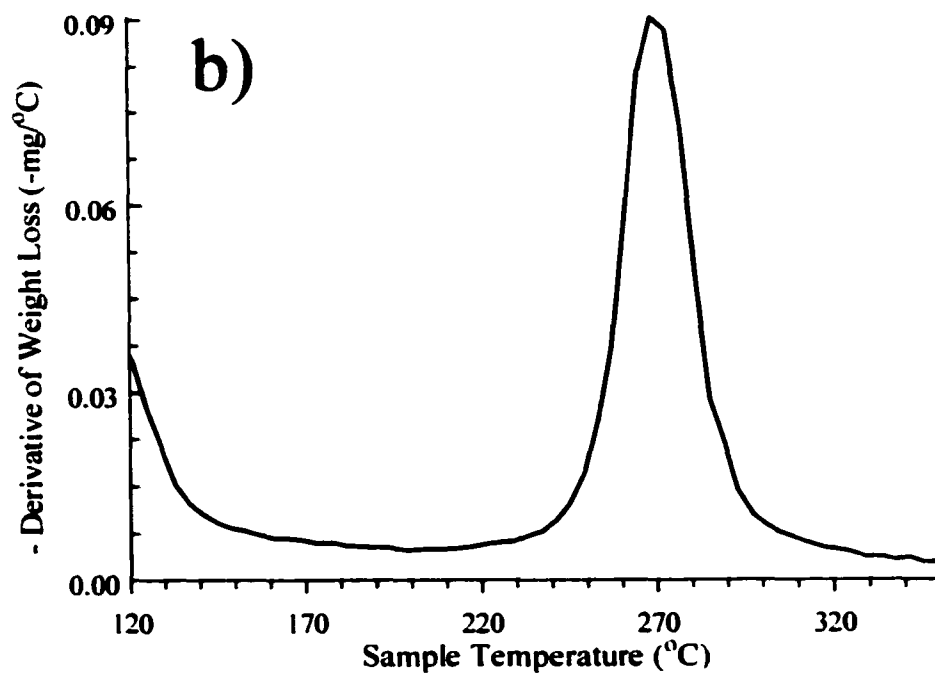
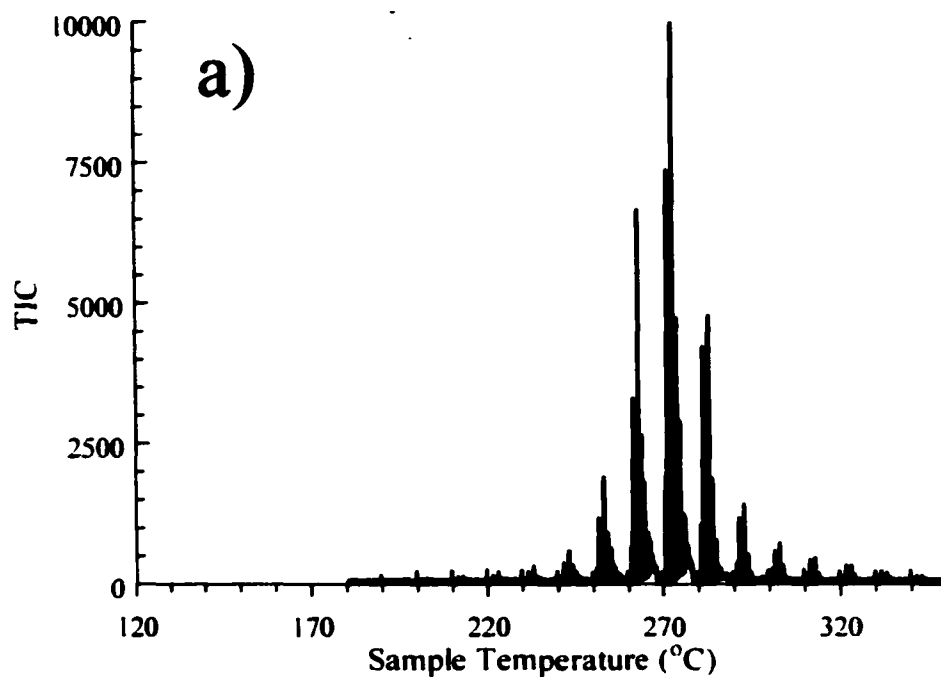


Figure 4-37: a) Repetitive injection chromatogram for LPE/HMCM-41 heated in helium b) Negative derivative of the weight loss obtained for LPE/HMCM-41 heated in helium by using TGA

Figure 4-37b shows the negative derivative ($-\Delta m g / \Delta^{\circ} C$) of the TGA weight loss curve for the LPE/HMCM-41 (He) sample. The small TGA plot decrease between 120-150 °C was due to desorption of water from the catalyst. A single polymer weight loss region was observed from 220-320 °C.

Figure 4-38 shows the repetitive injection chromatograms obtained at a) 250, b) 270, and c) 290 °C. The chromatograms in Figure 4-38 show that relative volatile hydrocarbon product yields did not change significantly while the LPE/HMCM-41 (He) sample was heated. The small air peak at $R_t \approx 4.8$ min in each Figure 4-38 chromatogram was caused by leakage of the six port injection valve when it was rotated back to the load position (Chapter 2).

Figure 4-39 shows the species-specific evolution profiles calculated for a) paraffin and b) olefin volatile products. The shapes of the volatile product evolution profiles versus temperature for volatile paraffin and olefin products were very similar (Figure 4-39a and 4-39b). The largest integrated TIC peak area calculated for the volatile paraffin products was less than 1/7 of the C_5 -olefin area at their respective maximum temperatures. The volatile product slate illustrated in Figure 4-39 shows that C_3 - C_{10} hydrocarbons were formed and that C_4 - C_7 olefins (Figure 4-39b) were the dominant volatile species. The temperature corresponding to the maximum olefin evolution rate was 270 °C (Figure 4-39b). No volatile alkyl aromatic volatile products were detected from the LPE/HMCM-41 (He) sample.

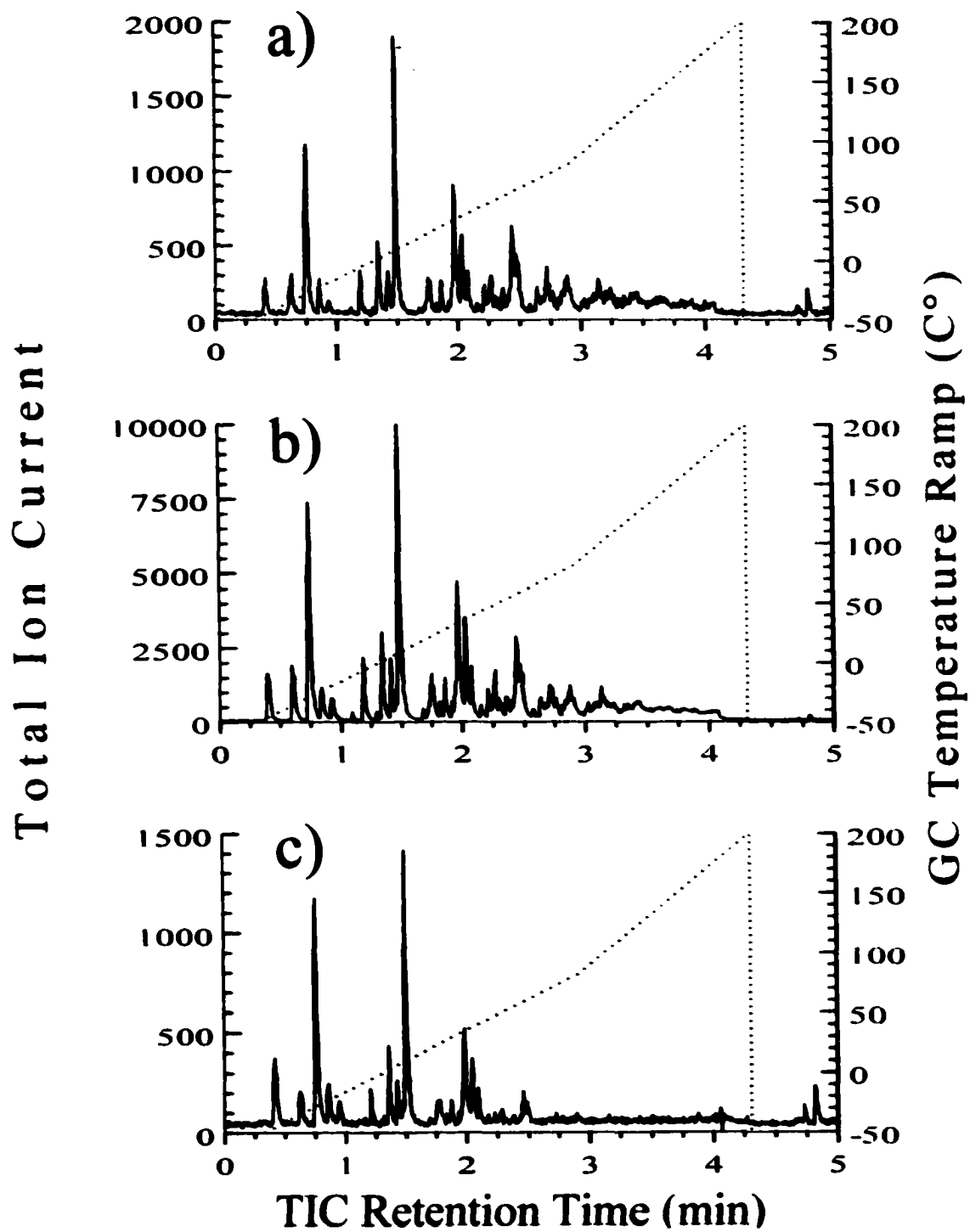


Figure 4-38: Repetitive injection chromatograms obtained from LPE/HMCM-41 heated in helium when the sample temperature reached a) 250 °C b) 270 °C c) 290 °C

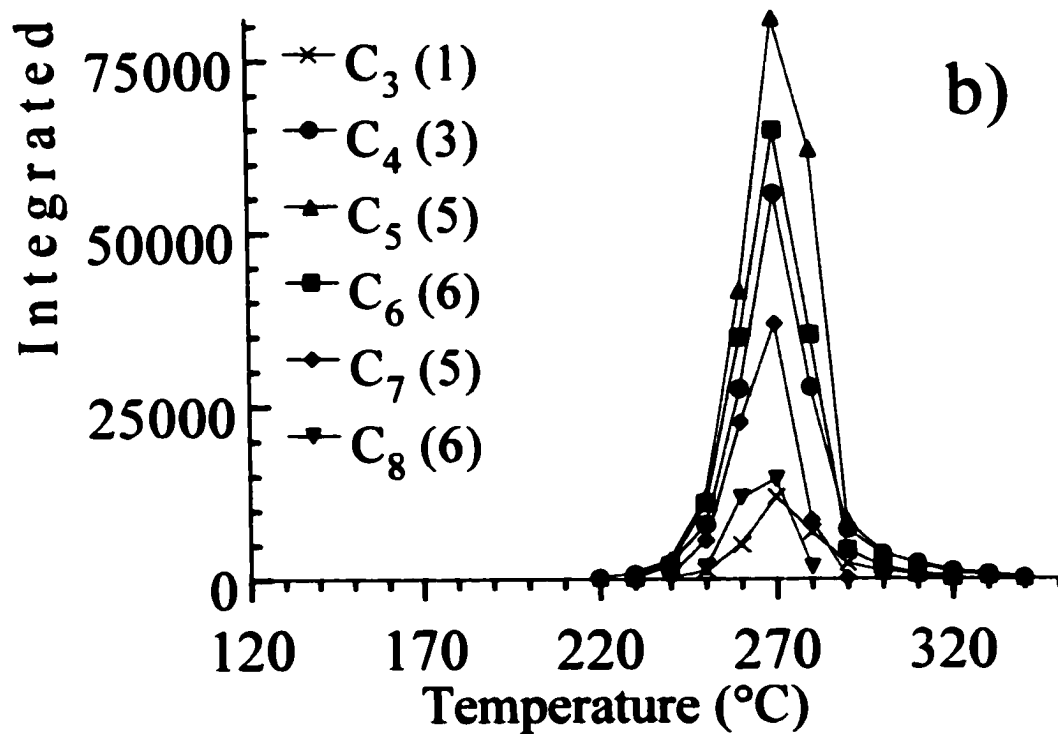
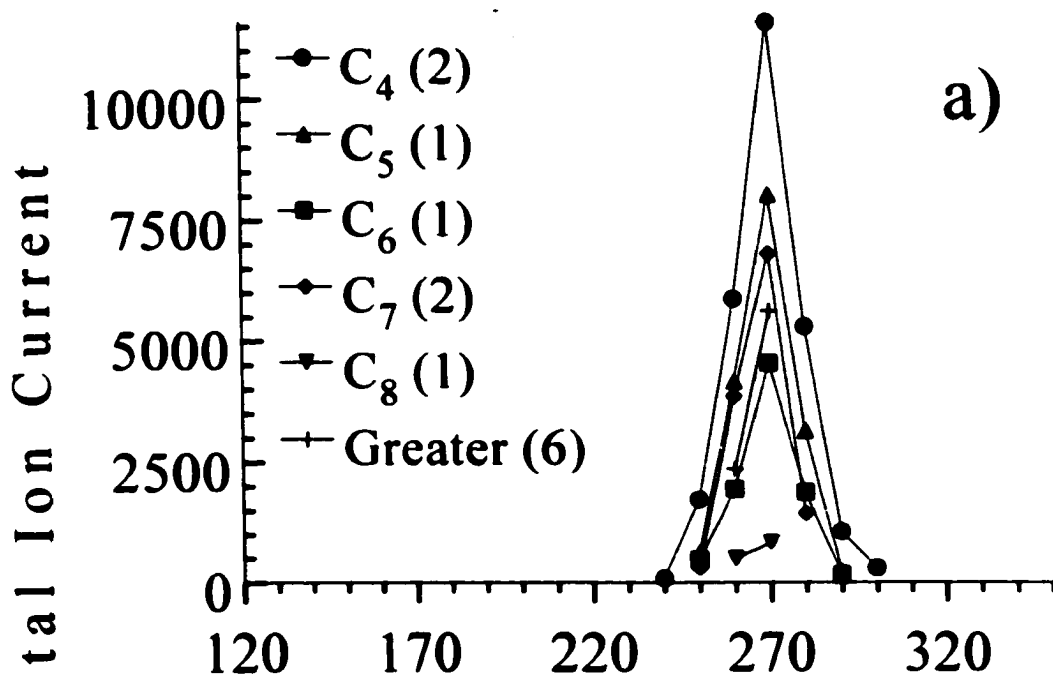


Figure 4-39: Volatile product evolution profiles for LPE/HMCM-41 heated in helium a) paraffins b) olefins
 [Values in parentheses represent the number of isomers detected]

4.2.9b TA-MS Results

The m/z 55 ion signal selectivity for olefins was 97% from 0.05-0.95 fractional integrated ion signal. The large error in E_a values in Figure 4-40 below 0.35 fractional integrated ion signal was due to low volatile olefin yields (low m/z 55 ion signal). The low ion signal intensity made it difficult to calculate temperatures corresponding to specific fractional integrated ion signal values. Above 0.50 fractional integrated ion signal (300 °C), the E_a value remained relatively constant near 26 kcal/mol until 0.95 fractional integrated ion signal (345 °C). Evolution profiles show that volatile paraffin formation occurred between 240-300 °C. Large errors in paraffin E_a values were attributed to low volatile paraffin yield and low m/z 57 paraffin selectivity. Consequently, the E_a vs. fractional integrated ion signal plot for paraffins is not included here.

4.2.10 LPE/HMCM-41 (H₂)

4.2.10a TA-GC/MS Results

Figure 4-41a shows the repetitive injection chromatograms obtained while heating the LPE/HMCM-41 (H₂) sample. Volatile products were detected over the same temperature range as for the LPE/HMCM-41 (He) sample (230-330 °C). A single volatile product evolution maximum was observed in the chromatograms at 270-280 °C. Figure 4-41b shows the negative derivative ($-\Delta mg/\Delta^\circ C$) of the TGA weight loss curve for the LPE/HMCM-41 (H₂) sample. The TGA plot decrease between 120-150 °C was due to desorption of water from the catalyst. A single polymer weight loss region was observed from 230-320 °C.

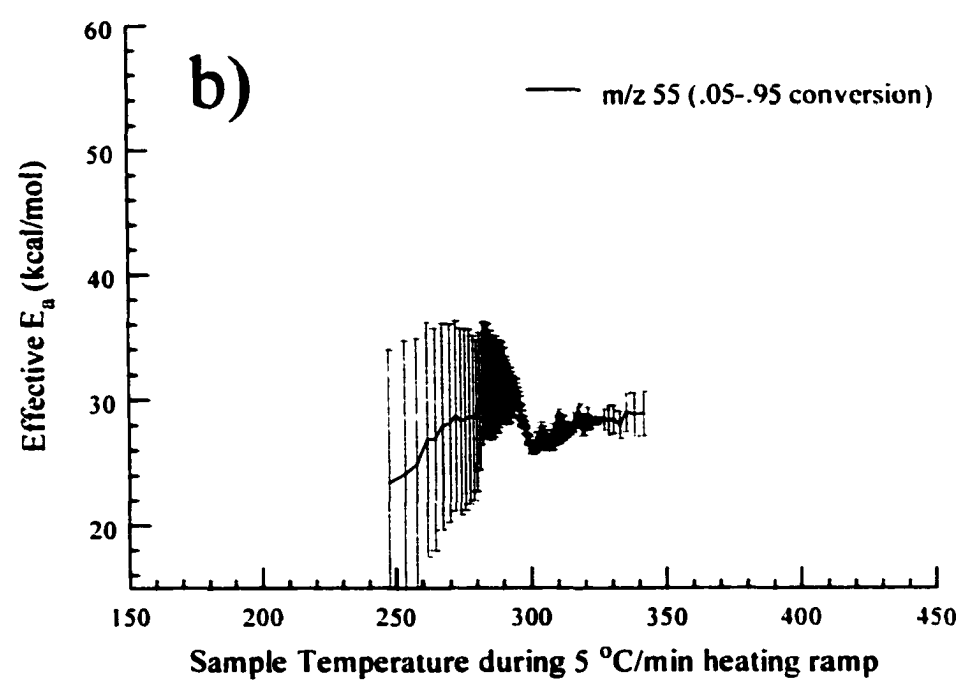
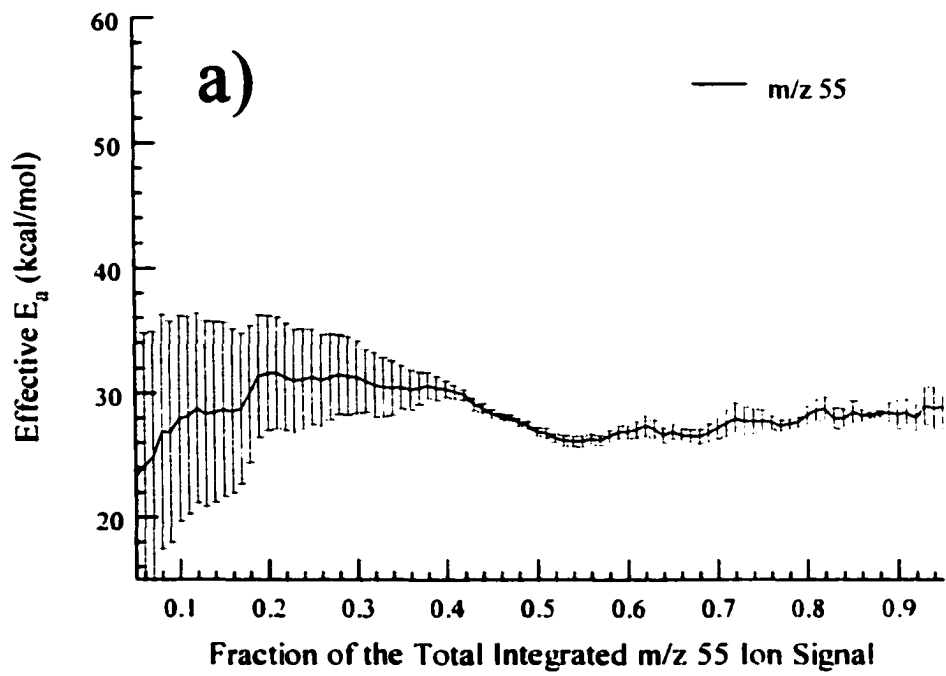


Figure 4-40: a) E_a vs. Fractional integrated ion signal b) E_a vs. Temperature plots for the formation of olefins (m/z 55) from LPE/HMCM-41 heated in helium

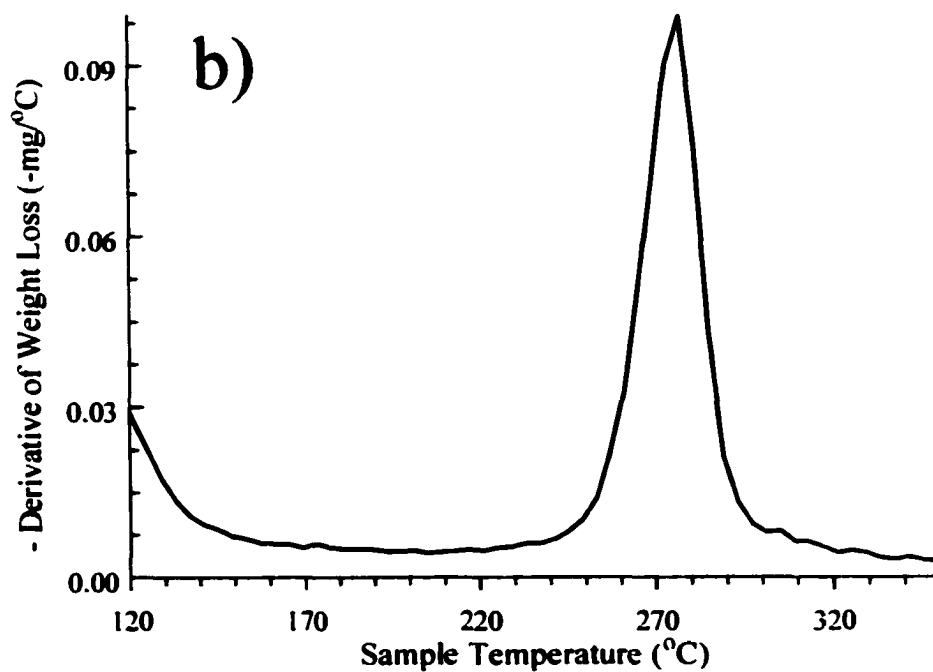
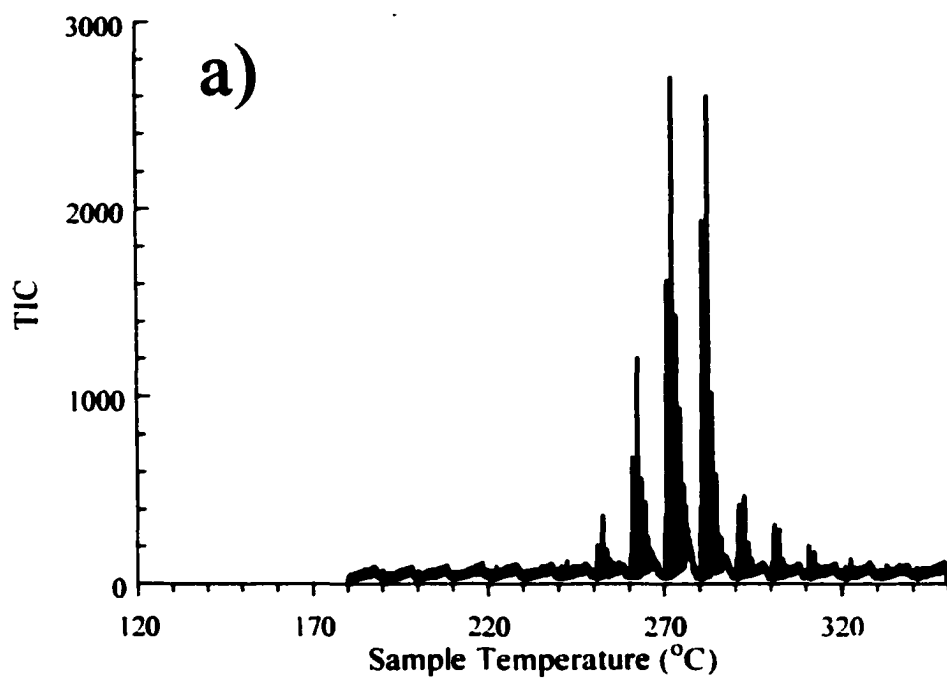


Figure 4-41: a) Repetitive injection chromatogram for LPE/HMCM-41 heated in hydrogen b) Negative derivative of the weight loss obtained for LPE/HMCM-41 heated in hydrogen by using TGA

Figure 4-42 shows the repetitive injection chromatograms obtained at a) 250, b) 270, and c) 290 °C. The chromatograms in Figure 4-42 show that relative volatile hydrocarbon product yields did not change significantly while the LPE/HMCM-41 (H₂) sample was heated.

Figure 4-43 shows the species-specific evolution profiles calculated for a) paraffin and b) olefin volatile products. The shape of the volatile product evolution profiles versus temperature for volatile paraffin and olefin products were very similar (Figure 4-43a and 4-43b). The largest integrated TIC peak area calculated for the volatile paraffin products was less than 1/7 of the C₅-olefin area at their respective maximum temperatures. The volatile product slate illustrated in Figure 4-43 shows that C₃-C₁₀ hydrocarbons were formed and that C₄-C₇ olefins (Figure 4-43b) were the dominant volatile species. The temperature corresponding to the maximum olefin evolution rate was 270 °C (Figure 4-43b). No volatile alkyl aromatic volatile products were detected from the LPE/HMCM-41 (H₂) sample.

4.2.10b TA-MS Results

The m/z 55 ion signal selectivity for olefins was 97% from 0.05-0.95 fractional integrated ion signal. The E_a value for olefin formation in Figure 4-44 was initially 22 kcal/mol at 0.05 fractional integrated ion signal (250 °C) and remained relatively constant until 0.60 fractional integrated ion signal (300 °C). Above 0.60 fractional integrated ion signal (300 °C), the E_a value increased to 26 kcal/mol by 0.95 fractional integrated ion signal (345 °C). The E_a values for the LPE/HMCM-41 (H₂) sample were 6 kcal/mol lower than those for the LPE/HZSM-5 (H₂) sample (Figure 4-10). Evolution profiles show that volatile paraffin formation occurred between 250-300 °C.

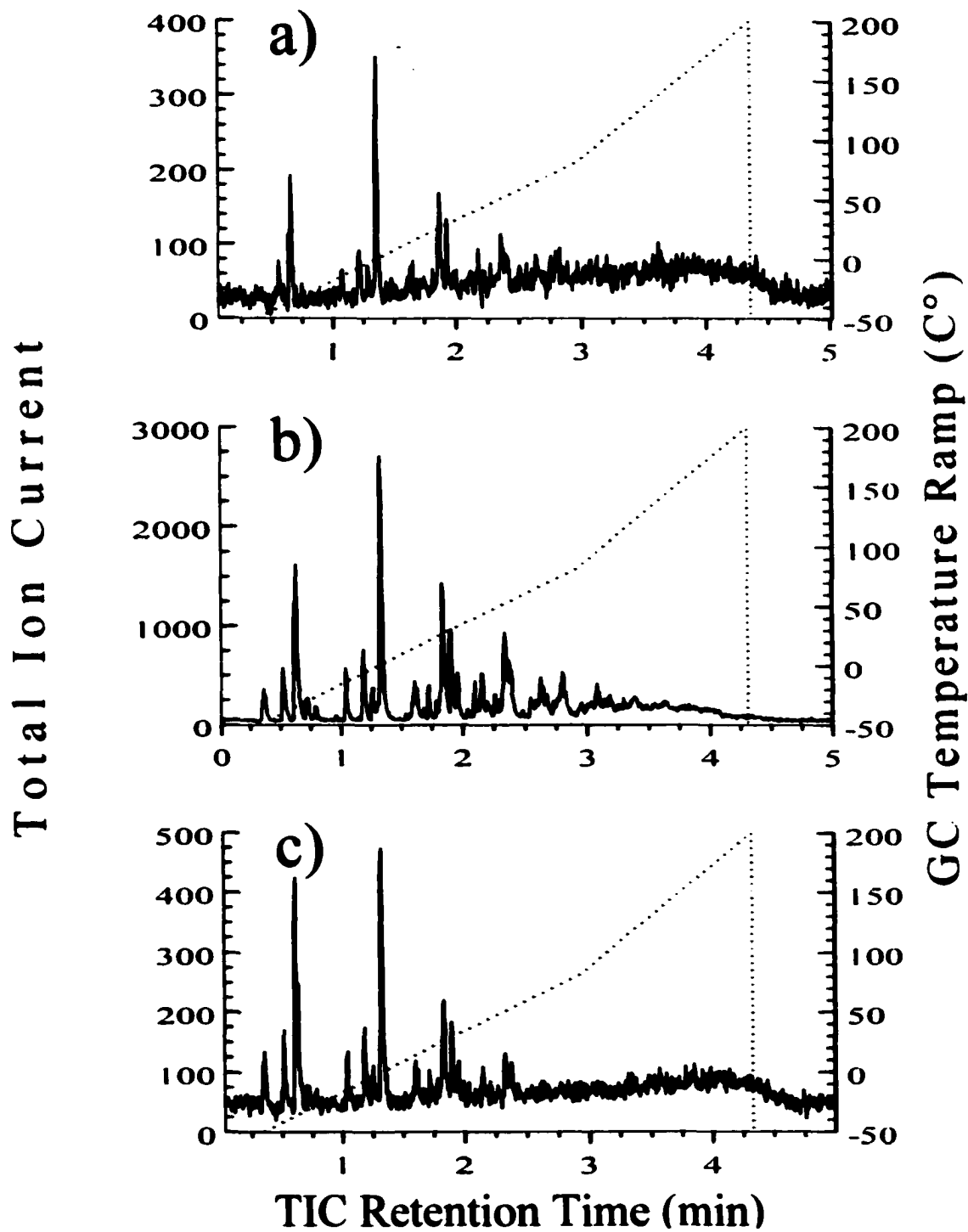


Figure 4-42: Repetitive injection chromatograms obtained from LPE/HMCM-41 heated in hydrogen when the sample temperature reached a) 250 °C b) 270 °C c) 290 °C

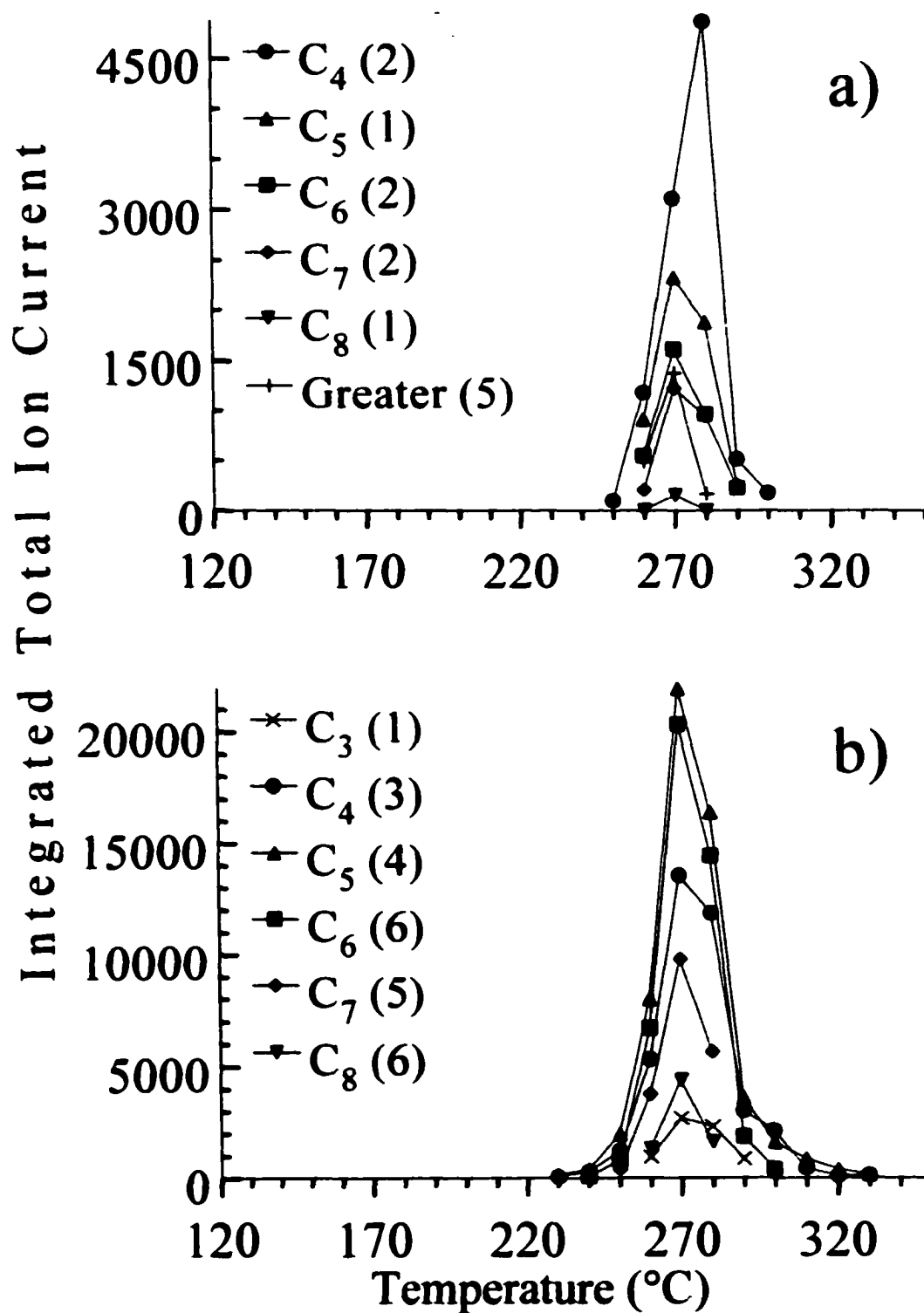


Figure 4-43: Volatile product evolution profiles for LPE/HMCM-41 heated in hydrogen a) paraffins b) olefins
 [Values in parentheses represent the number of isomers detected]

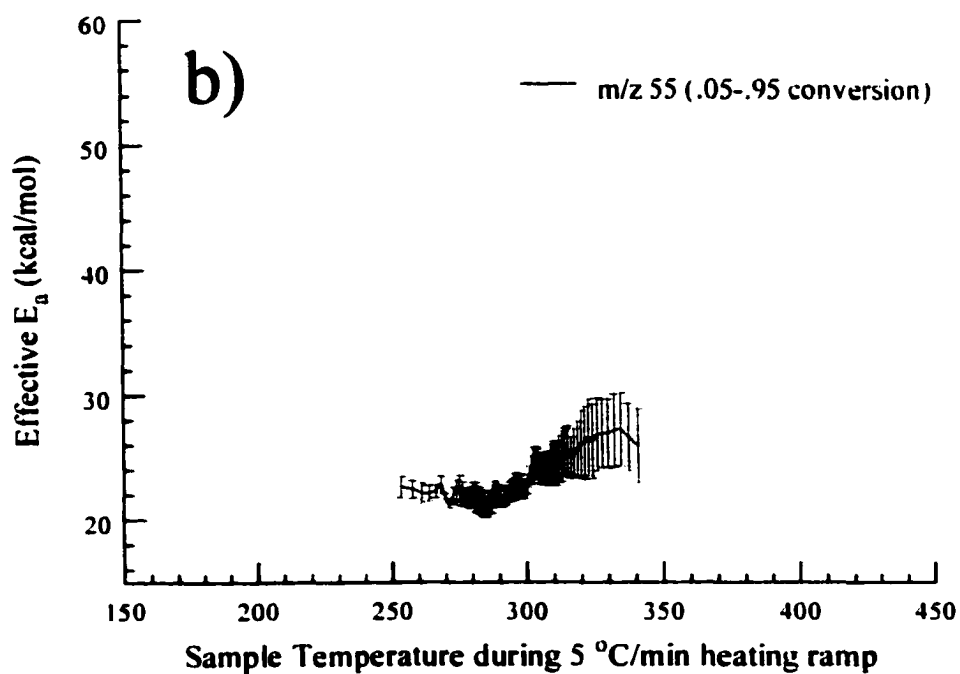
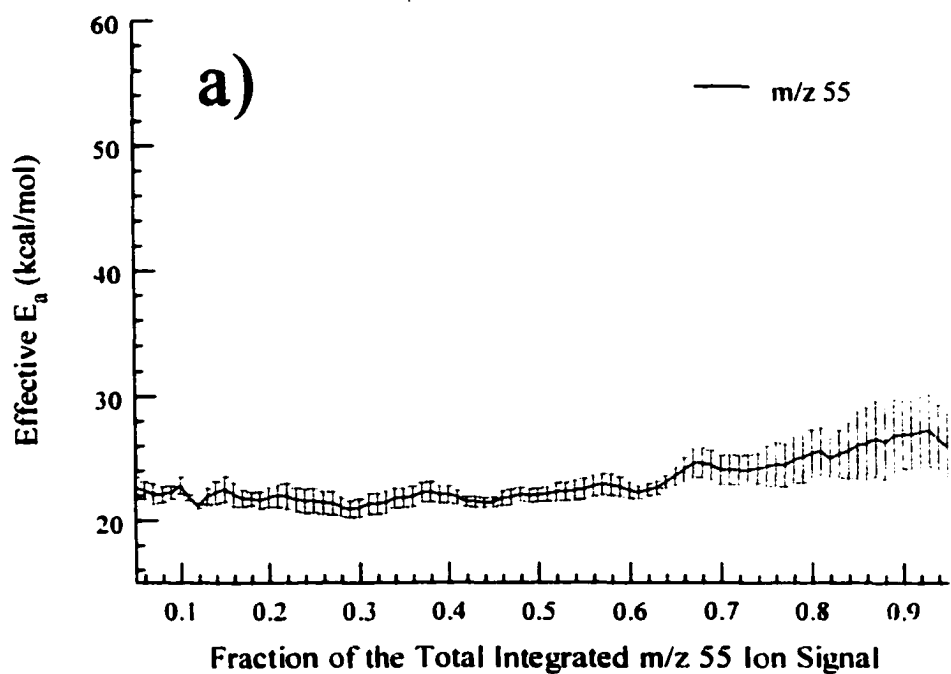


Figure 4-44: a) E_a vs. Fractional integrated ion signal b) E_a vs. Temperature plots for the formation of olefins (m/z 55) from LPE/HMCM-41 heated in hydrogen

Large paraffin E_a errors were attributed to low volatile paraffin yield and low m/z 57 paraffin selectivity. Consequently, the E_a vs. fractional integrated ion signal plot for paraffins is not included here.

4.2.11 LPE/PtHMCM-41 (He)

4.2.11a TA-GC/MS Results

Figure 4-45a shows the repetitive injection chromatograms obtained while heating the LPE/PtHMCM-41 (He) sample. Volatile products were detected between 180-300 °C. The initial temperature of volatile product evolution was 40 °C lower than for the LPE/HMCM-41 (He) sample. A single volatile product evolution maximum was observed in the chromatograms at 250 °C. Figure 4-45b shows the negative derivative ($-\Delta mg/\Delta^\circ C$) of the TGA weight loss curve for the LPE/PtHMCM-41 (He) sample. A single polymer weight loss region was observed between 170-300 °C.

Figure 4-46 shows the repetitive injection chromatograms obtained at a) 200, b) 250, and c) 290 °C. The chromatograms in Figure 4-46 show that relative volatile hydrocarbon product yields did not change significantly while the LPE/PtHMCM-41 (He) sample was heated.

Figure 4-47 shows the species-specific evolution profiles calculated for a) paraffin and b) olefin volatile products. The shape of the volatile product evolution profiles versus temperature for volatile paraffin and olefin products were very similar (Figure 4-47a and 4-47b). The largest integrated TIC peak area calculated for the volatile paraffin products was less than 1/10 of the C_5 -olefin area at their respective maximum temperatures.

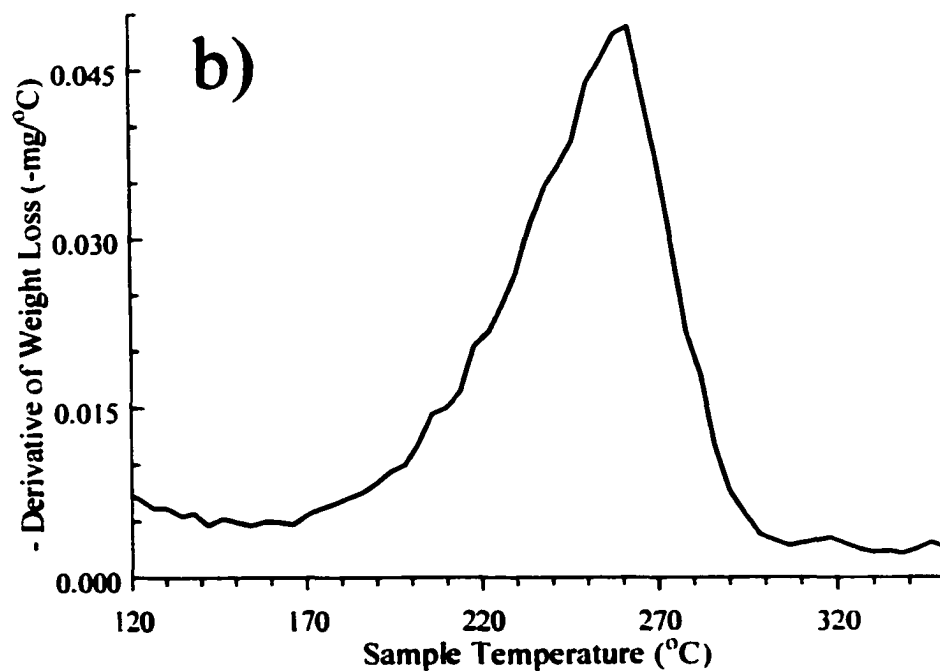
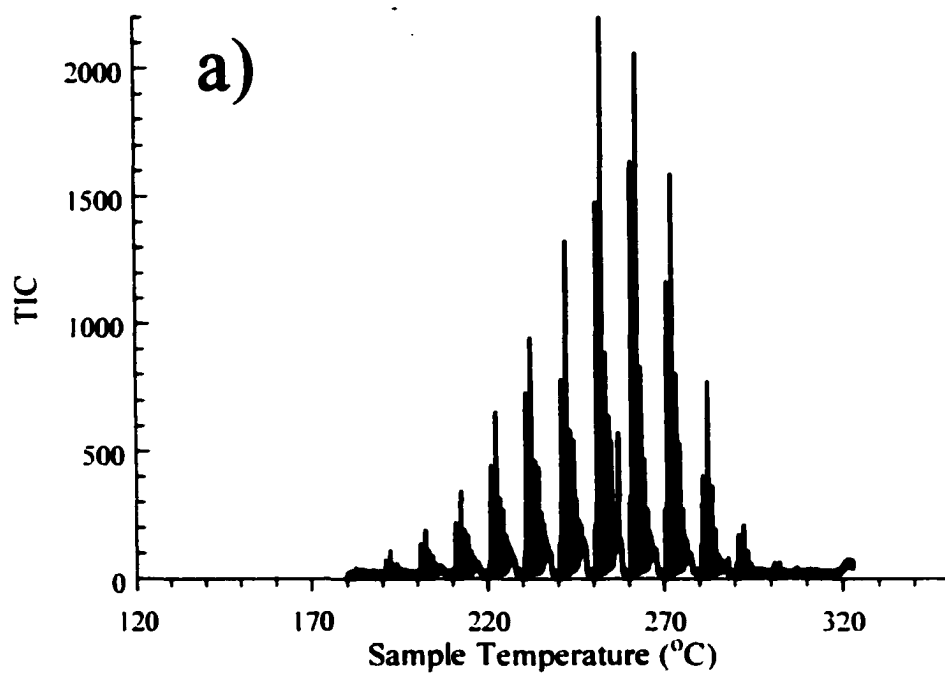


Figure 4-45: a) Repetitive injection chromatogram for LPE/PtHMCM-41 heated in helium b) Negative derivative of the weight loss obtained for LPE/PtHMCM-41 heated in helium by using TGA

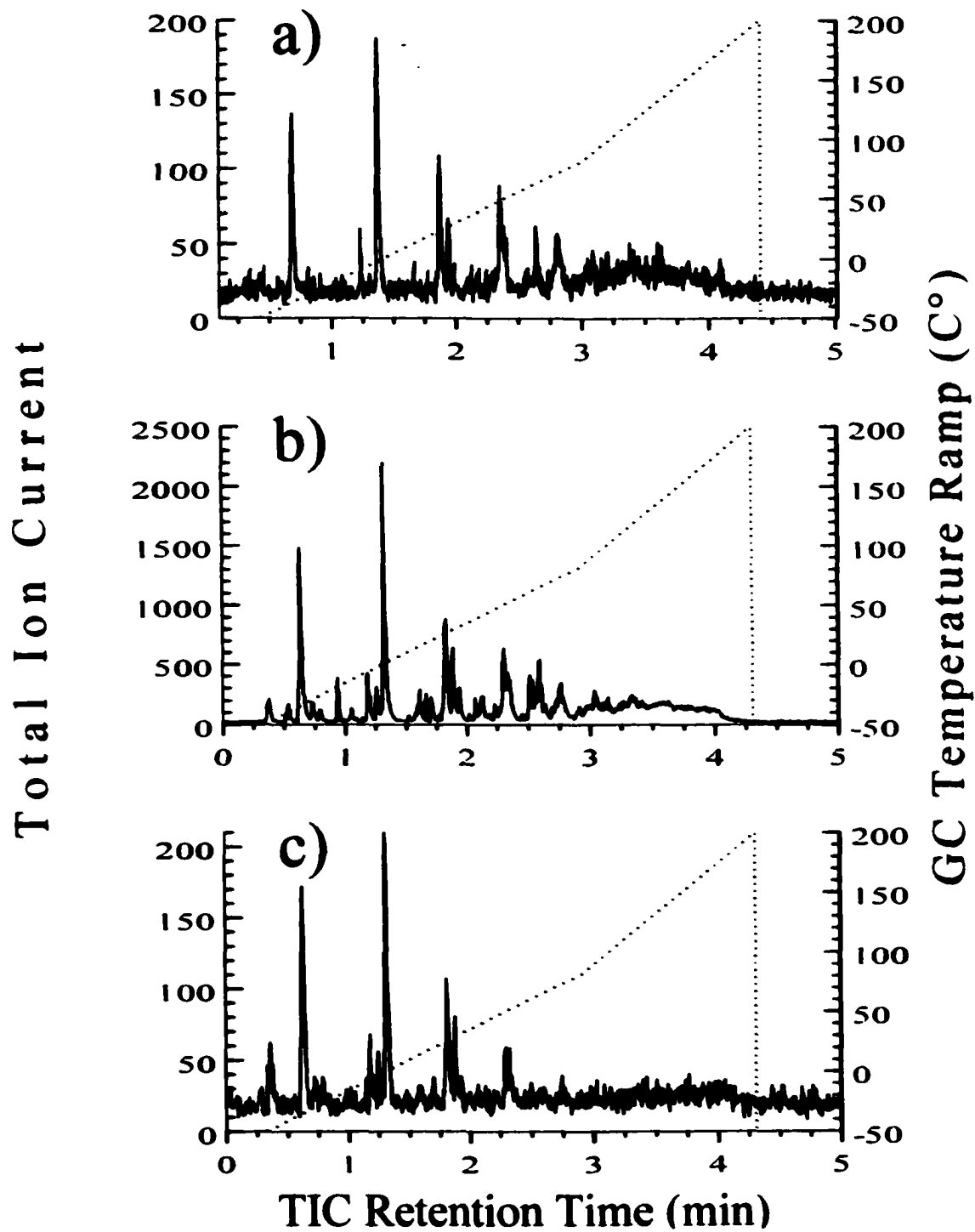


Figure 4-46: Repetitive injection chromatograms obtained from LPE/PtHMCM-41 heated in helium when the sample temperature reached a) 200 °C b) 250 °C c) 290 °C

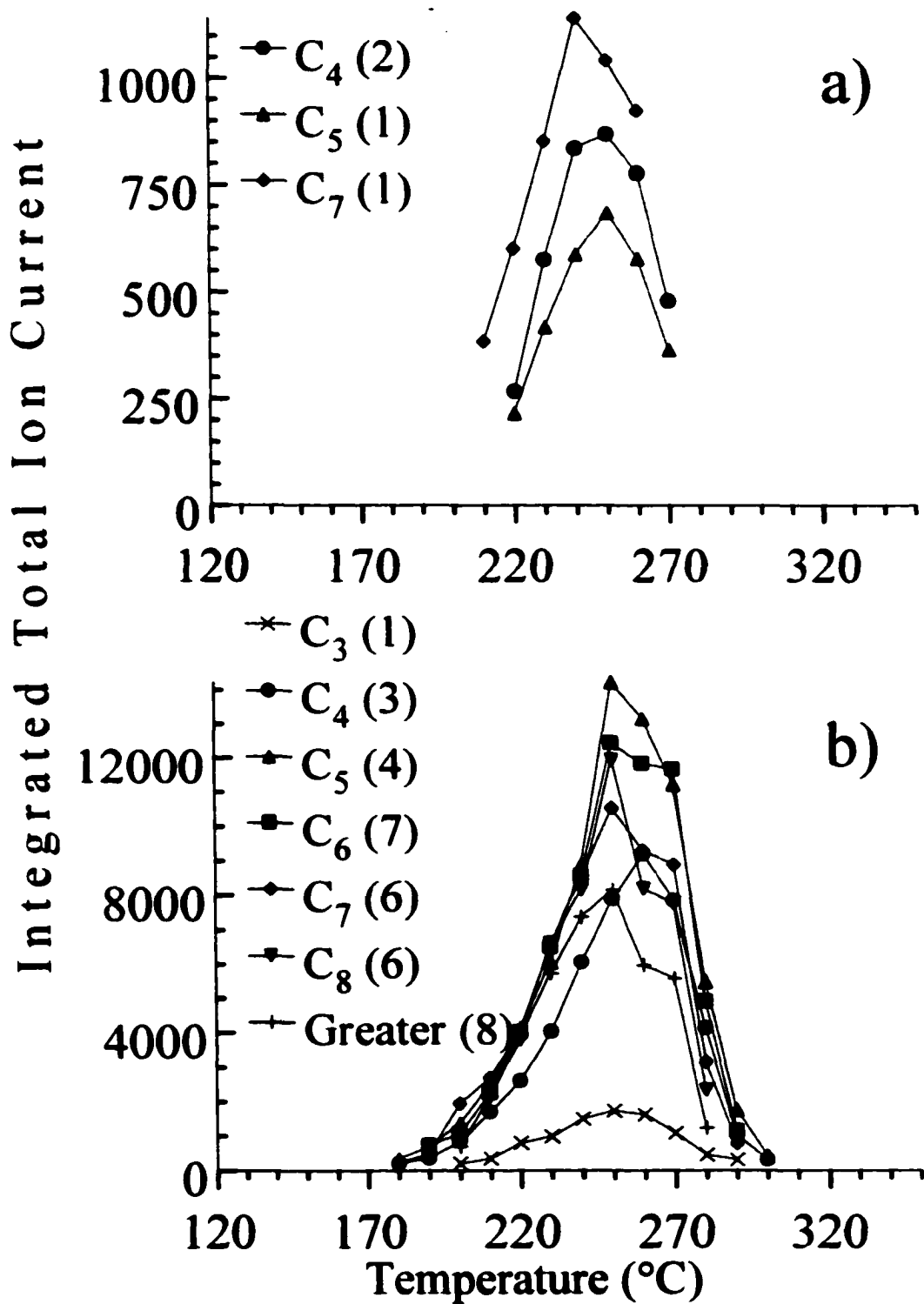


Figure 4-47: Volatile product evolution profiles for LPE/PtHMCM-41 heated in helium a) paraffins b) olefins
 [Values in parentheses represent the number of isomers detected]

The volatile product slate illustrated in Figure 4-47 shows that C₃-C₁₀ hydrocarbons were formed and that C₄-≥C₉ olefins (Figure 4-47b) were the dominant volatile species. The temperature corresponding to the maximum olefin evolution rate was 250 °C (Figure 4-47b). No volatile alkyl aromatic volatile products were detected from the LPE/PtHMCM-41 (He) sample.

4.2.11b TA-MS Results

The m/z 55 ion signal selectivity for olefins was 99% from 0.05-0.95 fractional integrated ion signal. The E_a value for olefin formation in Figure 4-48 was initially 36 kcal/mol at 0.05 fractional integrated ion signal (245 °C), but then decreased to 30 kcal/mol between 0.20-0.70 fractional integrated ion signal (270-325 °C). Above 0.70 fractional integrated ion signal (325 °C), the E_a value remained relatively constant at 30 kcal/mol until 0.95 fractional integrated ion signal (350 °C). The m/z 55 E_a vs. fractional integrated ion signal plot for the LPE/PtHMCM-41 was very similar to the LPE/PtHZSM-5 plot (Figure 4-15). Evolution profiles show that volatile paraffin formation occurred between 210-270 °C. Large paraffin E_a value errors were attributed to low volatile paraffin yields and low m/z 57 paraffin selectivity. Consequently, the E_a vs. fractional integrated ion signal plot for paraffins is not included here.

4.2.12 LPE/PtHMCM-41 (H₂)

4.2.12a TA-GC/MS Results

Figure 4-49a shows the repetitive injection chromatograms obtained while heating the LPE/PtHMCM-41 (H₂) sample. Volatile products were detected between 200-290 °C.

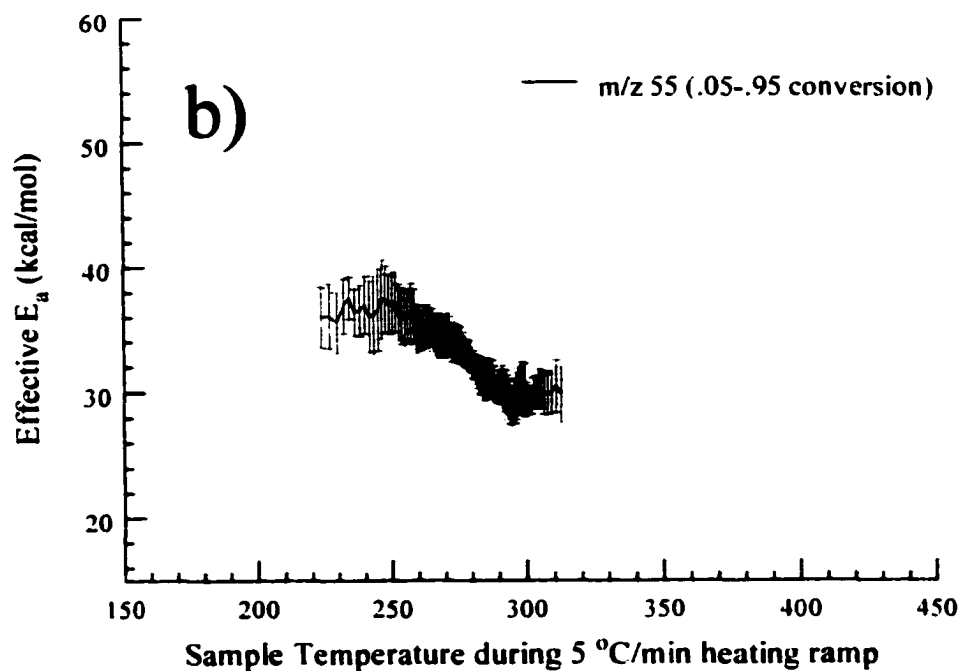
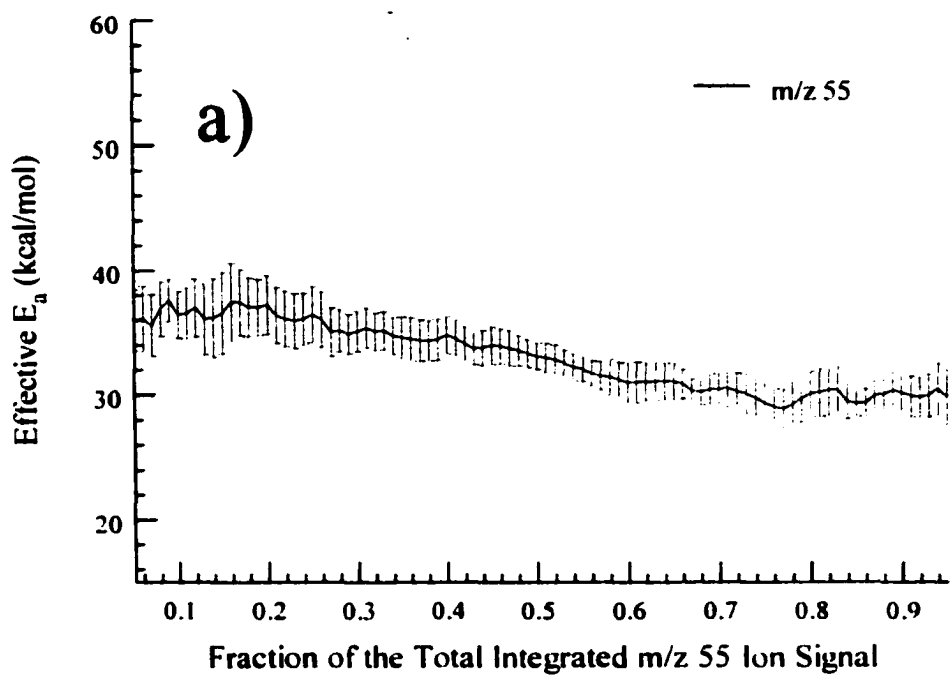


Figure 4-48: a) E_a vs. Fractional integrated ion signal b) E_a vs. Temperature plots for the formation of olefins (m/z 55) from LPE/PtHMCM-41 heated in helium

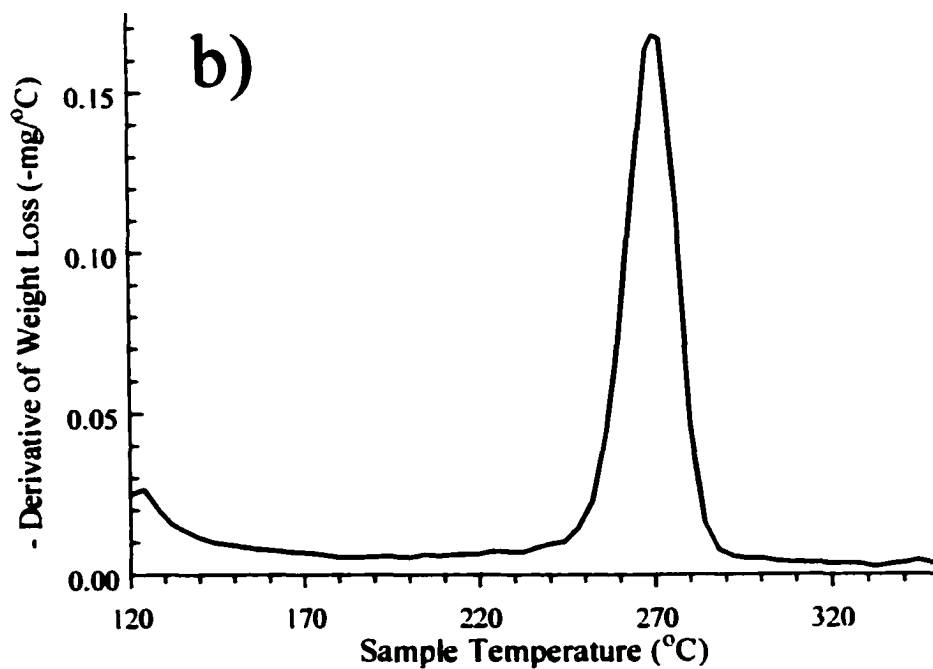
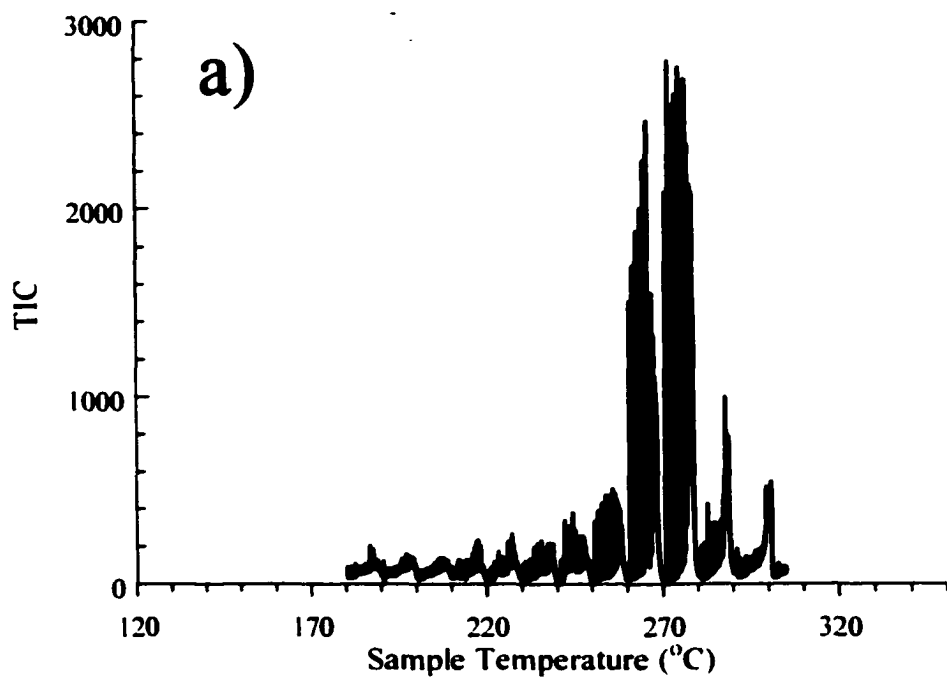


Figure 4-49: a) Repetitive injection chromatogram for LPE/PtHMCM-41 heated in hydrogen b) Negative derivative of the weight loss obtained for LPE/PtHMCM-41 heated in hydrogen by using TGA

The initial temperature of volatile product evolution was 20 °C higher than that for the LPE/PtHMCM-41 (He) sample. A single volatile product evolution maximum was observed in the chromatograms at 270 °C. Figure 4-49b shows the negative derivative ($-\Delta\text{mg}/\Delta^\circ\text{C}$) of the TGA weight loss curve for the LPE/PtHMCM-41 (H₂) sample. The TGA plot decrease between 120-140 °C was due to desorption of water from the catalyst. A single polymer weight loss region was observed from 240-290 °C. The chromatographic experiment was ended at 290 °C despite the continuous formation of volatile products (baseline increase) observed in Figure 4-49a. This was done to avoid possible clogging of the GC/MS interface because products formed above 280 °C were unable to fully elute from the GC during the heating ramp.

Figure 4-50 shows the repetitive injection chromatograms obtained at a) 250, b) 270, and c) 280 °C. The chromatograms in Figure 4-50 show that relative volatile hydrocarbon product yields changed slightly while the LPE/PtHMCM-41 (H₂) sample was heated. The baseline increase in the Figure 4-50 chromatograms was due to the formation of volatile products that had R_t values that were greater than 3.0 min. When the sample temperature reached 280 °C (Figure 4-50c), the heating ramp of the GC did not provide separation of the hydrocarbon isomers ($\geq\text{C}_9$).

Figure 4-51 shows the species-specific evolution profiles calculated for a) paraffin and b) olefin volatile products. The shapes of the volatile product evolution profiles versus temperature for volatile paraffins were similar (Figure 4-51a). Volatile paraffin products dominated the product slate from the LPE/PtHMCM-41 (H₂) sample, unlike the other three HMCM-41 samples.

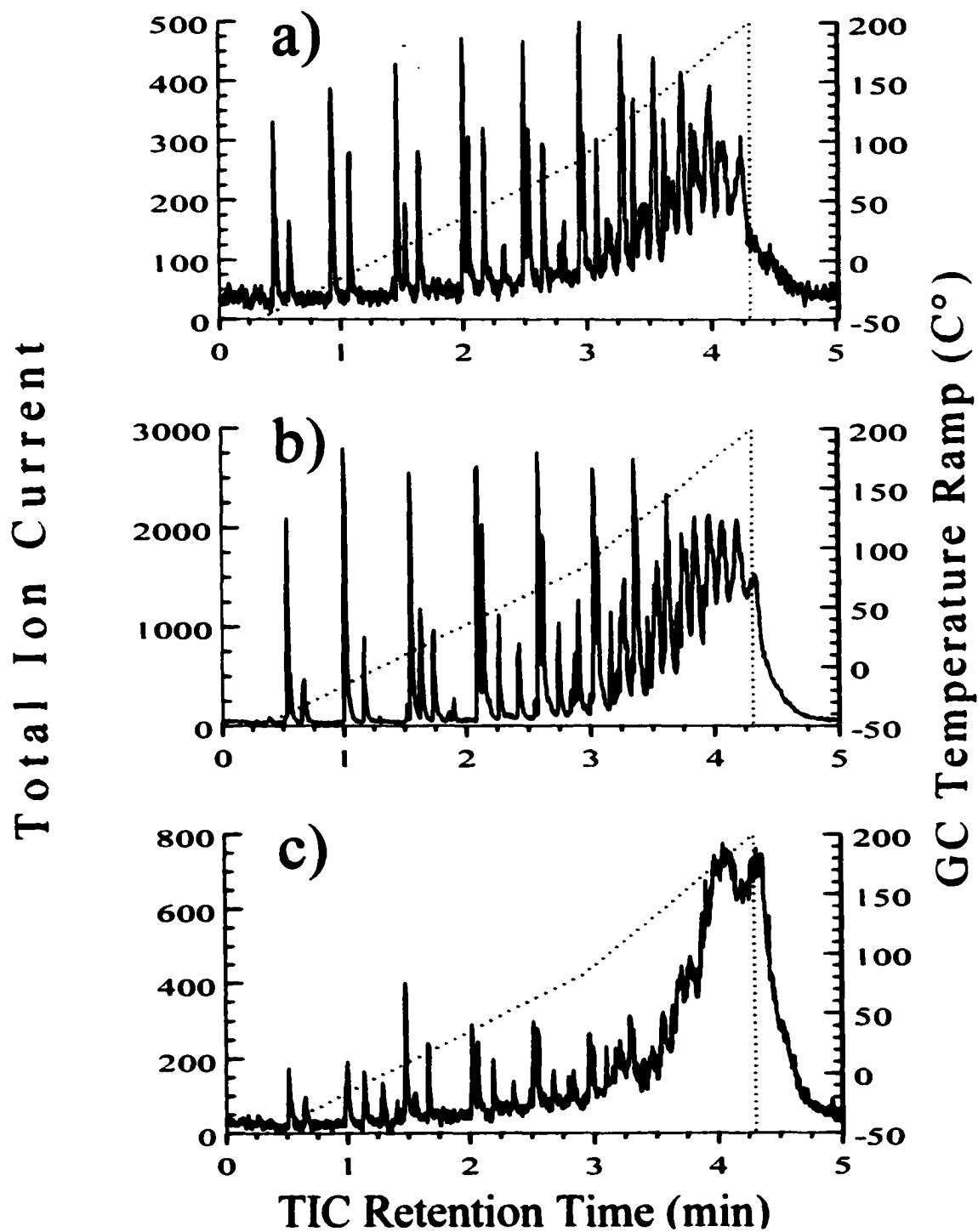


Figure 4-50: Repetitive injection chromatograms obtained from LPE/PtHMCM-41 heated in hydrogen when the sample temperature reached a) 250 °C b) 270 °C c) 280 °C

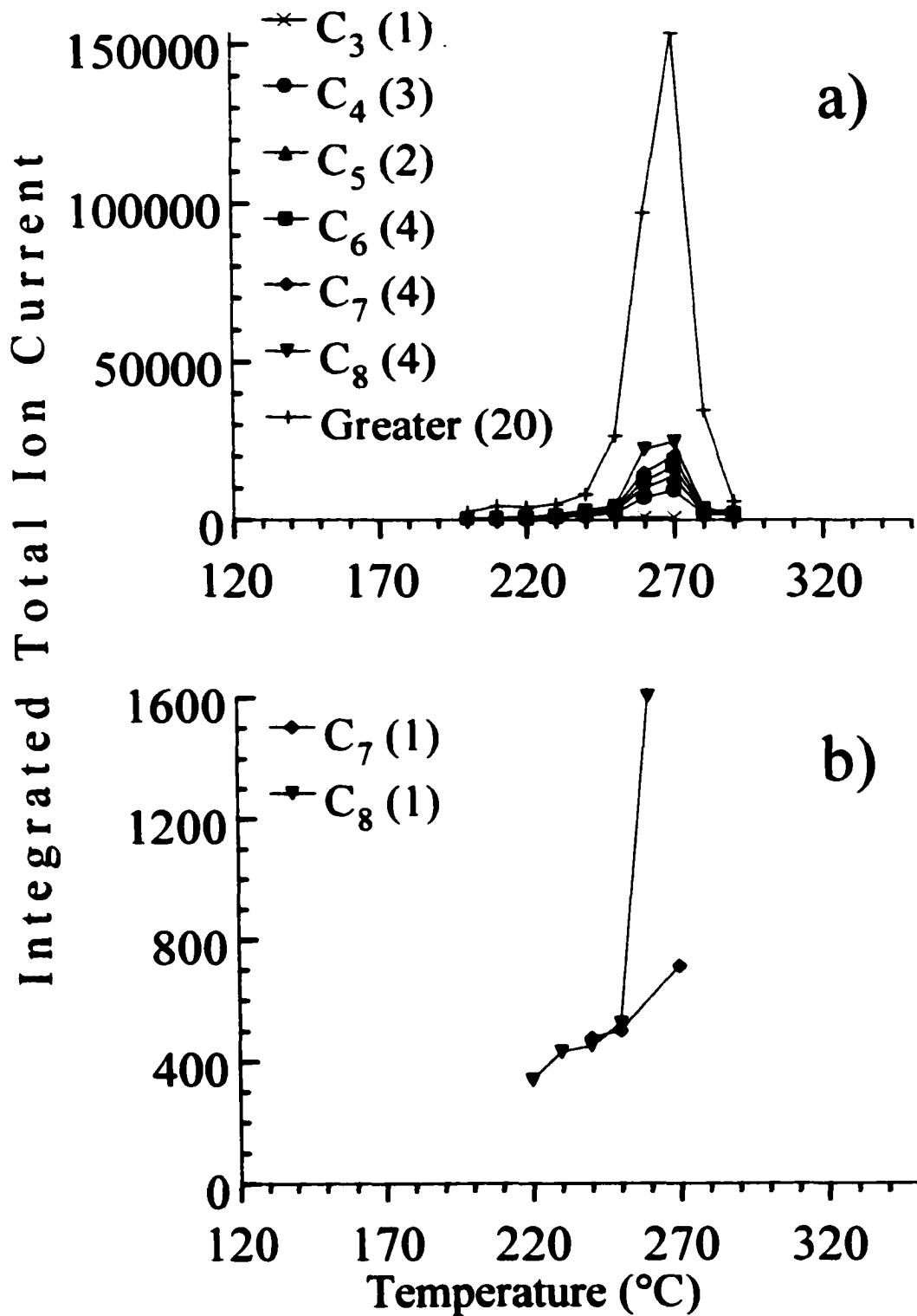


Figure 4-51: Volatile product evolution profiles for LPE/PtHMCM-41 heated in hydrogen a) paraffins b) olefins
 [Values in parentheses represent the number of isomers detected]

The largest integrated TIC peak area calculated for the volatile olefin products was less than 1/100 of the $\geq C_9$ -paraffin area at their respective maximum temperatures. The volatile product slate illustrated in Figure 4-51 shows that C_3 - $\geq C_9$ hydrocarbons were formed and that 20 isomers of $\geq C_9$ paraffins (Figure 4-51a) were the dominant volatile species. The temperature corresponding to the maximum paraffin evolution rate was 270 °C (Figure 4-51a). No volatile alkyl aromatic volatile products were detected for the LPE/PtHMCM-41 (H_2) sample.

4.2.12b TA-MS Results

The m/z 57 ion signal selectivity for paraffins was 99% from 0.05-0.95 fractional integrated ion signal. The initial E_a value for paraffin formation in Figure 4-52 was 36 kcal/mol at 0.05 fractional integrated ion signal (280 °C). The E_a value then decreased to 30 kcal/mol by 0.85 fractional integrated ion signal (320 °C) followed by a steep decrease to 16 kcal/mol by 0.95 fractional integrated ion signal (380 °C). The E_a vs. fractional integrated ion signal plot for the LPE/PtHMCM-41 (H_2) sample is very similar to that for the LPE/PtHY (H_2) sample (Figure 4-36) until the steep decrease above 0.85 fractional integrated ion signal. Evolution profiles show that volatile olefin formation occurred between 220-270 °C. Large olefin E_a value errors were attributed to low volatile olefin yield and low m/z 55 olefin selectivity. Consequently, the E_a vs. fractional integrated ion signal plot for olefins is not included here.

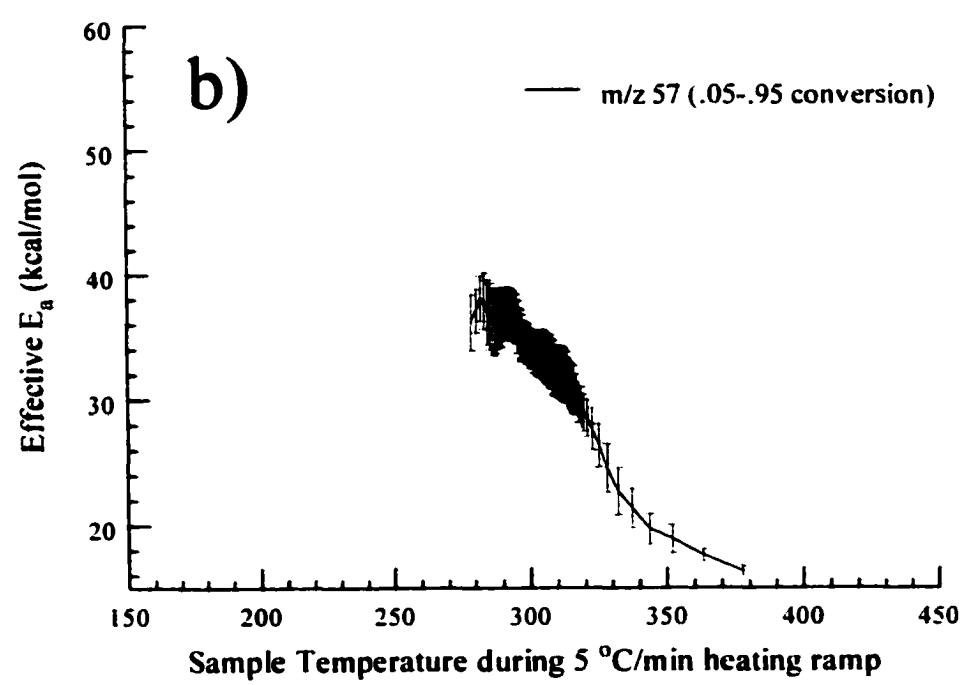
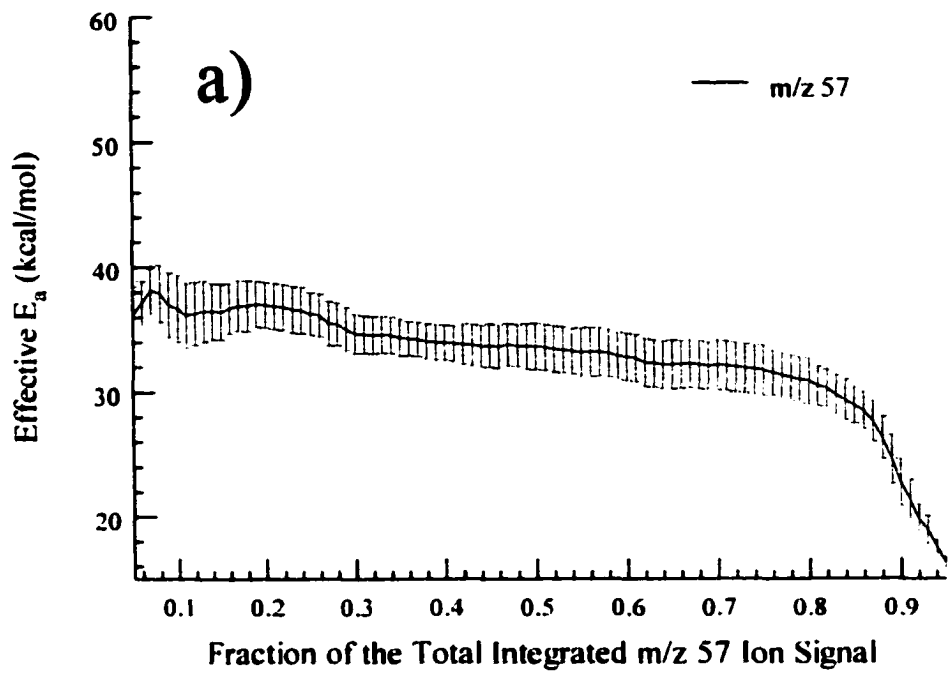


Figure 4-52: a) E_a vs. Fractional integrated ion signal b) E_a vs. Temperature plots for the formation of paraffins (m/z 57) from LPE/PtHMCM-41 heated in hydrogen

CHAPTER 5 - DISCUSSION OF EXPERIMENTAL RESULTS

5.1 Introduction

Results described in Chapter 4 show that volatile product slates change when various mono-functional and bifunctional catalysts crack polyethylene in helium or hydrogen. Catalytic cracking mechanisms were solely responsible for volatile product slates because products were detected well below temperatures at which thermal cracking occurs. In Chapter 1, various catalytic cracking mechanisms that are possible for small hydrocarbons on acid and metal catalyst functionalities were outlined. Reactions between catalysts and polymer may be similar to those observed for small hydrocarbons, but larger molecules can undergo a wider variety of reactions and may behave differently than small hydrocarbons. For example, unlike small molecules, large polymer molecules have limited access to catalyst active sites within pores. As polymer fragments become smaller due to cracking, pore accessibility improves. We are interested in the effects of adding platinum and/or hydrogen to LPE catalytic cracking processes when using HZSM-5, HY, and HMCM-41 acid catalysts. Our goal of this work was to examine the dependence of catalyst acidity, pore size, platinum, and hydrogen on the catalytic cracking mechanism(s) of LPE.

5.2 Temperature Changes During LPE Cracking

The temperature range of volatile product evolution from LPE/catalyst samples depends on the choice of catalyst. Previous work has shown that the temperature at which volatile products are first detected from catalytic cracking of polyethylene with solid acid catalysts depends on catalyst acid properties.¹⁻³ In general, the temperature at

which volatile products are detected decreases as the acid strength of the catalyst increases.

5.2.1 LPE/catalysts in Helium

Table 5-1 lists the temperatures at which volatile products were detected from LPE by using repetitive injection TA-GC/MS. Results are shown for LPE heated with HZSM-5, PtHZSM-5, HY, PtHY, HMCM-41, and PtHMCM-41 in helium and hydrogen. The temperatures listed in Table 5-1 were derived from the volatile product evolution profiles shown in Chapter 4. Temperatures corresponding to initial volatile product detection and maximum volatile product evolution rate are represented in Table 5-1 by Init. T and Max. T, respectively. ΔT denotes the temperature range over which volatile products were detected. For example, volatile products were detected initially from LPE/HZSM-5 (He) at 130 °C and continued to evolve until 350 °C (Init. T + ΔT = 350).

Catalyst acidity is an important parameter in determining the temperature at which volatile cracking products are formed. The acid strengths of the catalysts used in this study were characterized by ammonia desorption. Increased area under the ammonia TPD curve at higher temperatures indicates a larger fraction of strong (e.g. large K_a value) acid sites. Figure 2-19 shows that HZSM-5 possessed the largest fraction of strong acid sites, followed by HY and HMCM-41. Table 5-1 shows that for metal-free LPE/catalyst samples heated in helium, the lowest initial temperature for formation of volatiles correlates with the acid strength trend: LPE/HZSM-5 (130 °C) < LPE/HY (160 °C) < LPE/HMCM-41 (220 °C). However, initial polymer cracking likely occurs only at sites accessible to the large polymer molecules (e.g. external surfaces) and acid strength was determined for all acid sites accessible to ammonia.

Volatile Product Evolution Temperatures (°C) from TA-GC/MS Experiments				
Catalyst^a	Atm^b	Init. T	Max. T	ΔT^c
HZSM-5	He	130	240	220
HZSM-5	H ₂	130	240	200
PtHZSM-5	He	130	240	210
PtHZSM-5	H ₂	130	230	220
HY	He	160	210	170
HY	H ₂	160	210	130
PtHY	He	160	210	170
PtHY	H ₂	220	260	100
HMCM-41	He	220	270	120
HMCM-41	H ₂	220	270	100
PtHMCM-41	He	180	250	120
PtHMCM-41	H ₂	200	270	100

^aLPE/Catalyst sample ^bReaction condition (Atm) ^cTemperature range of volatile product evolution (Final T = Init. T + ΔT)

Table 5-1: Temperatures of volatile product evolution for LPE/Catalyst samples

Thus, because only a fraction of the total number of acid sites was initially accessible to the polymer, the correlation between acid strength and temperature of initial volatile product detection may have been a coincidence. During polymer cracking, access to acid sites within pores should be better for larger pore catalysts. Thus, HZSM-5 should have the smallest fraction of sites in contact with LPE at low temperatures. Furthermore, it has been reported that the strength of acid sites inside catalyst pores is greater than those on the external surface.⁴⁻⁷ Therefore, acid strength as measured by ammonia TPD is likely not representative of the initially accessible sites. As polymer cracking progresses with increased temperature, catalyst surfaces become coated with smaller polymer fragments that can more easily enter the pores, which increases the number of acid sites available for cracking. When all acid sites are accessible to polymer fragments, ammonia TPD acid strength would be expected to correlate with cracking effectiveness. However, temperatures corresponding to maximum volatile product evolution rates (Max. T) do not correlate with ammonia TPD acid strength (Table 5-1). This may have been due to deactivation of some acid sites during catalytic cracking. Catalyst acid strength and site density are factors that affect the rate of catalyst deactivation.⁸⁻¹⁴ An increase in the fraction of sites with high acid strength increases the rate of deactivation. Therefore, rapid deactivation of the strong HZSM-5 acid sites would be expected when they become accessible to polymer fragments.

5.2.2 LPE/catalysts in Hydrogen

When metal-free LPE/catalysts were heated in hydrogen, there was virtually no change in the initial and maximum temperatures of volatile product evolution compared to the same samples heated in helium (Table 5-1). However, the temperature ranges (ΔT)

of product evolution decreased by 20-40 °C when LPE/catalysts were heated in hydrogen. When helium is replaced by hydrogen, it is possible that hydrogenation can occur on metal-free acid catalysts. Many authors have reported that molecular hydrogen can be activated by metal impurities, alkali metals, and the Brønsted acid sites of metal-free catalysts.¹⁵⁻¹⁸ Molecular hydrogen activation during small hydrocarbon cracking was shown to be dependent on temperature and hydrogen pressure in addition to the acid strength, acid site density, and pore dimensions of the catalyst. The exact form of activated hydrogen species is unknown, but their presence can lead to hydrogenation reactions on the catalyst surface. It has also been proposed that the presence of hydrogen can increase the concentration of Brønsted acid sites on catalyst surfaces.^{16,19} If additional Brønsted acid sites were formed on LPE/catalyst surfaces by activated hydrogen species, they were not of adequate strength to reduce the initial temperature of volatile product evolution, but may have been responsible for the narrower volatile product evolution ranges. Even though the physical characteristics of each catalyst were different, the consistent decrease in the temperature range over which volatiles were detected suggests that the effects of hydrogen were similar for each catalyst.

5.2.3 LPE/Ptcatalysts in Helium

When a catalyst has two different types of active sites, it is termed bifunctional. Typically, bifunctional catalysts consist of a transition metal moiety (e.g. platinum) and an acid moiety. Classical bifunctional hydrocracking/hydroconversion involves hydrogenation reactions on the metal and isomerization and cracking reactions on the acid sites.²⁰ However, when small hydrocarbons react on bifunctional catalysts in the absence of hydrogen, the functionality of the metal can be altered.²⁰⁻²² Dehydrogenation,

cracking, and hydrogenolysis reactions can occur on the metal surface.²⁰⁻²² Small hydrocarbon dehydrogenation reactions have been reported to occur at temperatures as low as 150 °C on both platinum black and Pt-bifunctional catalysts.^{21,24-25} Hydrogenolysis reactions on a metal tend to occur at higher temperatures (>200 °C) and require surface species with high hydrogen content.^{21,24-25} Consequently, it is possible that volatile products formed by platinum catalyzed reactions may be formed as low as 150 °C for LPE/Ptcatalyst samples heated in helium. Therefore, the addition of platinum without hydrogen could affect the temperature at which initial volatile products are detected.

The addition of platinum did not significantly affect the acidity of the catalysts as evidenced by the similarity of ammonia TPD curves for catalyst samples with and without platinum (Figures 2-16 to 2-18). Similar TPD characterizations reported in the literature have shown that the addition of transition metals (i.e. platinum) does not affect catalyst acidity.²⁶⁻³⁰ Thus, the initial temperature at which volatile products were detected for catalysts containing platinum would be expected to be the same as for the metal-free catalysts. This was observed for the LPE/PtHZSM-5 (He) and LPE/PtHY (He) samples. Platinum catalyzed reactions did not cause a shift in the temperatures of volatile product detection for the LPE/PtHZSM-5 (He) and LPE/PtHY (He) samples compared to their metal-free analogs (Table 5-1). However, platinum catalyzed reactions did contribute to the formation of volatile products because changes in volatile product slates were detected for the LPE/PtHZSM-5 (He) and LPE/PtHY (He) samples compared to their metal-free analogs (*vide infra*).

The presence of platinum decreased the initial temperature (Init. T) at which volatiles were detected by 40 °C for the LPE/PtHMCM-41 (He) sample compared to the LPE/HMCM-41 (He) sample (Table 5-1). Volatile products were initially detected at 180 °C for the LPE/PtHMCM-41 (He) sample compared to 220°C for the LPE/HMCM-41 (He) sample. In addition, the temperature corresponding to the maximum volatile product evolution rate (Max. T) decreased by 20 °C for the platinum loaded sample. This would suggest that platinum in the LPE/PtHMCM-41 (He) sample contributed significantly to volatile product formation at 180 °C and that the importance of metal catalyzed reactions decreased, but was still significant at higher cracking temperatures. The relatively weak acidity of the PtHMCM-41 catalyst may be the reason that the effect of platinum on volatile product evolution temperatures was more apparent for this catalyst than for the PtHZSM-5 and PtHY catalysts.

5.2.4 LPE/Ptcatalysts in Hydrogen

The activation energy of hexane hydrocracking on metal-free acid catalysts is reportedly lower than on metal-loaded bifunctional analogs.³¹ Perrotin et al. and references therein describe the catalyst dependence on the activation energy of hexadecane hydroconversion.³² Catalyst trends in hydrocracking activation energies were: acid catalysts (40-50 kJ/mol) < bifunctional catalysts (105-135 kJ/mol) < metallic catalysts (230-295 kJ/mol).³² Acid catalyzed C-C bond rupture requires less energy than metal catalyzed C-C bond rupture. The hydrogen partial pressure has also been reported to affect hydrocracking activation energies.³²⁻³⁴ In general, an increase in hydrogen partial pressure leads to an increase in activation energy due to competitions between molecular hydrogen and hydrocarbons for acid sites. Platinum preferably catalyzes

hydrogen activation rather than cracking reactions. Therefore, an increase in energy is required for metal-catalyzed cracking reactions when excess hydrogen is present. Thus, it would be expected that the presence of both platinum and hydrogen would increase the activation energy for LPE cracking, which would result in an increase in the temperature required for reactions. In fact, TGA results reported by Liu et al. have shown that initial decomposition of commingled plastic by PtAl₂O₃ was indeed shifted to slightly higher temperatures in hydrogen compared to helium.³⁵

The initial volatile product evolution temperature for LPE/PtHY (H₂) was shifted 60 °C higher and the maximum product evolution rate was shifted 50 °C higher compared to the LPE/PtHY (He) sample (Table 5-1). Slight increases (20 °C) for the initial and maximum temperatures were also observed for LPE/PtHMCM-41 (H₂) compared to the same sample in helium. The temperature range for volatile product evolution decreased by 20 °C for LPE/PtHMCM-41 and 70 °C for LPE/PtHY in hydrogen compared to helium, which implies that the rate of volatile product evolution increased. There was no temperature shift observed for the LPE/PtHZSM-5 (H₂) sample compared to the LPE/PtHZSM-5 (He) or LPE/HZSM-5 (H₂) samples (Table 5-1). The fact that LPE/PtHZSM-5 (H₂) did not exhibit a temperature shift during TA-GC/MS experiments would suggest that pore size is important for this effect. However, the effect was larger for PtHY than for PtHMCM-41, which suggests that it cannot be attributed solely to pore size considerations.

5.3 Volatile Product Slate Comparisons

Volatile product evolution from LPE/catalyst samples depended on the choice of catalyst. Previous work has shown that the volatile products detected from cracking PE with solid acid catalysts depend heavily on catalyst pore size and acidity.¹⁻³

5.3.1a LPE/HZSM-5 (He) vs. LPE/HZSM-5 (H₂)

Table 5-2 lists the relative volatile product yields from the LPE/HZSM-5 (He), LPE/HZSM-5 (H₂), LPE/PtHZSM-5 (He), and LPE/PtHZSM-5 (H₂) samples obtained by TA-GC/MS. Plots of integrated TIC chromatographic peak area with respect to sample temperature for each volatile product category constitute their respective evolution profiles that were shown in Chapter 4. Percentages of the total (for all chromatograms) integrated TIC signals were calculated for each product category and grouped by carbon number and molecular type in Table 5-2. Calculated percentages were found to vary by less than 2% in consecutive analyses (Chapter 2). Percent residue was calculated by oxidative TGA weight loss after previously heating the respective sample in helium or hydrogen. The change in percent residue was found to be less than 1% in consecutive analyses (Chapter 2).

Catalyst pore size and acidity influence the volatile product distribution formed during catalytic cracking of PE.^{1-3,36-48} In general, smaller volatile products are obtained from catalysts with higher acid strength. Catalyst pores can act as molecular sieves that can also affect volatile product size. Therefore, the size of volatile products evolved from LPE cracking would be expected to increase with larger average pore size and lower acid strength: LPE/HZSM-5 < LPE/HY < LPE/HMCM-41.

Volatile Products		Percentage Yields ^{**} by Catalyst and Purge gas			
		HZSM-5 (He)	HZSM-5 (H ₂)	PtHZSM-5 (He)	PtHZSM-5 (H ₂)
Paraffin ↓	C ₃	-	-	-	4 (1)
	C ₄	10 ^a (2)	10 (3)	9 (2)	17 (3)
	C ₅	11 (2)	13 (2)	11 (2)	23 (2)
	C ₆	13 (3)	8 (3)	10 (3)	24 (3)
	C ₇	6 (3)	4 (3)	5 (3)	12 (3)
	C ₈	2 (3)	1 (2)	2 (3)	6 (3)
	≥C ₉	<1 (3)	1 (3)	1 (5)	6 (6)
Olefin ↓	C ₃	12 (1)	17 (1)	12 (1)	-
	C ₄	21 (3)	25 (3)	19 (3)	-
	C ₅	14 (4)	16 (4)	11 (3)	-
	C ₆	3 (4)	2 (4)	2 (4)	1 (1)
	C ₇	<1 (1)	<1 (1)	-	2 (3)
	C ₈	-	1 (2)	-	1 (3)
	≥C ₉	-	-	-	1 (3)
Aromatic ↓	Ben ^c	<1	-	<1	<1
	Tol ^d	2	1	4	1
	C ₂ -Ph ^e	2 (3)	1 (2)	10 (3)	1 (3)
	C ₃ -Ph	1 (2)	<1 (1)	3 (2)	<1 (2)
	C ₄ -Ph	-	-	<1 (1)	
% Total	Volatiles	97	99	99	99
P/O ^b		0.84	0.60	0.86	18
% R [*]		5	2	3	<1

^{**}LPE/Catalyst samples are listed along with the reaction atmosphere in parentheses (He = Helium, H₂ = Hydrogen) ^aPercentages calculated from integrated total ion current chromatographic peak areas. The maximum number of isomers detected for each product is labeled in parentheses. ^bP/O = Paraffin/Olefin Ratio ^cBen = Benzene ^dTol = Toluene ^ePh = Phenyl group ^{*}Percent residue (%R) was calculated by the weight loss in air divided by the total weight loss.

Table 5-2: Volatile product distribution, P/O ratio, and percent residue for the LPE/HZSM-5 and LPE/PtHZSM-5 samples heated in helium and hydrogen

Our results are not consistent with this trend, the largest volatile products were detected when LPE was cracked in helium and hydrogen by HY. This discrepancy could be due to the fact that LPE cracking reactions are dependent on pore accessibility and the strengths of accessible acid sites and both of these may change during sample heating.

Disproportionation reactions leading to paraffin formation should be favored on strong HZSM-5 acid sites. However, small HZSM-5 pores inhibit bimolecular reactions. Carbenium ions formed on strong acid sites inside small pores would have long residence times that would increase the probability for β -scission reactions (i.e. olefin formation).⁸ Many authors have reported that carbenium ion β -scission contributes significantly to the cracking mechanism of small hydrocarbons on HZSM-5 catalysts.⁴⁹⁻⁵¹ Similar trends toward increased olefin production have been reported when PE was cracked by HZSM-5 compared to larger pore zeolites.^{1-3,37-38}

Volatile olefins ranging from C₃-C₅ made up 47% and 58% of the total volatile product slates detected for the LPE/HZSM-5 (He) and LPE/HZSM-5 (H₂) samples, respectively (Table 5-2). Volatile paraffins (C₄-C₇) were 40% and 35% of the total product slates, respectively. These results are consistent with volatile product distributions previously reported for PE cracking by HZSM-5 where small (C₃-C₅) olefins were the principal volatile products formed.^{1-3,37-38} Disproportionation reactions were favored over β -scission at low temperatures (<200 °C) because the majority of the volatile product slate consisted of paraffins. Behrsing et al. have shown that the external acid sites of PtHZSM-5 are active for the hydroisomerization of branched olefins.⁵² Catalyst particle size was also reported to affect the volatile product distribution when cracking polymers.⁵³⁻⁵⁴ Therefore, disproportionation reactions may occur initially on the

external HZSM-5 surface because polymer segments are too large to diffuse into the pore structure. At higher temperatures (>200 °C), TA-GC/MS results from the LPE/HZSM-5 (He) and LPE/HZSM-5 (H₂) samples are consistent with literature reports that the combination of strong acid sites and small pore dimensions of HZSM-5 favor unimolecular β -scission and/or desorption reactions (i.e. olefin formation) over disproportionation.⁴⁹⁻⁵¹

Paraffin yield was expected to increase at the expense of olefin formation with the addition of hydrogen because of acid catalyzed hydrogenation reactions. In fact, Lugstien et al. reported that n-heptane cracking products for HZSM-5 heated in hydrogen at high pressure and low conversion (<10%) consisted of more C₃-C₄ paraffins and less C₃-C₄ olefins compared to helium.⁵⁵ The paraffin/olefin ratios (P/O) calculated for LPE/HZSM-5 were 0.84 in helium and 0.60 in hydrogen, which reflects a slight decrease in paraffin formation (Table 5-2). The individual percentages of volatile paraffin (C₄- \geq C₉) products listed in Table 5-2 are relatively constant in helium and hydrogen atmospheres, except for a 5% decrease in C₆ paraffin formation. This discrepancy relative to the Lugstein et al. report may result because LPE cracking was performed under very different reaction conditions (e.g. lower H₂ pressure and high polymer conversion).

The temperatures of initial volatile product evolution were the same for the LPE/HZSM-5 (He) and LPE/HZSM-5 (H₂) samples (Table 5-1). However, as the temperature increased and the catalyst became coated with smaller polymer fragments, the probability of hydrogenation increased. Hydrogen activation on metal-free HZSM-5 under 0.5 Atm hydrogen was reported to increase as catalyst temperatures increased from

100-400 °C.¹⁷ P/O ratios listed in Table 5-2 do not reflect the preferential increase in volatile paraffin formation at temperatures greater than 200 °C observed for the LPE/HZSM-5 (H₂) sample compared to the LPE/HZSM-5 (He) sample. At higher temperatures, a larger fraction of the total paraffin slate was evolved in hydrogen compared to helium as illustrated by the evolution profiles in Figure 5-1. Thus, P/O ratios plotted with respect to temperature were found to change (Figure 5-2). Below 220 °C, P/O ratios calculated for the sample heated in hydrogen were less than those for the sample heated in helium. The reduction in initial paraffin formation in hydrogen was followed by an increase at higher temperatures as shown by the increase in P/O ratio in hydrogen above 200 °C. Consequently, total paraffin yields detected in hydrogen were similar to that for helium (Table 5-2). The increase in P/O ratio for the LPE/HZSM-5 (H₂) sample above 200 °C may be explained by metal-free hydrogenation.

The combination of catalyst acidity and pore dimensions influence residue and volatile aromatics formation rates. Various cracking studies have found that increased catalyst pore size together with increased acidity promotes formation of surface residue.^{1-3,47-48,56-59} Volatile aromatic species are known to originate from accumulated unsaturated surface species.⁸⁻¹⁴ Residue formation during PE cracking was found to increase in the catalyst order: HZSM-5 < HMCM-41 < HY.¹ More volatile aromatic products were observed during PE cracking by HZSM-5 than HY because the smaller pore HZSM-5 was significantly more effective at facilitating cyclization than HY.^{1,37,48,56} Even though HZSM-5 was the strongest acid catalyst used in the study, the pores of HZSM-5 were only large enough to allow formation of small alkyl aromatics and formation of fused unsaturated residue species was inhibited.

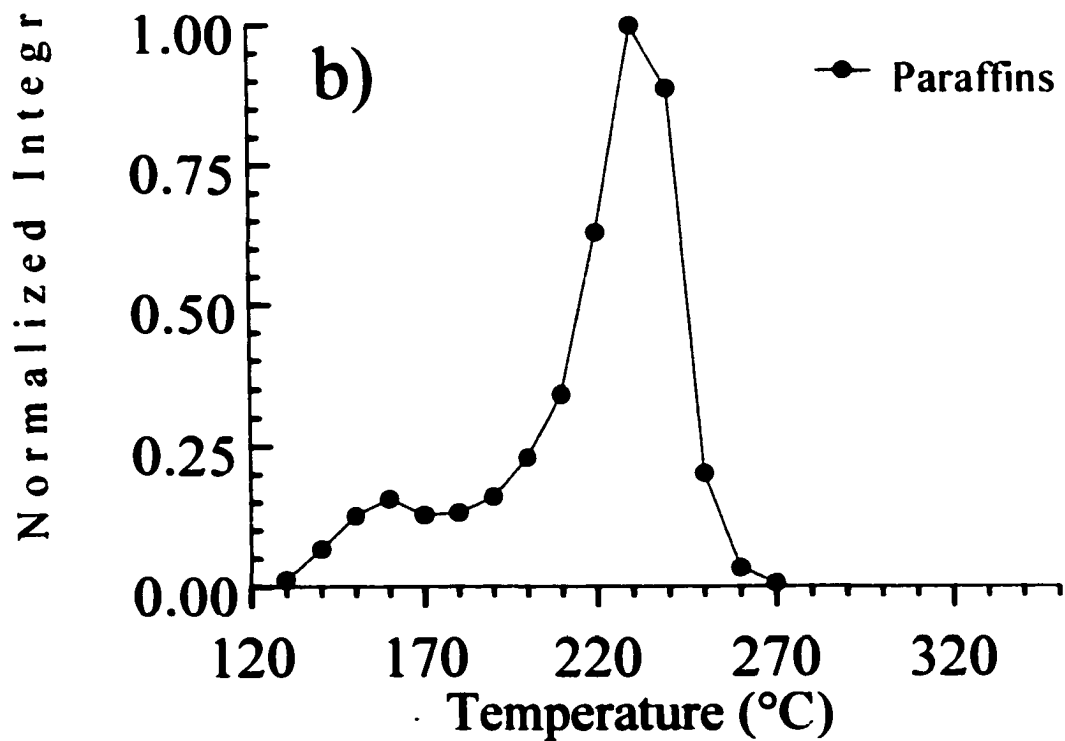
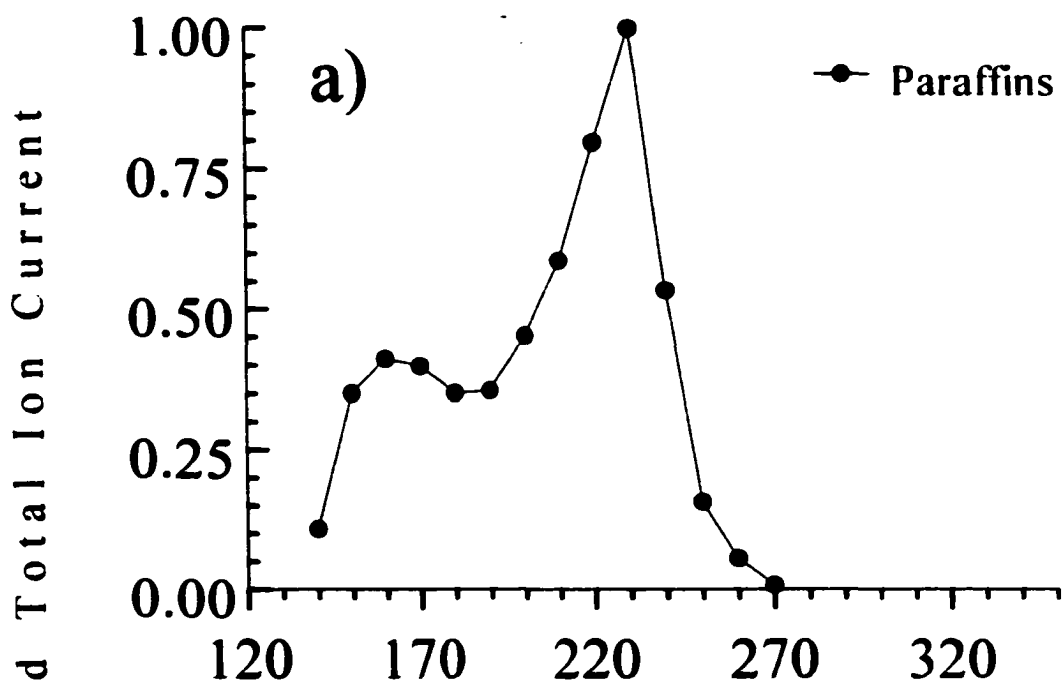


Figure 5-1 Normalized volatile paraffin profiles for a) LPE/HZSM-5 (He)
 b) LPE/HZSM-5 (H₂)

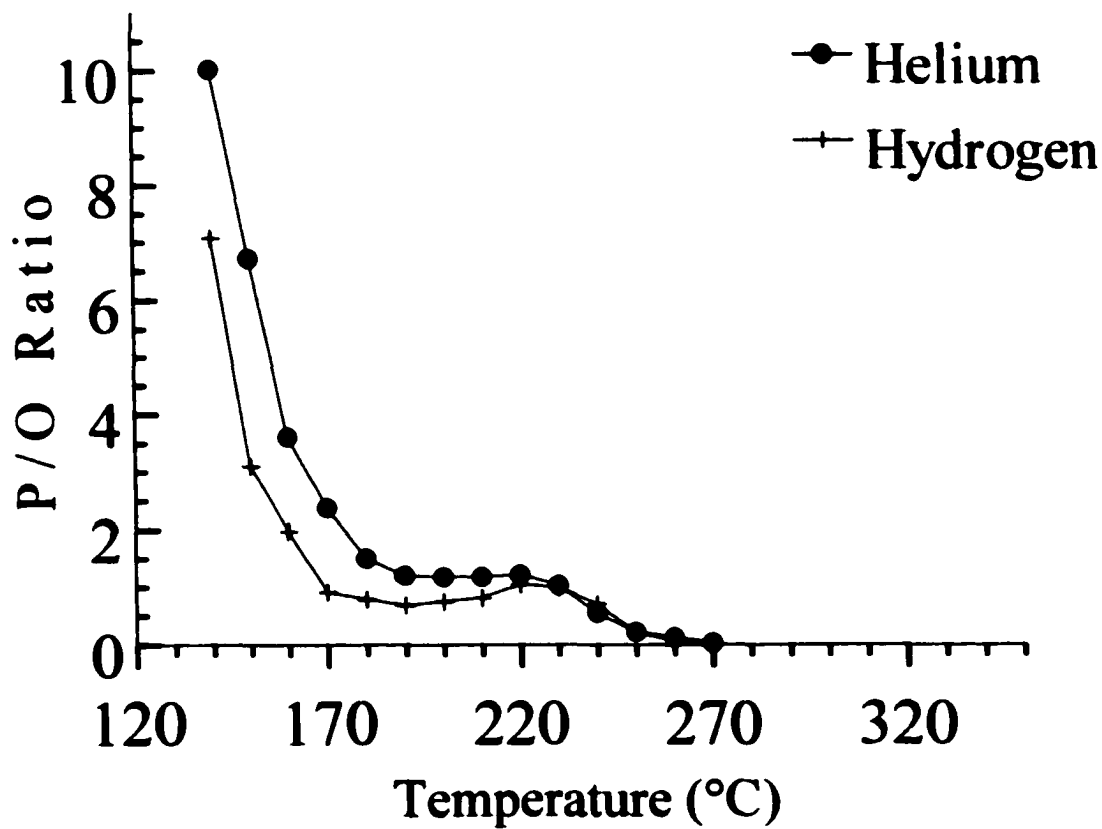


Figure 5-2: P/O ratio vs. temperature for LPE/HZSM-5 heated in helium and hydrogen

The small amount of residue found after cracking LPE by HZSM-5 is consistent with the literature reports that smaller pores restrict formation of large unsaturated species.

The percentage of volatile alkyl aromatic species was 5% of the total volatile product slate detected for the LPE/HZSM-5 (He) sample. In contrast, 2% was formed for the LPE/HZSM-5 (H₂) sample (Table 5-2). There was a 4-5% increase in C₃ and C₄ olefin yields along with reduced volatile aromatics yields in hydrogen compared to helium. Carbonaceous residue that remained on the LPE/HZSM-5 (He) sample amounted to 5% of the initial polymer weight. Only 2% residue remained on the LPE/HZSM-5 (H₂) sample. The presence of hydrogen contributes to hydrogenation reactions on metal-free catalysts that decrease residue.⁵⁷⁻⁶¹ Ding et al. have reported that less residue collects on HZSM-5 after the decomposition of HDPE in hydrogen versus nitrogen.⁶⁰ Apparently, the hydrogen activating ability of metal-free HZSM-5 is adequate to reduce residue and alkyl aromatic yields, but not sufficient to reduce olefin production. The formation of residue and alkyl aromatic products requires the presence of conjugated double bonds, which were reduced in concentration by hydrogenation. The 20 °C decrease in volatile product evolution temperature range for the LPE/HZSM-5 (H₂) sample compared to the LPE/HZSM-5 (He) sample (Table 5-1) can be explained by metal-free hydrogenation and the resulting decrease in volatile alkyl aromatics yield.

5.3.1b LPE/HZSM-5 (He) vs. LPE/PtHZSM-5 (He)

Dehydrogenation, cracking, and hydrogenolysis reactions may occur on platinum in the absence of molecular hydrogen.²⁰⁻²² Specific contributions from platinum catalyzed reactions may not be evident because volatile products may be the same as those formed on acid sites. For example, no significant differences in volatile product

slates were reported from n-heptane conversion by HZSM-5 and PtHZSM-5 in helium.⁵⁵ However, those studies were conducted at constant conversion with low n-heptane concentrations. At low conversion, volatile product slates are constant because catalyst active sites remain relatively unchanged. LPE cracking is a high conversion reaction in which catalyst properties may constantly change. Thus, changes in relative product yields are more likely to be detected for LPE cracking by platinum containing catalysts. Hydrogenolysis can form paraffins, but there is a very low probability for this reaction in hydrogen deficient environments. However, contributions from dehydrogenation and cracking reactions catalyzed by platinum could enhance olefin and aromatic yields in volatile product slates.

There was no significant change in P/O ratio between the LPE/HZSM-5 (He) and LPE/PtHZSM-5 (He) samples (Table 5-2). However, total volatile paraffin and olefin yields decreased by 5% when platinum was added. Increased unsaturation was evidenced by an increase in volatile alkyl aromatics formation for the LPE/PtHZSM-5 (He) sample compared to the LPE/HZSM-5 (He) sample. Volatile aromatic products amounted to 5% of the total volatile product slate detected for the LPE/HZSM-5 (He) sample. The volatile aromatics yield increased to 17% of the total product slate for the LPE/PtHZSM-5 (He) sample (Table 5-2).

A general trend of increased product size distribution has been reported for polymer cracking in nitrogen with bifunctional catalysts compared to metal-free acid catalysts.⁶²⁻⁶³ Increased formation of aromatics and/or larger olefin species reportedly cause a change in volatile product distribution that depends on catalyst properties. Dehydrocyclization reactions on platinum sites of bifunctional catalysts are additional

pathways for alkyl aromatics formation.⁶⁴⁻⁶⁶ Aromatic products reportedly form preferentially to skeletal isomers during hexane conversion over Pt black in absence of hydrogen.^{64,67} Gnep et al. reported that an increase in volatile aromatic species correlates with the presence of platinum during cyclization of propane on HZSM-5 and PtHZSM-5 in hydrogen deficient environments.⁶⁸ The acid catalyst structure of bifunctional catalysts was reported to be very important for dehydrocyclization reactions of hydrocarbons larger than C₇.⁶⁹ Thus, it is likely that the pore structure of HZSM-5 together with the presence of platinum combined to increase volatile aromatics yield at the expense of paraffin and olefin formation for the LPE/PtHZSM-5 (He) sample compared to the metal-free sample.

Carbonaceous residue that remained on the LPE/HZSM-5 (He) sample was 5% of the initial polymer weight. Only 3% of the initial polymer weight remained on the LPE/PtHZSM-5 (He) sample. Previous PE cracking studies revealed that increased residue formation on bifunctional catalysts could be correlated with increased aromatics formation.^{62-63,70} Bifunctional catalysts have been reported to collect more residue than metal-free catalysts under the same conditions.^{64,71} In contrast to literature reports, there were more volatile aromatics and less carbonaceous residue for the LPE/PtHZSM-5 (He) sample compared to the LPE/HZSM-5 (He) sample.

5.3.1c LPE/PtHZSM-5 (He) vs. LPE/PtHZSM-5 (H₂)

According to the classical bifunctional catalyst mechanism, the role of platinum is to promote dehydrogenation/hydrogenation reactions.²⁰ In section 5.2.3, it was discussed that platinum can be multi-functional. The hydrogenation ability of platinum is dramatically increased in the presence of molecular hydrogen due to a process called

hydrogen spillover.^{67,72-74} During bifunctional hydrocracking, molecular hydrogen is activated on platinum sites and then the activated species migrate (i.e. spillover) to another metal or acid site to participate in hydrogenation reactions. The exact form of activated hydrogen species is unknown, but hydrogen spillover has been proposed to occur by gas phase and surface transfer mechanisms.⁷²⁻⁷⁴

Volatile paraffins (C₄-C₇) were 35% of the total product slate detected for the LPE/PtHZSM-5 (He) sample (Table 5-2). Volatile paraffins (C₄-C₇) increased to 76% of the total product slate detected for the LPE/PtHZSM-5 (H₂) sample due to platinum catalyzed hydrogenation. The volatile paraffin/olefin ratios (P/O) were 0.86 and 18, respectively. No volatile C₃ paraffins were detected for the sample heated in helium, but 4% of the total volatile product slate for the sample heated in hydrogen were C₃ paraffins. There was also an increased relative abundance of C_n≥C₉ paraffins for the LPE/PtHZSM-5 (H₂) sample compared to the LPE/PtHZSM-5 (He) sample (Table 5-2).

Increased acid strength together with small pore size was shown to favor n-hexadecane hydrocracking. An increased amount of smaller paraffin isomers were detected from n-hexadecane hydrocracking by PtHZSM-5 compared to PtHY and PtMCM-41.⁷⁷ Many authors have reported that hydrogenation of olefins (formed by β-scission) contribute significantly to paraffin formation during hydrocracking of C₉-C₁₆ hydrocarbons over PtHZSM-5 catalysts.⁷⁸⁻⁸⁰ Therefore, the small pores and strong acid strength of PtHZSM-5 should promote LPE hydrocracking to form volatile paraffins with an increase in the amount of small isomers compared to cracking in helium, which is consistent with our measurements.

Volatile olefin and aromatic products made up only 5% of the total volatile product slate detected for the LPE/PtHZSM-5 (H₂) sample, which was much less than was detected for the LPE/PtHZSM-5 (He) sample (55%) (Table 5-2). Carbonaceous residue that remained on the LPE/PtHZSM-5 (H₂) sample amounted to <1% of the initial polymer weight (Table 5-2), which was much less than any of the other LPE/HZSM-5 samples. Studies of small hydrocarbon conversion on metal-free and bifunctional catalysts have shown that the accumulation of residue on the catalyst depends on hydrogen partial pressure.^{15,17,81} Hydrogenation has been suggested to inhibit surface residue formation.⁸²⁻⁸³ Residue and volatile aromatic yields during bifunctional cracking reactions can be correlated.⁷⁰ For example, Aberuagba et al. detected decreased aromatics and residue formation from the conversion of 2-heptene over PtAl₂O₃ in hydrogen compared to nitrogen.⁸⁴ Our results are consistent with this report, residue and volatile aromatics yield decreased when LPE/PtHZSM-5 was heated in hydrogen compared to helium.

5.3.2a LPE/HY (He) vs. LPE/HY (H₂)

Table 5-3 lists the relative volatile product yields for the LPE/HY (He), LPE/HY (H₂), LPE/PtHY (He), and LPE/PtHY (H₂) samples. Volatile paraffins ranging from C₄-≥C₉ made up 96% and 98% of the total volatile product slates for the LPE/HY (He) and LPE/HY (H₂) samples, respectively. P/O ratios were high for both samples and differed by about 20%. Disproportionation reactions, which yield paraffin products, are favored carbenium ion reactions at strong acid sites unless catalyst pore size restricts bimolecular reactions.⁸ Even with decreased acid strength, the increased pore size of HY compared to HZSM-5 appears to be adequate to accommodate these bimolecular reactions.

Volatile Products		Percentage Yields** by Catalyst and Purge gas			
		HY (He)	HY (H ₂)	PtHY (He)	PtHY (H ₂)
Paraffin ↓	C ₃	-	-	-	-
	C ₄	12 ^a (1)	12 (3)	9 (1)	7 (3)
	C ₅	17 (1)	16 (1)	10 (1)	11 (2)
	C ₆	19 (3)	19 (3)	16 (3)	14 (4)
	C ₇	20 (3)	21 (3)	15 (3)	18 (4)
	C ₈	17 (4)	19 (5)	13 (4)	19 (4)
	≥C ₉	11 (5)	11 (7)	12 (10)	29 (17)
Olefin ↓	C ₃	1 (1)	<1 (1)	1 (1)	-
	C ₄	1 (3)	2 (2)	2 (3)	-
	C ₅	1 (3)	2 (3)	1 (3)	-
	C ₆	<1 (1)	-	-	-
	C ₇	<1 (1)	-	<1 (1)	<1 (1)
	C ₈	<1 (1)	<1 (2)	-	1 (1)
	≥C ₉	-	-	-	-
Aromatic ↓	Ben ^c	-	-	-	-
	Tol ^d	-	-	-	-
	C ₂ -Ph ^e	-	-	2 (2)	-
	C ₃ -Ph	1 (2)	-	12 (3)	-
	C ₄ -Ph	<1 (1)	-	6 (1)	-
% Total	Volatiles	100	102	99	99
P/O^b		32	25	19	98
% R^e		19	13	26	9

**LPE/Catalyst samples are listed along with the reaction atmosphere in parentheses (He = Helium, H₂ = Hydrogen). ^aPercentages calculated from integrated total ion current chromatographic peak areas. The maximum number of isomers detected for each product is labeled in parentheses. ^bP/O = Paraffin/Olefin Ratio ^cBen = Benzene ^dTol = Toluene ^ePh = Phenyl group ^ePercent residue (%R) was calculated by the weight loss in air divided by the total weight loss.

Table 5-3: Volatile product distribution, P/O ratio, and percent residue for the LPE/HY and LPE/PtHY samples heated in helium and hydrogen

These results are consistent with previous literature reports. For example, paraffin rich products were detected during HDPE cracking with HY catalyst heated in nitrogen.³⁶⁻³⁷ Previous work in this laboratory has also shown that volatile paraffins are the principal species formed by HY during PE cracking in helium.¹

The competition between cracking at external sites and inside pores appears to be less important for the larger pore HY catalyst because, unlike HZSM-5, there was little change in volatile product slate in helium and hydrogen as the cracking temperature increased. Volatile paraffin products were the main species detected for the LPE/HY samples and the influence of hydrogen was not as obvious as for the LPE/HZSM-5 samples, except for the decrease in the volatile product evolution temperature range (Table 5-1). There was a large decrease in the amount of residue between the LPE/HY (He) and LPE/HY (H₂) samples. Carbonaceous residue that remained on the LPE/HY (He) sample amounted to 19% of the initial polymer weight and 13% of the initial polymer weight remained on the LPE/HY (H₂) sample (Table 5-3). The addition of metal-free hydrogenation reactions would be expected to decrease the amount of surface residue formed on a catalyst during hydrocracking.⁵⁷⁻⁶¹ Thus, the decrease in residue and volatile product evolution temperature range in the presence of hydrogen can be attributed to hydrogenation reactions.

The percentage of volatile alkyl aromatics species for the LPE/HY (He) sample was very small (1%) and no aromatics were detected from the LPE/HY (H₂) sample. More volatile aromatic products were detected during PE cracking by HZSM-5 than by HY because the smaller HZSM-5 pore was significantly more effective at cyclization of conjugated double bond systems than HY.^{1,37} Even though the LPE/HY samples

accumulated more residue than the LPE/HZSM-5 samples, aromatics formation was not favored by HY because the pores were not small enough to promote cyclization.

5.3.2b LPE/HY (He) vs. LPE/PtHY (He)

Volatile paraffins ranging from C_4 - $\geq C_9$ in size made up 96% and 75% of the total volatile product slate detected for the LPE/HY (He) and LPE/PtHY (He) samples, respectively (Table 5-3). There was an increase in the number of $\geq C_9$ paraffin isomers and a decrease in the C_5 - C_8 paraffin yields for the LPE/PtHY (He) sample. The large P/O ratio difference was due to the reduction in paraffin yield for the LPE/PtHY sample. Acid and platinum catalyzed reactions may contribute to the formation of volatile paraffins and olefins for the LPE/PtHY (He) sample. However, it was not possible to distinguish products formed by specific mechanisms of the bifunctional catalyst. Increased volatile product size has been reported for polymer cracking in nitrogen with bifunctional catalysts compared to metal-free acid catalysts.⁶²⁻⁶³ Thus, the addition of platinum likely caused the increase in $\geq C_9$ isomers detected for the LPE/PtHY (He) sample compared to the LPE/HY (He) sample.

An increase in residue (Table 5-3) and volatile aromatics yield were detected when platinum was added to the HY catalyst. A large increase in volatile aromatics yield at the expense of volatile paraffin yield is illustrated by the evolution profiles in Figure 5-3. The volatile alkyl aromatics yield from LPE/HY (He) was 1% (Table 5-3). However, volatile aromatic species were 20% of the total volatile product slate for the LPE/PtHY (He) sample. Carbonaceous residue that remained on the LPE/HY (He) sample amounted to 19% of the initial polymer weight and increased to 26% with the addition of platinum.

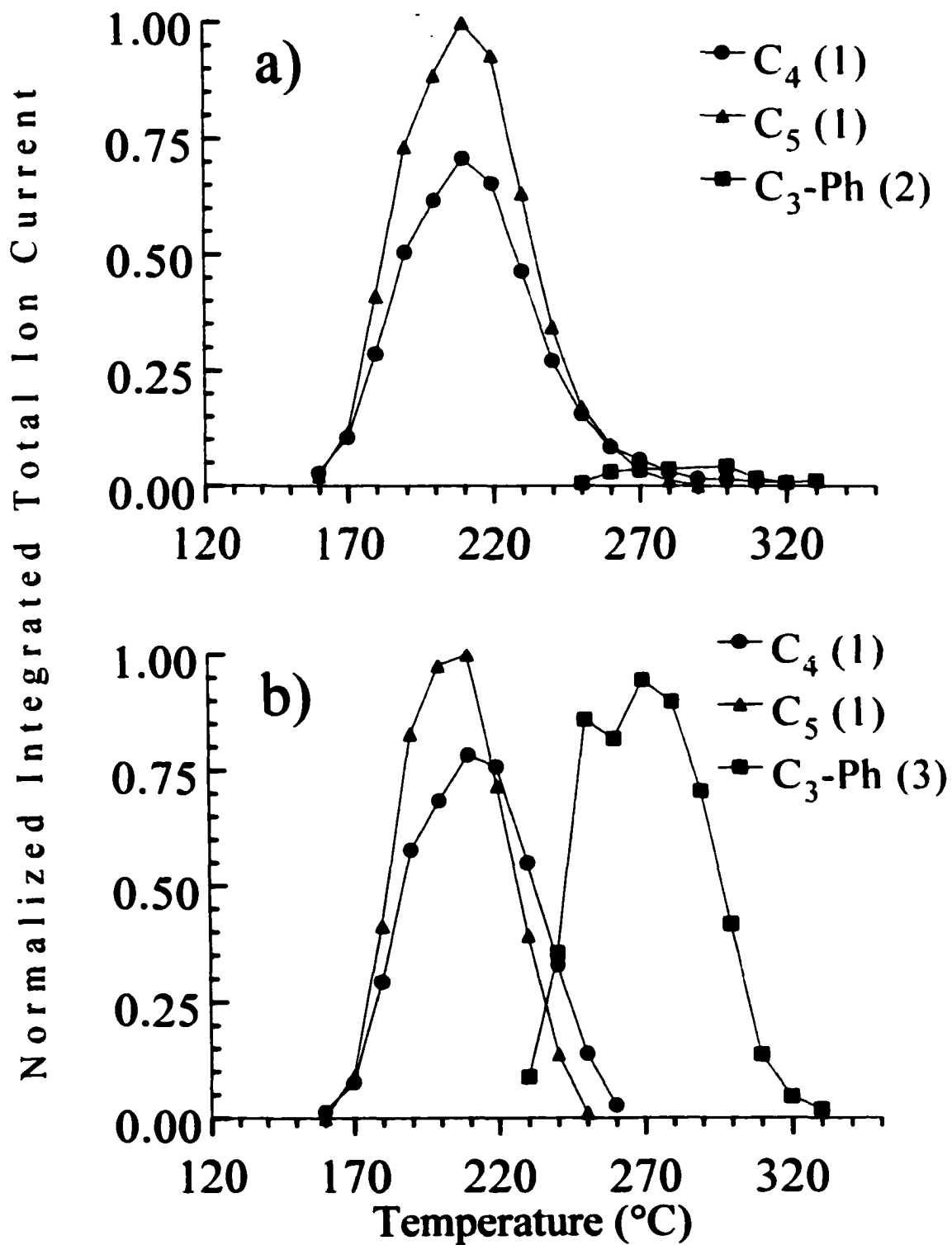


Figure 5-3: a) Normalized volatile C₄-C₅ paraffins and alkyl aromatic (C₃-Phenyl) evolution profiles for LPE/HY in helium b) Normalized volatile C₄-C₅ paraffins and alkyl aromatic (C₃-Phenyl) evolution profiles for LPE/PtHY in helium

These results are consistent with previous reports that bifunctional catalysts collect more residue and produce more volatile alkyl-aromatics than metal-free catalysts when the pore size allows.^{64,71} Thus, dehydrogenation reactions catalyzed by platinum increased the yield of volatile aromatic products and residue.

5.3.2c LPE/PtHY (He) vs. LPE/PtHY (H₂)

Volatile paraffins ranging from C₄-≥C₉ in size made up 75% and 98% of the total volatile product slate detected for the LPE/PtHY (He) and LPE/PtHY (H₂) samples, respectively (Table 5-3). There was an increase in the number and amount of ≥C₉ paraffin isomers detected from the LPE/PtHY (H₂) sample. The dramatic change in P/O ratio was due to the large increase in paraffin yield for the LPE/PtHY (H₂) sample. The percentage of volatile alkyl aromatic species formed from LPE/PtHY (He) was 20% and no aromatics were detected for the LPE/PtHY (H₂) sample. Carbonaceous residue that remained on the LPE/PtHY (He) sample amounted to 26% of the initial polymer weight and decreased to 9% with the addition of hydrogen. Bifunctional hydrogenation reactions have been previously shown to decrease the amount of residue and volatile alkyl aromatic yields.⁸²⁻⁸³

In the case of polymer hydrocracking, larger paraffin isomers should be observed under hydrogenating conditions compared to non-hydrogenating conditions. When surface species undergo hydrogenation reactions, there is increased probability that species will be released from the active site before cracking may occur.⁶⁷ Coonradt et al. reported that more paraffins (C₄-C₁₂) were formed during hexadecane hydrocracking over PtSiAl compared to cracking over SiAl in nitrogen (C₃-C₆).⁷⁵ They also reported negligible olefin formation during hydrocracking, but substantial olefin yields were

detected during cracking.⁷⁵ Lower HDPE oil conversion due to reduced polymer cracking on a bifunctional catalyst was observed in hydrogen compared to nitrogen.⁷⁶ In other words, bifunctional catalysts promote shorter carbenium ion residence times that lead to larger products, the degree to which this occurs depends on catalyst properties (e.g. pore size, acid strength, metal, and acid site density).⁷⁶ Compared to LPE/PtHZSM-5 results, the increased size of volatile products evolved by LPE/PtHY hydrocracking correlates with average pore size and acid strength: LPE/PtHZSM-5 < LPE/PtHY. Volatile paraffin products were the main species formed from both LPE/PtHY samples, but the hydrogenation function of platinum led to increased product evolution temperatures when hydrogen was present (Table 5-1).

5.3.3a LPE/HMCM-41 (He) vs. LPE/HMCM-41 (H₂)

Table 5-4 lists the relative yields of the volatile products for the LPE/HMCM-41 (He), LPE/HMCM-41 (H₂), LPE/PtHMCM-41 (He), and LPE/PtHMCM-41 (H₂) samples. Volatile olefins ranging from C₃-C₈ in size made up 89% and 90% of the total volatile product slates detected for the LPE/HMCM-41 (He) and LPE/HMCM-41 (H₂) samples, respectively (Table 5-4). Volatile paraffins (C₄-C₈) were 13% and 12% of the total product slates and P/O ratios were calculated to be 0.15 and 0.13, respectively. Volatile olefin products were the main species formed from the LPE/HMCM-41 samples, which was similar to what was observed for the LPE/HZSM-5 samples. Compared to HZSM-5 and HY, HMCM-41 had the fewest acid sites and lacked high acid strength sites. The high olefin yield for the LPE/HMCM-41 samples suggests that β -scission and desorption dominated rather than disproportionation during LPE cracking.

Volatile Products		Percentage Yields** by Catalyst and Purge gas			
		HMCM-41 (He)	HMCM-41 (H ₂)	PtHMCM-41 (He)	PtHMCM-41 (H ₂)
Paraffin ↓	C ₃	-	-	-	<1 (1)
	C ₄	4 ^a (2)	5 (2)	1 (2)	4 (3)
	C ₅	2 (1)	3 (1)	1 (1)	6 (2)
	C ₆	1 (1)	2 (2)	-	7 (4)
	C ₇	2 (2)	1 (1)	1 (1)	9 (4)
	C ₈	3 (1)	<1 (1)	-	11 (4)
	≥C ₉	1 (6)	1 (5)	-	61 (20)
Olefin ↓	C ₃	4 (1)	4 (1)	3 (1)	-
	C ₄	19 (3)	20 (3)	13 (3)	-
	C ₅	30 (5)	29 (4)	20 (4)	-
	C ₆	22 (6)	23 (6)	19 (7)	-
	C ₇	10 (5)	10 (5)	16 (6)	<1 (1)
	C ₈	4 (6)	4 (6)	15 (6)	1 (1)
	≥C ₉	-	-	12 (8)	-
Aromatic ↓	Ben ^c	-	-	-	-
	Tol ^d	-	-	-	-
	C ₂ -Ph ^c	-	-	-	-
	C ₃ -Ph	-	-	-	-
	C ₄ -Ph	-	-	-	-
% Total	Volatiles	102	102	101	99
P/O^b		0.15	0.13	0.03	98
% R^e		6	5	16	5

**LPE/Catalyst samples are listed along with the reaction atmosphere in parentheses (He = Helium, H₂ = Hydrogen). ^aPercentages calculated from integrated total ion current chromatographic peak areas. The maximum number of isomers detected for each product is labeled in parentheses. ^bP/O = Paraffin/Olefin Ratio ^cBen = Benzene ^dTol = Toluene ^ePh = Phenyl group ^ePercent residue (%R) was calculated by the weight loss in air divided by the total weight loss.

Table 5-4: Volatile product distribution, P/O ratio, and percent residue for the LPE/MCM-41 and LPE/PtHMCM-41 samples heated in helium and hydrogen

Disproportionation reaction rates depend on carbenium ion reactivities, which are determined by catalyst site acid strengths.⁸ Therefore, catalytic site acidities may have been too low for this reaction pathway to be favored. There appears to be no competition between cracking at external sites and within pores for the larger pore HMCM-41 catalyst because there was no significant change in volatile product slate in helium and hydrogen when the cracking temperature was increased.

There was an increase in the size of volatile olefins formed by HMCM-41 (C₄-C₇) compared to HZSM-5 (C₃-C₅). This trend is consistent with reports of increased volatile product size for hexadecane and PE batch reactions with increased catalyst pore size and decreased acid strength.^{45-46,77} However, HY and HMCM-41 do not follow this trend.

The size distribution of volatile products from the LPE/HMCM-41 (He) and LPE/HMCM-41 (H₂) samples were very similar. No volatile aromatic species were detected from either LPE/HMCM-41 sample. The carbonaceous residue that remained on the LPE/HMCM-41 (He) sample amounted to 6% of the initial polymer weight and 5% remained on the LPE/HMCM-41 (H₂) sample (Table 5-4). Previous PE cracking studies have found that formation of aromatic products was not favored by HMCM-41 catalysts.^{1,43} Compared to the HZSM-5 and HY catalysts, the increased pore size of HMCM-41 should facilitate the formation of large surface residue species. However, lower catalyst acidity should inhibit formation of residue.^{1,44,47} Hydrogenation on metal-free HMCM-41 does not appear to affect the volatile product slate or residue accumulation as much as for HY and HZSM-5. However, a slight decrease in the volatile product evolution temperature range (20 °C) was observed for the LPE/HMCM-41 (H₂) sample, which may be attributed to metal-free hydrogenation.

5.3.3b LPE/HMCM-41 (He) vs. LPE/PtHMCM-41 (He)

Cracking reactions that lead to volatile product formation may be supplemented by hydrocarbon reactions on platinum sites. Thus, changes in LPE relative product yields may be detected after the addition of platinum to the HMCM-41 cracking catalyst. Contributions from dehydrogenation and cracking reactions catalyzed by platinum would be expected to enhance olefin and aromatic yields in volatile product slates.

Volatile olefins ranging from C₄-C₈ in size made up 89% and 98% of the total volatile product slate detected for the LPE/HMCM-41 (He) and LPE/PtHMCM-41 (He) samples, respectively (Table 5-4). Decreased C₄-C₆ olefin yields were detected, but increased C₇-≥C₉ olefin yields were detected for the LPE/PtHMCM-41 (He) sample compared to the LPE/HMCM-41 (He). The volatile P/O ratios were 0.03 and 0.15, respectively. The initial temperature of volatile product evolution decreased by 40 °C with the addition of platinum to the catalyst (Table 5-1). No volatile aromatic species were detected for either sample. The carbonaceous residue that remained on the LPE/HMCM-41 (He) sample amounted to 6% of the initial polymer weight and 16% remained on the LPE/PtHMCM-41 (He) sample (Table 5-4).

The increased size distribution of volatile products formed from the LPE/PtHMCM-41 (He) sample compared to the LPE/HMCM-41 (He) sample was expected. The addition of platinum to HMCM-41 increased the amount of surface residue formed in helium, but did not promote volatile aromatics formation as was observed for the PtHY and PtHZSM-5 catalysts. Even with the addition of platinum, formation of aromatic products was not favored by the large pore size and/or low acidity of the HMCM-41 catalyst.

5.3.3c LPE/PtHMCM-41 (He) vs. LPE/PtHMCM-41 (H₂)

Volatile olefins made up 98% of the total volatile product slate detected for the LPE/PtHMCM-41 (He) sample (Table 5-4). However, volatile olefin yields made up 1% of the total volatile product slate detected for the LPE/PtHMCM-41 (H₂) sample. Volatile paraffins (C₄-C₇) made up 3% of the total volatile product slate for the LPE/PtHMCM-41 (He) sample. In contrast, 37% of the total volatile product slate were C₄-C₈ paraffins and 61% were ≥C₉ paraffins for the LPE/PtHMCM-41 (H₂) sample. The P/O ratios were 0.03 and 98, respectively. These results clearly show that the hydrogenation function of the platinum counteracted the tendency for HMCM-41 to form olefins. No volatile aromatics were detected for either sample. Carbonaceous residue that remained on the LPE/PtHMCM-41 (He) sample amounted to 16% of the initial polymer weight. Carbonaceous residue that remained on the LPE/PtHMCM-41 (H₂) sample amounted to 5% of the initial polymer weight. Thus, the hydrogenation activity of the platinum was responsible for the volatile product evolution temperature shift, the increased size of volatile paraffin isomers, and the decrease in residue for the LPE/PtHMCM-41 (H₂) sample.

5.4 Isoconversion E_a of LPE Cracking

The “effective” activation energy (E_a) value represents the minimum energy required for reaction processes that lead to a given result (i.e. volatile product class) (Chapter 3). E_a value changes during a temperature dependent reaction reflect changes in parallel reaction pathway(s). An increase in E_a with temperature denotes changing contributions from competing reaction mechanisms.⁸⁵ A decrease in E_a with temperature

reflects a change in the rate limiting step (RLS) for one or more parallel mechanisms.⁸⁵ E_a temperature profiles for LPE/catalyst samples heated in helium and hydrogen atmospheres were derived from three mass spectrometer ion signals: m/z 55, 57, and 91. As described in Chapter 3, these ions were chosen because of their high selectivities for $>C_3$ -olefin, $>C_3$ -paraffin, and alkyl aromatic volatile products, respectively. E_a versus temperature plots will be shown here because volatile products evolve over different temperature ranges for the LPE/catalyst samples. The temperature scales in the E_a plots were generated by assuming a 5 °C/min heating ramp. E_a versus temperature plots may not always correlate with volatile product evolution profiles because TA-GC/MS experiments employed a slightly slower heating rate (2 °C/min).

E_a value accuracies depend on the degree to which the ion signals used for calculating these values correlate with the target product class. Correlations between E_a value and reaction mechanism may be less meaningful when selectivities are low. Ion signal selectivities for paraffin (m/z 57) and olefin (m/z 55) formation varied between ca. 75-99% for the LPE/HZSM-5 (He), LPE/HZSM-5 (H₂), and LPE/PtHZSM-5 (He) samples. Ion selectivities for all other LPE/catalyst samples ranged from ca. 97-99%.

5.4.1 LPE/HZSM-5 Paraffin Formation E_a

The selectivity of m/z 57 for paraffins for the LPE/HZSM-5 (He) and LPE/HZSM-5 (H₂) samples changed with temperature and was dependent on the volatile product slate. Between 160-180 °C, the m/z 57 paraffin selectivity for the LPE/HZSM-5 (He) sample decreased from ca. 99 to 88% and then remained relatively constant at 88% until 250 °C (Figure 5-4, triangle). Above 250 °C, selectivity decreased dramatically.

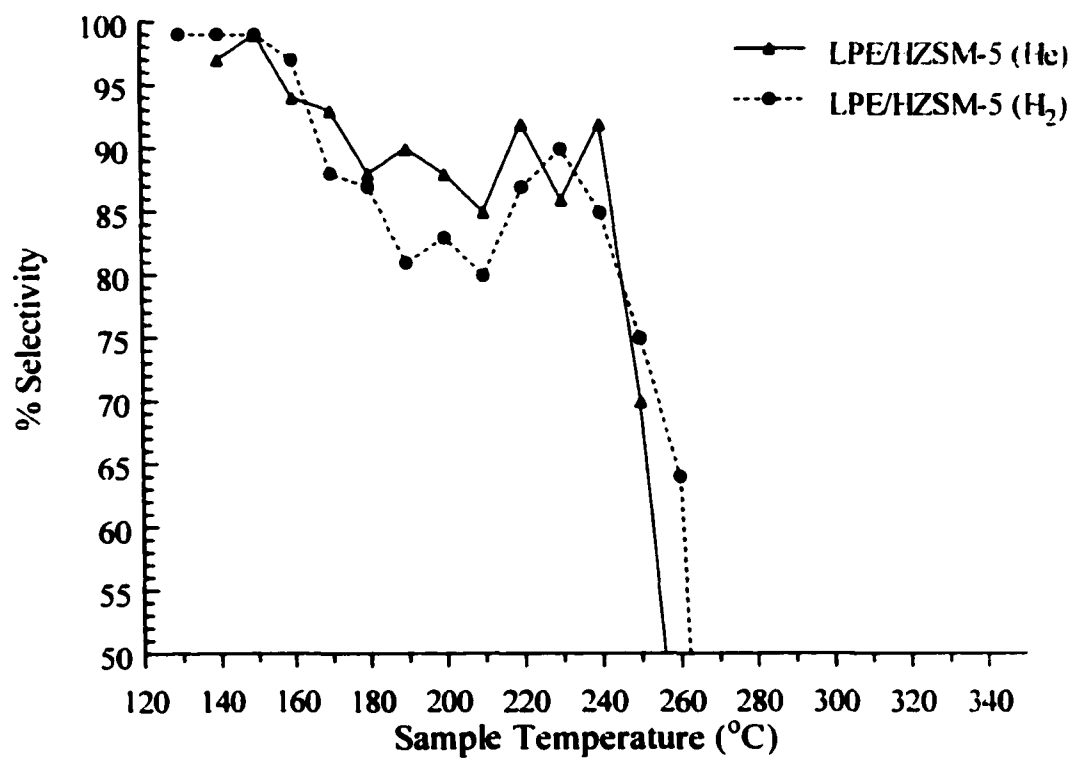


Figure 5-4: Plot of paraffin (m/z 57) selectivity vs. sample temperature calculated from TA-GC/MS results for LPE/HZSM-5 heated in helium and hydrogen

The high selectivity at low temperature indicates that E_a values calculated at these temperatures accurately represent volatile paraffin formation mechanisms. As the selectivity decreases, paraffin formation mechanisms may not be represented as well by E_a values. The trend in selectivity with respect to temperature for the LPE/HZSM-5 (H_2) sample was similar to that for the LPE/HZSM-5 (He) sample (Figure 5-4, circle). The selectivity of m/z 57 for paraffins for the LPE/PtHZSM-5 (He) sample remained relatively constant at ca. 89-92% over the 160-250 °C temperature range. Above 250 °C, very small amounts of volatile paraffins were formed by the LPE/HZSM-5 (He), LPE/HZSM-5 (H_2), and LPE/PtHZSM-5 (He) samples. Consequently, m/z 57 selectivities were very low and therefore these portions of the E_a versus temperature plots are not shown.

Figure 5-5 shows the E_a vs. temperature plots for the a) LPE/HZSM-5 (He) (solid line) and LPE/HZSM-5 (H_2) (dotted line) and b) LPE/PtHZSM-5 (He) samples. The shape of the E_a curve for each plot in Figure 5-5 follows the same general trend with respect to temperature. Large error in the E_a values calculated for the LPE/PtHZSM-5 (He) sample makes interpretation of E_a trends questionable for this sample (Figure 5-5b). E_a values remained relatively constant from 160-180 °C, which suggests that the mechanism(s) of volatile paraffin formation did not change significantly during this temperature range. An increase in E_a with respect to temperature from 180-225 °C was due to a change in the relative importance of paraffin formation by parallel reaction mechanisms. The E_a plateau from 225-250 °C suggests that mechanism(s) that form paraffins remained unchanged over this temperature range.

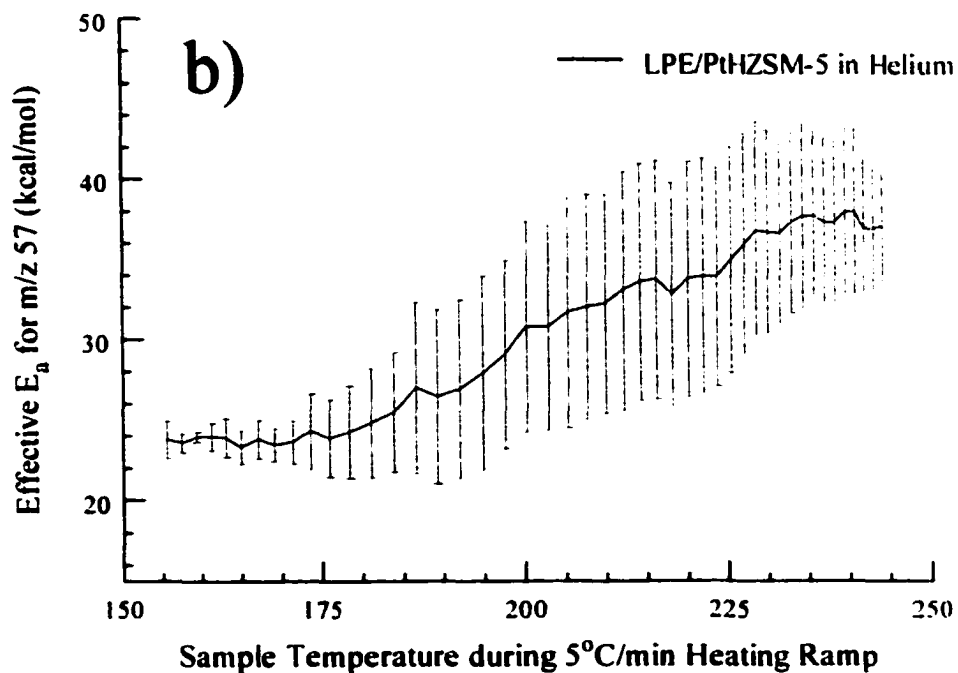
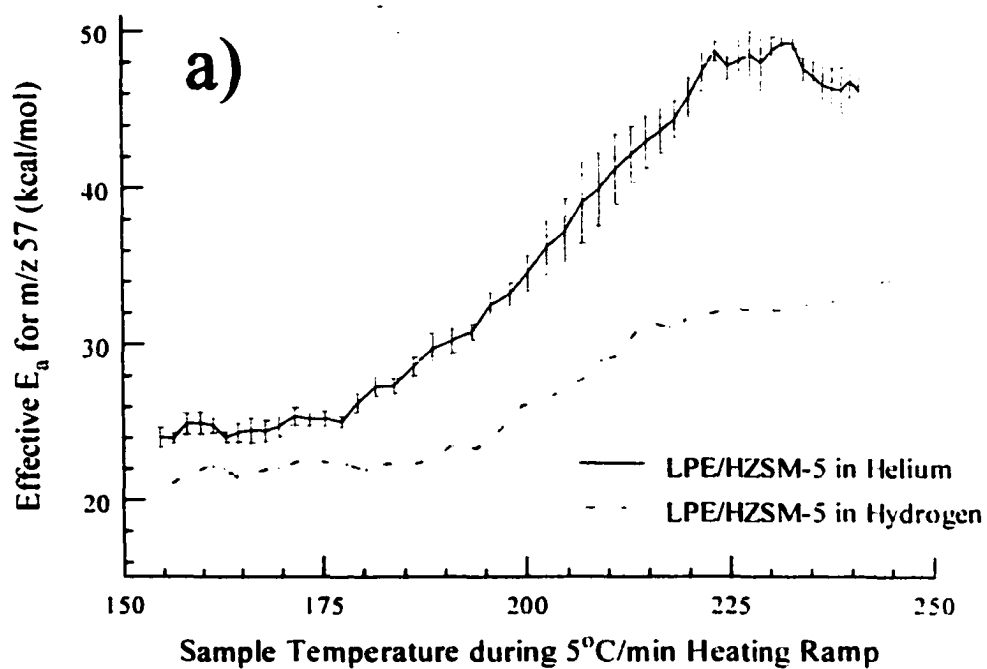


Figure 5-5: E_a vs. temperature plots for the formation of paraffins (m/z 57) by
 a) LPE/HZSM-5 heated in helium and hydrogen b) LPE/PtHZSM-5 heated in helium

Volatile product evolution profiles for the LPE/HZSM-5 samples show that paraffin formation was favored at temperatures below 200 °C. Acid catalyzed disproportionation reactions are believed to lead to the formation of volatile paraffins from reactions on HZSM-5 active sites that are initially accessible to LPE (i.e. external surfaces). Acid sites inside pores are known to be stronger than those on the external surface and stronger acid sites should better promote disproportionation. However, volatile product evolution profiles suggest that the combination of strong acid sites and small pore dimensions of HZSM-5 favor unimolecular β -scission and/or desorption reactions (i.e. olefin formation) over disproportionation at temperatures above 200 °C. Diffusion of large LPE molecules into the HZSM-5 pores and disproportionation at acid sites within pores are sterically inhibited processes. Therefore, an increase in E_a for paraffin formation would be expected for disproportionation reactions that occur inside pores compared to reactions on external acid sites. As the temperature increases, smaller polymer fragments can more easily diffuse into catalyst pores and competition between disproportionation reactions at external surfaces and inside pores would increase the effective E_a value for paraffin formation.

Relatively constant E_a values of 22-25 kcal/mol from 160-180 °C were calculated for the LPE/HZSM-5 (He), LPE/HZSM-5 (H₂), and LPE/PtHZSM-5 (He) samples, suggesting that the mechanism(s) of paraffin formation were not significantly affected by the addition of hydrogen or platinum at those temperatures. These results are consistent with paraffin formation by disproportionation on external catalyst surfaces.

The increase in E_a value from 25 to 48 kcal/mol for paraffin formation for the LPE/HZSM-5 (He) sample over the 180-225 °C temperature range is consistent with

competition between disproportionation reactions at external sites (lower E_a) and within pores (higher E_a) (Figure 5-5a, solid line). When hydrogen was present, the increase in E_a value was not as large (22 to 32 kcal/mol) over this temperature range (Figure 5-5a, dotted line). Metal-free hydrogenation reactions were previously reported to be favored at elevated temperature and can contribute additional pathway(s) for formation of volatile paraffins. Therefore, as the sample temperature increased, hydrogenation reactions on external catalyst surfaces competed with disproportionation inside HZSM-5 pores. The decreased rate of E_a value change between 180-225 °C may have been due to contributions from this additional parallel mechanism. E_a values also increased less for the LPE/PtHZSM-5 (He) sample, from 24 to 38 kcal/mol over the 180-250 °C temperature range, compared to the metal-free sample (Figure 5-5b). However, the large errors in the E_a values for the LPE/PtHZSM-5 (He) sample make interpretation of E_a variations highly speculative.

Figure 5-6 shows the E_a vs. temperature plot for the LPE/PtHZSM-5 (H_2) sample. The selectivity of m/z 57 for paraffins was ca. 99% over the entire volatile product evolution temperature range. Thus, E_a values can be expected to accurately represent volatile paraffin formation mechanisms for this sample. E_a values increased from 25 to 40 kcal/mol over the 165-210 °C temperature range. E_a values then decreased from 40 to 33 kcal/mol over the 210-260 °C temperature range and then remained relatively constant at 33 kcal/mol from 260-300 °C.

The E_a value at 165 °C (25 kcal/mol) in Figure 5-6 was nearly identical to the values for the other three LPE/HZSM-5 samples.

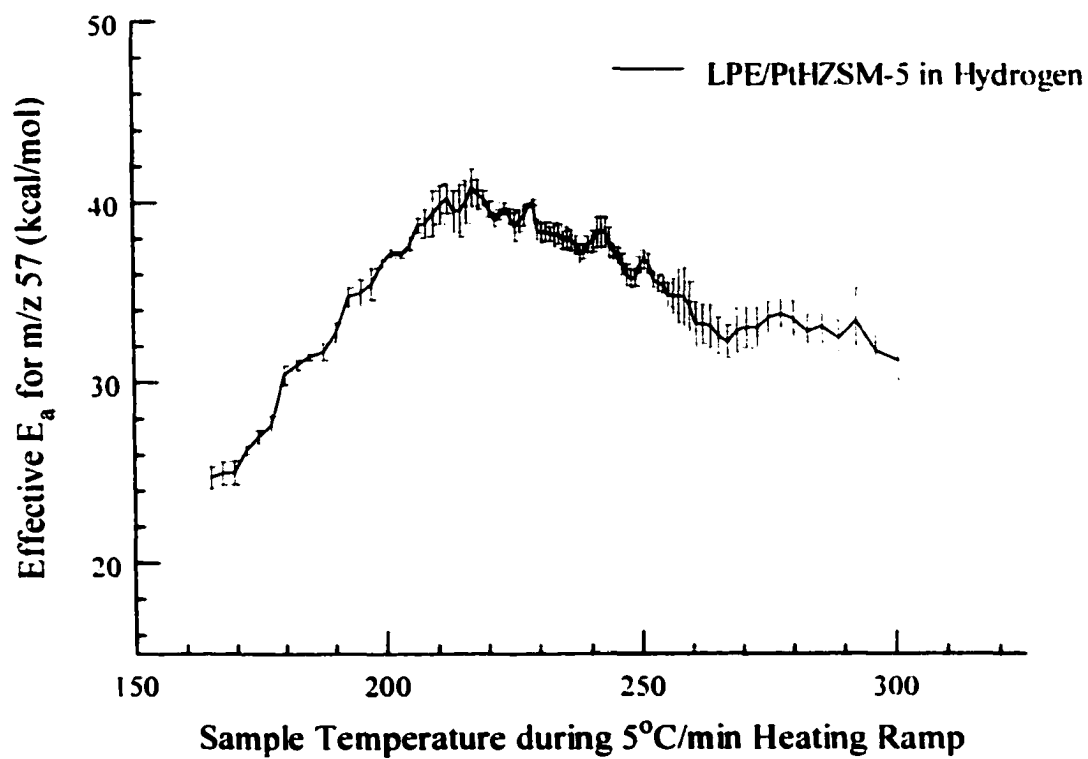


Figure 5-6: E_a vs. temperature plot for the formation of paraffins (m/z 57) by LPE/PtHZSM-5 heated in hydrogen

However, the amount of volatile paraffins detected at low temperatures (<200 °C) increased substantially for the LPE/PtHZSM-5 (H₂) sample compared to the other LPE/HZSM-5 samples as shown by the volatile product evolution profiles (Figures 4-3, 4-9, 4-14, and 4-19). The immediate increase in E_a value is due to a combination of platinum catalyzed hydrogenation and increased contributions from disproportionation inside catalyst pores.

The decrease in E_a value over the 210-260 °C temperature range for the LPE/PtHZSM-5 (H₂) sample (Figure 5-6) was not observed for the other LPE/HZSM-5 samples. The maximum volatile paraffin evolution rate for this sample occurred during this temperature range (Figure 4-19). A decrease in E_a value with respect to temperature indicates a change in the processes leading to paraffin formation. This change must be associated with changes in catalytic hydrogenation reactions with increasing temperature.

Volatile product evolution profiles show that small amounts of paraffins were formed above 250 °C for the LPE/HZSM-5 (He), LPE/HZSM-5 (H₂), and LPE/PtHZSM-5 (He) samples. Unsaturated volatile species (e.g. olefins and alkyl aromatics) were found to dominate evolution profiles for these samples above 250 °C. In contrast, significant volatile paraffin yields were detected above 250 °C for the LPE/PtHZSM-5 (H₂) sample. Platinum catalyzed hydrogenation likely inhibited unsaturated volatile product formation pathways, which resulted in the production of volatile paraffins above 250 °C.

5.4.2 LPE/HZSM-5 Olefin Formation E_a

The selectivity of m/z 55 for olefins changed with respect to temperature for the LPE/HZSM-5 (He) (triangle), LPE/HZSM-5 (H_2) (circle), and LPE/PtHZSM-5 (He) (square) samples. For example, m/z 55 olefin selectivity as a function of temperature is shown for the LPE/HZSM-5 (He), LPE/HZSM-5 (H_2), and LPE/PtHZSM-5 (He) samples in Figure 5-7. Selectivity increased from ca. 57 to 80% over the 140-180 °C temperature range. E_a values are not included in E_a versus temperature plots for this range because low selectivity made the accuracies of these values questionable. Volatile product evolution profiles show that olefin formation was favored over paraffin formation at temperatures above 180 °C for the LPE/HZSM-5 (He), LPE/HZSM-5 (H_2), LPE/PtHZSM-5 (He) samples. From 180-250 °C, selectivity remained relatively constant at about 80-85%. Above 250 °C, selectivity of m/z 55 for olefins increased to ca. 99%. Similar trends of selectivity with respect to temperature were observed for the LPE/HZSM-5 (H_2) and LPE/PtHZSM-5 (He) samples. Olefin yields were too low for calculation of E_a values for the LPE/PtHZSM-5 (H_2) sample.

Figure 5-8 shows E_a vs. temperature plots for olefin formation for the LPE/HZSM-5 (He) (solid line), LPE/HZSM-5 (H_2) (dotted line), and LPE/PtHZSM-5 (He) (dashed line) samples. The E_a curves for the LPE/HZSM-5 (He) and LPE/PtHZSM-5 (He) samples follow similar trends with respect to temperature. E_a values for the LPE/HZSM-5 (He) and LPE/PtHZSM-5 (He) samples increased from 30 to 40 kcal/mol and 34 to 38 kcal/mol over the 190-230 °C temperature range, respectively. Olefin m/z 55 selectivities were only about 80% for both samples in this temperature range.

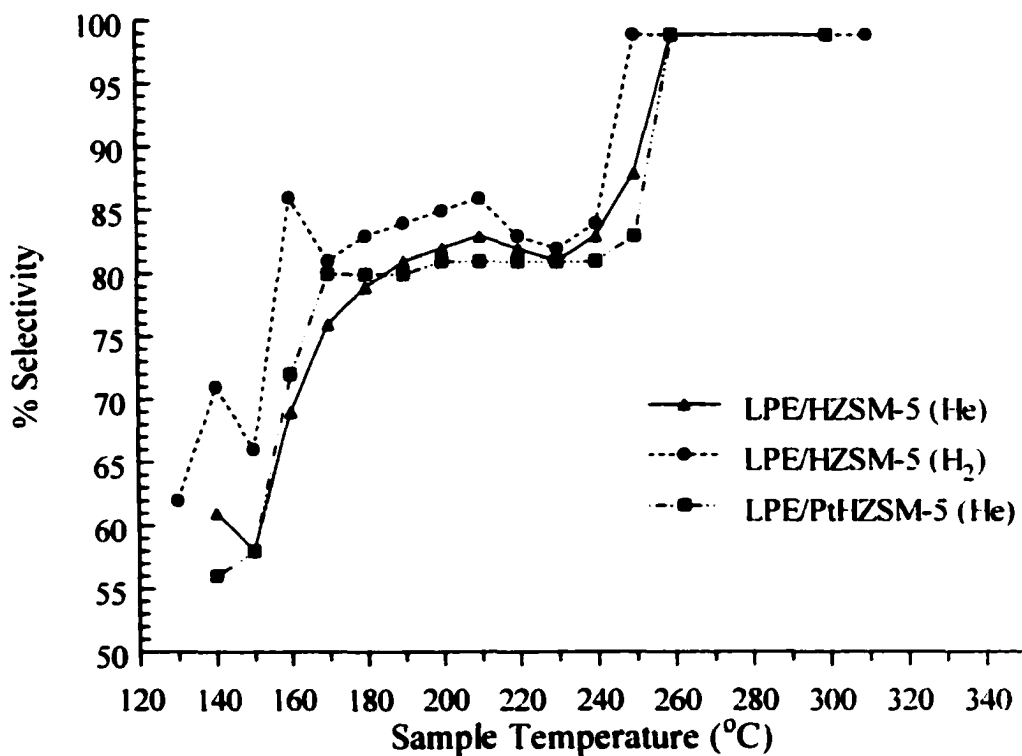


Figure 5-7: Plot of olefin (m/z 55) selectivity vs. sample temperature calculated from TA-GC/MS results for LPE/HZSM-5 and LPE/PtHZSM-5 heated in helium and LPE/HZSM-5 heated in hydrogen

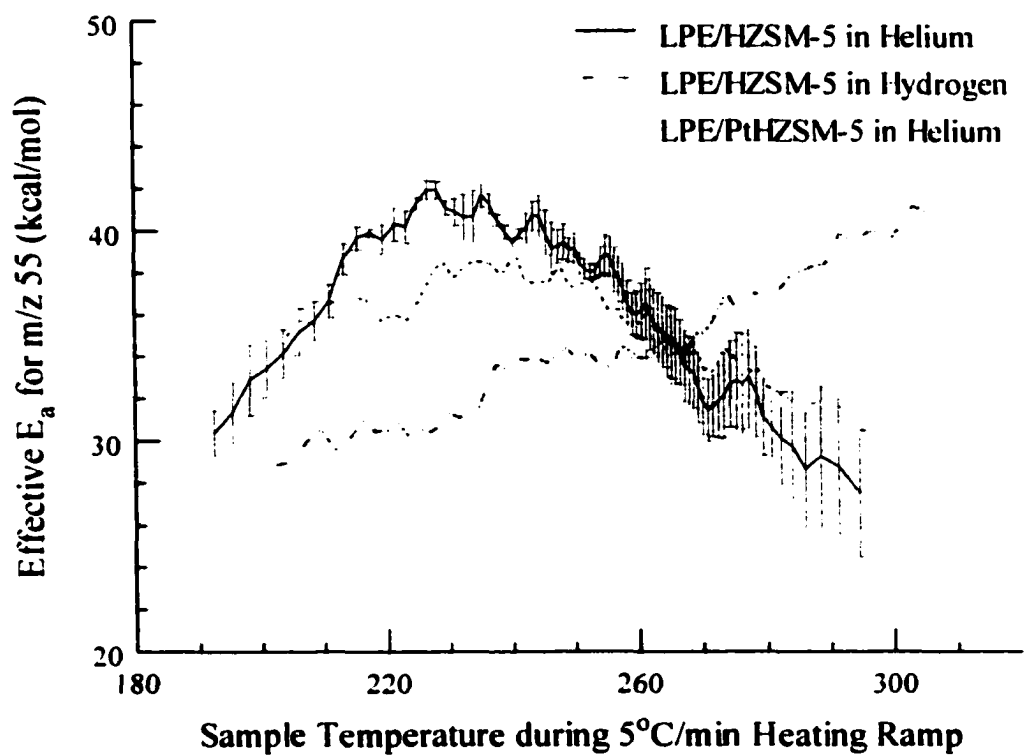


Figure 5-8: E_a vs. temperature plots for the formation of olefins (m/z 55) by LPE/HZSM-5, LPE/PtHZSM-5 heated in helium and LPE/HZSM-5 heated in hydrogen

Thus, the increase in E_a value over this temperature range may not necessarily reflect a change in olefin formation mechanisms. Rather, it may have been caused by changes in paraffin forming reactions, because the primary non-olefin contribution to m/z 55 in this temperature range was from paraffins. A decrease in E_a value was observed for both LPE/HZSM-5 (He) and LPE/PtHZSM-5 (He) samples from 40 to 28 and 38 to 30 kcal/mol over the 230-300 °C temperature range, respectively (Figure 5-8). This decrease in E_a value coincides with the detection of alkyl aromatic volatile products. The change in E_a at this temperature may signify mechanistic changes for olefin formation in which volatiles were derived from unsaturated surface residue rather than polymer fragments.

The trend in E_a versus temperature for the LPE/HZSM-5 (H_2) sample was quite different (Figure 5-8, dotted line). E_a values for this sample increased from 28 to 40 kcal/mol over the 190-310 °C temperature range. Alkyl aromatic products were detected in small amounts for this sample compared to the LPE/HZSM-5 (He) and LPE/PtHZSM-5 (He) samples. Therefore, the change in mechanism proposed for the LPE/HZSM-5 (He) and LPE/PtHZSM-5 (He) samples may not have been possible because the required unsaturated residue was not formed in the presence of hydrogen. Above 250 °C, m/z 55 selectivities for volatile olefin formation were better than 99% for the LPE/HZSM-5 (He), LPE/PtHZSM-5 (He), and LPE/HZSM-5 (H_2) samples, suggesting that E_a values should accurately reflect olefin formation mechanisms. Thus, the E_a value decrease for the LPE/HZSM-5 (He) and LPE/PtHZSM-5 (He) samples and the E_a value increase for the LPE/HZSM-5 (H_2) sample suggests that the presence of hydrogen affected the olefin forming reaction pathways above 250 °C.

5.4.3 LPE/HZSM-5 and LPE/PtHZSM-5 Alkyl Aromatics Formation E_a

Volatile alkyl aromatic yields for the LPE/HZSM-5 (H_2) and LPE/PtHZSM-5 (H_2) samples were too low for activation energy calculations. However, the m/z 91 selectivities for volatile alkyl aromatics formation were greater than 99% for the LPE/HZSM-5 (He) and LPE/PtHZSM-5 (He) samples. E_a versus temperature plots for the LPE/HZSM-5 (He) (solid line) and LPE/PtHZSM-5 (He) (dotted line) samples are shown in Figure 5-9. Activation energies for both samples were relatively constant throughout the temperature range over which alkyl aromatics were detected, suggesting that reaction mechanisms remained relatively unchanged with sample heating. E_a values for the LPE/PtHZSM-5 (He) sample were about 4 kcal/mol greater than those for the LPE/HZSM-5 (He) sample at the same temperature. The alkyl aromatics yield for the LPE/PtHZSM-5 (He) sample (19%) was significantly greater than the yield for the LPE/HZSM-5 (He) sample (6%). This three-fold increase in alkyl aromatics yield for the LPE/PtHZSM-5 (He) sample compared to the LPE/HZSM-5 (He) sample can be attributed to platinum catalyzed dehydrocyclization reactions. Consequently, the increase in E_a values for the LPE/PtHZSM-5 (He) sample compared to the LPE/HZSM-5 (He) sample was likely due to the addition of a platinum catalyzed pathway for alkyl aromatics formation.

5.4.4 LPE/HY Paraffin Formation E_a

Figure 5-10 shows paraffin formation E_a values versus temperature for the LPE/HY (He) (solid line) and LPE/HY (H_2) (dotted line) samples.

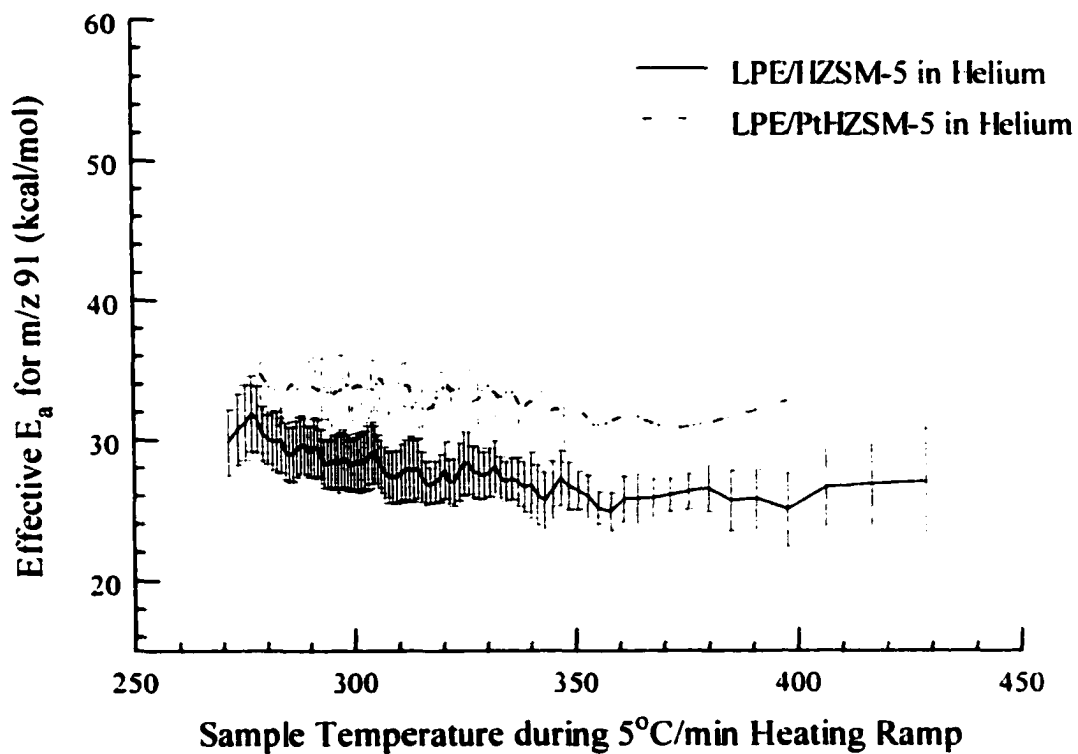


Figure 5-9: E_a vs. temperature plots for the formation of alkyl aromatics (m/z 91) by LPE/HZSM-5 and LPE/HZSM-5 heated in helium

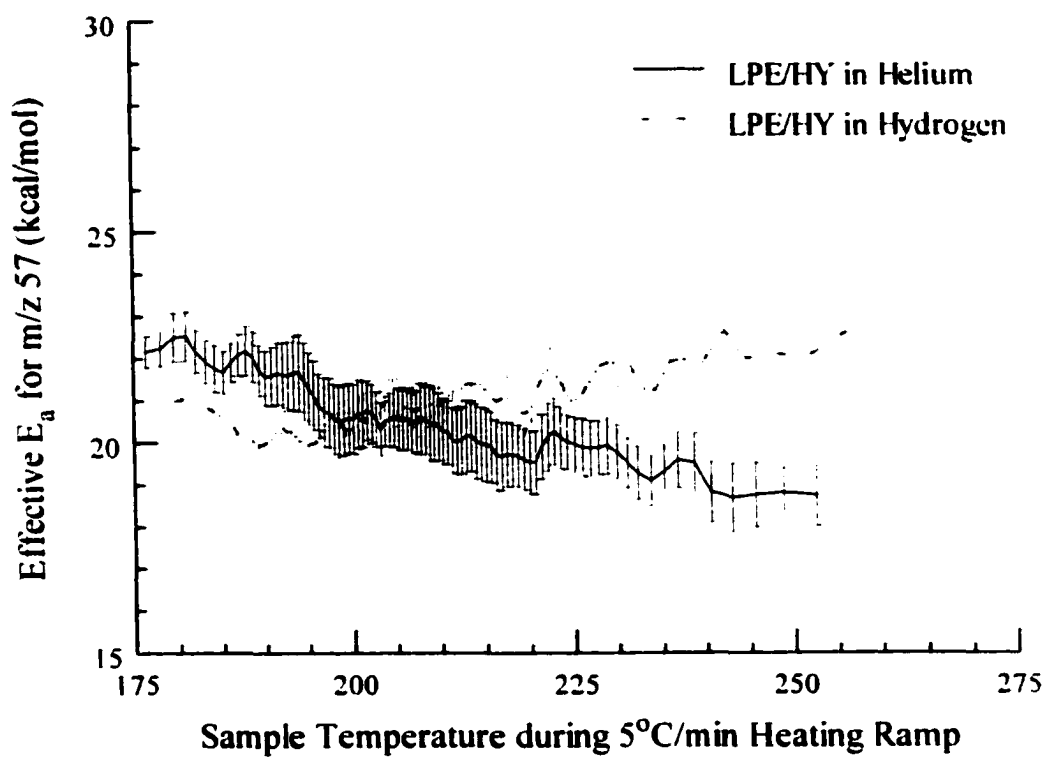


Figure 5-10: E_a vs. temperature plots for the formation of paraffins (m/z 57) by LPE/HY heated in helium and hydrogen

The temperature range for volatile product evolution and m/z 57 selectivities (ca. 99%) were about the same for both samples. - Neither plot in Figure 5-10 exhibits the dramatic increase in E_a value that was observed for the corresponding HZSM-5 samples (Figure 5-5). Apparently, the high activation energy HZSM-5 pathway for paraffin formation did not contribute to HY catalyzed reactions. The lack of this high activation energy pathway suggests that steric hinderance for reactions that occur within HY pores is much less than for reactions within HZSM-5 pores. The LPE/HY (He) E_a versus temperature plot exhibits a slight downward trend whereas the LPE/HY (H_2) plot exhibits a slight upward trend. The higher E_a value for the LPE/HY (H_2) sample compared to the LPE/HY (He) sample at 250 °C may reflect the effects of hydrogenation on paraffin production. Hydrogenation reaction contributions to volatile product yields would be expected to increase with increasing sample temperature, thus, E_a values would be expected to increase with temperature. Although the paraffin yield for the LPE/HY (H_2) sample was not significantly greater than for the LPE/HY (He) sample (Table 5-3), the effect of hydrogenation was evidenced by the fact that alkyl aromatics were detected for the sample heated in helium but not in hydrogen.

Figure 5-11 shows paraffin formation E_a values versus temperature for the LPE/PtHY (He) and LPE/PtHY (H_2) samples. The temperature range corresponding to volatile paraffin evolution was very different for the two samples. The m/z 57 selectivities for paraffin formation were nearly constant at ca. 99% for both samples. Both E_a versus temperature plots exhibit similar downward trends with increasing sample temperature.

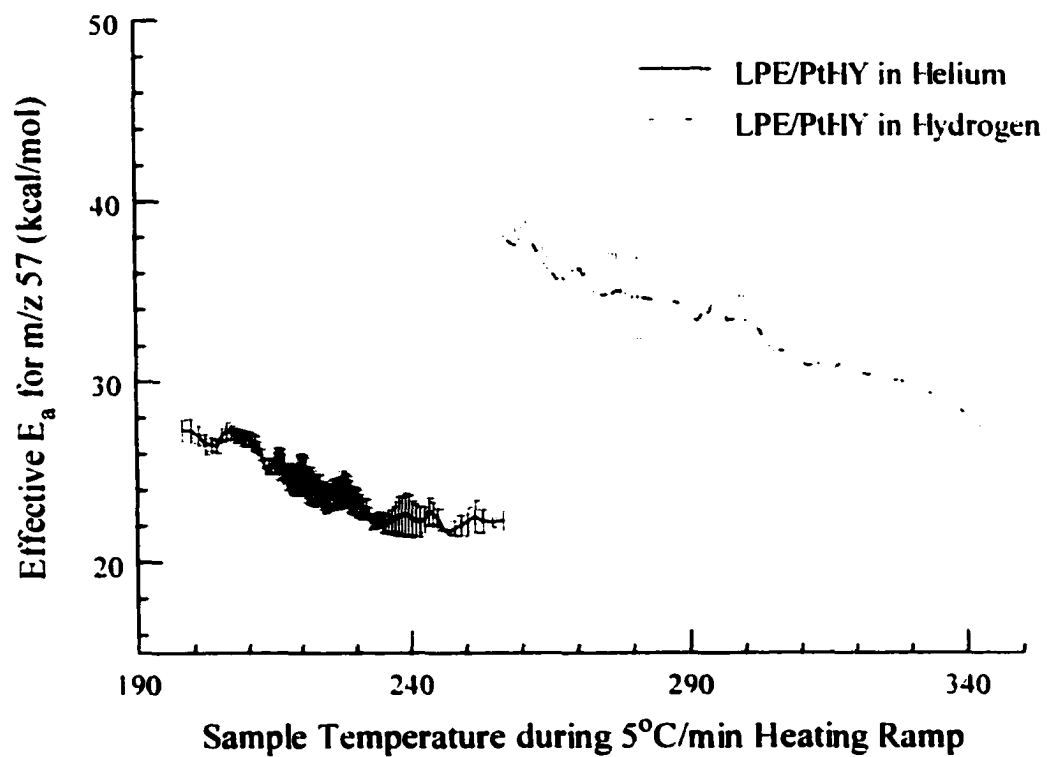


Figure S-11: E_a vs. temperature plots for the formation of paraffins (m/z 57) by LPE/PtHY heated in helium and hydrogen

However, the LPE/PtHY (H₂) sample plot is shifted to higher temperature (ca. 60 °C) and to higher activation energy (ca. 10 kcal/mol) relative to the LPE/PtHY (He) plot. This is consistent with literature reports that activation energies for hydrocracking with bifunctional catalysts are significantly higher than for acid catalyzed cracking³. Hydrocracking was also responsible for the dramatic increase in paraffin yield for the LPE/PtHY (H₂) sample (98%) compared to the LPE/PtHY (He) sample (75%). In the absence of hydrogen, the main effect of adding platinum to the HY catalyst was to increase the alkyl aromatics yield ten-fold (i.e. from 2% to 20%, Table 5-3).

5.4.5 LPE/HY Olefin Formation E_a

LPE/HY sample olefin yields ranged between 2-5% (Table 5-3). The poor signal-to-noise for m/z 55 ion signal versus temperature plots and low m/z 55 selectivities for olefin formation precluded activation energy calculations for this volatile product class.

5.4.6 LPE/PtHY Alkyl Aromatics Formation E_a

The LPE/PtHY (He) sample was the only sample containing HY catalyst that formed significant quantities of alkyl aromatics (Table 5-3). The E_a versus temperature plot for the LPE/PtHY (He) sample is shown in Figure 5-12. The m/z 91 selectivity for alkyl aromatics was ca. 99% over the volatile product evolution temperature range. The alkyl aromatics formation activation energy was relatively constant at 22-25 kcal/mol between 240 and 350 °C. Nearly all alkyl aromatics formed by the LPE/PtHY (He) sample can be attributed to dehydrocyclization reactions catalyzed by platinum.

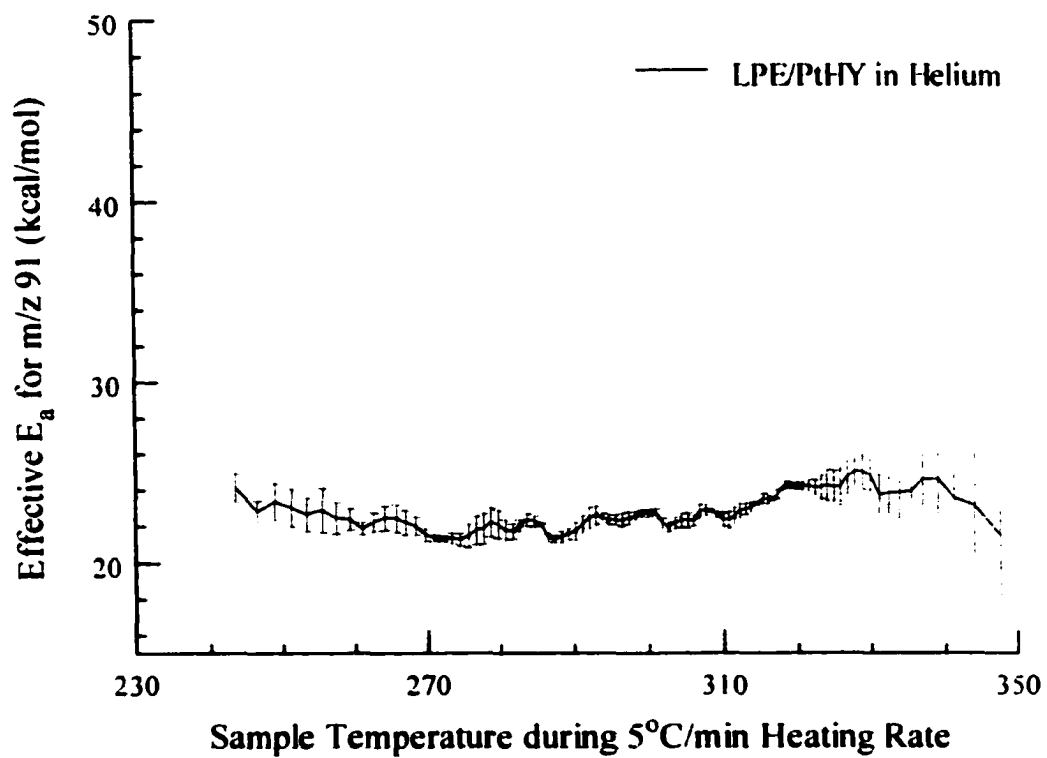


Figure 5-12: E_a vs. temperature plot for the formation of alkyl aromatics (m/z 91) by LPE/PtHY heated in helium

Thus, this reaction pathway for PtHY can be characterized by a 22-25 kcal/mol activation energy. In contrast, E_a values for the LPE/PtHZSM-5 (He) sample were more than 10 kcal/mol greater than for the LPE/PtHY (He) sample (Figure 5-9). The significantly higher E_a values for the PtHZSM-5 catalyst in helium suggests that platinum may preferentially reside within HZSM-5 pores, which would result in increased steric hinderance for dehydrocyclization reactions compared to the PtHY catalyst.

5.4.7 LPE/PtHMCM-41 Paraffin Formation E_a

Low paraffin yields and large contributions to m/z 57 ion signals from olefins precluded paraffin formation activation energy calculations for all but the LPE/PtHMCM-41 (H_2) sample. The E_a versus temperature plot for the LPE/PtHMCM-41 (H_2) sample is shown in Figure 5-13. The m/z 57 selectivity for paraffin formation for this sample was ca. 99% over the temperature range corresponding to volatile paraffin evolution. The high initial activation energy and downward trend with increasing sample temperature were similar to the LPE/PtHY (H_2) sample plot (Figure 5-11) and reflects the dominance of platinum catalyzed hydrogenation reactions for paraffin formation. This dominance is clearly illustrated by the dramatic increase in volatile paraffin yield for the LPE/PtHMCM-41 (H_2) sample (99%) compared to the LPE/PtHMCM-41 (He) sample (3%) (Table 5-4).

5.4.8 LPE/HMCM-41 Olefin Formation E_a

E_a value versus temperature plots for the LPE/HMCM-41 (He) (solid line) and LPE/HMCM-41 (H_2) (dotted line) samples are shown in Figure 5-14a. Figure 5-14b shows the E_a versus temperature plot for the LPE/PtHMCM-41 (He) sample.

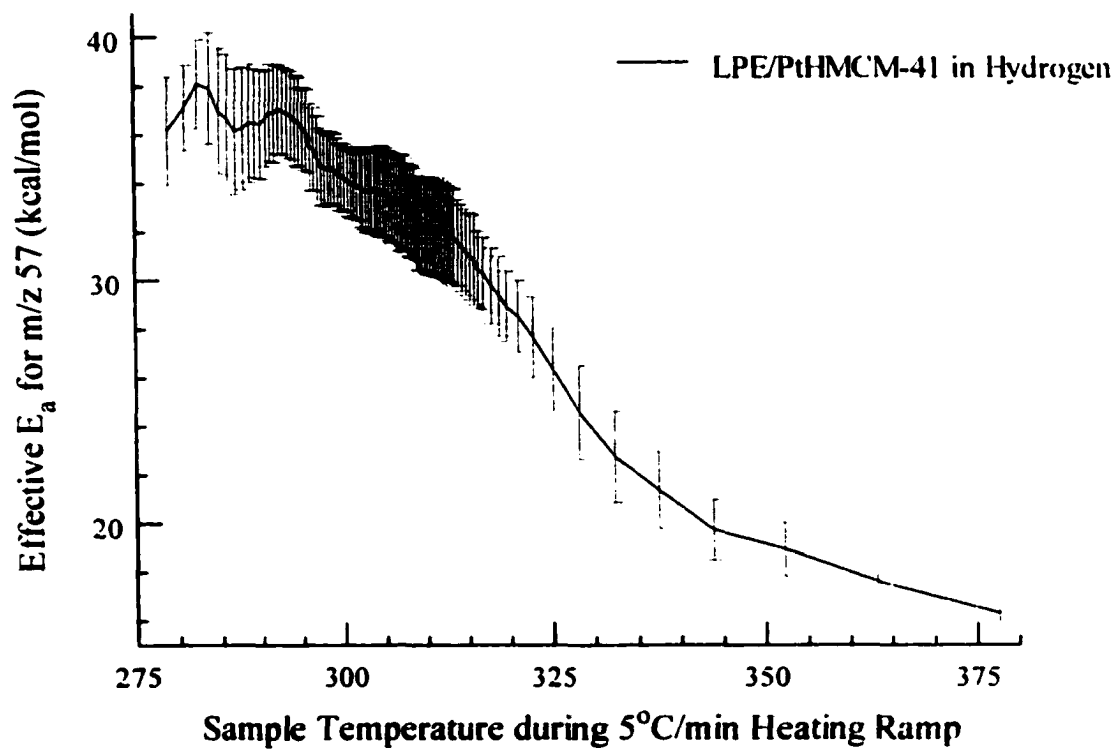


Figure 5-13: E_a vs. temperature signal plots for the formation of paraffins (m/z 57) by LPE/PtHMCM-41 heated in hydrogen

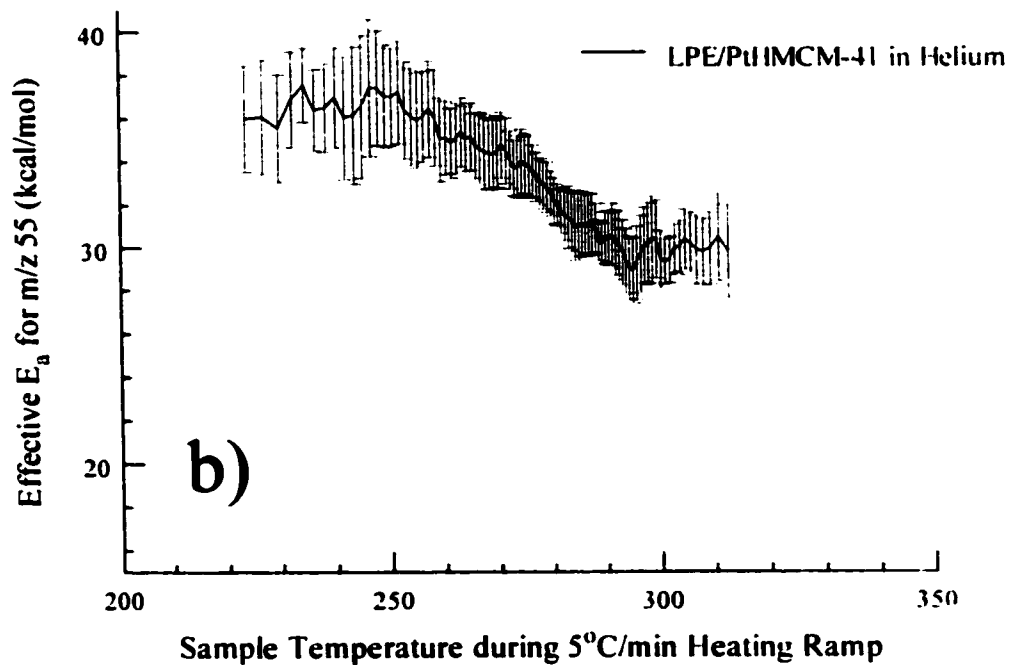
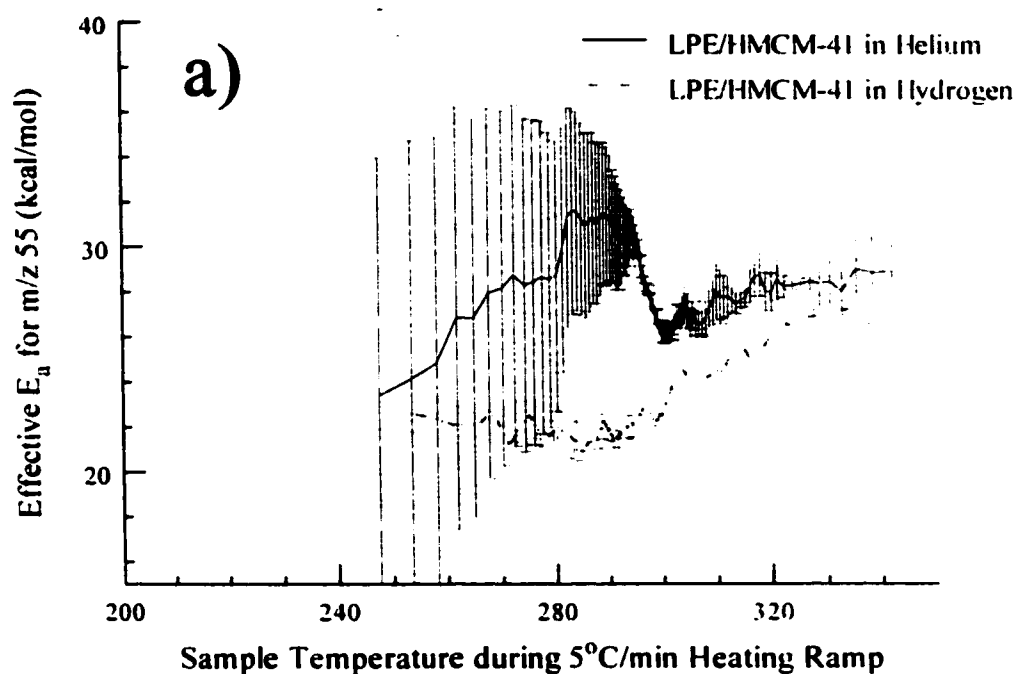


Figure 5-14: E_a vs. temperature plots for the formation of olefins (m/z 55) by
 a) LPE/HMCM-41 heated in helium and hydrogen
 b) LPE/PtHMCM-41 heated in helium

The selectivity for m/z 55 for olefins was better than 97% for all three samples over their respective olefin evolution temperature ranges. Very large E_a errors for the LPE/HMCM-41 (He) sample precluded any interpretation of activation energy trends below 290 °C for this sample. Above 300 °C, error bars for the LPE/HMCM-41 (He) and LPE/HMCM-41 (H₂) plots overlap, thus E_a values in this range cannot be considered to be statistically different for these samples. Volatile product distributions for these two samples were very similar (Table 5-4) confirming that replacing helium with hydrogen had little effect on LPE/HMCM-41 reaction mechanisms.

The E_a versus temperature plot for the LPE/PtHMCM-41 (He) sample in Figure 5-14b exhibits a downward trend with increasing temperature similar to that for the LPE/PtHZSM-5 (He) sample (Figure 5-8). Comparing volatile product distributions in Table 5-2 and Table 5-4 shows that volatile slate changes caused by addition of platinum to HZSM-5 were primarily associated with increased alkyl aromatics yield whereas changes attributed to addition of platinum to HMCM-41 were associated with increased volatile olefin yield. Table 5-3 shows that adding Pt to HY also resulted in a dramatic increase in alkyl aromatics yield. The smaller pores of HZSM-5 and HY relative to HMCM-41 may provide better steric alignment of hydrocarbon fragments, which facilitates platinum catalyzed dehydrocyclization reactions to form alkyl aromatics. The much larger HMCM-41 pores cannot provide this steric requirement, therefore an enhanced olefin yield was the principle result of platinum catalyzed reactions for the LPE/PtHMCM-41 (He) sample.

5.4.9 LPE/HMCM-41 Alkyl Aromatics Formation E_a

No significant yield of alkyl aromatics was detected for any of the LPE/HMCM-41 samples. Thus, activation energy versus temperature plots could not be generated.

5.5 Conclusions

Based solely on acid strength considerations, paraffin formation should have been most favored for the LPE/HZSM-5 (He) sample. Indeed, volatile paraffins were detected at the lowest temperatures for the LPE/HZSM-5 (He) sample compared to the LPE/HY (He) and LPE/HMCM-41 (He) samples. Volatile paraffin formation was favored by disproportionation reactions catalyzed by external acid sites as illustrated by the low E_a values for the LPE/HZSM-5 (He) sample at low temperatures (< 200 °C). However, as polymer fragments gained access into the small pores of HZSM-5, bimolecular disproportionation reactions were inhibited. This trend was evidenced by the large increase in E_a value for paraffin formation at higher temperatures for the LPE/HZSM-5 (He) sample (Figure 5-5). In helium, the highest paraffin yield for a metal-free sample was detected for the LPE/HY (He) sample. HY apparently had acid sites of adequate strength and larger pores compared to HZSM-5, which facilitated bimolecular reactions. The HY preference for paraffin formation resulted from the relatively constant and low paraffin formation E_a values over the entire volatile product evolution temperature range (Figure 5-10). In contrast, the low paraffin yield for the LPE/HMCM-41 (He) sample was likely due to the low acidity of the catalyst. Although the HMCM-41 pore size was large enough to facilitate disproportionation, catalytic site acidity was apparently too low for this reaction pathway to be favored.

Aromatic products were detected at temperatures above those at which volatile paraffin and olefin product evolutions maximized. The shift in alkyl aromatic evolution profiles to higher temperatures relative to paraffins and olefins is consistent with a mechanism in which unsaturated surface species are precursors for alkyl aromatic formation.⁸ Alkyl aromatic yields decreased in the order: LPE/HZSM-5 > LPE/HY > LPE/HMCM-41, which follows the trend of increased pore size. Very small amounts of aromatic products were detected when the LPE/HY (He) sample was heated and no aromatics were formed for the LPE/HMCM-41 (He) sample. Apparently, cyclization reactions were not favored within the larger HMCM-41 pores. Steric restrictions on reaction volume afforded by HZSM-5 and HY (to a lesser extent) promoted aromatic ring formation from conjugated unsaturated polymer segments.

Unsaturated residue formed during catalytic reactions that produced paraffins and olefins was likely the source of alkyl aromatics and non-volatile residue. It is well known that strong acid sites are more prone to accumulate residue. After heating, the LPE/HY (He) sample contained almost four times the amount of residue as the LPE/HZSM-5 (He) sample, despite the fact that HZSM-5 had stronger acid sites than HY. However, the larger HY pores facilitated the formation of non-volatile unsaturated residue. Even though the HMCM-41 pore size was much larger than the HY pore size, the amount of residue remaining on the LPE/HMCM-41 (He) sample was substantially less than for the LPE/HY (He) sample. This can be attributed the low acidity of HMCM-41 acid sites.

The general trends observed for LPE/catalyst samples heated in helium were also observed when the samples were heated in hydrogen. The magnitude of hydrogenation effects depended on catalyst acid strength. Thus, the LPE/HZSM-5 sample was the only

one for which both volatile product slate and residue content were significantly different in hydrogen compared to helium (Table 5-2). For the LPE/HY sample, a decrease in residue was observed in the presence of hydrogen (Table 5-3). No significant hydrogen effect was observed for the LPE/HMCM-41 sample. The magnitude of the hydrogenation effect was also reflected by E_a versus temperature curves. The differences between the LPE/HZSM-5 (H_2) and LPE/HZSM-5 (He) paraffin curves (Figure 5-5) were greater than the LPE/HY (H_2) and LPE/HY (He) differences (Figure 5-10).

The addition of platinum increased the volatile aromatic or olefin yield and/or residue content for the LPE/Ptcatalyst (He) samples compared to the corresponding LPE/catalyst (He) samples. This magnitude of the platinum catalyzed effect appears to be a function of catalyst pore size and acidity. The LPE/PtHZSM-5 (He) sample yielded less alkyl aromatics than LPE/PtHY (He) and formed the smallest amount of residue. The LPE/PtHY (He) sample yielded the most alkyl aromatics and the most residue compared to the other Pt/catalyst (He) samples. The LPE/PtHMCM-41 (He) sample yielded more large olefins and less residue than the LPE/HY (He) sample. The lower volatile aromatics yield for the LPE/PtHZSM-5 (He) sample (Table 5-2) compared to the LPE/PtHY (He) sample (Table 5-3) is consistent with a higher E_a value (Figures 5-9 and 5-12) and may be due to increased steric hindrance for platinum particles located inside HZSM-5 pores.

Bifunctional hydrogenation reactions dominated volatile product forming reactions for the LPE/Ptcatalyst (H_2) samples. Compared to the corresponding LPE/Ptcatalyst (He) samples, paraffin yields increased at the expense of olefins and aromatics. In addition, lower residue contents were detected for the LPE/Ptcatalyst (H_2)

samples. The size of volatile paraffins was found to depend on the catalyst pore size: HMCM-41 > HY > HZSM-5. However, paraffin formation temperatures depended on catalyst and cracking environment. Although there was no change in volatile paraffin formation temperature for the LPE/PtHZSM-5 (H₂) sample compared to the LPE/PtHZSM-5 (He) sample, temperature increases of ca. 60 °C and ca. 20 °C were observed for the LPE/PtHY (H₂) and LPE/PtHMCM-41 (H₂) samples compared to the same samples heated in helium. E_a value differences between the LPE/Ptcatalyst (H₂) and LPE/Ptcatalyst (He) samples may be responsible for the temperature shifts. Volatile product slate and E_a value trends cannot be explained by a single catalyst characteristic, such as pore size. Instead, the combined influence of acidity, pore size, and preferred cracking mechanism(s) for each sample must be considered.

The commercial value of hydrocarbon products obtained by plastic waste tertiary recycling depends on how they will be used. In general, gaseous products are less desirable because they can be difficult to transport and olefins are less stable than paraffins during long-term storage. A good cracking catalyst must convert a high percentage of polymer to hydrocarbon product and accumulate minimal residue during cracking. Thus, LPE/catalyst samples that form the highest percentage of liquid (>C₄) paraffin products while accumulating the least amount of residue would be the most attractive for commercial applications. HZSM-5 converted LPE to volatile hydrocarbons at the lowest temperatures and accumulated small amounts of residue. However, this catalyst produced large amounts of gaseous products. HY produced higher liquid fractions than HZSM-5 at slightly higher temperatures, but accumulated a high percentage of residue. The LPE/PtMCM-41 (H₂) sample provided the best product slate

compared to the other samples. Approximately 95% (by weight) of the LPE was converted mainly into paraffin products. Only ca. 4% of these products were gaseous at room temperature. In addition, very small amounts of liquid olefins (ca. 1%) were formed by this sample (Table 5-4).

A new method for calculating class-specific “effective” activation energies was featured in this work. Our unique TA-GC/MS and TA-MS instrumentation allows us to identify and quantify volatile products evolved from complex temperature-dependent systems. When TA-GC/MS results are used in combination with TA-MS, it is possible to relate isoconversion E_a values to volatile product reaction mechanisms. As shown here, activation energy and volatile product slate correlations can be used to characterize complex temperature-dependent reaction mechanisms. The methods described here are not restricted to polymer degradation studies and can be applied to any temperature-dependent reaction in which volatile products are formed. For systems in which mass spectrometer ions can be associated with specific substances, species-specific rather than class-specific correlations can be made.

5.6 References

1. Hesse, N.D.; Lin, R.; Bonnet, E.; Copper III, J.; White, R.L.; *J. Appl. Polym. Sci.* 2001, 82, 3118-3125 "In-situ Analysis of Volatiles Obtained from the Catalytic Cracking of Polyethylene"
2. Lin, R.; White, R.L.; *J. Appl. Polym. Sci.* 1995, 58, 1151-1159 "Effects of Catalyst Acidity and HZSM-5 Channel Volume on the Catalytic Cracking of Poly(ethylene)"
3. Lin, R.; Ph.D. Dissertation, University of Oklahoma. 1997 "Catalytic Cracking of Poly(ethylene) and Poly(styrene) by Silica-Alumina, HZSM-5 Zeolite, and Sulfated Zirconia"
4. Zhao, Q.; Chen, W-H.; Huang, S-J.; Wu, Y-C.; Lee, H-K.; Liu, S-B.; *J. Phys. Chem. B* 2002, 106, 4462-4469 "Discernment and Quantification of Internal and External Acid Sites on Zeolites"
5. Otero Arean, C.; Rodriguez Delgado, M.; Penarroya Mentrut, M.; Llabres i Xamena, F.X.; Morterra, C.; *Stud. Surf. Sci. Catal.* 2000, 130, 3137-3142 "The Combined use of Acetonitrile and Adamantane-Carbonitrile for FTIR Spectroscopic Characterization of Acidity in Zeolites"
6. Armaroli, T.; Bevilacqua, M.; Trombetta, M.; Milella, F. Gutierrez Alejandre, A.; Ramirez, J.; Notari, B.; Willey, R.J.; Busca, G.; *Appl. Catal. A* 2001, 216, 59-71 "A Study of the External and Internal Sites on MFI-type Zeolitic Materials Through the FT-IR Investigation of Adsorption of Nitriles"
7. Trombetta, M.; Armaroli, T.; Gutierrez Alejandre, A.; Gonzalez, H.; Ramirez Solis, J.; Busca, G.; *Catal. Today* 2001, 65, 285-292 "Conversion and Hydroconversion of Hydrocarbons on Zeolite-based Catalysts: an FTIR Study"
8. Wojciechowski, B.W.; *Catal. Rev. - Sci. Eng.* 1998, 40, 209-328 "The Reaction Mechanism of Catalytic Cracking: Quantifying Activity, Selectivity, and Catalyst Decay"
9. Gnep, N.S.; Roger, P.; Magnoux, P.; Guisnet, M.; *Prepr. Papers - Am. Chem. Soc. Div. Fuel Chem.* 1993, 38, 87-90 "Comparative Study of the Removal of Coke from Protonic Zeolites"
10. Groten, W.A.; Wojciechowski, B.W.; Hunter, B.K.; *J. Catal.* 1992, 138, 343-350 "On the Relationship between Coke Formation Chemistry and Catalyst Deactivation"
11. Holmes, S.M.; Garforth, A.; Dwyer, J.; *Thermochim. Acta* 1997, 294, 57-64 "Pyrolysis GC-MS Study of External Coke Composition on H-ZSM-5 Zeolite Catalysts"
12. Guisnet, M.; Magnoux, P.; *Appl. Catal. A* 2001, 212, 83-96 "Organic Chemistry of Coke Formation"

13. Bibby, D.M.; Milestone, N.B.; Patterson, J.E.; Aldridge, L.P.; J. Catal. 1986, 97, 493-502 "Coke Formation in Zeolite ZSM-5"
14. Guisnet, M.; Magnoux, P.; Catal. Today 1997, 36, 477-483 "Deactivation by Coking on Zeolite Catalysts. Prevention of Deactivation. Optimal Conditions for Regeneration"
15. Meusinger, J.; Corma, A.; J. Catal. 1995, 152, 189-197 "Activation of Hydrogen on Zeolites: Kinetics and Mechanism of n-Heptane Cracking on H-ZSM-5 Zeolites under High Hydrogen Pressure"
16. Ebitani, K.; Tsuji, J.; Hattori, H.; Kita, H. J. Catal. 1992, 138, 750-753 "Activation of Molecular Hydrogen into Protonic Acid Sites over Metal-Free H-ZSM-5 Catalyst"
17. Meusinger, J.; Liers, J.; Mosch, A.; Reschetilowski, W. J. Catal. 1994, 148, 30-35 "Cracking of n-Heptane on Metal-Free H-ZSM-5 Zeolite at High Hydrogen Pressure"
18. Kanai, J.; Martens, J.A.; Jacobs, P.A. J. Catal. 1992, 133, 527-543 "On the nature of the active sites for ethylene hydrogenation in metal-free zeolites"
19. Pajonk, G.M.; Appl. Catal. A 2000, 202, 157-169 "Contribution of spillover effects to heterogeneous catalysis"
20. Weisz, P.B.; Swegler, E.W. Science 1957, 126, 31-32 "Stepwise Reaction on Separate Catalytic Centers: Isomerization of Saturated Hydrocarbons"
21. Weisz, P.B.; Adv. Catal. 1962, 13, 137-190 "Polyfunctional Heterogeneous Catalysis"
22. Paal, Z.; Menon, P.G. Catal. Rev. – Sci. Eng. 1983, 25, 229-324 "Hydrogen Effects in Metal Catalysis"
23. Carter, J.L.; Cusumano, J.A.; Sinfelt, J.H.; J. Catal. 1971, 20, 223-229 "Hydrogenolysis of n-Heptane over Unsupported Metals"
24. Demirci, U.B.; Garin, F.; Catal. Lett. 2001, 76, 45-51 "From Bifunctional site to metal-proton adduct site in alkane reforming on sulfated-zirconia-supported Pt or Pd or Ir Catalysts"
25. Siffert, S.; Schmitt, J-L.; Sommer, J.; Garin, F.; J. Catal. 1999, 184, 19-28 "Influence of Acidity-Basicity in ¹³C-Labeled Hexane Isomerization Reactions on Exchanged Pt-β Zeolite: Mechanistic Studies"
26. Chupin, J.; Gnep, N.S.; Lacombe, S.; Guisnet, M.; Appl. Catal. A 2001, 206, 43-56 "Influence of the Metal and of the Support on the Activity and Stability of Bifunctional Catalysts for Toluene Hydrogenation"

27. Pirngruber, G.D.; Zinck-Stagno, O.P.E.; Seshan, K.; Lercher, J.A.; *J. Catal.* 2000, 190, 374-386 "The Effect of the Pore- Structure of Medium-Pore Zeolites on the Dehydroisomerization of n-Butane: A Comparison of Pt-FER, Pt-TON, and Pt-ZSM-5"
28. Pirngruber, G.D.; Seshan, K.; Lercher, J.A.; *J. Catal.* 1999, 186, 188-200 "Dehydroisomerization on n-Butane over Pt-ZSM-5 (I): Effect of the Metal Loading and Acid Site Concentration"
29. Jentys, A.; Lugstein, A.; Kingler, G.; Vinek, H.; Proceedings of the International Zeolite Conference, 12th, Baltimore, July 5-10, 1998 (1999), 2817-2824 "Hydroconversion of Heptane and Octane over Bifunctional Zeolites; Influence of Structure and Metal Distribution on Activity and Selectivity"
30. Alvarez, F.; Ribeiro, F.R.; Perot, G.; Thomazeau, C.; Guisnet, M.; *J. Catal.* 1996, 162, 179-189 "Hydroisomerization and Hydrocracking of Alkanes 7. Influence of the Balance between Acid and Hydrogenating Functions on the Transformation of n-Decane on PtHY Catalysts"
31. Ribeiro, F.; Marcilly, C.; Guisnet, M.; *J. Catal.* 1982, 78, 267-274 "Hydroisomerization of n-Hexane on Platinum Zeolites I. Kinetic Study of the Reaction on Platinum/Y-Zeolite Catalysts: Influence of Platinum Content"
32. Perrotin, L.; Finiels, A.; Fajula, F.; Cholley, T.; *Stud. Surf. Sci. Catal.* 2001, 135, 3838-3845 "Peculiarities in the Hydroconversion of n-Hexadecane over bifunctional Catalysts"
33. Wootsch, A.; Paal, Z.; *J. Catal.* 1999, 185, 192-198 "n-Hexane Reactions on EUROPT-1 at Different Hydrogen Pressures: The Possibility of Calculating Kinetic Parameters"
34. Bond, G.; *Catal. Today* 1999, 49, 41-48 "Kinetics of Alkane Reactions on Metal Catalysts: Activation Energies and the Compensation Effect"
35. Liu, K.; Meuzelaar H.L.C. *Fuel Proc. Tech.* 1996, 49, 1-15 "Catalytic reactions in waste plastics, HDPE and coal studied by high-pressure thermogravimetry with online GC/MS"
36. Manos G.; Garforth, A.; Dwyer, J.; *Ind. Eng. Chem. Res.* 2000, 39, 1203-1208 "Catalytic degradation of High-Density Polyethylene on an Ultrastable-Y Zeolite. Nature of Initial Polymer Reactions, Pattern of Formation of Gas and Liquid Products, and Temperature Effects"
37. Manos, G.; Garforth, A.; Dwyer, J.; *Ind. Eng. Chem. Res.* 2000, 39, 1198-1202 "Catalytic Degradations of High-Density Polyethylene over Different Zeolitic Structures"

38. Garforth, A.A.; Lin, Y-H.; Sharratt, P.N.; Dwyer, J.; *Appl. Catal. A* 1998, 169, 331-342 "Production of Hydrocarbons by Catalytic Degradation of High Density Polyethylene in a Laboratory Fluidised-Bed Reactor"
39. Gobin, K.; Koumantaropoulos, D.; Manos, G.; *Stud. Surf. Sci. Catal.* 2001, 135, 4989-4994 "One Stage Catalytic Cracking of Plastic Waste on Zeolite-Based Catalysts"
40. Satsuma, A.; Ebigase, T.; Inaki, Y.; Yoshida, H.; Kobayashi, S.; Uddin, Md.A.; Sakata, Y.; Hattori, T.; *Stud. Surf. Sci. Catal.* 2001, 135, 4001-4008 "Catalytic Sites of Mesoporous Silica in Degradation of Polyethylene"
41. Sharratt, P.N.; Lin, Y-H.; Garforth, A.A.; Dwyer, J.; *Ind. Eng. Chem. Res.* 1997, 36, 5118-5124 "Investigation of the Catalytic Pyrolysis of High-Density Polyethylene over a HZSM-5 Catalyst in a Laboratory Fluidized-Bed Reactor"
42. Ishihara, Y.; Hidesaburo, N.; Katsuhiko, S.; Ikemura, T.; Takesue, T.; *Bull. Chem. Soc. Jpn.* 1991, 64, 3585-3592 "Back Biting Reactions during the Catalytic Decomposition of Polyethylene"
43. Aguado, J.; Serrano, D.P.; Romero, M.D.; Escola, J.M.; *J. Chem. Soc. Chem. Comm.* 1996, 725-726 "Catalytic Conversion of Polyethylene in Fuels over Mesoporous MCM-41"
44. Lin, Y-H.; Sharratt, P.N.; Garforth, A.A.; Dwyer, J.; *Energy Fuels* 1998, 12, 767-774 "Catalytic Conversion of Polyolefins to Chemicals and Fuels over Various Cracking Catalysts"
45. Serrano, D.P.; Aguado, J.; Escola, J.M.; *Ind.Eng. Chem. Res.* 2000, 39, 1177-1184 "Catalytic Cracking of a Polyolefin Mixture over Different Acid Solid Catalysts"
46. Aguado, J.; Serrano, D.P.; Sotelo, J.L.; Van Grieken, R.; Escola, J.M.; *Ind. Eng. Chem. Res.* 2001, 40, 5696-5704 "Influence of the Operating Variables on the Catalytic Conversion of a Polyolefin Mixture over HMCM-41 and Nanosized HZSM-5"
47. Serrano, D.P.; Van Grieken, R.; Aguado, J.; Garcia, R.A.; Rojo, C.; Temprano, F.; *Stud. Surf. Sci. Catal.* 2000, 130, 1589-1594 "Study on the Initial Steps of the Polyethylene Cracking over Different Acid Catalysts"
48. Uemichi, Y.; Hattori, M.; Itoh, T.; Nakamura, J.; Sugioka, M.; *Ind. Eng. Chem. Res.* 1998, 37, 867-872 "Deactivation Behaviors of Zeolite and Silica-Alumina Catalysts in the Degradation of Polyethylene"
49. Lukyanov, D.B.; Shtral, V.I.; Khadzhiev, S.N.; *J. Catal.* 1994, 146, 87-92 "A Kinetic Model for the Hexane Cracking Reaction over H-ZSM-5"

50. Abbot, J.; Appl. Catal. 1990, 57, 105-125 "Cracking Reactions of C₆ Paraffins on HZSM-5"
51. Krannila, H.; Haag, W.O.; Gates, B.C.; J. Catal. 1992, 135, 115-124 "Monomolecular and Bimolecular Mechanisms of Paraffin Cracking: n-Butane Cracking Catalyzed by HZSM-5"
52. Behrsing, T.; Jaeger, H.; Mole, T.; Appl. Catal. 1989, 47, 67-73 "Hydroisomerization of Branched-Chain Olefins over Pt/HZSM-5 Zeolite"
53. Triantafillidis, C.S.; Evmirdis, N.P.; Ind. Eng. Chem. Res. 1999, 38, 916-927 "Performance of ZSM-5 as a Fluid Catalytic Cracking Catalyst Additive: Effect of the Total Number of Acid Sites and Particle Size"
54. Sotelo, J.L.; Van Grieken, R.; Aguado, J.; Serrano, D.P.; Escola, J.M.; Menendez, J.M.; Proc. 12th Int. Zeolite Conf., Baltimore, Maryland, July 1998, Eds. Treacy, M.M.J.; Marcus, B.K.; Bisher, M.E.; Higgins, J.B.; Materials Research Society, Warrendale, PA 1999
55. Lungstein, A.; Jentys, A.; Vinek, H. Appl. Catal. A 1998, 166, 29-38 "Hydroconversion of n-Heptane over Bifunctional HZSM-5 Zeolites. Influence of the Metal Concentration and Distribution on the Activity and Selectivity"
56. Abbot, J.; Corma, A.; Wojciechowski, B.W.; J. Catal. 1985, 92, 398-408 "The Catalytic Isomerization of 1-Hexene on H-ZSM-5 Zeolite: The Effects of a Shape-Selective Catalyst"
57. Henriques, C.A.; Bentes Jr., A.M.; Magnoux, P.; Guisnet, M.; Monteiro, J.L.F.; Appl. Catal. A 1998, 166, 301-309 "Characterization of the Coke Formed from o-Xylene over Mordenites at Different Pressures under N₂ and H₂"
58. Murty, M.V.S.; Grulke, E.A.; Bhattacharyya, D.; Poly. Deg. Stab. 1998, 61, 421-430 "Influence of Metallic Additives on Thermal Degradation and Liquefaction of High Density Polyethylene (HDPE)"
59. Deng, G.S.; McClennen, W.H.; Meuzelaar, H.L.C.; Prepr. Papers - Am. Chem. Soc. Div. Fuel Chem. 1997, 42, 987-992 "Catalytic Degradation of High Density Polyethylene and Waste Plastic Below 200 °C"
60. Ding, W.; Liang, J.; Anderson, L.L. Fuel Proc. Tech. 1997, 51, 47-62 "Thermal and Catalytic Degradation of High Density Polyethylene and Commingled Post-Consumer Plastic Waste"
61. Chen, W-H.; Pradhan, A.; Jong, S-J.; Lee, T-Y.; Wang, I.; Tsai, T-C.; Lui, S-B.; J. Catal. 1996, 163, 436-446 "Roles of Carrier Gases on Deactivation and Coking in Zeolite Beta during Cumene Disproportionation"

62. Van Grieken, R.; Serrano, D.P.; Aguado, J.; Garcia, R.; Rojo, C.; *J. Anal. Appl. Pyrol.* 2001, 58-59, 127-142 "Thermal and Catalytic Cracking of Polyethylene under Mild Conditions"
63. Park, D.W.; Hwang, E.Y.; Kim, J.R.; Choi, J.K.; Kim, Y.A.; Woo, H.C.; *Poly. Deg. Stab.* 1999, 65, 193-198 "Catalytic Degradation of Polyethylene over Solid Acid Catalysts"
64. Paal, Z.; Tetenyi, T.; *J. Catal.* 1973, 29, 176-179 "Isomerization of Hydrocarbons in the Presence of Platinum Black"
65. Paal, Z.; Tetenyi, T.; *J. Catal.* 1973, 30, 350-361 "The Mechanism of Aromatization on Platinum Black Catalysts; Dehydrocyclization of Hexadienes and Hexatrienes"
66. Mielczarski, E.; Bong Hong, S.; Davis, R.J.; Davis, M.E.; *J. Catal.* 1992, 134, 359-369 "Aromatization of n-hexane by Platinum-Containing Molecular Sieves II. n-Hexane Reactivity"
67. Paal, Z.; *Hydrogen Effects in Catalysis: Fundamentals and Practical Applications*, Eds. Paal, Z.; Menon, P.G.; Marcel Dekker, Inc., New York, 1988. Ch. 17
68. Gnep, N.S.; Doyemet, J.Y.; Seco, A.M.; Ribeiro, F.R.; Guisnet, M.; *Appl. Catal.* 1987, 35, 93-108 "Conversion of Light Alkanes into Aromatic Hydrocarbons. 1-Dehydrocyclodimerization of Propane on PtHZSM-5 Catalysts"
69. Meriaudeau, P.; Naccache, C.; *Catal. Rev. Sci. Eng.* 1997, 1-2, 5-48 "Dehydrocyclization of Alkanes over Zeolite-Supported Metal Catalysts: Monofunctional or Bifunctional Route"
70. Choudhary, V.R.; Mayadevi, S.; Akolekar, D.B.; *J. Catal.* 1993, 144, 16-29 "Influence of Coke Deposition on Acidity, Intercrystalline Mass Transfer, and Catalytic Properties of Pt/H-ZSM-5/Al₂O₃ Catalyst"
71. Ribeiro, F.; Marcilly, C.; Guisnet, M.; *J. Catal.* 1982, 78, 275-280 "Hydroisomerization of n-Hexane on Platinum Zeolites II. Comparison between the Reaction Mechanisms on Platinum/Y-Zeolite and on Platinum/Mordenite"
72. Baumgarten, E.; Niemeyer, I.; *React. Kinet. Catal. Lett.* 2000, 70, 371-377 "On the Role of Surfaces in Hydrogenation Reactions with Gas Phase Spillover Hydrogen"
73. Baumgarten, E.; Maschke, L.; *Appl. Catal. A* 2000, 202, 171-177 "Hydrogen Spillover through the Gas Phase Reaction with Graphite and Activated Carbon"
74. Roessner, F.; Roland, U.; *J. Mol. Catal. A* 1996, 112, 401-412 "Hydrogen Spillover in Bifunctional Catalysis"

75. Coonradt, H.L.; Garwood, W.E.; *Ind. Eng. Chem. Prod. Res. Dev.* 1964, 3, 38-45
"Mechanism of Hydrocracking Reactions of Paraffins and Olefins"
76. Ding, W.B.; Tuntawiroon, J.L.; Anderson, L.L.; *Fuel Proc. Tech.* 1996, 49, 49-63
"Depolymerization of Waste Plastics with Coal over Metal-Loaded Silica-Alumina Catalysts"
77. Park, K-C.; Ihm, S-K.; *Appl. Catal. A* 2000, 203, 201-209 "Comparison of Pt/zeolite Catalysts for n-Hexadecane Hydroisomerization"
78. Weitkamp, J.; Jacobs, P.A.; Martens, J.A.; *Appl. Catal.* 1983, 8, 123-141
"Isomerization and Hydrocracking of C₉ Through C₁₆ n-Alkanes on Pt/HZSM-5 Zeolite"
79. Hocht, M.; Kleber, Ch.; Jentys, A.; Vinek, H.; *Stud. Surf. Sci. Catal.* 2000, 130, 377-382 "In Situ Investigation of Hydrocarbon Reactions over Zeolite Based Bifunctional Catalysts"
80. Martens, J.A.; Parton, R.; Uytterhoeven, L.; Jacobs, P.A.; Froment, G.F.; *Appl. Catal.* 1991, 76, 95-116 "Selective Conversion of Decane into Branched Isomers - A Comparison of Platinum/ZSM-22, Platinum/ZSM-5, and Platinum/USY Zeolite Catalysts"
81. Baburek, E.; Novakova, J.; *Appl. Catal. A* 2000, 190, 241-251 "Effect of Platinum in Bifunctional Isomerization of n-Butane over Acid Zeolites"
82. Zaera, F.; *J. Mol. Catal* 1994, 86, 221-242 "Molecular Approach to the Study of the Mechanism of Alkyl Reactions on Metal Surfaces"
83. Ribeiro, F.; Marcilly, Ch.; Guisnet, M.; Freund, E.; Dexpert, H.; *Stud. Surf. Sci. Catal.* 1980, 5, 319-325 "Influence of Platinum Content on the Catalytic Activity of PtHY and PtHM Zeolites"
84. Aberuagba, F.; *React. Kinet. Catal. Lett.* 2000, 70, 243-249 "Aromatization of Heptene-2 on Pt/Al₂O₃ Catalysts"
85. Vyazovkin, S.; Lesnikovich, A.I.; *Thermochim. Acta* 1990, 165, 273-280 "An Approach to the Solution of the Inverse Kinetic Problem in the Case of Complex Processes Part 1. Methods Employing a Series of Thermoanalytical Curves"
86. Ribeiro, F.; Guisnet, M.; Marcilly, C.; *Appl. Catal.* 1985, 13, 281-288 "Influence of Coke on the Kinetics of n-Hexane Hydroisomerization on Platinum HY Catalysts"
87. Sermon, P.A.; Vong, M.S.W.; Matheson, M.; *Deactivation and Testing of Hydrocarbon-Processing Catalysts*, ACS Symp. Ser. 634, Eds. O'Connor, P.; Takatsuka, T.; Woolery, G.L.; American Chemical Society, Washington D.C., 1996, 91-98

88. Pirngruber, G.D.; Seshan, K.; Lercher, J.A.; *Catal. Lett.* 2000, 64, 232-238 "On the conversion of 1-Butene over Pt-ZSM5"